

**Pickering emulsion-based encapsulation strategies for
delivery of curcumin**

Andrea Araiza Calahorra

Submitted in accordance with the requirements for the degree of
Doctor of Philosophy
The University of Leeds
School of Food Science and Nutrition

March, 2020

The candidate confirms that the work submitted is his/her own, except where work which has formed part of jointly-authored publications has been included. The contribution of the candidate and the other authors to this work has been explicitly indicated below. The candidate confirms that appropriate credit has been given within the thesis where reference has been made to the work of others. Details of the jointly-authored publications and contribution of each authors are outlined on the next page.

This copy has been supplied on the understanding that it is copyright material and that no quotation from the thesis may be published without proper acknowledgement.

The right of Andrea Araiza Calahorra to be identified as Author of this work has been asserted by her in accordance with the Copyright, Designs and Patents Act 1988.

© 2020 The University of Leeds and Andrea Araiza Calahorra

Further details of the jointly-authored publications and the contributions of the candidate and the other authors to the work are included below:

Chapter 2

Araiza-Calahorra, A., Akhtar, M., and Sarkar, A. 2016. Recent advances in emulsion-based delivery approaches for curcumin: From encapsulation to bioaccessibility, *Trends in Food Science & Technology*. 71, pp. 155 – 169.

Chapter 3

Araiza-Calahorra, A., & Sarkar, A. 2019a. Pickering emulsion stabilized by protein nanogel particles for delivery of curcumin: Effects of pH and ionic strength on curcumin retention. *Food Structure*, 21, pp. 100 – 113.

Chapter 4

Araiza-Calahorra, A., & Sarkar, A. 2019b. Designing biopolymer-coated Pickering emulsions to modulate *in vitro* gastric digestion: a static model study. *Food & Function*, 10 (9), pp. 5498 – 5509.

Chapter 5

Araiza-Calahorra, A., Glover, Z., Akhtar, M., and Sarkar, A. 2020. Conjugate microgel-stabilized Pickering emulsions: Role in delaying gastric digestion. *Food Hydrocolloids*, 105, pp. 105794.

Chapter 6

Araiza-Calahorra, A., Wang, Y., Boesch, C., Zhao, Y., and Sarkar, A. A. Pickering emulsions stabilized by protein gel particles complexed/ conjugated with biopolymers to enhance bioaccessibility and cellular uptake of curcumin. *Current Research in Food Science*, 3, pp. 178 –188.

Details of authorship contributions:

Andrea Araiza-Calahorra: designed the question for literature search, collected and analysed data from the literature to summarize the findings from all the emulsion-based encapsulation strategies for curcumin, identified the knowledge gap, drafted and edited the manuscript and replied to the comments from reviewers.

Zachary J. Glover: contributed in the cross-correlation image analysis of the confocal images obtained by A. Araiza-Calahorra.

Yansheng Zhao: conducted the preliminary experiments for Caco-2 cell culture.

Yunqing Wang: conducted the final experiments for Caco-2 cell culture.

Anwasha Sarkar, Mahmood Akhtar and Christine Boesch: provided supervision and feedback on the literature research and contributed to the proofreading and editing of the manuscript.

List of accepted conference abstracts

Poster presentation:

Araiza-Calahorra, A., Exton, H., Akhtar, M., Sarkar, A. Encapsulation and gastric release of curcumin using Pickering emulsion-stabilized by protein nanogel. (2018). 17th Food Colloids Conference: Application of Soft Matter Concepts – Leeds, UK.

Araiza-Calahorra, A., Akhtar, M., Sarkar, A. Protein nanogel particle-stabilized Pickering emulsion: A delivery vehicle for curcumin. (2018). 32nd EFFoST International Conference – Nantes, France.

Araiza-Calahorra, A., Sarkar, A. Delivering curcumin using Pickering oil-in-water emulsions stabilized by whey protein nanogel particles: Role of pH and ionic strength on curcumin retention. (2019). 8th International Symposium on “Delivery of Functionality in Complex Food Systems” – Porto, Portugal. (Best poster award).

Araiza-Calahorra, A., Glover, Z., Akhtar, M., and Sarkar, A. Evaluating the fate of microgel-stabilised Pickering emulsions during *in vitro* gastric digestion: Role of electrostatic coating versus covalent-conjugation with polymers. (2020). Physics in Food Manufacturing 2020 Conference. – Leeds, UK. (Best poster award).

Oral presentations:

Araiza-Calahorra, A., Mackie, A., A., Sarkar, A. Designing polysaccharide-coated Pickering emulsions stabilised by protein nanogel particles to modulate *in vitro* gastric digestibility. (2019). Rank Prize Fund Symposium: Designing Food Structure to Control Digestion and Improve Health Impacts – Grasmere, UK.

Araiza-Calahorra, A., Mackie, A., A., Sarkar, A. Polymer-coated Pickering emulsions as a strategy to control *in vitro* gastric digestion. (2019). The Food Hydrocolloids Trust: 20th Gums & Stabilisers for the Food Industry Conference – San Sebastian, Spain.

Araiza-Calahorra, A., Akhtar, M., Sarkar, A. Protein-polysaccharide conjugate-based microgels for Pickering stabilization of oil-in-water emulsions: Influence on gastric digestion. (2019). 4th UK Hydrocolloids Symposium, from Food to Bioprocessing – Leeds, UK.

Acknowledgements

First and foremost, I would like to sincerely thank my main supervisor Dr. Anwesha Sarkar for all her guidance, persistent help, tolerance and consistent support as well as motivation throughout my PhD. Her office door was always open whenever I had a question and her support was truly crucial from the start up to the submission of my thesis. Thanks for being an excellent supervisor, I truly think I was very lucky to have you in this process and I am deeply grateful to have conducted my research project with such an incredible and supportive person. Thanks for helping me follow my dreams and for boosting up my confidence.

I would also like to acknowledge “Consejo Nacional de Ciencia y Tecnologia (CONACyT) (Mexico) for the financial support during my studies.

I would like to extend my thanks to all staff in the School of Food Science and Nutrition, who helped me directly or indirectly throughout my research, Miles Ratcliff, Dr. Joanne Brown, Amie Lister, Ian Hardy, Dr. Nataricha Phisarnchananan and Neil Rigby, many thanks for always be there to help and offer valuable technical support during my PhD.

Even though it is not possible to mention every single person in here, I would like to thank all my Food Science’s friends, specially Dr. Emma Krop, Suvro Saha, Vicente Miron, Dr. Yadira Gonzalez, Dr. Efren Andablo, Dr. Amelia Torcello, Dr. Mar Collado and Dr. Gurmeet Kaur for all the meals, parties, beers and laughs we shared together through my time as a PhD student.

I would also like to thank my friends and family members in Mexico, Maria Jose, Francisco, Prince and Yaya, many thanks for all your encouragement despite the distance. Ale, Rosy, Maya, Mariana, Dani and Sofia, thank you for your friendship and all the support though endless messages and conversations. Also, my friends and family in Spain, Ana, Nicolai, Valentin, Paco and Clara, thank you for all the love and comfort you have given us every time we visit you. I am also thankful and grateful for my friend Anna, for her joy, kindness and support, and for showing me that friendship is not defined by time or distance.

My endless gratitude goes to my parents, whose support, understanding and patience when they had to bear my moments of stress and frustration made it possible to overcome the hardship of these years. Dad, thank you for being an inspiration and role model through my life, mom, thank you for all the sacrifice and selflessness care you always give me, and Ale, thanks for your support and caring. Pa, ma, thanks for all the sacrifices that you have made on my behalf, los quiero muchisimo!

And finally, last but by no means least, my deepest appreciation goes to my best friend and life companion, my husband Alberto, thank you for the endless love, support, encouragement, positivity and emotional comfort you have given me all these years. None of this would have been possible without you. I love you and I am lucky and grateful to have you by my side.

Thanks/gracias

Abstract

Curcumin is a potent bioactive polyphenolic compound but its bioavailability when orally administered is limited because of its low solubility in aqueous environments and chemical/ metabolic degradation during gastrointestinal transit. Oil-in-water emulsions have been extensively used as delivery systems for curcumin to target physiological sites. Particularly, emulsions stabilized by solid particles, also known as Pickering emulsions, have gained remarkable research interest as delivery vehicles due to their exceptional resistance to coalescence over prolonged periods of time and the fact that these particles are not desorbed by intestinal biosurfactants (bile salts) because of their high detachment energies. This thesis focuses on the design of complex particulate Pickering interfaces using two types of interactions (*i.e.* electrostatic and covalent) between whey protein and polysaccharides (dextran sulphate or dextran). Hence, three different Pickering emulsions; whey protein isolate nanogel particle-stabilized (E_{WPN}), dextran sulphate coated-whey protein isolate nanogel particle-stabilized ($DxS-E_{WPN}$) and whey protein isolate-dextran conjugated (or Maillard) microgel particle-stabilized (E_{WPDxM}) Pickering emulsions were created as delivery vehicles for curcumin.

For E_{WPN} , controlled retention of curcumin was associated with the effect of pH and ionic strength on the partitioning of curcumin between the oil phase and the nanogel particle-laden interface. Also, by using an *in vitro* gastric model, pepsin hydrolysis was restricted in $DxS-E_{WPN}$ compared to E_{WPN} . In addition, Maillard conjugation was used to engineer novel conjugated microgel particles ($WPDxM$) that could stabilize Pickering emulsions (E_{WPDxM}) that exhibited gastric-stable properties as opposed to non-conjugated systems. Finally, the bioaccessibility and cellular uptake of curcumin by Caco-2 cells in the three different Pickering interfaces was evaluated after *in vitro* digestion. All three systems offered similar bioaccessibility due to similar degree of free fatty acid release during *in vitro* intestinal digestion. Nevertheless, the uniqueness was that $DxS-E_{WPN}$ and E_{WPDxM} had better cell viability and cellular internalization of curcumin in comparison to E_{WPN} .

In summary, findings from this PhD ranges from colloidal design of novel biocompatible Pickering emulsion-based delivery vehicles, to identifying the vehicles that offer optimized gastric stability of emulsions and cellular delivery of bioactives (curcumin). These insights can be used for rational design of functional foods, food supplements, and for oral pharmaceutical and cosmetic applications in the future.

Table of Contents

Acknowledgements	vi
Abstract	vii
Table of Contents	viii
List of Tables	xiv
List of Figures	xvi
List of Abbreviations	xxi
List of Symbols	xxv
Chapter 1 General Introduction	1
1.1 Overall research aim	2
1.2 General insights on emulsions	3
1.2.1 Pickering emulsions	3
1.3 Rationale behind the selection of biopolymers	4
1.3.1 Milk Proteins	4
1.3.1.1 Whey protein isolate for designing nanogel and microgel particles.....	4
1.3.1.2 Stabilization of emulsions by whey protein- based gel particles.....	5
1.3.2 Polysaccharides.....	6
1.3.3 Maillard Reaction	7
1.4 Rationale behind the selection of characterization techniques	8
1.4.1. Dynamic light scattering (DLS)	8
1.4.2 ζ -potential	10
1.4.3 Microscopy across scales (confocal laser scanning microscopy to scanning and transmission electron microscopy)	12
1.4.4 Static light scattering (SLS).....	14
1.4.5 Interfacial shear rheology.....	15
1.4.6 <i>In vitro</i> gastrointestinal processing.....	17
1.4.6 Assessment of gastric digestibility of the proteinaceous particles	19
1.4.7 Free fatty acid release	20
1.4.8 Cell viability and cellular uptake.....	21
1.4.9 High Performance Liquid Chromatography (HPLC).....	21
1.5 Outline of the thesis	22
1.6 References.....	25

Chapter 2 Recent advances in emulsion-based delivery approaches for curcumin: From encapsulation to bioaccessibility	31
2.1 Introduction	32
2.2 General aspects of curcumin	34
2.2.1 Structure of curcumin.....	34
2.2.2 Solubility of curcumin in solvents.....	37
2.3 Key challenges of delivery of curcumin.....	39
2.4 Emulsion-based delivery systems.....	40
2.4.1 Stability of O/W emulsions	47
2.4.2 Types of emulsion structure.....	47
2.5 Dispersion of curcumin into the oil phase	51
2.6 Physicochemical stability of curcumin–loaded emulsion systems.....	53
2.6.1 Loading efficiency	53
2.6.2 Droplet size of curcumin-loaded emulsions	56
2.7 <i>In vitro</i> gastrointestinal stability and bioaccessibility of curcumin-loaded emulsions	57
2.7.1 <i>In vitro</i> storage stability and release	58
2.7.2 <i>In vitro</i> gastrointestinal stability of curcumin	59
2.7.3 Bioaccessibility of curcumin-loaded emulsions.....	61
2.8 Conclusions and Future Outlook.....	63
2.9 References.....	65
Chapter 3 Pickering emulsion stabilized by protein nanogel particles for delivery of curcumin: Effects of pH and ionic strength on curcumin retention.....	76
3.1 Introduction	77
3.2 Materials and methods.....	79
3.2.1 Materials	79
3.2.2 Preparation of whey protein nanogel particles.....	80
3.2.3 Preparation of whey protein nanogel-stabilized emulsions (E _{WPN}), CUR-loaded emulsions (CUR-E _{WPN}) and whey protein isolate-stabilized emulsions (E _{WPI})	80
3.2.4 Transmission electron microscopy.....	81
3.2.5 Cryogenic- Scanning Electron Microscopy	81
3.2.6 Confocal scanning laser microscopy (CLSM)	82
3.2.7 Determination of adsorption efficiency by WPN.....	82
3.2.8 Interfacial shear viscosity.....	82

3.2.9 Droplet and particle size distribution	83
3.2.10 ζ -potential	84
3.2.11 Measurement of CUR retention in Pickering emulsions.....	84
3.2.12 CUR retention in Pickering emulsions	85
3.2.13 Fluorescence measurements.....	85
3.2.14 Statistical analysis.....	86
3.3 Results and discussion	86
3.3.1 Characteristics of aqueous dispersions of WPN.....	86
3.3.2 Characteristics of Pickering emulsions (EWPN).....	87
3.3.3 Characteristics of CUR-loaded Pickering emulsions	93
3.3.4 CUR retention in the CUR-E _{WPN}	95
3.3.5 Binding of CUR and WPN.....	98
3.4 Conclusions	101
3.5 References.....	102
Chapter 4 Designing biopolymer-coated Pickering emulsions to modulate <i>in vitro</i> gastric digestion: A static model study	109
4.1. Introduction	110
4.2 Materials and Methods.....	112
4.2.1 Materials	112
4.2.2 Preparation of whey protein nanogel particles (WPN).....	113
4.2.3 Preparation of Pickering oil-in-water emulsions.....	113
4.2.4 <i>In vitro</i> gastric digestion of particles and emulsions.....	114
4.2.5 Particle size and droplet size distribution.....	114
4.2.6 ζ -potential	115
4.2.7 Confocal scanning laser microscopy (CLSM).....	115
4.2.8 Quantification of protein hydrolysis	116
4.2.9 Sodium dodecyl sulphate polyacrylamide gel electrophoresis (SDS-PAGE)	116
4.2.10 Statistical analysis.....	117
4.3. Results and Discussion.....	117
4.3.1 Optimization of the biopolymer-coated Pickering emulsions.....	117
4.3.2 <i>In vitro</i> gastric digestion of aqueous dispersions of WPN and DxS+WPN	120
4.3.3 Physicochemical and microstructural characterization of E _{WPN} , DxS-E _{WPN} -40 and DxS-E _{WPN} -500 during <i>in vitro</i> gastric digestion.....	124

4.3.4 Protein composition of adsorbed phase of E _{WPN} , DxS-E _{WPN} -40 and DxS-E _{WPN} -500 during <i>in vitro</i> gastric digestion	129
4.4 Conclusions	132
4.5 References.....	133
Chapter 5 Conjugate microgel-stabilized Pickering emulsions: Role in delaying gastric digestion.....	138
5.1. Introduction	139
5.2 Materials and Methods.....	141
5.2.1 Materials	141
5.2.2 Preparation of whey protein isolate - dextran conjugate... ..	141
5.2.3 Determination of free amino groups.....	142
5.2.4 Preparation of heat-induced gels and microgel particles ..	143
5.2.5 Mechanical properties of heat-induced WPI-Dx gels	144
5.2.6 Preparation of Pickering oil-in-water emulsions.....	144
5.2.7 Interfacial shear viscosity.....	144
5.2.8 <i>In vitro</i> gastric digestion of conjugate microgel particles... ..	145
5.2.9 Particle size and droplet size distribution.....	145
5.2.10 ζ -potential	146
5.2.11 Cryogenic-Scanning Electron Microscopy	146
5.2.12 Confocal scanning laser microscopy (CLSM) and cross-correlation analysis	147
5.2.13 Sodium dodecyl sulphate polyacrylamide gel electrophoresis (SDS-PAGE)	148
5.2.14 Statistical analysis.....	148
5.3. Results and Discussion.....	149
5.3.1 Identifying the degree of conjugation (% DC).....	149
5.3.2 Mechanical properties of the conjugate WPI-Dx heat-set gels	151
5.3.3 Characteristics of conjugate microgel particles.....	153
5.3.4 Characteristics of conjugated microgel particles during <i>in vitro</i> gastric digestion	155
5.3.5 Characteristics of Pickering emulsions stabilized by WPD _{X10M} (E _{WPDx10M}).....	159
5.3.6 Characteristics of E _{WPDx10M} during <i>in vitro</i> gastric digestion	161
5.3.6.1 Stability under simulated gastric conditions.....	162

5.3.6.2 Cross-correlation image analysis of confocal microscopy images	164
5.4 Conclusions	166
5.5 References.....	167
Chapter 6 Pickering emulsions stabilized by protein gel particles complexed and conjugated with biopolymers to enhance bioaccessibility and cellular uptake of curcumin	174
6.1. Introduction	175
6.2 Materials and Methods.....	177
6.2.1 Materials	177
6.2.2 Methods	177
6.2.2.1 Preparation of CUR-loaded Pickering emulsion systems.....	177
6.2.2.1.1 Preparation of whey protein nanogel particles (WPN) and whey protein isolate+dextran conjugate microgel particles (WPDxM).....	177
6.2.2.1.2 CUR-loaded Pickering oil-in-water emulsion preparation.....	178
6.2.2.2 Particle and droplet size measurements.....	179
6.2.2.3 ζ -potential measurements.....	179
6.2.2.4 Apparent viscosity.....	179
6.2.2.5 <i>In vitro</i> gastrointestinal digestion (static model).....	180
6.2.2.6 Free fatty acid release	181
6.2.2.7 Bioaccessibility of CUR.....	182
6.2.2.8 Microstructural characterization	182
6.2.2.8.1 Confocal scanning laser microscopy (CLSM).....	182
6.2.2.8.2 Cryogenic-scanning electron microscopy.	182
6.2.2.9 Cell based assays.....	183
6.2.2.9.1 Cell culture.	183
6.2.2.9.2 Cytotoxicity assay.	183
6.2.2.9.3 Cellular curcumin uptake.	183
6.2.3 Statistical analysis.....	184
6.3. Results and Discussion.....	184
6.3.1 Characteristics of curcumin Pickering emulsions	184
6.3.2 Characteristics of CUR-loaded Pickering emulsions during <i>in vitro</i> gastrointestinal digestion.....	189
6.3.3 Influence of emulsion type on lipid digestion kinetics	192
6.3.4 Influence of emulsion type on CUR bioaccessibility	192

6.3.5 Cell viability and uptake in presence of CUR.....	194
6.4 Conclusions	196
6.7 References.....	197
Chapter 7 General discussion	202
7.1 Introduction	202
7.2 Summary of main results	205
7.2.1 Assessment of curcumin solubility in different types of oil	205
7.2.3 Assessment of nanogel and microgel particles.....	206
7.2.4 O/W emulsions.....	208
7.2.5 Properties of emulsions during <i>in vitro</i> gastrointestinal processing using static model.....	212
7.2.5.1 Curcumin-loaded Pickering emulsions	212
7.2.5.2 Stability after <i>in vitro</i> gastric digestion	213
7.2.5.3 Behaviour during <i>in vitro</i> intestinal digestion, curcumin bioaccessibility and cellular uptake	214
7.3 Future directions	216
7.4 References.....	218
Appendix A Supporting information of Chapter 3	220
Appendix B Supporting information of Chapter 4	224
Appendix C Supporting information of Chapter 5	230
Appendix D Supporting information of Chapter 6	237

List of Tables

Table 2.1. Solubility ($\mu\text{g}/\text{mL}$) of curcumin in various edible oils.....	38
Table 2.2. Composition and formation of nanoemulsions for delivery of curcumin.	41
Table 2.3. Composition and formation of conventional emulsions (protein-polysaccharide conjugates/ complexes-stabilized) and Pickering emulsions (particle-stabilized systems) for delivery of curcumin.	45
Table 3.1. Interfacial shear viscosities ($\eta_i / \text{mN s m}^{-1}$) O/W interface in presence of whey protein isolate (WPI) and whey protein nanogel particles (WPN) at pH 7.0. Values represent mean \pm SD of at least three independent experiments ($n \geq 3$).....	88
Table 3.2. Surface coverage of emulsion droplets by various concentrations of WPN.	92
Table 4.1. Droplet size and ζ -potential values for E_{WPN} , DxS- $E_{\text{WPN-40}}$ and DxS- $E_{\text{WPN-500}}$ at pH 3.0, respectively.	125
Table 5.1. Nomenclature, conjugation conditions and characterization of conjugates obtained <i>via</i> OPA analysis.....	142
Table 5.2. Mean hydrodynamic diameter (d_H , nm), polydispersity index and ζ -potential values of freshly prepared conjugated microgel particles in phosphate buffer at pH 7.0 and after addition of SGF at pH 3.0.	156
Table 6.1. Mean droplet size and ζ -potential of initial emulsions.	186
Table 7.1. Comparison of the characteristics of 1 wt% protein-based particles on their size (d_H) and ζ -potential at pH 7.0.	208
Table 7.2. Summary of surface coverage, absorption efficiency, mean d_{43} and ζ -potential values of Pickering emulsions stabilized with different concentrations of WPN at pH 7.0.....	210
Table 7.3. Comparison of the characteristics of Pickering emulsions (without curcumin) based on their size (d_{43} , d_{32}) and ζ -potential at pH 7.0.	210
Table 7.4. Comparison of the characteristics of curcumin-loaded Pickering emulsions based on their size (d_{43} , d_{32}) and ζ -potential at pH 7.0.	213
Table B1. Mean hydrodynamic diameter (d_H), polydispersity index (PDI) and ζ -potential values for WPN, WPN + DxS-40 and WPN+DxS-500 after formation at pH 3.0.	224

Table B2. Mean hydrodynamic diameter (d_H), polydispersity index (Pdl) and ζ -potential values of control samples for WPN, WPN + DxS-40 and WPN + DxS-500 in an *in vitro* gastric model at pH 3.0 in presence of SGF without pepsin, respectively..... **225**

List of Figures

Figure 1.1. Schematic representation of a Pickering emulsion <i>i.e.</i> emulsions stabilized by solid particles.	3
Figure 1.2. Molecular structure of dextran.....	7
Figure 1.3. Schematic representation of protein-polysaccharide conjugation <i>via</i> Maillard reaction adapted from de Oliveira et al., (2016).....	8
Figure 1.4. Schematic representation of dynamic light scattering measuring principle.....	9
Figure 1.5. Schematic representation of zeta potential adapted from Malvern Instruments (2015).	12
Figure 1.6. Schematic diagram of interfacial shear rheometer based on bicone method.	17
Figure 1.7. Schematic representation of sodium dodecyl sulfate-polyacrylamide gel electrophoresis (SDS-PAGE) (MW: molecular weight).	20
Figure 1. 8. Schematic framework of the thesis.	24
Figure 2.1. Functional groups in curcumin.	35
Figure 2.2. Scanning electron micrographs (SEM) of curcumin crystals dispersed at 10 mg/ mL in methanol (a), DMSO (b), and sunflower oil (c) in lower ($\times 5,000$, left) and higher magnifications ($\times 10,000$, right).....	36
Figure 2.3. Schematic diagram of conventional emulsion (a), multilayered emulsion (b) and Pickering emulsion (c). Preparation method of conventional and Pickeing emulsion (a) and multilayered emulsion (e).....	40
Figure 2.4. Schematic diagram of nanoemulsion (a) and its preparation method by high-intensity (b) and low-intesity (c) techniques.	50
Figure 3.1. a) Intensity distribution of WPN with inset representing the visual image and physicochemical characteristics of the WPN, and micrographs of 1 wt% WPN at various length scales: b) Cryo-SEM, and c) TEM.	87
Figure 3.2. Micrographs of 20 wt% MCT-oil-in-water emulsion stabilised by a) 1 wt% WPI and b) 1 wt% WPN at pH 7.0 with superimposed droplet size distribution at multiple length scales. In Cryo-SEM, 20 wt% heptane-in-water emulsions was used.....	89

Figure 3.3. a) Droplet size distribution of 20 wt% MCT- oil-in-water emulsions stabilized by 0.1 wt% (black, dashed line), 0.25 wt% (red, solid circle), 0.35 wt% (blue, solid square), 0.5 wt% (green, solid circle), 1 wt% (purple, solid triangle), 1.5 wt% (orange, solid diamond), 2 wt% (turquoise, open diamond), 3 wt% (brown, cross) WPN, respectively, where insert represents the corresponding visual images of the Pickering emulsions, with b) mean d_{43} values (black, solid square), and ζ -potential values (red, solid circle) at pH 7, and c) corresponding absorption efficiency of WPN (black, solid square) at the droplet surface. Error bars represent standard deviation..... **91**

Figure 3.4. a) Droplet size distribution of emulsion-stabilized by 1 wt% WPN without curcumin (E_{WPN}) (black, solid line) or loaded with (red, dashed line) (CUR- E_{WPN}) curcumin with inset representing the corresponding emulsions, respectively *i.e.* C and E are with and without curcumin, respectively. b) Cryo-SEM images of b1) 20 wt% heptane-in-water Pickering emulsion (E_{WPN}) stabilized by 1 wt% WPN and b2) CURE $_{WPN}$ stabilized by 1 wt% WPN..... **94**

Figure 3.5. a1, b1) Confocal micrographs of original CUR- E_{WPN} droplets, a2, b2) after incubation at 37 °C in buffered solutions (15% v/v ethanol) at pH 3.0, and a3, b3) after incubation at 37 °C in buffered solutions (15% v/v ethanol) at pH 7.0 respectively. Top images a) represent staining oil by Nile Red and WPN by Fast Green, whereas b) images in bottom has no added stain but uses auto-fluorescence of CUR..... **97**

Figure 3.6. a) Percentage of CUR retained (black) in CUR- E_{WPN} droplets and bound (red, diagonal stripes) to WPN in the interface during incubation at 37 °C in buffered solutions (15% v/v ethanol) at 0 mM NaCl/ CaCl₂, 50 mM NaCl, and 10 mM CaCl₂, and b) double reciprocal plot $1/[CM]$ versus $1/\Delta FI$ b). Error bars represent standard deviation..... **99**

Figure 3.7. Schematic representation of the binding interaction of WPN with CUR at a) pH 3.0, and b) pH 7.0, respectively. The grey spheres represent WPN..... **100**

Figure 4.1. Change in a) mean ζ -potential values, b) mean droplet size (d_{43} and d_{32}) and c) mean droplet size distribution of 20 wt% MCT oil-in-water emulsions (DxS- E_{WPN}) at pH 3.0 containing 1 wt% WPN on addition of dextran sulphate (DxS) of (1) 40 kDa and (2) 500 kDa molecular weights, respectively. Error bars in figures a) and b) represent standard deviations, respectively..... **119**

Figure 4.2. a) SDS-PAGE image and b) percentage of intact protein bands of (1) 1 wt% WPN and 1 wt% WPN with addition of 0.2 wt% DxS of (2) 40 kDa or (3) 500 kDa molecular weights, respectively, as a function of in vitro gastric digestion time. Error bars in figure b represent standard deviations..... **121**

- Figure 4.3.** Free amino acid content of 1 wt% WPN (dark) and 1 wt% WPN with addition of 0.2 wt% DxS of 40 kDa (lined pattern) or 500 kDa (dotted pattern) molecular weights, respectively, as measured by OPA spectrophotometric and as a function of *in vitro* gastric digestion time. Error bars in figure represent standard deviations..... **123**
- Figure 4.4.** a) Droplet size distribution and b) mean droplet size (d_{43}) and ζ -potential values of (1) E_{WPN}, (2) DxS-E_{WPN}-40 and (3) DxS-E_{WPN}-500 after *in vitro* gastric digestion, respectively. Error bars in figure b represent standard deviations..... **126**
- Figure 4.5.** Confocal micrographs of (1) E_{WPN}, (2) DxS-E_{WPN}-40 and (3) DxS-E_{WPN}-500 at 0 min (a), after 30 min (b), and 120 min (c) of *in vitro* gastric digestion in presence of SGF containing pepsin, respectively. Note, 0 min represents the behavior in presence of SGF buffer without added pepsin. Green colour represents WPN stained by Fast Green; red colour represents the oil droplets stained by Nile Red, and the blue colour represents the FITC-labelled dextran sulfate. **128**
- Figure 4.6.** a) SDS-PAGE image and b) percentage of intact protein bands of the adsorbed phase of (1) E_{WPN}, (2) DxS-E_{WPN}-40, and (3) DxS-E_{WPN}-500 as a function of *in vitro* gastric digestion time. Error bars in figure b represent standard deviations..... **131**
- Figure 4.7.** Schematic diagram of interaction of E_{WPN} and DxS-E_{WPN}-500 on digestion with SGF. The grey shaded circles represent the WPN particles, the long coil red structures represent the DxS-500 kDa electrostatically attached at the interfacial layer and the smaller green structures represent the pepsin. **132**
- Figure 5.1.** SDS-PAGE patterns of the protein marker (first lane), WPI solution and WPI-Dx conjugates with different degrees of conjugation, respectively. The dotted region represents the beta-lactoglobulin band in 2nd-5th lane and the arrow in the 5th lane represents the oligomers that was not efficiently resolved in the resolving gel..... **150**
- Figure 5.2.** Fracture stress and Young's modulus of heat-treated WPI gels and heat-treated WPI-Dx conjugate gels and corresponding images of the thermo-set hydrogels of a) WPI, b) WPI-Dx₁₀, c) WPI-Dx₂₀ and d) WPI-Dx₃₀ (top). **152**
- Figure 5.3.** Particle size distribution of a) WPDx₁₀M, b) WPDx₂₀M, c) WPDx₃₀M particles (black full line: freshly prepared samples in phosphate buffer at pH 7.0, black dashed line: in SGF buffer at pH 3.0 without added pepsin) with inset representing the visual aspect of the particles..... **154**
- Figure 5.4.** SDS-PAGE patterns of a) WPDx₁₀M, b) WPDx₂₀M, c) WPDx₃₀M particles as a function of *in vitro* gastric digestion time..... **157**

- Figure 5.5.** Free amino acid content of 1 wt% WPD_{x10M} (dark), WPD_{x20M} (lined pattern) and WPD_{x30M} (white), respectively, as measured by OPA spectrophotometric as a function of *in vitro* gastric digestion time. Error bars represent standard deviations..... **159**
- Figure 5.6.** a) Droplet size distribution of E_{WPD_{x10M}}, with inset representing the visual image and physicochemical characteristics and b) cryo-SEM micrographs at 150,000× magnifications of Pickering Emulsions stabilized by 1 wt% WPD_{x10M} (scale bar 1 μm) and c) interfacial shear viscosity at n-tetradecane-water interface against time of 0.5 wt% WPD_{x10M} (blue triangle) and WPN (dark square) as control after 24 hrs of adsorption. Error bars represent standard deviation. **160**
- Figure 5.7.** Change in a) mean droplet size distribution, b) mean droplet size (d_{43}) and mean ζ-potential values of 20 wt% MCT oil-in-water emulsions (E_{WPD_{x10M}}) containing 1 wt% WPD_{x10M} as a function of *in vitro* gastric digestion time. Error bars represent standard. **162**
- Figure 5.8.** Confocal micrographs of E_{WPD_{x10M}} (a) initially without addition of SGF, (b) after addition of SGF at 0 min and (c) after 120 min of *in vitro* gastric digestion in presence of SGF containing pepsin, respectively. Note, 0 min represents the behavior in presence of SGF buffer without added pepsin. The left column with red filled colour represents the oil droplets stained by Nile Red, middle column with green outline represents WPD_{x10M} stained by Fast Green; and the right column represent both the Nile Red and Fast Green channels. Scale bar is 5 μm..... **163**
- Figure 5.9.** a) Pickering emulsion droplet (a) E_{WPN} and (b) E_{WPD_{x10M}} at time 0 min (t₁) and at time 5 -10 min (t₂) and corresponding mean integrated cross-correlation intensity around the droplet as a function of angle at time points t₁ and t₂. Cross-correlation intensities are scaled to the radius of the droplet in the image to account of minor changes in z-position over time. Scale bar is 2 μm. **165**
- Figure 5.10.** Schematic representation of the protective properties of the conjugated microgel particles-stabilized emulsion (E_{WPD_{x10M}}) as compared to non-conjugated counterparts against complete *in vitro* gastric digestion by pepsin..... **166**
- Figure 6.1.** Cryo-SEM images of the three Pickering emulsions used for delivering curcumin *i.e.* a) CUR-E_{WPN} emulsion (magnification of 15,000× (a1), and 50,000× (a2), respectively), b) CUR-DxS+E_{WPN} (magnification of 25,000× (b1), and 50,000× (b2), respectively) and c) CUR-E_{WPD_{xM}} (magnification of 10,000× (c1), and 20,000× (c2), respectively). Arrows indicate the nanogel particle in a2, nanogel particle aggregated with dextran sulphate in b2, and conjugate microgel particles in c2. **185**

- Figure 6.2.** Confocal images with superimposed droplet size distribution of the freshly-prepared Pickering emulsions *i.e.* CUR-E_{WPN}, CUR-DxS+E_{WPN} and CUR-E_{WPDxM} and after their exposure to 120 min of *in vitro* gastric or 180 min of *in vitro* sequential gastrointestinal digestion conditions. 187
- Figure 6.3.** Flow curves of freshly prepared Pickering emulsions *i.e.* CUR-E_{WPN} (black squares) CUR-DxS+E_{WPN} (blue triangles) and CUR-E_{WPDxM} (red circles) at 37 °C. Data points represent the average of at least three measurements on triplicate sample. Error bars indicate the standard deviations. Solid lines are the best fits to the experimental data predicted using the Ostwald de Waele model (Equation 6.1). 188
- Figure 6.4.** Average droplet diameter (d_{43}) (1) and ζ -potential value (2) of CUR-E_{WPN} (black bars) CUR-DxS+E_{WPN} (blue bars with diagonal lines) and CUR-E_{WPDxM} (red bars with horizontal lines) after *in vitro* gastric digestion (a) and *in vitro* intestinal digestion (b). 0 min in each case indicates the behaviour of the emulsions in presence of SGF (a) and SIF (b) buffer without any added enzymes. Error bars represent the standard deviations. (For interpretation of the references to colour in this figure legend, the reader is referred to the Web version of this article)..... 191
- Figure 6.5.** Percentage of free fatty acid (% FFA) released (a) from CUR-E_{WPN} (black squares), CUR-DxS+E_{WPN} (blue triangles) and CUR-E_{WPDxM} (red circles) with insets representing maximum FFA release (Φ_{max} , %), lipolysis rate constant (k , $\mu\text{mol s}^{-1} \text{m}^{-2}$) and the time to achieve 50% digestion ($t_{1/2}$, s), and bioaccessibility (b) of CUR after *in vitro* gastrointestinal digestion from the micellar phase of the aforementioned emulsions. The solid lines connecting the data points in the %FFA curves (a) are the best fits to the experimental data predicted using the mathematical model (Equation (6.2)). Data presented are mean with standard deviation of three independent experiments. Different letters indicate significant differences. (For interpretation of the references to colour in this figure legend, the reader is referred to the Web version of this article)..... 193
- Figure 6.6.** Cell viability (a) of MCT-dissolved CUR (non-emulsified) systems and the three Pickering emulsion-based delivery vehicles (CUR-E_{WPN}, CUR-DxS+E_{WPN} and CUR-E_{WPDxM}) at different concentrations of CUR against Caco-2 cells incubated for 2 h along with the digested blank emulsion without any curcumin (blank bars with diagonal lines), and cellular uptake (b) of CUR by the Caco-2 cells in the three Pickering emulsion-based delivery vehicles. Data presented are mean with standard deviation of three independent experiments. Different letters indicate mean significant differences between CUR concentrations (0.5 μM – 6.0 μM) for cell viability, and significant differences between emulsion types (CUR-E_{WPN}, CUR-DxS+E_{WPN} and CUR-E_{WPDxM}) for cellular uptake. 195

Figure 7.1. Schematic framework of the thesis.	204
Figure 7.2. Solubility ($\mu\text{g}/\text{mL}$) of curcumin in various edible oils. SFO: sunflower oil, MCT: medium chain triacylglycerol, SBO: soybean oil, OA: oleic acid, RT: room temperature.	206
Figure 7.3. TEM micrographs of 1 wt% a) WPN and b) WPD _{x10M}	207
Figure 7.4. CLSM with superimposed particle size distribution and cryo-SEM images of E _{WPN} , DxS+E _{WPN} and E _{WPD_{xM}} emulsion.	211
Figure 7.4. CLSM with superimposed particle size distribution and cryo-SEM images of E _{WPN} , DxS+E _{WPN} and E _{WPD_{xM}} emulsion.	211
Figure 7.4. CLSM with superimposed particle size distribution and cryo-SEM images of E _{WPN} , DxS+E _{WPN} and E _{WPD_{xM}} emulsion.	211
Figure 7.4. CLSM with superimposed particle size distribution and cryo-SEM images of E _{WPN} , DxS+E _{WPN} and E _{WPD_{xM}} emulsion.	211
Figure A1. Solubility ($\mu\text{g}/\text{mL}$) of CUR in sunflower oil, a), soybean oil, b), medium chain triacylglycerol, c) and oleic acid, d), respectively. Error bars represent standard deviations.	220
Figure A2. Visual appearance of CUR-EWPN sample extracts (methanol) a) and CUR after dilution with 1:1 (v/v) methanol/ buffer (25 °C), b) as a function of different pH.	221
Figure A3. Mean concentration of CUR ($\mu\text{g}/\text{mL}$) estimated based on absorbance measurements (425 nm) of stock CUR-methanol solutions (500 $\mu\text{g}/\text{mL}$) in acidic state (pH 2.0) with 1:1 (v/v) methanol/ buffer (25 °C), at different pH values (2.0 – 7.0) (low-to-high). Cero represent the control solution (stock CUR solution diluted in pure methanol).	222
Figure A4. Emission spectra of curcumin showing the variations of curcumin fluorescence intensity and blue-shift on binding to WPN. A 10 μM concentration of curcumin was titrated against an increasing concentration of WPN (0 - 40 μM).	223
Figure B1. Mean ζ -potential values of aqueous dispersions of WPN, DxS-40 kDa and DxS-500 kDa as a function of pH, respectively.	226
Figure B2. Change in mean ζ -potential values of 1 wt% WPN without or with the addition of 0.2 wt% DxS-40 kDa or 0.2 wt% DxS-500 kDa in an <i>in vitro</i> gastric model at pH 3.0 in presence of SGF containing pepsin, respectively.	227
Figure B3. Droplet size distribution, mean d_{43} values and ζ -potential values of control samples for a) E _{WPN} b) DxS-E _{WPN} -40 and c) DxS-E _{WPN} -500 after <i>in vitro</i> gastric digestion in presence of SGF buffer without pepsin, respectively.	228

Figure B4. Confocal micrographs of initial FITC-DxS-E _{WPN} -40 and FITC-DxS-E _{WPN} -500 samples. Simultaneous recording of the emission of Fast Green and FITC-DxS dyes without the addition of Fast Green in the samples. Blue colour represents the FITC-labelled DxS.	229
Figure C1. Images of conjugate powder of a) WPI-Dx ₁₀ , b) WPI-Dx ₂₀ , c) WPI-Dx ₃₀	230
Figure C2. Fracture stress and Young's modulus of non-conjugated WPI-Dx gels.	231
Figure C3. Intensity distribution of non-conjugated microgel particles (N-WPD _x M) with inset representing the visual image and physicochemical characteristics.	232
Figure C4. Photographs of vials containing 1 wt% aqueous solutions of conjugated microgel particles <i>i.e.</i> 1) WPD _{x10} M, 2) WPD _{x20} M, and 3) WPD _{x30} M, as a function of pH and ionic strength; a) 0 M NaCl/ CaCl ₂ , b) 50 mM NaCl and c) 10 mM CaCl ₂	233
Figure C5. Hydrodynamic diameter of WPD _{x10} M, WPD _{x20} M, and WPD _{x30} M as a function of pH and ionic strength; a) 0 M NaCl/ CaCl ₂ , b) 50 mM NaCl and c) 10 mM CaCl ₂	234
Figure C6. SDS-PAGE patterns of a) whey protein nanogel particles (WPN) (Araiza-Calahorra and Sarkar, 2019) and b) non-conjugated microgel particles as a function of <i>in vitro</i> gastric digestion time.	235
Figure C7. Interfacial shear viscosity at <i>n</i> -tetradecane-water interface against time of 0.5 wt% non-conjugated (N-WPD _x M) after 24 h of adsorption. Error bars represent standard deviation.	236
Figure D1. Cytotoxicity of bile salts towards Caco-2 cells following a 2 h incubation in the simulated digestion medium (<i>i.e.</i> simulated gastric and intestinal fluids without emulsion or CUR). Data are mean with SD from three independent experiments performed in duplicate.	237

List of Abbreviations

BSA	Bovine serum albumin
CLSM	Confocal laser scanning microscopy
Cryo-SEM	Cryo scanning electron microscopy
CUR	Curcumin
CUR-DxS- E _{WPN}	Dextran sulphate coated-whey protein nanogel-stabilized Pickering emulsion loaded with curcumin
CUR-E _{WPDxM}	Whey protein-dextran conjugated microgel-stabilized Pickering emulsion loaded with curcumin
CUR-E _{WPN}	Whey protein nanogel-stabilized Pickering emulsion loaded with curcumin
d ₃₂	De Broukere mean
d ₄₃	Sauter mean
DC	Degree of conjugation
DLS	Dynamic light scattering
Dx	Dextran
DxS	Dextran sulphate
DxS-E _{WPN}	Dextran sulphate coated-whey protein nanogel-stabilized Pickering emulsion
E _{WPDxM}	Whey protein-dextran conjugated microgel-stabilized Pickering emulsion
E _{WPN}	Whey protein nanogel-stabilized Pickering emulsion
FFA	Free fatty acids
GI	Gastrointestinal
HPLC	High-performance liquid chromatography
MCT	Medium chain triglyceride
MW	Molecular weight
N-WPDxM	Non-conjugated whey protein-dextran microgel
O/W	Oil-in-water
OPA	o-phthaldialdehyde

pl	Isoelectric point
SGF	Simulated gastric fluid
SIF	Simulated intestinal fluid
WPDxM	Conjugated whey protein-dextran microgel
WPI	Whey protein isolate
WPI-Dx	Whey protein isolate-dextran conjugate
WPN	Whey protein nanogel
α -la	α -lactalbumin
β -lg	β -lactoglobulin

List of Symbols

a	Particle radius
D	Translational diffusion coefficient
d_H	Hydrodynamic diameter
$f(K_a)$	Henry's function
g_f	Geometric factor
k	Electrical double layer thickness
k	Torsion constant
K	Consistency index
K_a	Binding constant
k_B	Boltzmann constant
M	Molar
n	Flow behaviour index
T	Temperature
V	Volume
ΔFI	Change in fluorescence intensity
ΔFI_{max}	Maximal change in fluorescence intensity
ϵ_0	Permittivity of vacuum
ϵ_r	Relative permittivity/dielectric constant
ζ	Zeta-potential
η	Viscosity
η_a	Apparent viscosity
η_i	Interfacial shear viscosity
θ	Equilibrium deflection of the disc in the presence of the film
θ_0	Equilibrium deflection in the absence of the film
σ	Standard deviation
ω	Angular velocity of the dish
$\dot{\gamma}$	Shear rate

Chapter 1

General Introduction

Many industries use emulsion technology to produce a wide variety of foods and beverages. In particular, emulsions form an integral part of the food either as the finished product or as an ingredient. An emulsion consists of a mixture of two immiscible liquids, where one of the liquids is dispersed (*i.e.* continuous phase) in the other (*i.e.* dispersed phase) as small spherical droplets. In the food context, emulsion droplets diameter normally is in the range of 0.1 – 100 μm and consist of oil and water mixed together with a relative balance varying widely depending on the product type (McClements, 2004). Due to the large interfacial area between the finely dispersed phase droplets and the continuous phase, emulsions are thermodynamically unstable systems, which means that they will eventually separate into oil and water phases through a variety of instability mechanisms. To form emulsions that are kinetically stable, emulsifiers such as small-molecular surfactants, phospholipids, proteins, polysaccharides and solid particles are often used.

Depending on their relative spatial distribution of the oil and the aqueous phase, conventional emulsions can be classified into oil-in-water (O/W) emulsion (*i.e.* oil droplets dispersed in an aqueous phase) or water-in-oil (W/O) emulsion (*i.e.* water droplets dispersed in an oil phase). In food products, milk, cream, dressings and mayonnaise are some examples of O/W emulsions, whereas margarine and butter are examples of W/O emulsions. To create emulsions, homogenization is generally carried out using high-energy mechanical devices such as high-speed blenders, high-pressure valve homogenizers, and colloid mills that facilitate droplet break-up to increase the surface area. Formation of emulsions by homogenization is a dynamic process that starts with the violent disruption of droplets, whilst the surface-active molecules rapidly move from the bulk liquid to the interfacial region to provide electrostatic (charged interface) or steric (viscoelastic interface) stabilization against immediate coalescence. In simple terms, it can be considered that conventional emulsions consist of three distinct regions: droplets, the continuous phase, and the interface.

Emulsions as delivery vehicle for either aqueous- or oil-based bioactives (or both) compounds have been widely investigated in the food and pharmaceutical industries as these systems are able to protect and increase the bioavailability and

controlled delivery of bioactive compounds (Appelqvist et al., 2007) which is why they have been investigated as the delivery vehicle in this thesis.

1.1 Overall research aim

Curcumin is a highly potent bioactive compound which is widely acknowledged due to its health benefits. However, poor solubility in aqueous media and metabolic degradation of curcumin during gastrointestinal transit remain as the key factors that limit its bioaccessibility and bioavailability. In addition, its extremely low water solubility (11 ng/ mL) also makes it difficult to incorporate into many food products (Tønnesen et al., 2002). Studies have shown that emulsion-based delivery systems can greatly increase the bioavailability of curcumin as compared to crystalline curcumin dispersed in water (Zheng et al., 2017). To date, nanoemulsions are often cited as the leading emulsion-based delivery vehicles for curcumin and this field has been extensively investigated. Although scarce in literature, recent evidence has shown that curcumin can be protected in an *in vitro* gastrointestinal setting using emulsions stabilized by solid particles rather than surfactants, due to the high desorption energies associated with particles once they adsorb at the O/W interface (Marefati et al., 2017). Thus, there is a knowledge gap in the literature on the design and use of biocompatible Pickering stabilizers to design emulsions encapsulating curcumin and investigate how such emulsions can be beneficial in preventing degradation of curcumin during gastrointestinal transit.

Thesis objective: The overarching goal of this thesis was to design novel Pickering emulsion-based encapsulation strategies to protect encapsulated curcumin during gastrointestinal processing, improve bioaccessibility and eventually deliver them to cells. Different biopolymers and processing techniques were used to design Pickering stabilizers and consequently Pickering emulsions that can be less sensitive to physiological conditions controlling the delivery of curcumin. In this thesis, besides the design of novel Pickering stabilizers *i.e.* whey protein nanogel particles, the innovative aspects involved capitalizing two types of interactions (*i.e.* electrostatic and covalent) of whey protein with polysaccharides (dextran sulphate or dextran) to create complex particulate interfaces.

Thesis hypothesis: The hypothesis was that by creating a complex interfacial layer at the droplet surface, it would be possible to offer a better protection to the oil droplets against gastrointestinal degradation during *in vitro* simulated regime and increase the bioaccessibility of encapsulated curcumin.

1.2 General insights on emulsions

This thesis is focused on targeting intestinal release of the curcumin-containing oil droplets, since it has been reported that most of curcumin gets absorbed in the intestine and the liver (Prasad et al., 2014). The rationale behind the selection of Pickering emulsions used are discussed in the following section.

1.2.1 Pickering emulsions

Solid particles can adsorb at liquid–liquid interfaces to stabilize emulsions and form the so- called “Pickering emulsions” (Figure 1.1). In fact, the concept of Pickering stabilized emulsions has been used for decades in different food products such as homogenized and reconstituted milks, where oil droplets are stabilized by casein micelles, or in margarines and fatty spreads where water is stabilized by triglyceride crystals (Dickinson, 2012). Nevertheless, it is only since the past decade that a ‘neo-Pickering era’ has commenced (Dickinson, 2020), that there has been increasing interests in the stabilization of droplets by solid particles in food, cosmetic and pharmaceutical industries due to their high resistance against droplet coalescence. More importantly, the ‘biocompatible’ character of the Pickering particles that are bio-derived such as those prepared using polysaccharides, starches, organic crystals (e.g. flavonoids) make them even more attractive to several application fields due to growing demands of sustainable Pickering emulsions. The key rationale for using Pickering emulsions in this thesis is that these emulsions not only provide ultrastability against coalescence but also offer in-body stability against desorption mediated by bile salts in the gastrointestinal phase (Sarkar et al., 2019). The latter is of paramount importance to control gastrointestinal digestion kinetics and degree of free fatty acid release and consequently bioaccessibility of bioactive compounds (curcumin in this case), latter has not been fully understood to date.

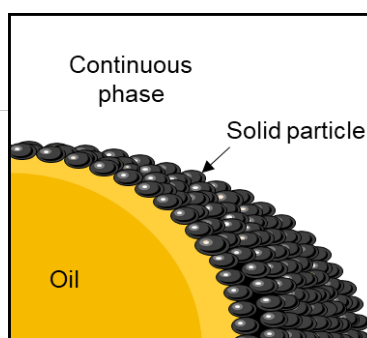


Figure 1.1. Schematic representation of a Pickering emulsion *i.e.* emulsions stabilized by solid particles.

1.3 Rationale behind the selection of biopolymers

Specific biopolymers and techniques were used to design particles and emulsions depending on the physicochemical and protective properties of the biopolymers at specific physiological conditions. In order to understand their structural differences, the following section includes details about the structure of whey protein isolate, their use to design nano-microgel particles, as well as the use of such whey protein nano-micro gel particles as Pickering stabilizers. In addition, structure of dextran and covalent interactions between protein and polysaccharides through Maillard reaction were also included in this section.

1.3.1 Milk Proteins

Milk proteins are very well-characterized in literature and are mainly divided into two groups: caseins and whey proteins. The main whey proteins are β -lactoglobulin (β -lg) and α -lactalbumin (α -la) and represent about 80% and 15% respectively of the mass of industrially purified whey protein isolate (WPI) (de Wit, 1998). β -lg is a globular protein with a secondary structure mainly composed by β -sheets. It contains 162 amino acid and two disulphide bonds and a free thiol group and has a molecular weight of 18.4 kDa. In the case of α -la, it is also globular, but it exhibits a helical secondary structure. It is composed of 123 amino acids with 4 disulphide bonds and has a molecular weight of 14.2 kDa (Nicolai et al., 2011). Both proteins possess a net negative charge at neutral pH and have an isoelectric point (pI) close to pH 5.0. Particularly whey protein has been used as a chief source in this thesis (**Chapters 3 – 4 and 6**) to make the gel particles as Pickering stabilizers because of the unique ability of whey protein to form thermo-set gel by virtue of free thiol groups to allow disulphide crosslinking.

1.3.1.1 Whey protein isolate for designing nanogel and microgel particles

Besides the various polymers available for the production of temperature responsive microgels, food-grade proteins such as milk proteins or egg albumin have attracted significant attention since they offer the potential of creating heat-set gel structures with well-defined properties for food and biomedical applications (Nicolai, 2016). Whey protein was used to design thermally cross-linked whey protein gels, which were then sheared into nanometric size *i.e.* < 100 nm (novel nanogels) to stabilize oil-in-water Pickering emulsions as a delivery vehicle for curcumin (**Chapter 3**). Also, they were used as primary building blocks for the layer-by-layer deposition design of polymer-coated Pickering emulsions (**Chapter 5**), for protein-polysaccharide-Maillard conjugated Pickering emulsions (**Chapter 6**), and for lipolysis and cellular uptake assessed in **Chapter 7**.

When aqueous dispersions of WPI are heated above 65 °C, protein gelation occurs due to heat-induced aggregation. For example, at neutral pH, heat treatment causes unfolding of the tertiary structures as well as some secondary structures of the otherwise folded β -lg molecule. The unfolding of the globular structure causes the exposure of the free sulfhydryl group and the inner hydrophobic amino acids. Initially hydrophobic interactions followed by formation of intramolecular sulfhydryl/disulphide- leads to protein aggregation and dimer formation. Further sulfhydryl-catalysed disulphide-bond interchange between the dimers create larger species, some of which are also associated with non-covalent interactions (Croguennec et al., 2004, Nicolai et al., 2011).

Depending on the pH, ionic strength, protein concentration and heating conditions, different morphologies of the aggregates can be obtained. For example, long fibrillar aggregates can be obtained at low pH (<2.0) and low ionic strength, whereas particulated aggregates can be formed at high protein concentrations when the pH of the system is around the *pI* (pH 5.7 - 5.9), which can be broken down into microgels or nanogels by controlled shearing process, latter is used in this thesis in **Chapter 3**.

1.3.1.2 Stabilization of emulsions by whey protein-based gel particles

Very stable oil-in-water Pickering emulsions can be formed using WPI-based microgels when the pH is away from the *pI* and the ionic strength is low (Destribats et al., 2014). Interestingly, these emulsions demonstrated high stability against coalescence even with a partially covered droplet surface due to bridging of the interfaces of neighbouring drops by the particles leading to flocculation of the droplets. Shelf-stable Pickering high internal phase emulsions (HIPE) have been also studied using whey protein microgel particles (Zamani et al., 2018). In this study, it was observed that substantially greater shelf and thermal stabilities over HIPE prepared using whey protein microgels was achieved compared to either Tween 20 or WPI as surfactants. In a gastrointestinal regime, it has been shown that in the presence of pure lipase and bile salts, gastrointestinal-stable Pickering emulsions can be produced when using heat-induced whey protein microgel particles to stabilize oil–water interfaces (Sarkar et al., 2016a). The gastrointestinal-stable character of the system arises possibly from the very strong binding of the particles to the interface, which makes them hard to be displaced by the bile salts, meaning that large portion of the surface is not available for the adsorption of the lipase/colipase complex. Although whey protein-based microgels have been well-reported in literature, nanometric sized gel particles *i.e.* ‘nanogel’ have never been reported in literature. Such nanogels can be useful to design smaller emulsion droplets as compared to those coated by

microgel particles as it is known that the size of droplets is generally 50-100 times larger than the size of the Pickering particles stabilizing the droplets. Hence, in this thesis whey protein nanogel was designed and used for the first time (**Chapters 3 – 4 and 6**) to create smaller-sized Pickering emulsion droplets, which will have eventually impact on degree and kinetics of lipolysis and bioaccessibility of the encapsulated curcumin.

1.3.2 Polysaccharides

Polysaccharides are widely used as thickeners, binders, and stabilizing agents. They are classified according to their amount of carbon-chain length or by their functional groups, which determines the type of reactions they will present such as esterification, amination, reduction, or oxidation (Pilnik and Rombouts, 1985). The chemical structure of polysaccharides can be as diverse as their origin, but in general they have a large number of highly hydrophilic hydroxyl groups, which have the ability to hydrate and form hydrogen bonds.

In this thesis, negatively charged dextran sulphate (**Chapters 5**) and neutral dextran (**Chapters 6**) were used for electrostatic and covalent interactions with the protein, respectively. Dextran is mainly composed of a linear chain of glucose residues linked by bonds α -(1,6), with some ramifications α -(1-3) (Figure 1.2). They are structurally diverse but are characterized according to the percentage, nature and distribution of their bonds.

Dextrans are usually produced by the lactic acid bacteria of the *Leuconostoc spp.* species in sucrose-rich cell cultures. When bacteria cells are growing, they secrete an extracellular enzyme that converts the excess sucrose into dextran, releasing fructose into the medium (Santos et al., 2000). Currently, dextran is the most important commercially available polysaccharide produced by bacteria strains and through this method it is possible to obtain dextran of a wide range of molecular weights from 5 to 500,000 Da (Sun and Mao, 2012).

Dextran has been used for conjugation with proteins in **Chapter 6**, since they are reductive in nature and possess a neutral charge, which inhibits the formation of electrostatic complexes. When in aqueous solution, dextrans are very flexible molecules and are unable to form gel-like structures, which is ideal for protein gelation studies as required in this thesis, where protein gelation is a key step for designing the microgel particles (Sun et al., 2011). Dextran sulphate is the polyanionic form produced by sulphation of dextran, which allows electrostatic interaction with protein

microgels particularly at gastric pH, where the proteinaceous species are positively charged and hence the sulphated form is used in **Chapter 5**.

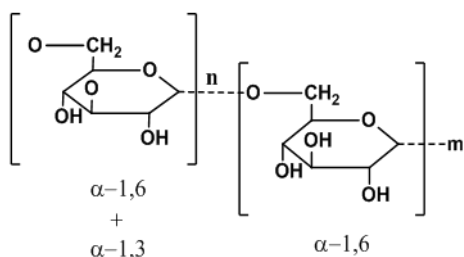


Figure 1.2. Molecular structure of dextran.

1.3.3 Maillard Reaction

Functional properties of proteins are often modified using interaction with polysaccharides (Jiménez-Castaño et al., 2007). Protein-polysaccharide interactions can be achieved *via* non-covalent (hydrogen bonding, hydrophobic interactions, etc.) or covalent bondings. The most common covalent bonds are disulphide bridges between cysteine residues which can be appreciated in protein gelation as mentioned previously. Nevertheless, covalent bonds between proteins and sugars or polysaccharides with reducing sugar ends can also be introduced *via* Maillard reaction (Oakenfull et al., 1997).

The Maillard reaction (MR) is the covalent attachment between the amino groups of proteins (especially ϵ -amino group of lysine residues) and the terminal reducing group of the carbonyl of polysaccharides through a non-enzymatic browning reaction, or glycosylation reaction as shown in Figure 1.3. This covalent bonding between a protein and a polysaccharide is also known as protein-polysaccharide conjugate. The glycosylation (or conjugation) of proteins with polysaccharides, *via* the MR, has been extensively studied to improve the functional properties of food proteins such as emulsifying capacity, ionic strength, pH and thermal stability and improved solubility (Qi et al., 2009; Mu et al., 2018; Álvarez et al., 2012; Kasran et al., 2013). The application of these conjugates is oriented to food and other fields, since the reaction generally does not require any chemical catalyst or enzymes and under well controlled conditions it is possible to arrive at the desired products of the Maillard reaction (Oliver et al., 2006). In this thesis, Maillard reaction was used in **Chapter 6** to design whey protein + dextran Maillard conjugates, which were eventually used to design Pickering gel particles also termed as 'conjugate gel particle'. The main purpose of designing this gel particles *via* Maillard conjugation was to protect the emulsions from gastric destabilization by improving the resilience of the proteinaceous part of the interface

from pepsinolysis. To our knowledge, this is the first study that uses protein+polysaccharide Maillard conjugates for making conjugate microgels for preparing Pickering emulsions and using them for delivery of curcumin.

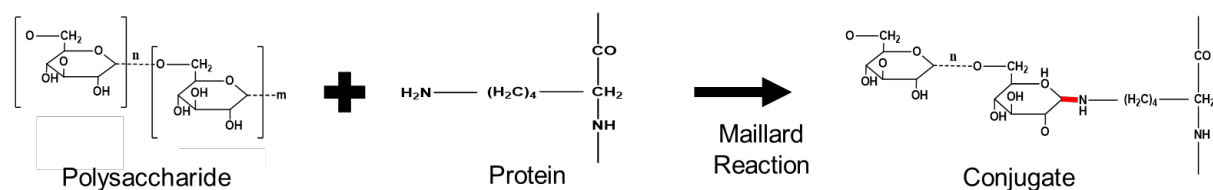


Figure 1.3. Schematic representation of protein-polysaccharide conjugation *via* Maillard reaction adapted from de Oliveira et al., (2016).

1.4 Rationale behind the selection of characterization techniques

To understand the different microstructures and the physicochemical characteristics of the particles and emulsions developed, several analytical instruments were employed. The theoretical and technical properties of the main characterization tools employed during this PhD are discussed below.

1.4.1. Dynamic light scattering (DLS)

To characterise the particle size of the whey protein isolate-based nanogel (**Chapters 3 and 4**) and whey protein isolate-dextran conjugate microgel particles (**Chapter 5**), dynamic light scattering (DLS) was employed. DLS is used for characterizing the size distribution of particles suspended in a solvent (usually water). The size range for the DLS technique ranges from 1 nm to 1 μ m. DLS-based sizing instruments have been used extensively to characterize a wide range of particulate systems, including small emulsion droplets, protein aggregates, surfactant micelles, and other nanoparticles.

DLS is based on the analysis of the interaction between a laser beam and a particle, which scatters light in all directions (Figure 1.4). In dispersions, particles are not stationary; they diffuse in a random way due to the Brownian motion (caused by collisions of neighbouring solvent molecules). DLS relies on the measurements of the scattered waves arriving at the detector that fluctuate randomly in time, due to fluctuations in the positions of the particles that scatter those waves. The connection between random fluctuations and particle sizing is perhaps more easily understood by considering that smaller particles will have a faster Brownian motion than larger ones. In other words, small particles will create rapid fluctuations of the intensity signal, whereas larger particles will diffuse more slowly resulting in a slow varying intensity

(Dalglish and Hallett, 1995). The hydrodynamic diameter (d_H) derived from the DLS refers to the diameter of an equivalent hard sphere that diffuses at the same rate as the analysed particle. In a dilute solution, where only single-scattering events occur, the Stokes-Einstein equation, which defines the velocity of the Brownian motion as the translational diffusion coefficient (D), will be ultimately employed to calculate the hydrodynamic diameter, d_H (equation 1.1):

$$d_H = \frac{k_B T}{3\pi\eta D} \quad (1.1)$$

where k_B is the Boltzmann constant, T is the temperature in Kelvin, η is the zero-shear viscosity of the medium and D is the translational diffusion coefficient. Thus, it is important to input the correct temperature and viscosity values of the dispersant (buffer at relevant pH in this thesis) used at the specific measurement temperature.

Analysis of the autocorrelation function will yield estimates of the true particle size distribution and the z-average value can be obtained as the intensity-weighted mean hydrodynamic diameter of the particle. A second important parameter that can be derived from DLS measurement is the polydispersity index, which is a measure of the width of the particle size distribution. Polydispersity indices less than 0.1 are typically referred to as "monodisperse". The equation 1.2 for polydispersity is shown below:

$$PdI = \left(\frac{\sigma}{d_H}\right)^2 \quad (1.2)$$

where, σ refers to the standard deviation and d_H is the mean diameter.

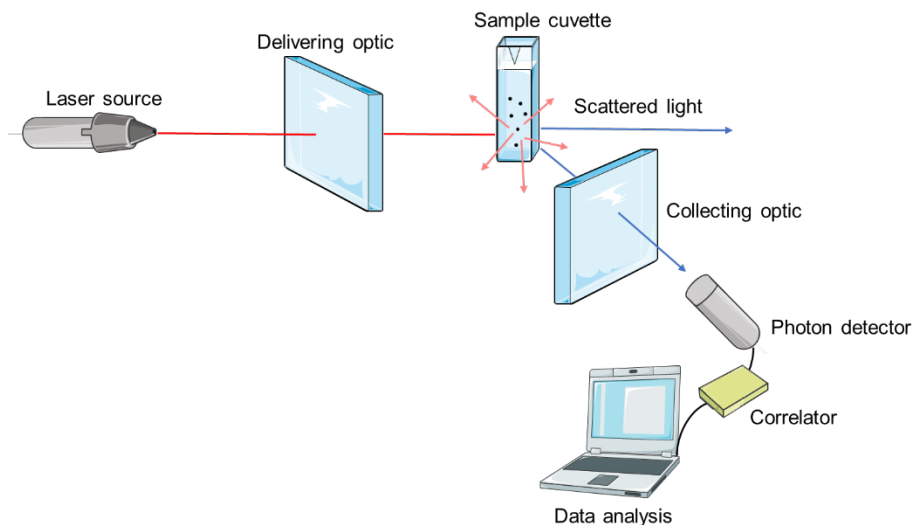


Figure 1.4. Schematic representation of dynamic light scattering measuring principle.

1.4.2 ζ -potential

The electrical characteristics of the different particles and emulsions was analysed in this thesis in terms of zeta (ζ) potential when they were initially prepared, as well as during gastrointestinal *in vitro* conditions (**Chapters 3 – 6**). The electrical characteristics are important parameter that gives an indication about electrostatic stability and physicochemical properties of an emulsion. The sign and magnitude of the ζ -potential on emulsion droplets will dictate the electrostatic interactions between emulsion droplets, their response to changes in pH and ionic strength, as well as the tendency for various types of electrically charged compounds such as biopolymers, antioxidants, pro-oxidants, and flavours to accumulate at the droplet surfaces (McClements, 2004).

The electrical properties of interfaces arise from the surface charge due to the ionization of the functional groups in the biopolymers and the concentration and types of ions in the solution. For example, ions of opposite charge to the surface (*i.e.* counter ions) will be attracted toward a charged surface, whereas ions of similar charge (*i.e.* co-ions) will be repelled from it. For convenience, the distribution of counterions near a highly charged surface is divided into two regimes: an inner region and an outer region (Figure 1.5).

In the inner region (also referred to as “Stern layer”), the counter-ions are strongly attracted to the charged droplet or particle surface and therefore, the counter-ions are relatively immobile. Further away from the particle, in the outer region (also referred to as the “diffuse region”), the counter-ions are more loosely associated. These two layers are collectively referred to as the electrical “double layer”, and the boundary between the inner and outer regions is referred to as the “Stern plane” (Figure 1.5). When a particle moves (*e.g.* due to gravity or Brownian motion), a distinction is created between the ions on the “diffuse layer” that move with the particle, and the ions in the bulk dispersant. The electrostatic potential at this boundary or “slipping plane” is referred to as the zeta (ζ)-potential (Hunter, 2013). However, since ζ -potential cannot be directly measured, it is deduced from the measurement of the electrophoretic mobility (μ_e) under an applied electric field (*i.e.* electrophoresis). Electrophoretic mobility is defined as the velocity of a particle (V_p) in a unit electric (E) ($\mu_e = V_p / E$). From the obtained μ_e , the ζ -potential can be calculated using the Henry’s equation (1.3):

$$\mu_e = \frac{2\varepsilon_r\varepsilon_0\zeta f(ka)}{3\eta} \quad (1.3)$$

where ϵ_r is the relative permittivity/dielectric constant, ϵ_0 is the permittivity of vacuum, ζ is the ζ -potential, $f(K_a)$ the Henry's function which refers to the ratio of the particle radius (a) to the electrical "double layer" thickness (k) and η the viscosity of the medium at experimental temperature in this case water at 20 °C ($\eta = 8.9 \cdot 10^{-4}$ Pa s).

The main assumption for the validity of the aforementioned equation is that the thickness of the electric double layer has to be much smaller compared to the particle radius (*i.e.* big particles up to 1 μm) when particles are suspended in aqueous solutions of high salt concentration (10–2 M). When this assumption is met, the value of $f(K_a)$ is taken as 1.5 and the Henry's equation then modifies into the Helmholtz-Smoluchowski equation (1.4):

$$\mu_e = \frac{\epsilon_r \epsilon_0 \zeta}{\eta} \quad (1.4)$$

On the contrary, if the thickness of the electric "double layer" is larger than the particle itself due to small particles (≤ 100 nm) dispersed in low salt concentration (10–5 M) the value of $f(K_a)$ is taken as 1 and the Henry's equation can be modified as the Hückel equation (1.5):

$$\mu_e = \frac{2\epsilon_r \epsilon_0 \zeta}{3\eta} \quad (1.5)$$

The general dividing line between stable and unstable emulsions can be taken at either +30 or -30 mV. Thus, emulsion or particles with a ζ -potential higher than +30 mV or more negative than -30 mV are normally considered stable (McClements, 2004).

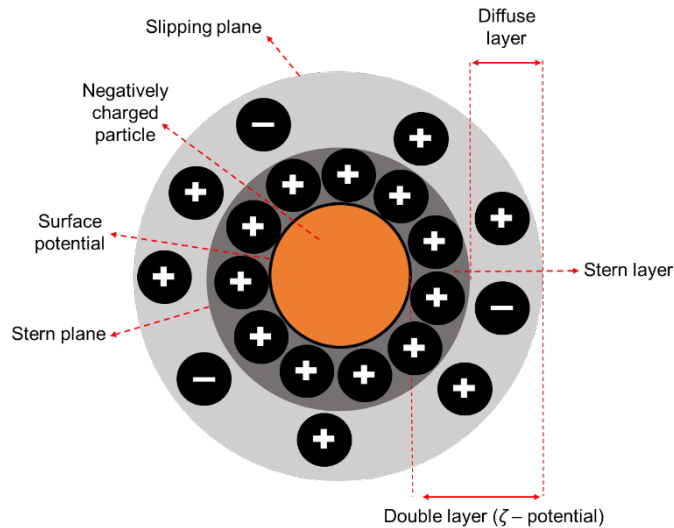


Figure 1.5. Schematic representation of zeta potential adapted from Malvern Instruments (2015).

1.4.3 Microscopy across scales (confocal laser scanning microscopy to scanning and transmission electron microscopy)

Since components of emulsions are in the micron (for droplets) and submicron (for Pickering particles) scales, microscopy across length scales has been used in this thesis (**Chapters 3 – 6**) to study the particles and the Pickering emulsions with or without loading with curcumin. The microscopy techniques include confocal laser scanning microscopy (CLSM), transmission electron microscopy (TEM) and cryo-scanning electron microscopy (cryo-SEM).

As optical light microscopy provides a limited resolution ($>0.2 \mu\text{m}$), high-resolution images of the microstructure of emulsions can be obtained using confocal laser scanning microscopy (CLSM). CLSM is a very useful optical tool for examining shear and/ or compression-sensitive samples such as emulsions. The confocal microscope is based on the principle that the image of a light source is focused on a well-defined depth in the specimen. The information from this focal point is then projected onto a pinhole in front of a detector, which is located in the same focal plane of the imaging lens as the light source (Auty, 2013). Incident light is absorbed by a fluorophore within the sample and emitted at a longer wavelength, which is deflected onto a photon detector. The intensity of the signal received in the photon detector is then amplified and converted into pixels. The main advantage of using CLSM for food research is that it is possible to produce optical sections through a three-dimensional (3-D) specimen.

To visualise the structures in the CLSM specific fluorescent dyes are used since most food ingredients are not naturally auto fluorescent. Labelling with fluorescent probes generally relies in passive diffusion of the dye molecules to the site of interest, thereby emulsion disturbance is minimum. In the case of the emulsions in this thesis, it is relatively straightforward to stain and visualise the distribution of fat and protein. In this thesis, Nile Red, an oxazone derivative of Nile Blue, was used to stain the oil phase via hydrophobic interactions, whereas protein gel particles were stained using Fast Green FCF *via* hydrogen bonding, and the polysaccharide dextran was stained using fluorescein isothiocyanate (FITC) (de Belder and Granath, 1973; Auty, 2013).

Besides imaging of samples, CLSM was also used to do cross-correlation image analysis in **Chapter 5** to derive quantitative information about digestion of emulsions. The method of cross-correlation analysis was used to calculate the typical distance between a fat droplet interface to a maximum local distribution of protein around the fat droplet by giving each pixel in the emulsion image a polar co-ordinate. The image was split into radial segments and for every radial segment, the intensity of the fat and protein was radially averaged using MATLAB. The cross-correlation intensity was integrated for every radial segment and the integrated values were scaled to the radius of the droplet in the selected region. Through this method it was possible to quantify the amount of proteinaceous microgel particles located at the droplet interface before and after *in vitro* gastric digestion and evaluate the degree of pepsin-induced hydrolysis.

To evaluate the ultrastructure of the emulsions, cryo-scanning electron microscopy (cryo-SEM) was used. SEM constructs an image by detecting reflected electrons. When a beam of highly accelerated electrons, which carry a significant kinetic energy, are focused on the surface of a material, interaction with the sample decelerate the incident electrons in the solid sample dissipating the energy as a variety of signals (*i.e.* scattering energy). These signals include secondary electrons and backscattered electrons (among others) that produce SEM images. The use of the accelerated electrons beam in SEM featured by short wavelength causes the diffraction effects to occur at much smaller physical dimension, which in turn helps resolve atomic features ranging from nanometre to micrometre particle size (Cosgrove, 2010). Particularly, cryo-scanning electron microscopy (cryo-SEM) technique can be a useful technique to characterise micrometre size emulsions since it enables the sample to remain in a frozen-hydrated state under high vacuum conditions. The freezing step allows the preservation of the original structure and the technique is relatively fast and requiring few preparation steps. Preparation for cryo-SEM typically consists of rapidly freezing the sample and transferring it under vacuum conditions to a preparations chamber. The sample is then fractured, sublimated

('etched') and coated with a conductive metal by sputtering to be imaged under SEM (JEOL Ltd, 2011).

For cryo-SEM imaging in this thesis, heptane was preferred as the dispersed phase over the medium chain triglyceride (MCT) used for emulsion preparation, to avoid oil crystallization during the freezing step as heptane solidification allows the droplets to remain spherical with a smooth interface. In addition, because of the cryo-SEM conditions used, heptane allowed a slight sublimation of the sample to discern the nano and microgel particles at the interface before inserting the sample in the observation chamber (Destribats et al., 2014). Both systems (heptane or MCT emulsions) were shown to display the same overall macroscopic and microscopic characteristics, which means that the acquired cryo-SEM images for heptane emulsions can be extrapolated to MCT systems.

In addition, to characterize samples with length scales $< 0.2 \mu\text{m}$ such as the Pickering particles designed in this thesis, transmission electron microscopy (TEM) was also used. TEM can be considered an inverted light microscope in which the sample is illuminated by an electron beam. The contrast is acquired by either absorption or scattering of the electrons by the material, while the rest is transmitted. The amount of electrons transmitted by a material will depend on its electron density, so if the material possess a low electron density a higher fraction of the electrons will be transmitted, and the image will appear darker. In food systems, the differences in electron densities in food components is intrinsically small so it is necessary to increase the density contrast between components by selective staining with higher electron density materials such as heavy metal salts like lead, tungsten, or uranium, latter being used in this thesis (Kuntsche et al., 2011). Due to its speed and simplicity, negative staining (stained with uranyl acetate) was used in this thesis as the preparation method for the evaluation of the particles. In negative staining, the metal salts will bind to the surrounding material and the material will be seen against a dark background. However, when staining samples using negative staining process, it is important to consider that structural alterations of the colloids may occur due to the staining and drying steps involved in the process.

1.4.4 Static light scattering (SLS)

The Pickering emulsions designed in **Chapters 3 – 6** were characterized in terms of their size using static light scattering (SLS). SLS is another optical technique used to measure the size distribution of droplets dispersed in a medium in the order of 100 nm -1000 μm size range. SLS was used to measure the droplet size distribution of the emulsions before and after gastrointestinal digestion. SLS uses typically a He-Ne or

Ar, where the laser is focused on an optically clear cylindrical cell containing the sample. Most of the light passes directly through the sample but a small portion of the light is scattered. This scattered light intensity is detected at an angle, typically from about 15 – 180° from the incident beam by a photomultiplier or photodiode. The angle and intensity of the scattered light detected by the photodiode is then input into an algorithm that uses the “Mie theory”, which converts the intensity of scattered light into particle size distribution data. The “Mie theory” makes certain assumptions such as that the particle is spherical and dispersed in an homogeneous solution, and that the refractive index of the particle and the dispersed medium is known.

The most common approach for expressing SLS results is to report the d_{43} (De Brouckere mean diameter) and d_{32} (Sauter mean diameter) values based on a volume and surface area distribution (equations 1.6 and 1.7), respectively. The d_{32} is most sensitive to the presence of fine particulates, whereas the d_{43} is most sensitive to the presence of large particulates in the size distribution and thus more relevant when measuring gastrointestinal structuring of emulsion droplets.

$$d_{43} = \frac{\sum_1^n d_i^4 V_i}{\sum_1^n d_i^3 V_i} \quad (1.6)$$

$$d_{32} = \frac{\sum_1^n d_i^3 V_i}{\sum_1^n d_i^2 V_i} \quad (1.7)$$

where d is the diameter and V the volume of the i^{th} particle.

1.4.5 Interfacial shear rheology

Interfacial rheology has been defined as “the study of the mechanical and flow properties of adsorbed films at fluid interfaces” (Murray and Dickinson, 1996). In this thesis, the interfacial rheology of particles adsorbed at oil-in-water interfaces has been of interest (see **Chapters 3** and **5**) because the structural and mechanical properties of particulate layers designed in these studies (nanogels and conjugate microgels) can be an important parameter to indirectly determine the stability of an emulsion (Murray et al., 1995).

When an emulsion is formed, there are two types of disturbances that are created at the interface due to possibly strong and turbulent hydrodynamic flow field (Murray and Dickinson, 1996). The “interfacial dilatational” disturbance refers to the disturbance of the fluid interface that causes a change in the area, but the shape

remains the same. “Interfacial shear” disturbances are those where there is distortion of the shape when different stresses are applied (McClements, 2004). The way interfacial rheology is related to emulsion stability relies on the principle that coalescence occurs when disturbances grow causing bridging between two droplets. Disturbances are created when the thickness of the interface becomes too thin that it breaks. The rate of growth and propagation of these disturbances is related to the interfacial rheology because the flow of the liquid in the film becomes coupled to the flow of elements in the interface (Murray and Dickinson, 1996).

Interfacial shear rheology (η_i) is particularly useful for providing information about adsorption kinetics, competitive adsorption, and the structure and intermolecular interactions of the molecules at the interface in both air–water and the oil–water interfaces (Bos and van Vliet, 2001). For low molecular weight surfactants, the interfacial shear viscosity is usually several orders of magnitude less than that of the biopolymer layers. This is because biopolymers interact laterally with each other through various forces such as hydrogen bonding, hydrophobic and covalent bonding, and electrostatic interactions. In addition, these interactions between adsorbed protein molecules may vary strongly depending on the protein structure in the adsorbed state. For example, the surface shear rheology of adsorbed caseins are approximately two orders of magnitude lower than those of the globular whey proteins. This has been attributed to greater internal cohesion owed by the lower deformability of the whey proteins or to stronger intermolecular physical and covalent bonds as compared to a more flexible structure from the casein (Castle et al., 1987). Due to their sensitivity to interactions between the adsorbed protein molecules and the possible conformational changes involved, interfacial shear rheological parameters change as function of the ageing time of the adsorbed layer (Roth et al., 2000). Hence, in this thesis the interfacial rheology is characterized over a period of 2 to 24 hours.

The characterization of the shear rheology of surfaces and interfaces can be done through a variety of experimental methods. In this thesis, we use a two-dimensional Couette-type viscometer (Figure 1.6) since this system can be easily aligned in order to ensure reproducible measuring conditions. The method has been fully described elsewhere but a short description is introduced here (Murray and Dickinson, 1996; Jourdain et al., 2009; Erni et al., 2003). Briefly, a disk suspended by a torsion wire is located in the interfacial region between oil and water. The cup is rotated at a controlled torque or rotational speed, while the disk remains stationary. A laser beam is reflected from a mirror attached to the spindle of the disk onto a scale, and the angular deflection is measured. Surface shear rheology measurements is sensitive to variables such as emulsifier concentration, temperature and ionic strength (McClements, 2004).

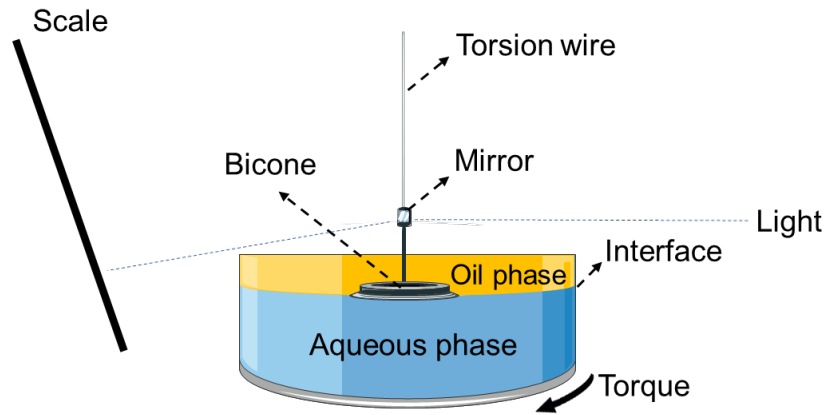


Figure 1.6. Schematic diagram of interfacial shear rheometer based on bicone method.

1.4.6 *In vitro* gastrointestinal processing

To study the gastrointestinal behaviour of the particles (nanogels or microgels) in aqueous dispersions and the emulsions, an *in vitro* gastrointestinal method was used. *In vitro* methods are particularly useful because they mimic the physiological conditions *in vivo* (e.g. pH, enzymes concentrations, ions etc.) in a fast, non-expensive, less labour-intensive way without the need of any ethical approval. In addition, it is easy to sample at the site of interest and allows measurement of multiple samples. They normally include oral, gastric and small intestinal phases.

Contrary to “semi-dynamic” or “dynamic” digestion models, which try to mimic the gentle mixing by controlling the shear and turbulent flow and the calorie-dependent gastric processing and emptying from the stomach, “static” models reproduce environments where constant ratios of meal to enzymes, salt, bile acids etc. at each step of digestion are produced (Alegría et al., 2015). Therefore, static models can be effectively used as preliminary trials for digestion studies of model food systems to produce evidence on the influence of digestion of different structures, composition and processing conditions. These models can be further use to produce bioaccessible micellar fractions to address further mechanistic questions such as intestinal transport by employing Caco-2 cells. However, some of the limitations of static models is that they lack the feedback mechanisms, complex peristaltic movements, gastric emptying or continuous changes in pH and secretion flow rates that are involved at physiological conditions. This means that the uptake, absorption, transport kinetics of curcumin or competition with other food components at the site of absorption as occurs *in vivo* cannot be assessed using this technique (Alegría et al., 2015).

As the main question in this thesis was to investigate the protection and breakdown mechanisms of the O/W emulsions during gastrointestinal digestion and to evaluate the microstructure at the end of digestion, a “static” *in vitro* model was considered sufficient and provided reasonable information to address the research question. For this, we have used the static harmonized INFOGEST model (Minekus et al., 2014) in **Chapters 4 – 6**.

Briefly, the process of digestion begins in the mouth, then the esophagus, stomach and the small and large intestines. Since, there is no starch used in this thesis, the oral digestion step was removed from the scope of this thesis. In the stomach, the parietal cells secrete HCl and pepsinogen, an active precursor that is converted into the proteolytic enzyme pepsin upon contact with acid (Bornhorst and Singh, 2014). The acidic conditions in the stomach are achieved when the gastrointestinal tract senses the food bolus releasing three main stimulants of the proton pump in parietal cells: gastrin, histamine, and acetylcholine (Schubert and Makhlof, 1992). Pepsin is activated when the pH of the stomach is between 1.5 and 2, a pH where active pepsin can digest proteins by hydrolysing peptide bonds of non-terminal amino-acid, preferentially peptide bonds between hydrophobic and aromatic amino acids such as phenylalanine, tryptophan and tyrosine (Powers et al., 1977). Pepsin digestion is investigated in **Chapters 4 – 6** as this is considered to be one of the main factor contributing to the degradation the proteinaceous particles and modification was therefore employed to improve the gastric resistance of the microgel particles to pepsin. Finally, physical breakdown of food in the stomach is caused by antral contraction waves or peristaltic contractions of the stomach wall that crush and grind food particles until they pass through the pyloric sphincter into the small intestine.

Once in the small intestine, the chyme is broken down into molecules small enough to be absorbed through the epithelial cells and carried into the bloodstream. The small intestine is divided into three sections: duodenum, jejunum and ileum. In the duodenum, bicarbonate is secreted to neutralize the gastric acid and provide an appropriate pH for enzymatic digestion. In this section, the secretions of bile and enzymes from the liver and pancreas are received. In the jejunum it occurs the majority of nutrient absorption, whereas in the ileum nutrient absorption is completed being the only location where vitamin B12 and bile salts can be absorbed (Bornhorst and Singh, 2014). Nutrient absorption from the chyme is aided by segmentation and peristaltic muscle contractions allowing a large amount of the chyme material to get in contact with the intestinal walls.

Pancreatic lipase is the most important of the intestinal lipases. The enzyme is activated when it encounters lipids, which initiates hydrolysis of triacylglycerols and

diacylglycerols by attacking triacylglycerol acyl groups which are on the 1(3)-positions of glycerols (*i.e.* terminal fatty acid groups of triacylglycerols) and it is a bile-dependent enzyme. Bile salts are highly surface-active species that generally displace initial interfacial materials from the droplets to promote lipid digestion (Sarkar et al., 2010; Sarkar et al., 2016b; Macierzanka et al., 2019). Hence, investigating whether the newly created particles (nanogels and microgels) in this thesis were also resilient to competitive desorption by bile salts and altered lipid digestion kinetics when used in Pickering emulsions was of interest in **Chapter 6**. The pancreatic lipase has a pH optimum of about 8.5 and is irreversibly inactivated below pH 4.0 (Holt, 1972; Bauer et al., 2005). The hydrolysis of lipids and of proteins is considered almost complete at the end of the small intestine.

1.4.6 Assessment of gastric digestibility of the proteinaceous particles

Sodium dodecyl sulphate polyacrylamide gel electrophoresis (SDS-PAGE) was used to assess the extent of protein hydrolysis of the particles during and after *in vitro* gastric digestion stage (**Chapters 4 – 5**). The use of SDS-PAGE allows the separation of proteins based on their molecular weight.

SDS-PAGE is based upon the principle that a charged molecule will migrate towards an electrode of the opposite charge when an electric field is applied. In the case of proteins, samples need to be treated so that they acquire a uniform negative charge and the electrophoretic mobility depends only on the molecular size rather than the charge. For this, proteins are denatured using sodium dodecyl sulphate (SDS), which is a detergent that binds to the protein backbone. In the presence of SDS and a reducing agent (*e.g.* mercaptoethanol or dithiothreitol), disulphide bonds are cleaved causing protein unfolding into linear chains and giving them a negative charge proportional to the peptide chain length. Negatively charged proteins are then loaded onto a polymerized acrylamide (polyacrylamide) gel that acts as a molecular sieve and aids in the separations of the proteins depending on their molecular size (Figure 1.7). After loading, an electric field is applied, and the protein gel particles migrate towards the positively charged electrode (anode). After staining the gel with a protein-specific technique (*e.g.* Coomassie Blue), it is possible to calculate the size of the protein by comparing its migration pattern with that of a known molecular weight marker (or ladder) using a densitometry equipment.

Under the conditions described in this thesis, SDS-PAGE allowed the visualisation and quantification of protein gel particle fractions with a molecular weight ≥ 14 kDa. Since it was not possible to detect smaller peptides, application of the

technique was limited to those proteins within the gel particles that were not hydrolysed in a great extent.

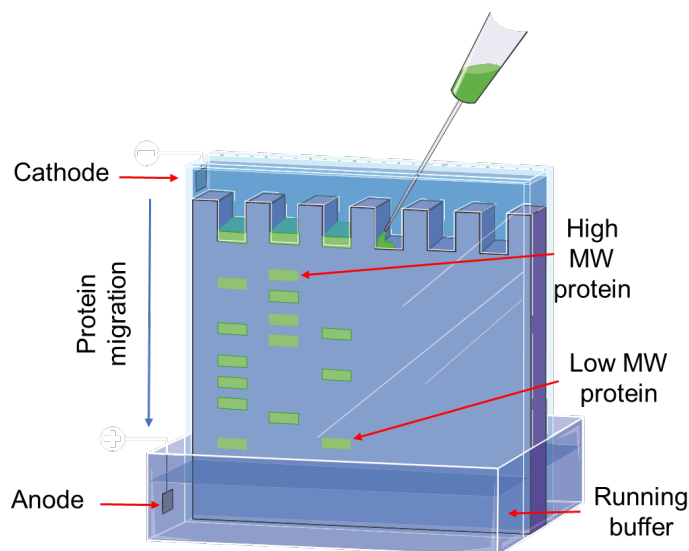


Figure 1.7. Schematic representation of sodium dodecyl sulfate-polyacrylamide gel electrophoresis (SDS-PAGE) (MW: molecular weight), figure from Creative Commons Servier Medical Art by Servier, unported license.

1.4.7 Free fatty acid release

To analyse the free fatty acid released in the intestinal phase, pH-stat titration method is a classical approach that is used to monitor the intestinal phase of *in vitro* digestions systems. The pH-stat method was used to monitor the rate of lipid hydrolysis of the emulsions during the *in vitro* intestinal stage in presence of simulated intestinal fluid containing bile salts and pancreatin (**Chapter 6**).

After addition of lipase at pH values close to neutral, lipid hydrolysis leads to the generation of two free fatty acids (FFAs) and one monoacylglycerol (MAG) per triacylglycerols (TAG) molecule. By maintaining the pH at the initial pre-set value (*e.g.* pH 7.0), the volume of sodium hydroxide (NaOH) titrated into the digestion cell to neutralize any FFA produced by lipid digestion can be recorded versus time using a pH-stat instrument (Li et al., 2011; Li and McClements, 2010).

The percentage of FFAs released can be then calculated based on the assumption that two moles of NaOH are required to neutralize one mole of digested triglyceride. However, if all the FFA released are not readily ionized, which depends on the pH and the *pK* of the fatty acids, this assumption is not applicable (Mat et al., 2016).

1.4.8 Cell viability and cellular uptake

In this thesis in **Chapter 6**, neutral red cell cytotoxicity assay was carried out to detect cell viability after exposure to micellar phase of emulsions containing curcumin after the *in vitro* gastrointestinal digestion.

The principle of this assay is based on the detection of viable cells *via* the uptake of the dye neutral red, a eurhodin dye that stains lysosomes in live cells. Neutral red is taken up by viable cells *via* non-ionic diffusion and is accumulated into their lysosomes. Damaged or dead cells cannot take up the chromophore, which is then removed after washing. Viable cells can release the incorporated dye under acidified extraction conditions and the amount of released dye can be used to quantitatively determine the total number of viable cells measuring the absorbance at 540 nm (Repetto et al., 2008).

1.4.9 High Performance Liquid Chromatography (HPLC)

High Performance Liquid Chromatography (HPLC) was used to quantify curcumin in this thesis. Liquid chromatography has been extensively used for curcumin quantification in biological samples since is a method that presents adequate selectivity, sensitivity, precision and accuracy for curcumin detection and is easy and fast to perform (Ireson et al., 2001; Pak et al., 2003; Heath et al., 2003; Ma et al., 2007). Liquid chromatographic methods for curcumin separation involve the sample to be dispersed in a solvent (*i.e.* mobile phase) and forced under high-pressure conditions through a column with chromatographic packing material (*i.e.* stationary phase). When curcumin passes through the column, it interacts between the two phases at different rate, primarily due to the different polarities of the molecule.

Compounds that have the least amount of interaction with the stationary phase or the most amount of interaction with the mobile phase will exit the column faster. The time taken for a particular compound to travel through the column to the detector is known as its “retention time”, and it will vary depending on the interaction between the stationary phase, the compounds being analysed, and the solvent, or solvents used.

Hence, quantification of curcumin before and after (bioaccessible curcumin) the *in vitro* gastrointestinal stage and the curcumin that is taken up by the Caco-2 cells in **Chapter 6** was performed using HPLC.

1.5 Outline of the thesis

This thesis starts with a literature review on the application of different oil-in-water emulsion-based approaches that have been specifically used to deliver curcumin. It continues with the design and characterization of Pickering particles and corresponding emulsions encapsulating curcumin, the measurement of *in vitro* gastrointestinal stability, release, bioaccessibility and cellular uptake of the encapsulated curcumin. The outline of this thesis is highlighted in Figure 1.8 and follows four main lines of investigation.

Chapter 2 includes a literature review to understand the key factors that influence curcumin delivery. A summary of types of oils used, their processing, and different types of oil-in-water emulsion-based approaches that have been used in recent years is discussed. In this chapter, a knowledge gap was identified on Pickering emulsions to set the scene for the experimental studies. The literature review forming this chapter was published in peer-reviewed journal, 'Trends in Food Science & Technology'.

Chapter 3 discusses the preparation and properties of oil-in-water Pickering emulsions stabilized by whey protein isolate gel particles of nanometric size (nanogels). The influence of particle concentration on the structure and stability of the emulsions containing medium chain triglyceride (MCT)-oil stabilized by these nanogel particles was investigated. The microstructure at multiple length scales, droplet size and interfacial shear viscosity of particles was studied. Furthermore, emulsions were used to encapsulate curcumin and the effects of pH and ionic strength on curcumin retention and quantitative aspects of binding of curcumin to the proteinaceous nanogel particles were investigated. The innovative aspect was that the formation of nanometric-size whey protein isolate gel particles acting as Pickering stabilizers was reported for the first time. The formation of whey protein isolate nanogel particle-stabilized Pickering emulsions for encapsulation of curcumin was also reported for the first time. The results of this chapter were published in the peer-reviewed journal 'Food Structure'.

In **Chapter 4**, the influence of a biopolymeric coating of negatively charged dextran sulphate of two molecular weights (40 kDa and 500 KDa) on gastric protection of the whey protein nanogel stabilized-Pickering emulsions was evaluated in the context of an *in vitro* static gastric digestion model. Droplet size, ζ -potential, microstructure (confocal microscopy with fluorescently-labelled dextran) and protein hydrolysis *via* SDS-PAGE were monitored. The results from this chapter were published in peer-reviewed journal, 'Food & Function'.

In **Chapter 5**, the influence of the degree of Maillard conjugation on the development of a covalently conjugated whey protein isolate-dextran-based gel particles of micrometric-size (microgels) was examined on gastric stability of emulsions. The formation of Pickering emulsion stabilized by a selected microgel particle was characterized followed by the structural and *in vitro* gastric digestion stability properties of the particles and corresponding Pickering emulsions. The formation of whey protein isolate-dextran conjugate microgels and Pickering emulsions, as well as confocal image cross-correlation analysis of emulsions after *in vitro* gastric digestion to appreciate the digestion of the interfacial layer has been reported for the first time. The results from this chapter were published in peer-reviewed journal, 'Food Hydrocolloids'.

Chapter 6 presents the ability of dextran sulphate-coated Pickering emulsions and whey protein isolate-dextran conjugate microgel-stabilized Pickering emulsions, as compared to whey protein nanogel-stabilized Pickering emulsions to protect droplets from coalescence during *in vitro* simulated digestion phase. The free fatty acid release, bioaccessibility of curcumin and cellular uptake in Caco-2 cells was also evaluated. The results from this chapter have been submitted to peer-reviewed journal, 'Current Research in Food Science'.

The final **Chapter 7** includes a general summary and discussion of the main results of this PhD project. Areas for future studies are also included in this chapter.

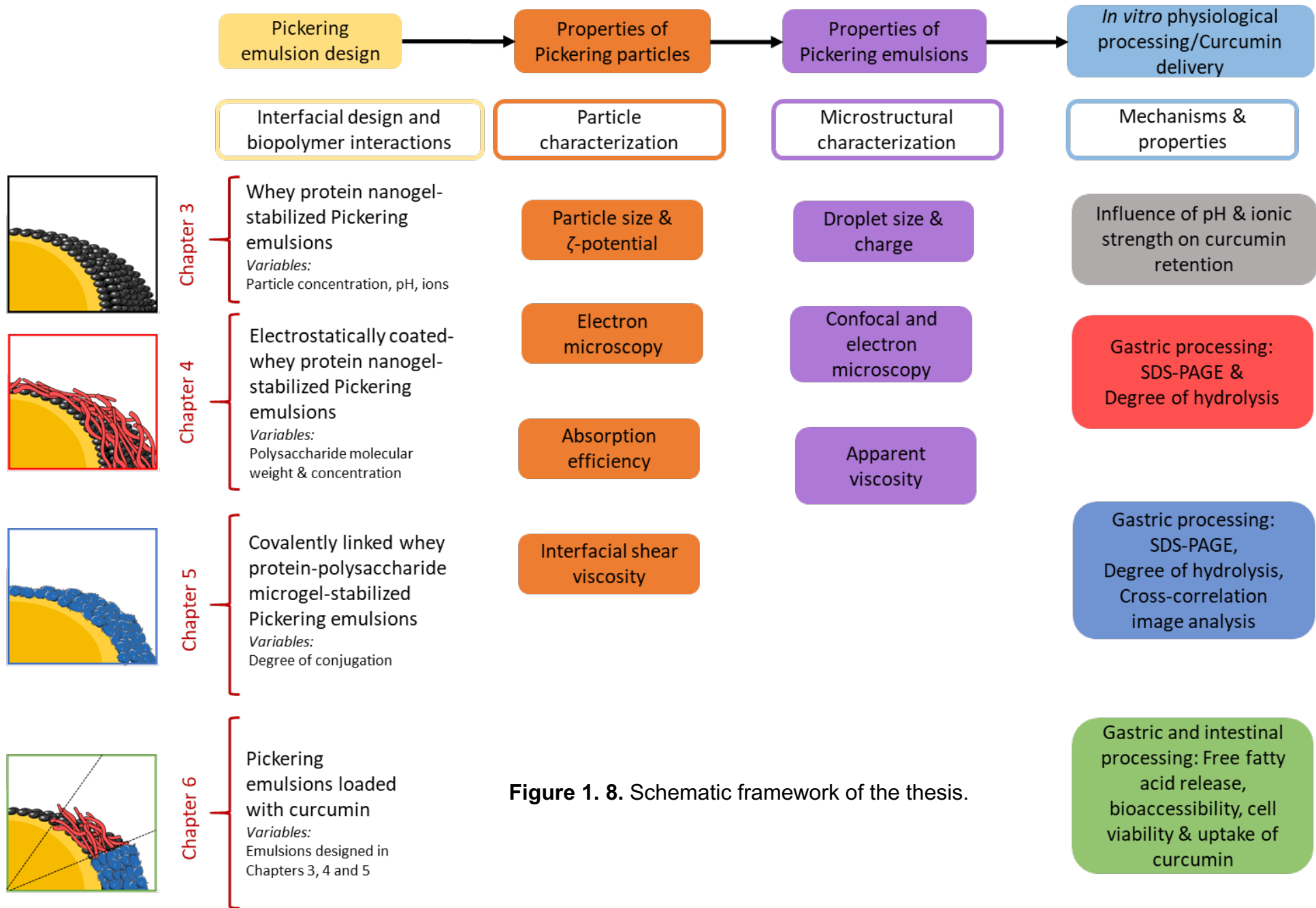


Figure 1. 8. Schematic framework of the thesis.

1.6 References

- A. Bos, M. & van Vliet, T. (2001). Interfacial rheological properties of adsorbed protein layers and surfactants: a review. *Advances in Colloid and Interface Science*, 91, 437-471.
- Alegría, A., Garcia-Llatas, G. & Cilla, A. (2015). Static Digestion Models: General Introduction. In: *The Impact of Food Bioactives on Health: in vitro and ex vivo models* (edited by Verhoeckx, K., Cotter, P., Lopez-Exposito, I., Kleiveland, C., Lea, T., Mackie, A., Requena, T., Swiatecka, D. & Wichers, H.). Pp. 3-12. Cham: Springer International Publishing.
- Álvarez, C., García, V., Rendueles, M. & Díaz, M. (2012). Functional properties of isolated porcine blood proteins modified by Maillard's reaction. *Food Hydrocolloids*, 28, 267-274.
- Appelqvist, I. A. M., Golding, M., Vreeker, R. & Zuidam, N. J. (2007). Emulsions as Delivery Systems in Foods. In: *Encapsulation and Controlled Release Technologies in Food Systems* (edited by Lakkis, J. M.). Pp. 41-81. Blackwell Publishing
- Auty, M. A. E. (2013). 4 - Confocal microscopy: principles and applications to food microstructures. In: *Food Microstructures* (edited by Morris, V. J. & Grovers, K.). Pp. 96-P8. Woodhead Publishing.
- Bauer, E., Jakob, S. & Mosenthin, R. (2005). Principles of Physiology of Lipid Digestion. *Asian-Australas Journal of Animal Science*, 18, 282-295.
- Bornhorst, G. M. & Singh, R. P. (2014). Gastric Digestion *In Vivo* and *In Vitro*: How the Structural Aspects of Food Influence the Digestion Process. *Annual Review of Food Science and Technology*, 5, 111-132.
- Castle, J., Dickinson, E., Murray, B. S. & Stainsby, G. (1987). Mixed-Protein Films Adsorbed at the Oil-Water Interface. In: *Proteins at Interfaces*. Pp. 118-134. American Chemical Society.
- Cosgrove, T. (2010). *Colloid science: principles, methods and applications*: John Wiley & Sons.
- Croguennec, T., O'Kennedy, B. T. & Mehra, R. (2004). Heat-induced denaturation/aggregation of β -lactoglobulin A and B: kinetics of the first intermediates formed. *International Dairy Journal*, 14, 399-409.
- Dalgleish, D. G. & Hallett, F. R. (1995). Dynamic light scattering: applications to food systems. *Food Research International*, 28, 181-193.

de Belder, A. N. & Granath, K. (1973). Preparation and properties of fluorescein-labelled dextrans. *Carbohydrate Research*, 30, 375-378.

de Oliveira, F. C., Coimbra, J. S. R., de Oliveira, E. B., Zuñiga, A. D. G. & Rojas, E. E. (2016). Food Protein-polysaccharide Conjugates Obtained via the Maillard Reaction: A Review. *Critical Reviews in Food Science and Nutrition*, 56, 1108-1125.

de Wit, J. N. (1998). Nutritional and Functional Characteristics of Whey Proteins in Food Products. *Journal of Dairy Science*, 81, 597-608.

Destribats, M., Rouvet, M., Gehin-Delval, C., Schmitt, C. & Binks, B. P. (2014). Emulsions stabilised by whey protein microgel particles: towards food-grade Pickering emulsions. *Soft Matter*, 10, 6941-54.

Dickinson, E. (2012). Use of nanoparticles and microparticles in the formation and stabilization of food emulsions. *Trends in Food Science & Technology*, 24, 4-12.

Dickinson, E. (2020). Advances in food emulsions and foams: reflections on research in the neo-Pickering era. *Current Opinion in Food Science*, 33, 52-60.

Erni, P., Fischer, P., Windhab, E. J., Kusnezov, V., Stettin, H. & Lauger, J. (2003). Stress- and strain-controlled measurements of interfacial shear viscosity and viscoelasticity at liquid/liquid and gas/liquid interfaces. *Review of Scientific Instruments*, 74, 4916-4924.

Heath DD, Pruitt MA, Brenner DE and Rock CL. (2003). Curcumin in plasma and urine: quantitation by high-performance liquid chromatography. *Journal of Chromatography B*, 783, 287–295.

Holt, P. R. (1972). The Roles of Bile Acids During the Process of Normal Fat and Cholesterol Absorption. *Archives of Internal Medicine*, 130, 574-583.

Hunter, R. J. (2013). Zeta Potential in Colloid Science: Principles and Applications. Pp. 398. Academic Press Limited.

Ireson C, Orr S, Jones DJ, Verschoyle R, Lim CK, Luo JL, Howells L, Plummer S, Jukes R, Williams M, Steward WP and Gescher A. (2001). Characterization of metabolites of the chemopreventive agent curcumin in human and rat hepatocytes and in the rat in vivo, and evaluation of their ability to inhibit phorbol ester-induced prostaglandin E2 production. *Cancer Research*, 61, 1058–1064.

Instruments, M. (2015). Zeta potential - An introduction in 30 minutes. In: Technical Note.

JEOL Ltd. (2011). Introducing Cryo Scanning Electron Microscopy. *JEOL Application Data Sheet*, SEM, SM-B-004-00E.

- Jiménez-Castaño, L., Villamiel, M. & López-Fandiño, R. (2007). Glycosylation of individual whey proteins by Maillard reaction using dextran of different molecular mass. *Food Hydrocolloids*, 21, 433-443.
- Jourdain, L. S., Schmitt, C., Leser, M. E., Murray, B. S. & Dickinson, E. (2009). Mixed Layers of Sodium Caseinate + Dextran Sulfate: Influence of Order of Addition to Oil–Water Interface. *Langmuir*, 25, 10026-10037.
- Kasran, M., Cui, S. W. & Goff, H. D. (2013). Emulsifying properties of soy whey protein isolate–fenugreek gum conjugates in oil-in-water emulsion model system. *Food Hydrocolloids*, 30, 691-697.
- Kuntsche, J., Horst, J. C. & Bunjes, H. (2011). Cryogenic transmission electron microscopy (cryo-TEM) for studying the morphology of colloidal drug delivery systems. *International Journal of Pharmaceutics*, 417, 120-137.
- Li, Y., Hu, M. & McClements, D. J. (2011). Factors affecting lipase digestibility of emulsified lipids using an *in vitro* digestion model: Proposal for a standardised pH-stat method. *Food Chemistry*, 126, 498-505.
- Li, Y. & McClements, D. J. (2010). New Mathematical Model for Interpreting pH-Stat Digestion Profiles: Impact of Lipid Droplet Characteristics on *in Vitro* Digestibility. *Journal of Agricultural and Food Chemistry*, 58, 8085-8092.
- Ma Z, Shayeganpour A, Brocks DR, Lavasanifar A and Samuel J. (2007). High-performance liquid chromatography analysis of curcumin in rat plasma: application to pharmacokinetics of polymeric micellar formulation of curcumin. *Biomedical Chromatography*, 21, 546– 552.
- Macierzanka, A., Torcello-Gómez, A., Jungnickel, C. & Maldonado-Valderrama, J. (2019). Bile salts in digestion and transport of lipids. *Advances in Colloid and Interface Science*, 274, 102045.
- Marefati, A., Bertrand, M., Sjöö, M., Dejmek, P. & Rayner, M. (2017). Storage and digestion stability of encapsulated curcumin in emulsions based on starch granule Pickering stabilization. *Food Hydrocolloids*, 63, 309-320.
- Mat, D. J. L., Le Feunteun, S., Michon, C. & Souchon, I. (2016). *In vitro* digestion of foods using pH-stat and the INFOGEST protocol: Impact of matrix structure on digestion kinetics of macronutrients, proteins and lipids. *Food Research International*, 88, 226-233.
- McClements, D. J. (2004). *Food Emulsions: Principles, Practices, and Techniques*. CRC Press, Taylor & Francis Group

Minekus, M., Alming, M., Alvito, P., Ballance, S., Bohn, T., Bourlieu, C., Carrière, F., Boutrou, R., Corredig, M., Dupont, D., Dufour, C., Egger, L., Golding, M., Karakaya, S., Kirkhus, B., Le Feunteun, S., Lesmes, U., Macierzanka, A., Mackie, A., Marze, S., McClements, D. J., Ménard, O., Recio, I., Santos, C. N., Singh, R. P., Vegarud, G. E., Wickham, M. S. J., Weitschies, W. & Brodkorb, A. (2014). A standardised static *in vitro* digestion method suitable for food – an international consensus. *Food & Function*, 5, 1113-1124.

Mu, L., Zhao, H., Zhao, M., Cui, C. & Liu, L. (2018). Physicochemical properties of soy protein isolates-acacia gum conjugates. *Czech Journal of Food Science*, 29, 129-136.

Murray, B. S. & Dickinson, E. (1996). Interfacial Rheology and the Dynamic Properties of Adsorbed Films of Food Proteins and Surfactants. *Food Science and Technology International*, Tokyo, 2, 131-145.

Nicolai, T. (2016). Formation and functionality of self-assembled whey protein microgels. *Colloids and Surfaces B: Biointerfaces*, 137, 32-38.

Nicolai, T., Britten, M. & Schmitt, C. (2011). β -Lactoglobulin and WPI aggregates: Formation, structure and applications. *Food Hydrocolloids*, 25, 1945-1962.

Oakenfull, D., Pearce, J. & Burley, R. W. (1997). Protein Gelation. In: Food protein and their applications (edited by Damodaran, S. & Paraf, A.). New York: Marcel Dekker, Inc.

Oliver, C. M., Melton, L. D. & Stanley, R. A. (2006). Creating Proteins with Novel Functionality via the Maillard Reaction: A Review. *Critical Reviews in Food Science and Nutrition*, 46, 337-350.

Pak Y, Patek R and Mayersohn M. (2003). Sensitive and rapid isocratic liquid chromatography method for the quantitation of curcumin in plasma. *Journal of Chromatography B*, 796, 339–346.

Pilnik, W. & Rombouts, F. M. (1985). Polysaccharides and food processing. *Carbohydrate Research*, 142, 93-105.

Powers, J. C., Harley, A. D. & Myers, D. V. (1977). Subsite Specificity of Porcine Pepsin. In: Acid Proteases: Structure, Function, and Biology (edited by TANG, J.). Pp. 141-157. New York, NY: Springer US.

Prasad, S., Tyagi, A. K. & Aggarwal, B. B. (2014). Recent developments in delivery, bioavailability, absorption and metabolism of curcumin: the golden pigment from golden spice. Cancer research and treatment. *Official journal of Korean Cancer Association*, 46, 2-18.

- Qi, J.-R., Yang, X.-Q. & Liao, J.-S. (2009). Improvement of functional properties of acid-precipitated soy protein by the attachment of dextran through Maillard reaction. *International Journal of Food Science & Technology*, 44, 2296-2302.
- Repetto, G., del Peso, A. & Zurita, J. L. (2008). Neutral red uptake assay for the estimation of cell viability/cytotoxicity. *Nature Protocols*, 3, 1125-1131.
- Roth, S., Murray, B. S. & Dickinson, E. (2000). Interfacial Shear Rheology of Aged and Heat-Treated β -Lactoglobulin Films: Displacement by Nonionic Surfactant. *Journal of Agricultural and Food Chemistry*, 48, 1491-1497.
- Santos, M., Teixeira, J. & Rodrigues, A. r. (2000). Production of dextransucrase, dextran and fructose from sucrose using *Leuconostoc mesenteroides* NRRL B512(f). *Biochemical Engineering Journal*, 4, 177-188.
- Sarkar, A., Horne, D. S. & Singh, H. (2010). Interactions of milk protein-stabilized oil-in-water emulsions with bile salts in a simulated upper intestinal model. *Food Hydrocolloids*, 24, 142-151.
- Sarkar, A., Murray, B., Holmes, M., Ettelaie, R., Abdalla, A. & Yang, X. (2016a). *In vitro* digestion of Pickering emulsions stabilized by soft whey protein microgel particles: influence of thermal treatment. *Soft Matter*, 12, 3558-69.
- Sarkar, A., Ye, A. & Singh, H. (2016b). On the role of bile salts in the digestion of emulsified lipids. *Food Hydrocolloids*, 60, 77-84.
- Sarkar, A., Zhang, S., Holmes, M. & Ettelaie, R. (2019). Colloidal aspects of digestion of Pickering emulsions: Experiments and theoretical models of lipid digestion kinetics. *Advances in Colloid and Interface Science*, 263, 195-211.
- Schubert, M. L. & Makhlof, G. M. (1992). Neural, hormonal, and paracrine regulation of gastrin and acid secretion. *The Yale journal of biology and medicine*, 65, 553-623.
- Sun, G. & Mao, J. J. (2012). Engineering dextran-based scaffolds for drug delivery and tissue repair. *Nanomedicine (Lond)*, 7, 1771-84.
- Sun, W.-W., Yu, S.-J., Yang, X.-Q., Wang, J.-M., Zhang, J.-B., Zhang, Y. & Zheng, E.-L. (2011). Study on the rheological properties of heat-induced whey protein isolate-dextran conjugate gel. *Food Research International*, 44, 3259-3263.
- Tønnesen, H. H., Másson, M. & Loftsson, T. (2002). Studies of curcumin and curcuminoids. XXVII. Cyclodextrin complexation: solubility, chemical and photochemical stability. *International Journal of Pharmaceutics*, 244, 127-135.

Zamani, S., Malchione, N., Selig, M. J. & Abbaspourrad, A. (2018). Formation of shelf stable Pickering high internal phase emulsions (HIPE) through the inclusion of whey protein microgels. *Food & Function*, 9, 982-990.

Zheng, B., Zhang, Z., Chen, F., Luo, X. & McClements, D. J. (2017). Impact of delivery system type on curcumin stability: Comparison of curcumin degradation in aqueous solutions, emulsions, and hydrogel beads. *Food Hydrocolloids*, 71, 187-197.

Chapter 2

Recent advances in emulsion-based delivery approaches for curcumin: From encapsulation to bioaccessibility¹

Abstract

Background

Curcumin has been widely acknowledged for its health-promoting effects. However, its application is often limited by its poor water solubility and biochemical/structural degradation during physiological transit that restricts its bioavailability. Emulsion based approaches have attracted the most research attention to encapsulate curcumin and improve its stability, bioaccessibility and bioavailability.

Scope and approach

This review summarizes the recent advances in application of different oil-in-water emulsion-based approaches, such as, conventional emulsions (surfactants-, protein- and protein-polysaccharide-stabilized emulsions), nanoemulsions, and Pickering emulsions that have been specifically used to deliver curcumin. Particular emphasis is given to factors affecting curcumin solubility, change in crystalline structure of curcumin upon dispersion and encapsulation efficiency. Changes in the droplet size and emulsion stability during *in vitro* oral-to-gastrointestinal digestion are discussed, with clear focus on the bioaccessibility of the encapsulated curcumin.

Key findings and conclusions

Key factors that influence curcumin delivery include emulsion droplet size, oil composition, volume fraction, dispersion conditions of curcumin in the oil phase and the type of interfacial materials. Nanoemulsions have been the preferred choice for delivery of curcumin up to now. Although scarce in literature, emulsions stabilized by edible Pickering particles as shown by recent evidence are effective in protecting curcumin in an *in vitro* gastrointestinal setting due to their high coalescence stability. Further studies with emulsions stabilized by food-grade particles and accurate tracking of the physiological fate (*in vitro* to human trials) of different emulsion-based delivery

¹ Published as: Araiza-Calahorra, A., Akhtar, M., and Sarkar, A. 2016. Recent advances in emulsion-based delivery approaches for curcumin: From encapsulation to bioaccessibility, *Trends in Food Science & Technology*. 71, 155 – 169. DOI: <https://doi.org/10.1016/j.tifs.2017.11.009>

vehicles are essential for rational designing of curcumin-rich functional foods with high bioaccessibility.

2.1 Introduction

Curcumin is a natural low-molecular-weight polyphenolic compound found in the rhizome of the perennial herb, turmeric (*Curcuma longa*) (Sharma et al., 2005). *Curcuma longa* is comprised of 3 - 5% curcuminoids, with the four main types being curcumin (77%), demethoxycurcumin (17%), bisdemethoxycurcumin (3%), and cyclocurcumin (Goel et al., 2008; Heger et al., 2014). Curcumin has a molecular weight of 368.37 g mol⁻¹ and a melting point of 183 °C (Tapal and Tiku, 2012). In the last few decades, curcumin has gained significant research attention owing to its wide range of health-promoting properties, such as anti-inflammatory, anticarcinogenic, and antioxidant activities (Ak and Gülçin, 2008; Fujisawa et al., 2004; Selvam et al., 2005). Hence, research has been conducted extensively in recent years to design food-based encapsulation vehicles that can deliver curcumin effectively in targeted physiological sites.

The main challenge in delivering curcumin effectively in human physiology is that curcumin is a highly lipophilic compound, which limits its absorption in the human body. Besides its poor water solubility, the relatively high rate of metabolic degradation during physiological transit, inactivity of the metabolic end-products, and rapid elimination from the body reduce the bioavailability of curcumin (Bansal et al., 2011). To overcome these challenges and to improve the bioavailability of curcumin upon ingestion, many studies have attempted to encapsulate curcumin using delivery systems, such as hydrogels (Gong et al., 2013), nanoparticles (Bisht et al., 2007), and liposomes (Hasan et al., 2014).

Particularly, food colloid scientists have shown that emulsions can be facile templates to encapsulate lipophilic curcumin and improve its stability and bioavailability by manipulating the bioaccessibility of these colloidal delivery systems. Essentially, two main emulsion-based approaches have been used to deliver curcumin: emulsion-based delivery systems and excipient emulsion systems. In emulsion-based delivery systems, the isolated curcumin is solubilized first within the oil phase of an oil-in-water emulsion during the formation of the emulsion. Preliminary evidence has suggested that emulsion-based delivery systems can be used to encapsulate curcumin to increase its oral bioaccessibility, permeability, and resistance to metabolic processes during physiological transit (Zhang and McClements, 2016). On the other hand, in excipient emulsion systems, the curcumin is kept within its natural environment (used in its original form, such as a powdered spice) and is co-

ingested with an oil-in-water excipient emulsion. Detailed information about excipient emulsion systems that have been used to deliver curcumin can be found in recent literatures (McClements et al., 2016; Zhang and McClements 2016; Zou et al., 2015b; Zou et al., 2016). For excipient emulsion systems the curcumin-free emulsion needs to be consumed with a curcumin-rich food or food ingredient (Zhang and McClements, 2016), whereas, for emulsion-based delivery systems, the curcumin-loaded emulsion can be used as a sole nutraceutical application, the latter has attracted considerable research attention.

There has been a strong upsurge in research efforts, in recent years, in delivering curcumin using emulsions of different sizes, structures and properties, and assessing the ability of these emulsions to protect curcumin during *in vitro* oral-to-gastrointestinal digestion. The droplet size distribution and the microstructure of the emulsions have been tailored to improve the bioaccessibility of curcumin. To the best of our knowledge, there is no literature source that has systematically reviewed the emulsion-based delivery systems that have been used for encapsulating curcumin and identified the specific factors affecting the stability of the encapsulated curcumin pre- and post-ingestion as well as its bioaccessibility. Such information is crucial in order to exploit emulsion-based approaches to design next generation curcumin-rich functional foods, functional ingredients and pharmaceutical applications.

Hence, the aim of this review is to provide an update of the recent advances in emulsion-based approaches for the delivery of curcumin. We have specifically focussed on emulsion-based delivery systems, such as, conventional oil-in-water (O/W) emulsions, Pickering emulsions, and nanoemulsions stabilized by a surfactant, protein-polysaccharide conjugates and complexes, solid particles that have specifically been used to encapsulate curcumin. Firstly, we have discussed the structure and physicochemical properties of curcumin, including research work at our own laboratory, which are key parameters for selecting the appropriate delivery approach. Specifically, we have discussed the solubility and crystalline structure of curcumin in different solvents in order to enable the optimal selection of the oils and/or fatty acids, and identified the key challenges encountered in poor dispersibility. Secondly, we have discussed the specific factors in designing the emulsion-based systems that affect the loading and encapsulation efficiency of curcumin, droplet size change after curcumin incorporation, and *in vitro* gastrointestinal stability of the encapsulated curcumin. We have critically analysed the release properties and bioaccessibility of curcumin in oral, gastric and intestinal regimes. Finally, we have highlighted the key research gaps and future trends in the research domain of delivery and bioaccessibility of curcumin using emulsion-based approaches.

The literature search was systematically conducted using three key search engines: ScienceDirect, PubMed and American Chemistry Society (ACS). In addition, 'Google Scholar' was also used to search for publications and additional information. Keywords used were 'curcumin', 'curcumin structure', 'curcumin emulsion(s)', 'curcumin nanoemulsion', and 'curcumin Pickering emulsion'. The initial selection of publications was made on the basis of the title of the publication, keywords, and abstract screening. Full-text articles were analysed for inclusion in the review. The reference list of each paper was carefully checked to identify any relevant previous studies and full-text screening was conducted for the same.

2.2 General aspects of curcumin

2.2.1 Structure of curcumin

Curcumin is a yellowish powder, with an ordered crystal structure (Rachmawati et al., 2013; Zhao et al., 2015). From a structural viewpoint, curcumin is comprised of two aromatic rings with methoxyl and hydroxyl groups in the ortho position with respect to each other (Figure 2.1). The aromatic rings are connected through seven carbons that contain two α , β -unsaturated carbonyl groups. As a result, curcumin exists in three possible forms, two isomers in an equilibrating *keto-enol* tautomeric form, and a β -diketonic tautomeric form (Payton et al., 2007). Under slightly acidic and neutral conditions, the keto-form of curcumin dominates (Jovanovic et al., 1999). However, when dissolved in ethanol at 70 °C in the dark and in aqueous solutions at pH > 8, curcumin exists primarily in its enolic form; the latter provides its radical-scavenging ability (Jovanovic et al., 1999; Kolev et al., 2005).

In crystalline phase, the molecule prefers the *enol* configuration stabilized by strong intramolecular hydrogen-bonding (H-bonding) (Tønnesen et al., 1982). However, as a result of this intermolecular H-bonding, the molecule loses its planarity (Kolev et al., 2005). Polymorphism of crystal structures of curcumin depends on the crystallization conditions. Curcumin crystals can adopt different shapes, such as monoclinic (acicular), orthorhombic (rice seed like), and amorphous (Liu et al., 2015; Mishra et al., 2014; Sanphui et al., 2011).

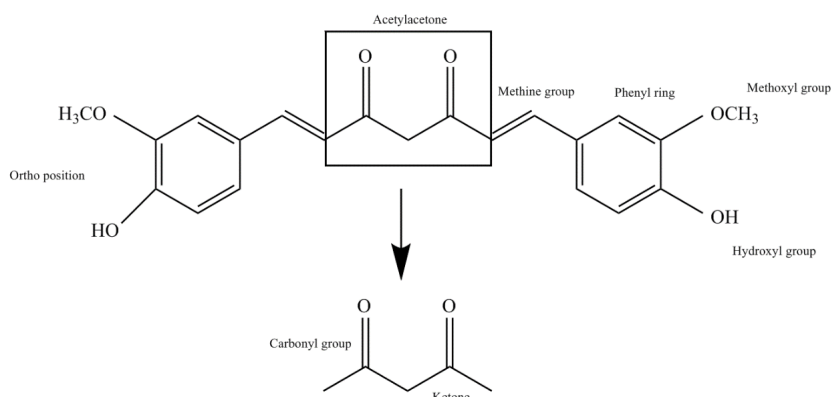


Figure 2.1. Functional groups in curcumin.

Using scanning electron microscopy (SEM), to analyse curcumin particles, in our laboratory has revealed interesting morphological characteristics, that was dependent on the solvent in which curcumin was dispersed. Figure 2.2a presents a SEM image of the curcumin particles dispersed in methanol. Curcumin showed a long plate-like morphology of around 20-31 μm length and aspect ratio (length-to-width) varied from 4:1 to 6:1, which is in agreement with previous reports (Kurniawansyah et al., 2017; Thorat and Dalvi, 2014, 2015). Formation of the repeated stacks of curcumin plates as observed in Figure 2.2a has also been described by other authors as an end-to-end attachment of curcumin particles (Thorat and Dalvi, 2014). This end-to-end attachment creates larger sized aggregates of the curcumin plates. However, with time, the particles appeared to be more fused and such stacks were less visible. Figure 2.2b presents the SEM image of the curcumin crystals dispersed in dimethyl sulfoxide (DMSO). In DMSO, there appeared to be a shift in aspect ratio to nearly 2:1 to 3:1 with appearance of needle-shaped attachments. The appearance of these acicular structures suggests an uncontrolled growth of the curcumin particles from dense non-uniform and highly supersaturated zones in the solution. This uncontrolled nucleation prompted the growth of secondary particles from the main crystal stem (Kurniawansyah et al., 2017; Thorat and Dalvi, 2014). In presence of edible oils, such as sunflower oil, curcumin crystals with dimensions of 13-23 μm (length) and 3-5 μm (width) were observed (Figure 2.2c). The particles appeared more fused; possibly caused by a rapid accretion of primary units into single particles, or by particle growth through the process of molecule-by-molecule bonding (Thorat and Dalvi, 2014). However, the exact mechanism of such crystal fusion remains to be uncovered.

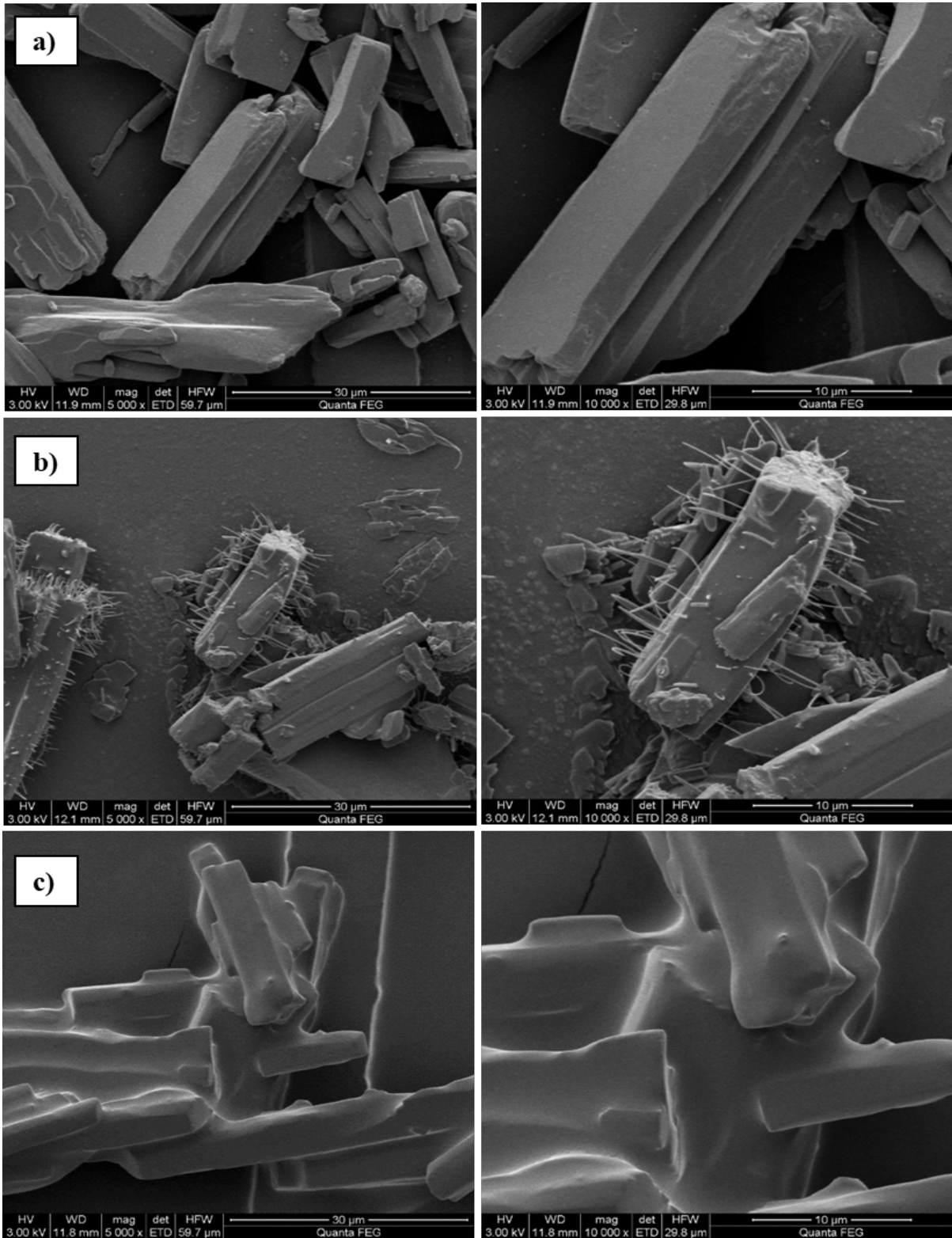


Figure 2.2. Scanning electron micrographs (SEM) of curcumin crystals dispersed at 10 mg/mL in methanol (a), DMSO (b), and sunflower oil (c) in lower ($\times 5,000$, left) and higher magnifications ($\times 10,000$, right).

2.2.2 Solubility of curcumin in solvents

The log P value of curcumin (*i.e.* the measure of the extent to which a solute preferentially partitions in octanol over the aqueous phase) has been reported to be 3.29 (PubChem-969516). This confirms that the curcumin molecule is highly lipophilic with a low intrinsic water solubility (11 ng/ mL, ambient temperature) (Tønnesen et al., 2002). The hydrophobic nature of curcumin is given by an aliphatic chain (bridge), which separates the highly polar enolic and phenolic groups (Balasubramanian 2006). The bridge is composed of lipophilic methine-rich segments connecting the polar regions of the molecule (Balasubramanian, 2006; Heger et al., 2014).

Curcumin is highly soluble in polar solvents, such as acetone (7.75 mg/ mL), 2-butanone (2.17 mg/ mL), ethanol (5.6 mg/ mL), methanol (4.44 mg/mL), 1,2-dichloroethane (0.5125 mg/ mL) and isopropanol (3.93 mg/ mL) (Heger et al., 2014; Khopde et al., 2000). The DMSO is one of the most commonly used solvents for dispersing curcumin as it can dissolve curcumin up to a concentration of ~20 mg/ mL, an order of magnitude higher as compared to most alcohols (Khopde et al., 2000).

Authors have reported that in alkaline conditions (> pH 7), curcumin can be dissolved sparsely in water as the acidic phenolic group in curcumin donates its H⁺ ion, forming the phenolate ion enabling dissolution (Jagannathan et al., 2012; Tønnesen and Karlsen, 1985). However, under alkaline conditions, curcumin is more susceptible to degradation, partly due to the formation of phenylated anion; this can increase the production of curcumin radicals. These radicals successively mediate degradation of the molecule by reacting with other curcumin radicals to form dimeric catabolites, or by reacting with biomolecules in the cells (Heger et al., 2014). For *in vitro* and *in vivo* studies, curcumin as a free molecule is commonly dissolved in the least toxic-miscible solvents according to their lethal 50% dose values (Heger et al., 2014). Curcumin is also soluble in different edible oils (Table 2.1) and such solubility depends on the degree of mixing, temperature-time conditions, which is discussed in detail in Section 2.5.

Table 2.1. Solubility ($\mu\text{g}/\text{mL}$) of curcumin in various edible oils.

Oil	Solubility ($\mu\text{g}/\text{mL}$)	Curcumin dispersion conditions	References
Corn oil	7580	AT/ 48 h	(Setthacheewakul et al., 2010)
	70	60 °C/ 10 min, 20 min sonication	(Joung et al., 2016)
	2.76	60 °C/ 10 min, 20 min sonication	(Ahmed, et al., 2012)
Soybean oil	7380	AT/ 48 h	(Setthacheewakul et al., 2010)
	0.1834	AT/ 10 min	(Lin, et al., 2009)
Oleic acid	1390	AT/ 48 h	(Setthacheewakul et al., 2010)
MCT	250	60 °C/ 10 min, 20 min sonication	(Joung et al., 2016)
	7.505	60 °C/ 10 min, 20 min sonication	(Ahmed, et al., 2012)
Ethyl oleate	310.59	37°C/ 24 h	(Cui et al., 2009)
	12170	AT/ 48 h	(Setthacheewakul et al., 2010)
	0.348	AT/ 10 min	(Lin et al., 2009)
Peppermint oil	0.2694	AT/ 10 min	(Lin et al., 2009)
Peanut oil	129.22	37°C/ 24 h	(Cui et al., 2009)
Castor oil	256.59	37°C/ 24 h	(Cui et al., 2009)
Coconut oil	100	60 °C/ 10 min, 20 min sonication	(Joung et al., 2016)
Olive oil	80	60 °C/ 10 min, 20 min sonication	(Joung et al., 2016)

Abbreviations: AT, ambient temperature; MCT, medium chain triacylglycerol

2.3 Key challenges of delivery of curcumin

A strong scientific consensus exists that orally administered curcumin has poor bioavailability due to the poor solubility and limited absorption from the gut of the latter. The bioavailability of curcumin is determined by its bioaccessibility; latter defined as the fraction of the quantity of bioactive initially ingested that is solubilized within the gastrointestinal fluid, in a form that can be absorbed by the epithelium cells (Fernández-García et al., 2009). Since early 1980's, substantial research has been conducted with respect to curcumin bioavailability in rat models. Ravindranath & Chandrasekhara (1980) reported that after oral administration of 400 mg of curcumin in rats, only a trace amount (less than 5 $\mu\text{g}/\text{mL}$) of curcumin remained in the portal blood during 15 min to 24 hours. More recently, Sharma, et al. (2004) found that after an oral dose of 3.6 g of curcumin, maximum curcumin level in plasma was 11.1 nmol/L after an hour of dosing. However, no curcumin was found in plasma from patients who received a lower dose of curcumin. It has been identified that, in rat plasma, glucuronide and sulphate are the major products of curcumin biotransformation (Sharma et al., 2001). Enzymatic hydrolysis of curcumin through glucuronidase and sulfatase may explain its efficient metabolism and its poor bioavailability when administered orally (Cheng et al., 2001; Sharma et al., 2001).

According to the Nutraceutical Bioavailability Classification Scheme (NuBACS), curcumin is classified as B*(-) L, S A*(+) T*(-) C, M. The full classification scheme has been discussed in detail elsewhere (Zhang and McClements, 2016; Zou et al., 2015b). Briefly, this suggests that the poor degree and rate of release of curcumin from the food structure (L) and the poor solubility in the gastrointestinal fluids (S) are the key factors (-) limiting the bioaccessibility (B*) of curcumin. Furthermore, curcumin absorption (A*) has no major influence on the bioavailability of curcumin. However, the chemical (C) or metabolic (M) degradation of curcumin during its gastrointestinal passage remains as the key limiting factor (-) on the transformation (T*) of curcumin. Hence, it is important to understand how emulsion-based delivery systems can be designed to address these specific challenges. In this review, we have only focused on bioaccessibility, which has yielded most of the publications in the last decade.

2.4 Emulsion-based delivery systems

Considering the high hydrophobicity of curcumin and our physiology being largely an aqueous-based system, an oil-in-water (O/W) emulsion-based approach has been the most obvious choice to deliver curcumin. In the last decade, a wide range of curcumin-encapsulated emulsion-based systems (Figure 2.3), such as conventional emulsions stabilized by surfactants, monolayers or multilayers of biopolymers (proteins, polysaccharides), nanoemulsions and Pickering emulsions, have been designed to deliver curcumin (Tables 2.2 and 2.3).

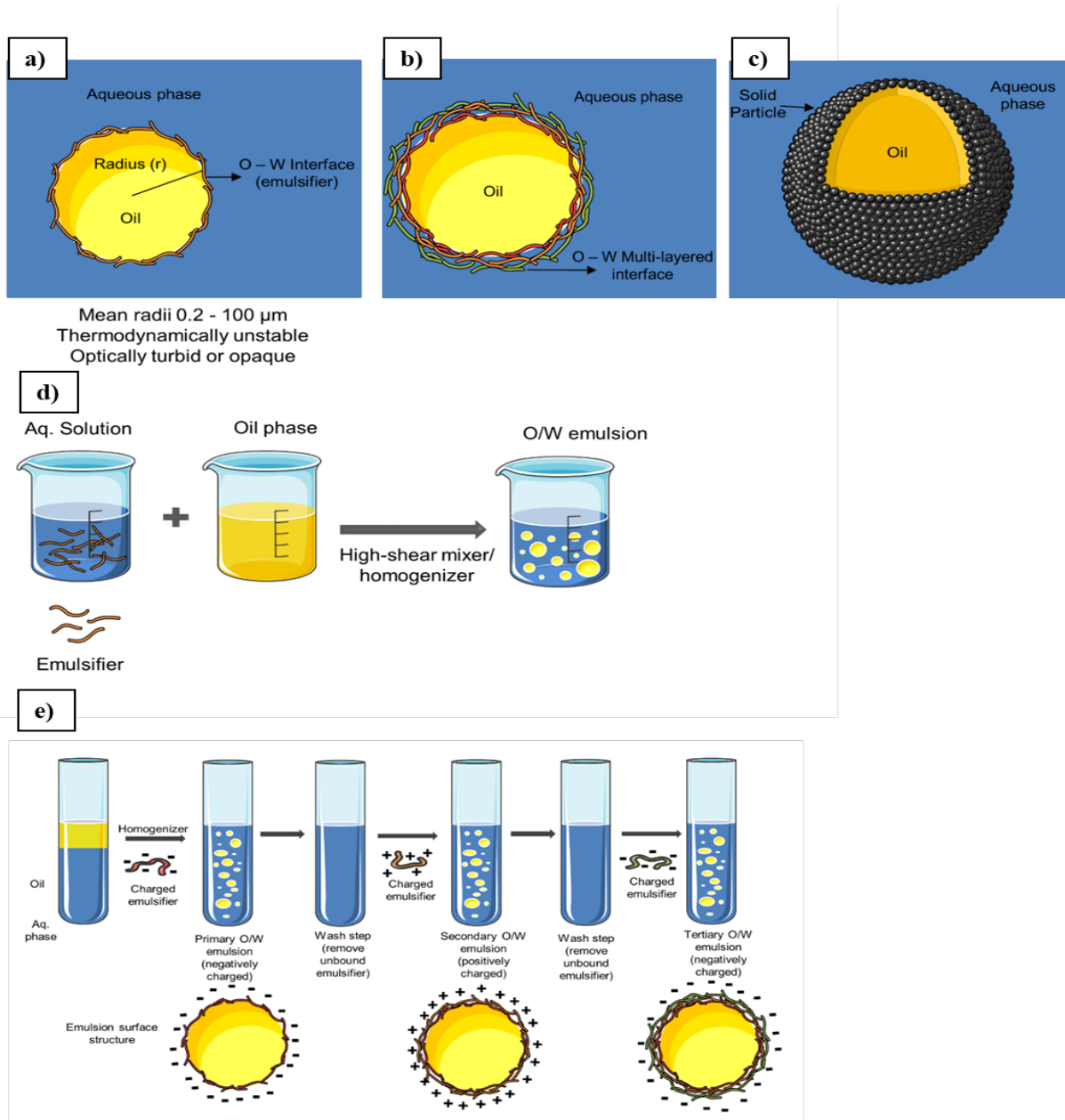


Figure 2.3. Schematic diagram of conventional emulsion (a), multilayered emulsion (b) and Pickering emulsion (c). Preparation method of conventional and Pickering emulsion (a) and multilayered emulsion (e).

Table 2.2. Composition and formation of nanoemulsions for delivery of curcumin.

Emulsifier(s)	Oil (wt%)	Curcumin loading in oil phase (wt%)	Curcumin dispersion method	Emulsification process	References
Octenyl-succinic-anhydride (OSA) modified starch, OSA modified starch - coated with chitosan or sodium carboxymethyl cellulose	MCT (0.02 – 0.14)	0.00028 – 0.0020	Magnetic stirring (100 °C, 7 min)	High-speed blender (14,000 rpm, 2 min/ High-intensity sonication (20 kHz, 1-13 min, 40-45 °C).	(Abbas et al., 2014; Abbas et al., 2015)
Hydrogenated L- α -phosphatidylcholine (HEPC) (surfactant), Tween 80 and Polyoxyethylene hydrogenated castor oil 60 (co-surfactant)	Soybean Oil (~3)	0.041 – 0.66	Curcumin initially dissolved in chloroform, then oil, evaporation of chloroform	Rotary evaporation, vacuum desiccation (3-5 h) / Hydrate in bath type sonicator (55-60 °C) / Vigorous mixing and sonication (5 min) / Sonication (30-60 min, N ₂ atmosphere, 55-60 °C).	(Anuchapree da et al., 2012b)

β -lactoglobulin	LCT, MCT, SCT, LCT: SCT (10)	0.15	Magnetic stirring (60°C, 10 min, 20 min sonication)	High-speed blender (2 min) / High-pressure homogenizer (9,000 psi, 5 cycles)	(Ahmed et al., 2012)
Tween 20, 60 and 80	Soybean oil (10 – 20)	0.03, 0.07, 0.1	Magnetic stirring (15 min)	Peristaltic pump (mechanical stirring 300-500 rpm) / 30 min (Inversion point (EIP) method)	(Borrin et al., 2016)
Tween 20	Olive Oil, Coconut oil, Corn Oil and MCT (1.9 – 55.5)	0.3	-	High-speed homogenizer (13500 rpm, 15 min) / High-pressure homogenizer (1,000 bar, 5 cycles).	(Joung et al., 2016)
Tween 80 (surfactant), lecithin (co-surfactant) – coated with high, medium and low molecular-weight chitosan	MCT (10)	0.65	Heating and stirring (overnight)	Stirring (10 min) / High-speed blender (1600 rpm, 5 min) / Ultrasonication (20 min, 150 W).	(Li et al., 2016)

Tween 80, lecithin, Acacia gum and whey protein	MCT, Canola Oil, Linseed Oil, Sunflower Oil (0.5 – 3)	1.18	Ultra-sonication	High-speed blender (6 min, 10000 rpm) / High-pressure homogenizer (60 MPa, 3 cycles)	(Ma et al., 2017a)
Poloxamer-407, Tween 20, Sodium dodecyl sulphate (SDS), Dodecyltrimethylammonium bromide (DTAB)	Cottonseed Oil (0.0010 – 0.0.0048*)	0.220 – 1.099*	Magnetic stirring (70°C, 1000 rpm)	Magnetic stirring (~70 °C, 1,000 rpm) / Magnetic stirring (650 rpm, 45 min).	(Malik et al., 2016)
Lactoferrin, lactoferrin coated with alginate, Tween 20 (T20), sodium dodecyl sulphate (SDS) and dodecyltrimethylammonium bromide (DTAB)	Corn oil (5)	0.1	-	High-speed blender (2 min) / High-pressure or Microfluidizer (20,000 psi, 5-20 cycles).	(Pineiro et al., 2016; Pineiro et al., 2013)
Sodium caseinate	Milk fat (1)	0.05	-	Sonication (60 °C, 5 min) / Sonication (30 min) / Spray dried	(Rao and Khanum, 2016)

Tween 80 (surfactant), whey protein concentrate 70 (co-surfactant)	MCT (0.5 – 2)	0.0047 – 0.075	-	Magnetic stirring/ Sonication	(Sari et al., 2015)
Phosphatidylcholine 80%, coated with chitosan and chitosan 2-iminothiolane conjugate	Soybean Oil (24)	2.2	High-speed blender (60 °C, 500 rpm), Sonication	Sonication / High- pressure homogenization (2,000 bar).	(Vecchione et al., 2016)
Tween 20	MCT (10)	1	-	High-speed homogenizer (10 min) or high- pressure homogenizer (6 cycles)	(Wang et al., 2008)
Papain hydrolysate soy protein isolate (SPIH) – coated with microcrystalline cellulose (MCC)	MCT (10)	0.1	-	Two-speed hand-held homogenizer (3 min) / Microfluidizer (50 MPa, 3 cycles)	(Xu et al., 2016)

* mol/ kg. Abbreviations: NE, nanoemulsion

Table 2.3. Composition and formation of conventional emulsions (protein-polysaccharide conjugates/ complexes-stabilized) and Pickering emulsions (particle-stabilized systems) for delivery of curcumin.

Emulsifier(s)	Oil (wt%)	Curcumin loading in oil phase (wt%)	Curcumin dispersion method	Emulsification process	References
Tween 80	Corn oil (10)	0.00279	Stirring (85 °C, 2 h)	High shear mixer / High-pressure homogenizer (12,000 psi, 5 cycles)	(Zheng et al., 2017)
Bovine serum albumin - dextran conjugate (BSA-dextran)	MCT (20 or 40)	0.22 – 0.56	Heating (90 °C, dark, 1 h)	Homogenizer (10,000 rpm, 1 min) / High-pressure homogenizer (900 bar, 4 min) / Samples heated (90 °C, dark, 1 h)	(Wang, et al., 2016)
Casein - soybean soluble polysaccharide complex (CN/SSPS)	MCT (16.7)	0.15	Solutions of 10% ethanol, 90% MCT	Homogenizer (10,000 rpm, 1 min) / High-pressure homogenizer (800 bar, 4 min)	(Xu, et al., 2017)

Particles					
Kafirin	Vegetable Oil (0.2 - 0.8)	0.0005 – 0.002	-	High-speed homogenizer (13,000 rpm, 3 min)	(Xiao, et al., 2015)
OSA quinoa starch granules	MCT (7)	0.0016	Rotor-stator high- shear homogenizer (22,000 rpm, 20 min)	High-shear homogenizer (22,000 rpm, 20 and 70 °C, 30 s)	(Marefati, et al., 2017)
Chitosan- tripolyphosphat e nanoparticles	MCT and LCT (5 – 50)	0.1	-	Stirring overnight / High- speed blender (10,000 rpm, 3 min)	(Shah, et al., 2016a; Shah, et al., 2016b)
Colloidal silica	Canola Oil (5)	0.0046	Vigorously mixed (20 min)	Hand-held dispenser (8,000 rpm) / Single-stage homogenizer (600 bar)	(Tikekar, et al., 2013)

In order to set the scene in terms of encapsulation efficiency, protection, retention, stability and release of curcumin, we have included an overview of emulsion-based delivery vehicles, focussing on the design principles, formation and stability of emulsions in the next section.

2.4.1 Stability of O/W emulsions

An emulsion consists of small droplets of one liquid dispersed in another immiscible liquid. Typically, these two immiscible liquids are oil and an aqueous phase (McClements, 2015; Sarkar and Singh, 2016). Depending on their arrangement, they are usually classified as oil-in-water (O/W) or water-in-oil (W/O) emulsions. Emulsions are thermodynamically unstable systems due to the large interfacial area between the two immiscible phases. Emulsions can destabilize over time due to their thermodynamic instability, causing creaming, sedimentation, flocculation and coalescence of the systems (Dickinson, 2009; McClements, 2015). Creaming and sedimentation are main forms of gravitational separation. When two or more droplets come together and aggregate, but retain their individual integrity, droplets are said to flocculate. Such flocculation might occur due to electrostatic attraction (bridging) or osmotic pressure effects (depletion). When two or more droplets merge together to form a single large droplet, droplets are said to coalesce. "Oiling-off" occurs when excessive droplet coalescence happens, and a separate layer of oil is formed on top of the aqueous phase.

2.4.2 Types of emulsion structure

Conventional emulsions. Conventional emulsions have mean droplet radii in the range of 0.2- 100 μm (Figure 2.3a). They are thermodynamically unstable systems and tend to be optically turbid or opaque as they scatter light because of the droplet dimension being similar to the wavelength of light. The droplet size is mainly determined by the oil phase, as the thickness of the interfacial layer ($\delta \approx 1\text{-}15\text{ nm}$) is much smaller than the radius (r) of the oil droplet core ($\delta \ll r$). The interfacial layer is generally made up of surfactants (e.g. tweens (polyethoxylated sorbitan esters or polysorbates), spans (sorbitan esters), polyoxyethylene (20) sorbitan monolaurate, monooleate and monopalmitate) or monolayers of biopolymers (e.g. milk proteins (caseins, whey proteins), plant proteins (pea protein, soy protein), and polysaccharides, such as gum Arabic). The preparation method for the formation of conventional emulsions involves using a high shear mixer or two-stage valve

homogenizer to homogenize the two immiscible phases, as illustrated schematically in Figure 2.3d.

Multi-layered emulsions. A multi-layered emulsion consists of emulsion droplets electrostatically stabilized by layers of alternatively charged emulsifiers (Figure 2.3b). In recent years, there has been growing interest in the utilization of the layer-by-layer (LbL) electrostatic deposition method to form such multilayer emulsion structures. In this method, a charged polyelectrolyte is absorbed through electrostatic attraction onto an oppositely charged droplet surface. Multiple layers can be formed by alternating adsorption of oppositely charged polyelectrolytes or charged emulsifiers leading to the formation of a multi-layered structure at the interface (Figure 2.3e) (Dickinson, 2009; McClements, 2015).

Protein-polysaccharide conjugate-stabilized emulsions. Proteins and polysaccharides possess different inherent characteristics (Goh et al., 2008, 2014). Proteins are known to adsorb at oil/water interface due to their surface-active properties, and polysaccharides are known for their water-binding, gelling and thickening properties. Covalently linked proteins and polysaccharides *via* Millard reaction between the amino groups of protein and reducing sugar groups of the polysaccharide are used to combine and improve their individual characters and stabilize oil-in-water emulsion with better kinetic stability (Akhtar and Ding, 2017).

Pickering emulsion. Pickering emulsions are stabilized by solid particles that are irreversibly adsorbed to the oil-water interface (Figure 2.3a) (Aveyard et al., 2003; Dickinson, 2012, 2017; Pickering, 1907; Ramsden, 1903). These particles at the interface should have an average size at least 10-100 times smaller than the emulsion droplet size in order to achieve effective Pickering stabilization. The stabilization mechanism for a Pickering emulsion is different from that of a conventional emulsion. In a conventional emulsion, the interfacial materials (*e.g.* surfactants, biopolymers) with amphiphilic properties impart kinetic stability to the droplets by decreasing the interfacial tension and by generating electrostatic repulsion/ steric hindrance between the droplets.

When compared to conventional emulsions, the irreversible absorption of particles creates a mechanical (steric) barrier in Pickering emulsions that adds long-term physical stability against coalescence and Ostwald ripening. Solid particles in Pickering emulsion present a partial wettability by both the oil and water phase. Depending on their degree of wettability in either of the phases and location at the interface defined by the contact angle of the particle (θ) they can either stabilize O/W or W/O emulsions (Dickinson, 2009, 2012, 2017). If the contact angle is smaller than 90° ($\theta < 90^\circ$), the particle will be preferentially wetted by the aqueous phase, favouring

the formation of an O/W emulsion. Pickering emulsions can be prepared in a similar way to that of conventional emulsions (Figure 2.3d).

Depending on the size of the particles, oil droplets of $<10 \mu\text{m}$ diameter can be achieved. However, in most case, food-grade Pickering emulsions prepared using starch and protein-based microgel particles have a considerably higher droplet size ($>10 \mu\text{m}$), as the particles used to stabilize these droplets are generally sub-micron to micron-sized (Sarkar et al., 2016a; Yusoff and Murray, 2011). The concept of Pickering emulsion has been present in different food products since long, such as homogenized and reconstituted milk (oil-in-water (O/W) emulsions stabilized by casein micelles) (Dickinson, 2012), it is only recently that there has been an upsurge of research interests to understand the interfacial properties of particles in O/W emulsions. This is largely due to the laboratory-manufactured food-grade particles of controlled size being available now, e.g. whey protein microgel, pea protein microgel, starch, zein, flavonoids etc (de Folter et al., 2012; Luo et al., 2012; Sarkar et al., 2016a; Shao and Tang, 2016; Yusoff and Murray, 2011).

Nanoemulsions. Nanoemulsions have a mean radii between 50 and 200 nm (Figure 2.4a). They tend to be transparent or slightly opaque and have much better stability to aggregation as compared to that of conventional emulsions due to their very small droplet size. The overall droplet composition is mainly constituted by the emulsifier layer as the thickness of the emulsifier layer is similar to that of the radius of the oil droplet ($\delta = r$) (McClements and Rao, 2011). Fabrication methods for nanoemulsions are typically categorized as either high-intensity or low-intensity and consist of two stages: the pre-emulsification and emulsification stage. High-intensity methods include use of a high-speed blender, high-pressure valve homogenizers, microfluidizers and ultrasonic bath or sonicator (Figure 2.4b) (McClements and Rao, 2011). These mechanical devices are capable of creating intense disruptive forces that break up the oil phase into small droplets. The low-intensity methods include phase inversion and solvent mixing methods (Figure 2.4c) (Borrin et al., 2016). In these methods, the spontaneous formation of tiny oil droplets within the mixed oil–water–emulsifier systems are formed, when the environmental conditions are altered.

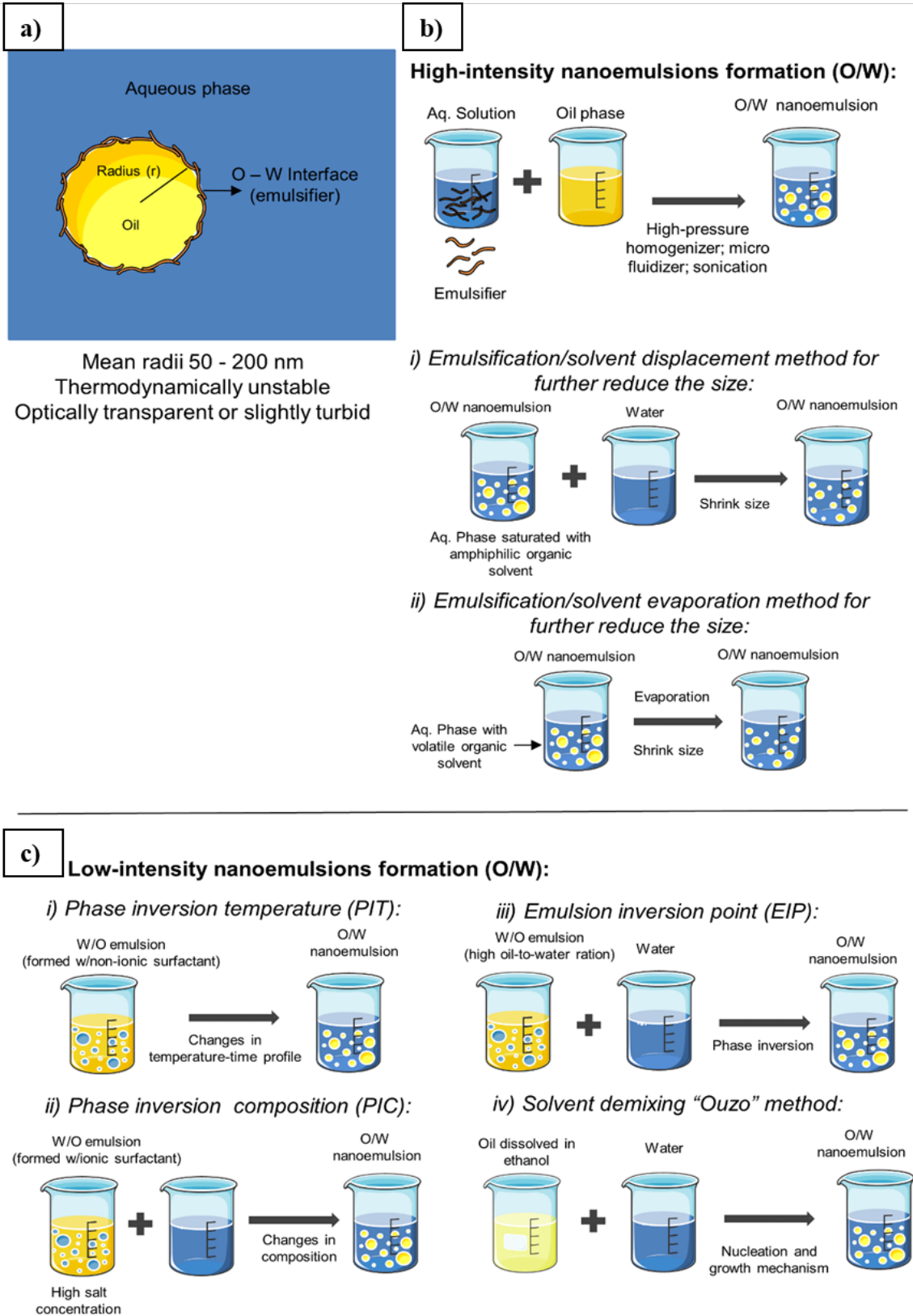


Figure 2.4. Schematic diagram of nanoemulsion (a) and its preparation method by high-intensity (b) and low-intensity (c) techniques.

2.5 Dispersion of curcumin into the oil phase

Proper dispersion of bioactive compounds into the carrier phase is a key factor for improving the solubility, dissolution behaviour, and administration orally (Zhang and McClements, 2016). Curcumin is crystalline at ambient temperature and must therefore be dispersed in a suitable carrier before it can be incorporated into a colloidal delivery system. In an oil-in-water emulsion, the lipid acts as the carrier phase for lipophilic bioactive components. Table 2.1 summarizes the solubility values (non-exhaustive) of curcumin dispersed in different types of edible oils. The dispersion ability of oil is commonly referred to in the literature, as the 'loading capacity' or 'loading percentage'. The numerical value of the loading capacity is obtained by calculating the quantity of curcumin dispersed in the oil as a percentage of the total quantity of curcumin added. The loading capacity of an oil can vary depending on the molecular weight and polarity of the carrier oil, as well as the physical conditions applied, such as temperature and times used either in the dispersion or in the incubation process.

Molecular weight and polarity of the carrier oil. Direct experimental evidence suggests that quantity of curcumin that can be solubilized in a carrier oil is inversely proportional to the average molecular weight of the latter (Ahmed et al., 2012). For instance, short chain triglycerides (SCT) have more polar groups (oxygens) per unit mass than long chain triglycerides (LCT). Hence, SCT present more dipole-dipole interactions between their polar groups and the curcumin molecules, thereby favouring curcumin solubilization. Also, greater solubilisation is achieved in SCT compared to LCT due to an excluded volume effect. When curcumin molecules are incorporated into the oil phase, a depletion zone is formed around curcumin molecules. In this region, the centre of the lipid molecules is excluded, in other words, the lipid concentration is zero. The thickness of the depletion zone increases with increasing molecular weight of the lipid molecules (Ahmed et al., 2012). For example, Joung et al. (2016) reported that the solubility of curcumin in MCT oil was higher when compared to coconut oil (LCT: MCT), olive oil (LCT) and corn oil (LCT) (0.25, 0.1, 0.08, 0.07 mg/ mL, respectively) (Table 2.1). These results were also consistent with a recent study by Ma et al. (2017a), who reported that solubility of curcumin in MCT was nearly three times as much as canola oil, and twice as much as in linseed oil, corn oil and sunflower oil (12.4, 4, 7, 6.2 and 5.4 mg/ mL , respectively).

Temperature dependence. Solubility of curcumin is highly temperature dependent. When a crystalline material is fully dissolved, it is said that the material has reached an equilibrium, but above this level, it will form crystals (supersaturation) (McClements, 2012a). From a theoretical perspective, increasing the temperature increases the average kinetic energy of both, the solution and the crystalline

molecules. This increase in kinetic energy destabilizes the solid state of the solute (less able to hold together) and allows the solvent to break apart the solute molecules more effectively and dissolving it more rapidly.

To characterize the temperature dependence of the dissolution of crystalline curcumin in oil, the common method used is to determine the reduction in magnitude of turbidity of the oil using a UV-Vis spectrophotometer. For instance, Zou et al. (2015a) observed that the turbidity of curcumin in corn oil mixtures (LCT) decreased appreciably upon heating from 25 to 100 °C. At a concentration of 3 mg/ mL, the turbidity almost reached a value close to zero at 100 °C indicating that the crystals were fully dissolved at this temperature (Table 2.3-2.1). Interestingly, upon cooling, turbidity of the oil was low indicating that the curcumin still remained dissolved within the oil. This might be attributed to either curcumin being below its saturation temperature even at 25 °C, or the curcumin concentration did not exceed the supersaturation level to form curcumin crystals (McClements, 2012a). At 4 mg/ mL, the turbidity also decreased as the temperature was increased. Nonetheless, the final turbidity at 100 °C was considerably greater than that observed for the sample containing 3 mg/ mL curcumin, which implies that excess curcumin crystals had not dissolved completely. When samples were cooled, the turbidity remained high and even increased slightly, which further highlights that the solubility of curcumin decreased with decreasing temperature, as well as the amount of curcumin present was above the saturation level.

Similarly, Ma et al. (2017b) observed increased curcumin concentrations in MCT oil when using a boiling bath for 3 min as compared to that of ultrasonic (390 W, one second interval for 30 min) and microwave treatments (780 W, 30 sec). Also, Abbas et al. (2014) reported that a curcumin concentration of ≤ 6 mg/ mL was successfully dissolved in MCT oil at 100 °C, without a noticeable sedimentation during one month storage period when incorporated into a nanoemulsion. However, prolonged heat exposure during solubilization of curcumin in the oil phase can cause decomposition of curcumin. In fact, Wang et al. (2016) reported 10% of curcumin decomposition after a heat treatment at 90 °C for 1 hour in the dark.

Time dependence. Dissolution rate of curcumin depends on the nature of the crystals (*e.g.* surface area, crystallinity, morphology, structure), the nature of the solvent (*e.g.* polarity), and the physical conditions applied (*e.g.* stirring speed, temperature and sonication) (McClements, 2012a) (Table 2.1). Soluble curcumin concentration values varied significantly for soybean oil when mixed for 48 h (ambient temperature) (7380 $\mu\text{g}/\text{mL}$) (Setthacheewakul et al., 2010) as compared to that for 10 min (0.1834 $\mu\text{g}/\text{mL}$) (Lin et al., 2009). In MCT oil, a soluble curcumin concentration

range of 7.50 - 250 $\mu\text{g}/\text{mL}$ has been reported when mixed at 60 °C for 10 min, with subsequent 20 min of sonication (Ahmed et al., 2012; Joung et al., 2016). Overall, the results suggest that solubility of curcumin depends on the nature of the oil, the curcumin-oil interactions, and the processing conditions (temperature, agitation time); such factors are critical for the maximum incorporation of curcumin into the oil phase. Various studies have shown that a higher curcumin concentration is generally favoured by MCT oil when high temperatures (≥ 60 °C) and appropriate agitation times (10 - 30 min) are applied.

2.6 Physicochemical stability of curcumin-loaded emulsion systems

Tables 2.2 and 2.3 summarize a non-exhaustive list of the emulsion-based approaches used for delivering curcumin, such as nanoemulsions and macroemulsions stabilized by surfactants, protein-polysaccharide conjugates, and Pickering particles respectively. In this Section, we reviewed various factors that can influence the retention capacity of curcumin, the effect of curcumin incorporation on the droplet size distribution of emulsions and the structural characteristics that promote retention of curcumin during storage and *in vitro* release.

2.6.1 Loading efficiency

In literature, the terms, such as “yield”, “encapsulation efficiency”, “incorporation efficiency” and “loading efficiency” have often been used interchangeably for emulsion-based encapsulation systems. In each case, it essentially refers to the entrapment capacity of an emulsion system. Quantitative information is obtained by measuring the mass of curcumin entrapped into the delivery system as a percentage of the total curcumin added (McClements et al., 2009). Since curcumin is required in high concentrations to show therapeutic benefits, one of the prerequisites in the delivery research is high entrapment of bioactive molecules. The loading efficiency of emulsions is highly dependent on the type of emulsifier and its structural arrangements at the interface.

Curcumin-surfactant interactions. Curcumin molecules contain mainly hydrophobic but also some hydrophilic groups that can directly interact with surfactant molecules mainly via hydrophobic and electrostatic interaction, respectively (Yu and Huang, 2010). It has been reported that the enolic and phenolic groups of curcumin underwent electrostatic interactions with positively charged head group of cationic-

non-ionic surfactant micelles mixtures (e.g. Dodecylethyldimethylammonium bromide (DDAB), Polyoxyethylene 10 oleyl ether, Tyloxapol, Polysorbate 80), while the methylene rich chain of curcumin interacted with the hydrophobic part of the surfactant micelles mixture (Kumar et al., 2016). The authors revealed using transmission electron microscopy (TEM) that curcumin was not located within the core of the surfactant micelles but was rather interacting with the polar part of the surfactants (head group). This suggests that in emulsions stabilized by mixed surfactant systems, both hydrophilic and hydrophobic parts of the surfactants might contribute to the solubilisation of curcumin. Such favourable microenvironment mediated by the surfactant systems might enable enhancing the solubilisation of curcumin molecules inside the emulsions leading to a high loading efficiency. For example, when 15 mg of curcumin was added in nanoemulsions stabilized by optimized mixtures of hydrogenated L- α -phosphatidylcholine (HEPC) (surfactant) and Polyoxyethylene hydrogenated castor oil 60 (HCO-60) (co-surfactant) or HEPC and Tween 80, loading efficiencies of 100% or ~97%, respectively, were obtained (Anuchapreeda et al., 2012a).

Curcumin-protein interactions. Sodium caseinate, a mixture of α 1-, α 2- and β - caseins and κ -casein is commonly used to stabilize oil droplets (Sarkar and Singh, 2016). The α 1-, α 2- and β - caseins are phosphoproteins and are more hydrophobic than κ -casein. This is because α 1-casein contains two tryptophan residues at positions 164 and 199, whereas κ -casein has one tryptophan residue at position 143 (Liu and Guo, 2008). It is highly likely that when sodium caseinate-stabilized emulsions are used to encapsulate curcumin, any or all of these tryptophan (hydrophobic) residues directed towards the oil phase could bind to curcumin molecules through hydrophobic interactions and contribute to increasing the loading efficiency of an emulsion (Pan et al., 2013). For example, Rao and Khanum (2016) observed a considerable increase in the loading efficiency when the sodium caseinate concentration was increased from 2.5% (89.6%) to 10% (92.3%) in nanoemulsions at a constant curcumin-milk fat ratio of 1:0.05% (w/w) (Table 2.2).

Curcumin-polysaccharides interactions. Curcumin-polysaccharide interactions can also affect the loading efficiency. Recently, Li et al. (2016) have investigated the influence of chitosan multilayer on the physicochemical properties of curcumin-loaded nanoemulsions. The loading efficiency was found to be 95.1% when a curcumin concentration of 0.548 mg/ mL was used. This was presumably due to the interactions between keto groups of curcumin in either the *diketo* or the *cis-enol* form, and the amine groups of chitosan (Anitha et al., 2011). Chitosan, which is rich in protonated amino groups possibly facilitated the electrostatic interaction between the cationic groups located on the polyglucosamine chains of the molecule and the

negatively charged anionic curcumin. In addition, at physiological pH (7.4) conditions, the hydrophobic interactions of curcumin with chitosan was reported to be more pronounced in the presence of non-ionic surfactant (Tween 80) than in the presence of cationic surfactants, such as, cetyl trimethyl ammonium bromide (CTAB). In Tween 80 systems, the binding process was hypothesized to be driven by hydrophobic, electrostatic and hydrogen bond formation between curcumin and chitosan (Boruah et al., 2012).

Interfacial structure. The development of a protein-polysaccharide conjugate has been reported to act as a physical barrier that prevents the diffusion of loaded curcumin into the aqueous phase (Qi et al., 2013; Wang et al., 2016). Often, one or more co-solvents or surfactants are added to the formulation to assist the solubilisation of high concentrations of curcumin in the system. For example, Wang et al. (2016) investigated protein-polysaccharide conjugates-stabilized emulsions that are suitable for delivery of curcumin (Table 2.3). They used a combination of MCT oil with a co-solvent ethanol (90:10 (v/v)) to prepared bovine serum albumin and dextran conjugate (BSA-dextran)-stabilized emulsion, the conjugate was formed between the e-amino group in BSA and the reducing-end carbonyl group in the dextran. It was observed that the conjugates form a BSA film at the oil/water interface with the dextran shell, the latter acted as a steric barrier retaining the loaded curcumin by preventing its diffusion into the aqueous phase, latter would have been facilitated by the carrier-acting ethanol otherwise. At BSA concentration of 15 mg/ mL in the aqueous phase, the curcumin loading efficiency was higher than 99% (Qi et al., 2013; Wang et al., 2016). Xu, Wang and Yao (2017) used a similar oil mixture (90% MCT and 10% ethanol (v/v)) and observed similar behaviour for casein-soy soluble polysaccharide (CN/SSPS) conjugate-stabilized emulsions at pH 3-4.5, at this pH the protein and the polysaccharide carried opposite charges forming a rather integrated interfacial film via electrostatic interactions (Table 2.3). About 99.9% of curcumin was encapsulated in the droplets (Xu et al., 2017).

Irreversible adsorption of individual particles in Pickering emulsion forms a porous interfacial layer (pores referring to space between the stabilizing particles at the interface) that may reduce the curcumin content by facilitating the diffusion of oxidation initiators into the oil droplets, latter may promote oxidative degradation/ modification or alkaline hydrolysis of curcumin (Tønnesen et al., 1986; Tønnesen et al., 2002). Previously, it has been estimated that the gaps between particles in a whey protein microgel-stabilized emulsion is ~110 nm for microgel particles of size $d_0 = 300$ nm (Sarkar et al., 2016a). However, such gap dimension can effectively be controlled by fusing the particles together forming a discrete layer or using smaller-sized particles. This was successfully shown in emulsions stabilized by smaller-sized kafirin

particles (size range of 92 - 434 nm), where a loading efficiency of ~90% was achieved because of the reduced gap dimension, latter limited the degradation of curcumin (Table 2.3). In another study, emulsions stabilized by non-heated (NHT) octenyl succinate (OSA) modified quinoa starch granules (2 μm) had a relatively low loading efficiency of curcumin (~80%) due to potential diffusion of oxidation initiators through the larger gaps in between the particles (Marefati et al., 2017; Xiao et al., 2015; Xiao et al., 2016) (Table 2.3). Interestingly, a thermal treatment of OSA modified starch granule-stabilized emulsions had created a rather fused layer of partially gelatinized starch granules, reducing the gaps between particles and favouring a higher protection of curcumin in undegraded form within the system.

2.6.2 Droplet size of curcumin-loaded emulsions

In theory, incorporation of curcumin should not alter the droplet size of a system if emulsion droplets are in the order of few microns (McClements and Li, 2010). Curcumin crystal size and emulsifier concentration can influence the extent of increase of droplet size after curcumin incorporation, particularly relevant in the case of nanoemulsions.

Curcumin crystal size. Nanoemulsion droplets usually have a mean diameter between 50 and 200 nm. Hence, it is highly likely that under specific dispersion conditions (*e.g.* temperature), curcumin crystal growth could interfere with the droplet size of the nanoemulsions. This clearly limits the amount of curcumin that can be successfully incorporated within the nanoemulsion droplets, since the concentration should always remain below the saturation limit (McClements and Rao, 2011). For instance, incorporation of curcumin into surfactant-stabilized nanoemulsions has been reported to increase the average droplet size of the emulsion, thereby destabilizing the system. Borrin et al. (2016) observed that encapsulating 0.1% curcumin into nanoemulsion stabilized by Tween 80 caused a statistically significant increase in the hydrodynamic diameter from 200 to 270 nm, after 60 days of storage. However, the increase was not observed in nanoemulsions containing less curcumin (0.03 - 0.07%). (Table 2.2). Similar findings were reported by Anuchapreeda, et al. (2012a) where increasing the amount of curcumin from 15 to 240 mg increased the mean hydrodynamic diameter of nanoemulsion from 48 to 78 nm.

On the contrary, in conventional emulsions and emulsions stabilized by protein-polysaccharide complex as well as edible Pickering particle-stabilized emulsions (Table 2.3), the size of curcumin crystals remains comparatively smaller (10 - 1000 times) as compared to that of the emulsion droplets. Hence, in these systems no significant change in the emulsion droplet size distribution occurs after curcumin

encapsulation (Marefati et al., 2017; Shah et al., 2016a; Wang et al., 2016; Xu et al., 2017). Thus, changes in the droplet size after curcumin incorporation is mainly a phenomenon in nanometre-sized emulsions. Bioactive components are required in high concentrations to show therapeutic benefits; therefore, the quantity of curcumin that can be incorporated into nanoemulsions without altering the droplet size can be a potential limiting factor. Furthermore, protein-polysaccharide conjugates/complexes, Pickering emulsion systems with a larger droplet size appear to be rather less sensitive to such alteration in droplet size after curcumin incorporation.

2.7 *In vitro* gastrointestinal stability and bioaccessibility of curcumin-loaded emulsions

An important parameter for characterizing the effectiveness of a delivery system is the protection of the encapsulated material until it reaches the targeted location. For curcumin, oxidative degradation/ modification that are mediated by reactive oxygen species (ROS), such as, hydroxyl radical ($\cdot\text{OH}$), superoxide anion ($\text{O}_2^{\cdot-}$), peroxy radicals and alkaline hydrolysis are the two major challenges encountered in *in vitro* stability studies that hinder the use of curcumin as a pharmaceutical (Wang et al., 1997). The most common pharmaceutical approach to assess *in vitro* degradation and release of curcumin from emulsion based systems involves addition of a buffer solution at different pH, or phosphate buffer containing cosolvents, such as, ethanol/ methanol, salts (e.g. CaCl_2) and in some cases bile salts in a dialysis bag (e.g. 3,500 - 8,000 Da) subjected to mechanical forces (e.g. shaking, stirring) at temperature in the range of 22-37 °C. In these pharmaceutical approaches, the degradation of curcumin under various pH conditions are investigated. In other cases, release of curcumin is facilitated by the use of polar solvents mixed with the buffer solution, here, the quantity of curcumin released from the emulsion to the buffer containing ethanol/ methanol is generally expressed as the percentage of the original curcumin encapsulated within the emulsion systems. However, for *in vitro* digestion models used by food scientists, this “release” term can be misleading as no such cosolvents are employed. In these studies, curcumin can only be released from an emulsion as part of an oil phase *i.e.* within the free fatty acids (FFAs), mono and/or diacylglycerols released during lipid digestion in the intestinal phase. Since pH change is a crucial parameter in *in vitro* gastrointestinal models and curcumin degradation is highly dependent on pH conditions, *in vitro* digestion results can be better interpreted in terms of degradation of curcumin rather than release, latter is only relevant when discussing the curcumin release along with the lipid digestion products as indicated above.

2.7.1 *In vitro* storage stability and release

Encapsulation of curcumin in Pickering emulsions have shown to significantly improve the storage stability of curcumin. For example, Tikekar et al. (2013) assessed the storage stability comparing the rate of curcumin degradation between curcumin solubilized in a buffer solution (3% (v/v) methanol) at pH 5.7, and curcumin encapsulated in silica-stabilized Pickering emulsions at pH 6.5. When incorporated into a Pickering emulsion system the time required for 50% reduction in curcumin concentration (half-life) was approximately 87 hours, compared to 50 minutes observed for free curcumin (Table 2.3). Considering that the stability of curcumin decreases in buffered systems at neutral to alkaline pH conditions (Wang et al., 1997), these results show that encapsulation of curcumin in Pickering emulsion significantly improved the storage stability of curcumin.

Unfortunately, the non-biodegradable and non-digestible character of silica has limited its application as delivery systems; increasing the interest in food-based particles, such as protein-based, and carbohydrate-based particles as Pickering emulsion stabilizers (Sarkar et al., 2016a; Yusoff and Murray, 2011). Chitosan-tripolyphosphate nanoparticles (CS-TPP-NPs) have been recently used due to its non-toxic (solvent free) and easy formation technique through ionic gelation process (Table 2.3). The CS-TPP nanoparticles were formed by cross-linking the primary positively charged amino groups of CS with the polyanion TPP, which is negatively charged. Shah et al. (2016a) observed that the curcumin degradation was ~14 wt% after 24 hours storage in the dark (22 °C) for CS-TPP-NPs emulsions prepared with 5 and 20 wt% MCT oil. The half-life (50 wt%) of curcumin was more than 120 hours.

Additionally, during an *in vitro* release model consisting of phosphate buffer containing ethanol (15% v/v) at acidic conditions (pH 2), which relates to gastric conditions, the release of curcumin from CS-TPP-stabilized Pickering emulsion after 24 and 96 hours was 56% and 82%, respectively. In almost neutral conditions (pH 7.4), which relates to blood fluid, 37% and 74% of curcumin was released within the same time interval. This lower curcumin retention, under acidic conditions, was also reported by Kakkar et al. (2011) for curcumin-loaded solid lipid nanoparticles and attributed to the increase of solubility of curcuminoids under acidic conditions previously discussed in section 2.2.1. Compared to silica-stabilized Pickering emulsions, curcumin storage stability was higher in Pickering emulsions stabilised with CS-TPP-NPs (Table 2.3).

2.7.2 *In vitro* gastrointestinal stability of curcumin

In vitro digestion models are commonly used to study the stability and digestibility of encapsulated bioactive compounds in different parts of the gastrointestinal tract (GIT) (Laguna et al., 2017; Minekus et al., 2014; Sarkar et al., 2010a; Sarkar et al., 2009b; Sarkar et al., 2010b, 2010c; Sarkar et al., 2016a; Sarkar et al., 2016b; Singh and Sarkar, 2011). Simulated gastric fluids (SGF) involve the addition of salts (e.g. NaCl), acids (e.g. HCl) and digestive enzymes (e.g. pepsin) at a highly acidic pH value (e.g. 1.2- 4) for a fixed period of time (e.g. 2 hours) at a body temperature of 37 °C. Simulated intestinal fluids (SIF) involve the addition of bile salts (or bile extract), pancreatin (trypsin, amylase, lipase) and salts (e.g. CaCl₂, NaCl, KH₂PO₄), at around neutral to alkaline pH values (e.g. 6.5 - 7.5) for a fixed period of time (e.g. 2- 3 hours) at a body temperature of 37 °C. In some digestion models, an initial oral stage is also included, which contains salts, glycoproteins (e.g. mucin) and α -amylase, around a neutral pH value for a fixed period of time (e.g. 5 - 10 min.) at a body temperature of 37 °C (Sarkar et al., 2009a; Sarkar and Singh, 2012; Sarkar et al., 2017a).

Proteolysis and/or displacement of interfacial materials. The structural conformations of proteins determine the ability of pepsin to hydrolyse the proteins. Native β -lactoglobulin has been reported to be resistant to pepsin breakdown in simulated gastric digestion due to its compact globular structure (Fu et al., 2002; Sarkar et al., 2010a; Sarkar et al., 2009b; Scanff et al., 1990; Singh and Sarkar, 2011). However, when present at the interface, it can be hydrolysed by gastric and pancreatic enzymes (Sarkar et al., 2009b; Sarkar et al., 2017b). This is particularly important for protein-based particle stabilized interfaces, such as whey protein microgel, kafirin and bovine serum albumin. Kafirin's structure comprises of an α -helix and β -sheet secondary structure and exhibits extensive disulphide-induced cross-linking (Belton et al., 2006). Xiao et al., (2016) observed that under gastric digestion, without the addition of pepsin, curcumin loaded kafirin-stabilised Pickering emulsions (KPE) suffered less droplet coalescence after 30 min of digestion as compared to that in the presence of pepsin (Table 2.3). With the addition of pepsin to the SGF, KPE showed coalescence with the appearance of larger droplets within 30 min. At the end of the gastric treatment (1 hour), the majority of the oil droplets lost their integrity and macro-scale phase separation occurred.

Protein-stabilized interfaces are highly responsive to intestinal conditions. Bile salt, a bio-surfactant in intestinal fluids can competitively displace the β -lactoglobulin protein from the droplet interface (Sarkar et al., 2010b; Sarkar et al., 2016a; Sarkar et al., 2016b), thereby favouring lipase activity and degradation of curcumin through exposure to ROS such as hydroxyl radical. For example, Sari et al. (2015) reported

that curcumin nanoemulsions, stabilized by whey protein concentrate (WPC) and composed of 50-60% β -lactoglobulin, were stable to gastric digestion (2 hours) with 90% of the encapsulated curcumin stable in the nanoemulsion (Table 2.2). However, during intestinal digestion 77% of the curcumin was degraded, attributed to the destabilization of the emulsions after 2 hours of incubation in the intestinal phase.

Barrier properties of interfacial materials. When treated under specific thermal conditions, Pickering particle-based interface can provide a certain degree of barrier to the access of bile salts or lipase to the oil-water interface. For example, in case of Pickering emulsions stabilized by gelatinised starch (Marefati et al., 2017) or whey protein microgel (Sarkar et al., 2016a), a thermal treatment was necessary for the formation of a fused barrier layer of connected particles at the interface (as discussed in Section 6) and might restrict the penetration of bile salts and/or enzymes. For example, Marefati et al. (2017) reported higher curcumin stability after 60 min of oral (~95%) and 2 hours of intestinal (~86%) digestion for heated Pickering-stabilized emulsions (HT) stabilized with OSA-treated quinoa starch granules, as compared to that of the non-heated samples (NHT) (~70% and ~40%, respectively) (Figure 2.3). However, no statistically significant difference between these samples was seen after 120 min of gastric digestion (Table 2.5a) (~82% for HT and ~86% NHT). This suggests that a fused layer of starch granules was significantly effective as a barrier layer against amylase attack (oral and intestinal regimes) as compared to that of intact starch granules, by reducing the gap dimensions. A recent study has shown that gastric destabilization of protein stabilized interfaces can be hindered by binding a secondary layer of oppositely charged polysaccharide-based particles, such as cellulose nanocrystals (Sarkar et al., 2017b). As cellulose nanocrystals are not digested by pepsin and provide a high surface viscosity, they provide a strong barrier to the pepsin attacking the whey protein at the droplet surface (Sarkar et al., 2017b). However, use of such secondary layer of particles in a proteinaceous particle-stabilized interface and role of such secondary layer of particles at interface in protecting curcumin in the entire gastrointestinal regime is yet to be explored in literature.

Through the implementation of *in vitro* digestion models, it has been demonstrated that, curcumin degradation is higher during simulated intestinal digestion or neutral pH than in simulated gastric digestion, regardless of the emulsion-based approach. Emulsions stabilized by ionic surfactants, proteins and electrostatically charged protein-polysaccharide multi-layered complexes are highly sensitive to any pH and ionic strength alterations, which are essentially abundant in physiology. In *in vitro* digestion regimes, Pickering particles appear to be more capable to protect curcumin from degradation in emulsions than that of the low molecular

weight emulsifiers/ protein owing to the strong adsorption of the particles to the oil-water interface and not being displaced by 'bio-surfactant' bile salts (Sarkar et al., 2016a). The effective formulation of emulsion systems exhibiting a mass transport barrier to enzyme attack, stability to changes in pH and delayed act of bile salts and lipid-lipase interactions through the establishment of a protective fused interface enclosing the droplet can be an effective strategy to encapsulate curcumin (Marefati et al., 2017).

2.7.3 Bioaccessibility of curcumin-loaded emulsions

Oil droplets are composed of digestible lipids such as triacylglycerols and they generate free fatty acids (FFAs) and monoacylglycerols (MAGs) upon digestion. Mixed micelles are formed by the interactions of these FFAs and MAGs that are released from the oil droplets, phospholipids, bile salts, and cholesterol (Devraj et al., 2013). These mixed micelles have non-polar domains capable of solubilizing hydrophobic bioactive compounds, and certain types of micelles are small enough to transport the bioactives through the mucus layer to the epithelium cells where they are absorbed (Zhang and McClements, 2016). In particular, bioaccessibility of curcumin is influenced by many factors, including oil composition, droplet size and curcumin-emulsifier interactions.

Oil composition. Various studies have revealed that the bioaccessibility of curcumin is clearly dependent on the type and amount of carrier lipid. Ahmed et al. (2012) observed that the bioaccessibility of curcumin in β -lactoglobulin-stabilized nanoemulsions increased substantially when the carrier lipid was composed of medium-chain triacylglycerols (MCT) or long-chain triacylglycerols (LCT) due to their ability to form mixed micelles (~41% for LCT and ~58% for MCT oil at a lipid concentration of 2 wt%) (Table 2.3). The authors also reported higher curcumin bioaccessibility values when the total lipid concentration of MCT oil was increased because more mixed micelles were formed to solubilise the curcumin (~8% at 1% lipid concentration and ~58% at 2% lipid concentration). However, for LCT oil, the bioaccessibility was similar with increased lipid content because a greater fraction of lipid phase was not digested, this means that some of the curcumin was not solubilised from the droplets into the surrounding micellar phase (~20% at 1% lipid concentration, ~40% at 1.5% lipid concentration and ~41% at 2% lipid concentration) (Table 2.3).

Conversely, other authors have reported that micelles are more likely to be formed by LCT than for MCT fatty acids. Medium chain triglycerides form a mixed micellar phase that contains hydrophobic domains that could not be large enough to accommodate large hydrophobic bioactive molecules such as curcumin (Zou et al.,

2016). For example, Shah et al. (2016b) deliberately prepared chitosan-tripolyphosphate nanoparticle-stabilized Pickering emulsions (PMCT, PLCT) and nanoemulsions stabilized by non-ionic surfactants (Span 80: Tween 80) (NEMCT, NELCT). A significant difference in curcumin bioaccessibility was reported when using MCT and corn oil (LCT) as the carrier lipids (Tables 2.2 and 2.3). The bioaccessibility was ~32% for NEMCT; ~65% for NELCT against 21% for PMCT and 53% for PLCT.

Droplet size. Emulsions with a smaller droplet size have higher lipid/water surface area to volume ratio that may result in higher degree of lipolysis (Armand, et al., 1999). Under physiological conditions, lipases are in excess relative to the quantity of oil droplets, hence a larger lipid/water interface will allow the anchoring of more lipase molecules to the oil/water interface (Armand et al., 1999). For example, Pinheiro et al. (2013) reported nearly 10-fold increase in curcumin bioaccessibility during sequential digestion (initial, stomach, duodenum, jejunum, ileum) for nanoemulsions stabilized by Tween 20 (e.g. ~15% in ileum) when compared with nanoemulsions stabilized by dodecyltrimethylammonium bromide (DTAB) (e.g. ~1.5% in ileum) (Table 2.3). This increased bioaccessibility for Tween 20 nanoemulsions correlated well with the reduced size of the emulsion droplet that was present throughout the simulated digestion (~100 - 310 nm), especially during duodenum, jejunum and ileum phases as compared to that of the size of DTAB nanoemulsions (~80 - 890 nm) (Table 2.2). Increasing the concentration of surfactants in nanoemulsions can decrease the emulsion droplet size (McClements, 2012b) and consequently the degree of lipid digestion. On the other hand, studies have found that increasing the surfactant concentration can also result in barrier effect that could also hinder the amount of FFA released (Joung et al., 2016). This suggests that the amount of surfactant concentration in curcumin nanoemulsions affects the FFA release and the size of the emulsion droplets (the lipid/water interfacial area), which is a key physicochemical factor in curcumin bioaccessibility. Other studies comparing the bioaccessibility of curcumin in β -lactoglobulin-stabilized conventional and nanoemulsions observed that the bioaccessibility of curcumin was fairly similar for both samples, with 58% for nanoemulsions, and 59% for conventional emulsions (Ahmed et al., 2012) (Table 2.3). Hence, it appears that there is no consensus in findings so far on advantages of using nanoemulsions over conventional emulsions to encapsulate curcumin from bioaccessibility standpoint.

Curcumin-emulsifier interactions. Some multilayer-stabilized nanoemulsions studies have shown that curcumin in these systems had relatively low total curcumin bioaccessibility, potentially due to emulsifier-curcumin interactions (Pinheiro et al., 2016). For example, nanoemulsions stabilized by lactoferrin (L-NE) and lactoferrin/alginate (L/A-NE) multilayer structure have shown relatively low curcumin

bioaccessibility of around ~2.5- 3.1% in jejunum and ileum. These results may be explained by the fact that curcumin may have been bound to the lactoferrin molecules or digestion products of lactoferrin after lipid hydrolysis, hence curcumin was not detected in the micellar phase (Tokle et al., 2013). Similarly, it has been suggested that cationic polymers may electrostatically inhibit lipase and bile salt action during lipolysis in the small intestine, decreasing the bioaccessibility of lipophilic compounds (Kido et al., 2003). However, experiments with chitosan-coated nanoemulsions stabilized by Tween 80 have suggested that chitosan coating had a very limited effect on the bioaccessibility of curcumin despite the possible interactions between curcumin and the amine groups of chitosan (Li et al., 2016). Hence, further studies using standardized *in vitro* digestion protocol is needed to arrive at a clear consensus on the influence of droplet size and emulsifier charge on curcumin bioaccessibility.

2.8 Conclusions and Future Outlook

Oil-in-water emulsions have been used as delivery systems for encapsulating and orally administering curcumin. The key factors affecting the stability, release, and bioaccessibility of curcumin in various emulsion-based systems are emulsion droplet size, oil composition and volume fraction, dispersion conditions of curcumin in the oil phase/oil type and structure/density/

type of interface and susceptibility of the interface to physiological breakdown. These factors may act either individually or synergistically.

Extensive studies have been performed to optimize and design effective nanoemulsion systems with improved physicochemical stability, release and bioaccessibility. Emulsions with smaller particle size tend to have better kinetic stability than that of conventional emulsions. Nevertheless, higher emulsifier concentrations are needed to produce smaller droplet size and some surfactants are allowed at significantly low levels. Furthermore, the size of the nanoemulsions seems to be altered on incorporation of micron-sized curcumin crystals. There are some evidences that nanoemulsions might result in higher degree of lipid digestion products by virtue of their high interfacial area and thus, form of higher quantities of mixed micelles. However, there is still debate on specific advantage from the bioaccessibility point of view, in using nanoemulsions versus conventional emulsions to encapsulate curcumin, which requires further investigation. Conventional emulsions on the other hand, particularly the ones stabilized by ionic surfactants, biopolymers, protein-polysaccharide complexes suffer from destabilization in the gastrointestinal regime due to their responsiveness to physiological pH, ionic strengths and enzymes. Thus,

they cannot protect the curcumin from physiological destabilization and oxidation before the encapsulated curcumin can reach the targeted sites.

Literature on Pickering emulsion for encapsulating curcumin is relatively scarce till date due to the very recent availability of laboratory-designed food-grade Pickering stabilizers. Nevertheless, at this early stage, Pickering emulsion shows promises in terms of *in vitro* gastrointestinal stability and barrier property to bile salts-induced displacement. Although bioaccessibility studies in nanoemulsions have been well documented in literature, very few studies have been conducted to assess the bioaccessibility of curcumin using Pickering emulsion approach. Further research is needed in this area of Pickering emulsions stabilized by intact or fused layer of particles of biodegradable origin to create highly stable emulsion that can be used to deliver curcumin. It will be important to identify innovative design principles for these Pickering emulsions to release the encapsulated curcumin in a controlled manner in targeted sites in human physiology and generate mechanistic insights in mixed micelles formation. Finally, designing emulsion structures loaded with curcumin together with mapping of their physical, chemical and biological fates during physiological lipid digestion (using *in vitro*, *in vivo* and clinical trials) is necessary to rationally design future curcumin-rich food, pharmaceuticals and nutraceuticals.

Based on the knowledge gap identified, in this thesis focus will be given to the fabrication of biocompatible soft heat-set gel particles (*i.e.* nano and microgel particles in this thesis) from whey protein isolate and dextran, and two types of interactions (*i.e.* electrostatic and covalent) between the same constituents to create complex particulate Pickering interfaces. Pickering emulsions stabilized by whey protein isolate nanogels will be studied as encapsulation systems for curcumin as a function of different pH values and ionic strengths (**Chapter 3**). Then, the electrostatic interaction between the developed Pickering emulsion and the polysaccharide dextran sulphate will be studied and the degree of *in vitro* gastric destabilization will be assessed (**Chapter 4**). Covalent conjugation at different degrees will be used to develop novel microgel particles and the stability of the corresponding Pickering emulsions during *in vitro* gastric digestion will be evaluated (**Chapter 5**). Finally, the bioaccessibility and cellular uptake of curcumin will be examined once it is encapsulated in the three different Pickering emulsions and their fate after *in vitro* gastrointestinal digestion will be examined (**Chapter 6**).

2.9 References

- Abbas, S., Bashari, M., Akhtar, W., Li, W. W., & Zhang, X. (2014). Process optimization of ultrasound-assisted curcumin nanoemulsions stabilized by OSA-modified starch. *Ultrasonics Sonochemistry*, 21, 1265-1274.
- Abbas, S., Karangwa, E., Bashari, M., Hayat, K., Hong, X., H. R. Sharif, & Zhang, X. (2015). Fabrication of polymeric nanocapsules from curcumin-loaded nanoemulsion templates by self-assembly. *Ultrasonics Sonochemistry*, 23, 81-92.
- Ahmed, K., Li, Y., McClements, D. J., & Xiao, H. (2012). Nanoemulsion- and emulsion-based delivery systems for curcumin: Encapsulation and release properties. *Food Chemistry*, 132, 799-807.
- Ak, T., & Gülçin, İ. (2008). Antioxidant and radical scavenging properties of curcumin. *Chemico-Biological Interactions*, 174, 27-37.
- Akhtar, M., & Ding, R. (2017). Covalently cross-linked proteins & polysaccharides: Formation, characterisation and potential applications. *Current Opinion in Colloid & Interface Science*, 28, 31-36.
- Anitha, A., Deepagan, V. G., Divya Rani, V. V., Menon, D., Nair, S. V., & Jayakumar, R. (2011). Preparation, characterization, *in vitro* drug release and biological studies of curcumin loaded dextran sulphate–chitosan nanoparticles. *Carbohydrate Polymers*, 84, 1158-1164.
- Anuchapreeda, S., Fukumori, Y., Okonogi, S., & Ichikawa, H. (2012a). Preparation of Lipid Nanoemulsions Incorporating Curcumin for Cancer Therapy. *Journal of Nanotechnology*, 2012, 1-11.
- Anuchapreeda, S., Fukumori, Y., Okonogi, S., & Ichikawa, H. (2012b). Preparation of lipid nanoemulsions incorporating curcumin for cancer therapy. *Journal of Nanotechnology*, 2012, 11.
- Armand, M., Pasquier, B., André, M., Borel, P., Senft, M., Peyrot, J., Salducci, J., Portugal, H., Jaussan, V., & Lairon, D. (1999). Digestion and absorption of 2 fat emulsions with different droplet sizes in the human digestive tract. *The American Journal of Clinical Nutrition*, 70, 1096-1106.
- Aveyard, R., Binks, B. P., & Clint, J. H. (2003). Emulsions stabilised solely by colloidal particles. *Advances in Colloid & Interface Science*, 100, 503-546.
- Balasubramanian, K. (2006). Molecular orbital basis for yellow curry spice curcumin's prevention of alzheimer's disease. *Journal of Agricultural and Food Chemistry*, 54, 3512-3520.

Bansal, S. S., Goel, M., Aqil, F., Vadhanam, M. V., & Gupta, R. C. (2011). Advanced drug-delivery systems of curcumin for cancer chemoprevention. *Cancer prevention research (Philadelphia, Pa.)*, 4, 1158-1171.

Belton, P. S., Delgadillo, I., Halford, N. G., & Shewry, P. R. (2006). Kafirin structure and functionality. *Journal of Cereal Science*, 44, 272-286.

Bisht, S., Feldmann, G., Soni, S., Ravi, R., Karikar, C., Maitra, A., & Maitra, A. (2007). Polymeric nanoparticle-encapsulated curcumin ("nanocurcumin"): a novel strategy for human cancer therapy. *Journal of Nanobiotechnology*, 5, 3.

Borriñ, T. R., Georges, E. L., Moraes, I. C. F., & Pinho, S. C. (2016). Curcumin-loaded nanoemulsions produced by the emulsion inversion point (EIP) method: An evaluation of process parameters and physico-chemical stability. *Journal of Food Engineering*, 169, 1-9.

Boruah, B., Saikia, P. M., & Dutta, R. K. (2012). Binding and stabilization of curcumin by mixed chitosan–surfactant systems: A spectroscopic study. *Journal of Photochemistry and Photobiology A: Chemistry*, 245, 18-27.

Cheng, A.-L., Hsu, C.-H., Lin, J.-K., Hsu, M.-M., Ho, Y.-F., Shen, T.-S., Ko, J.-Y., Lin, J.-T., Lin, B.-R., & Ming-Shiang, W. (2001). Phase I clinical trial of curcumin, a chemopreventive agent, in patients with high-risk or pre-malignant lesions. *Anticancer Research*, 21, 2895-2900.

Cui, J., Yu, B., Zhao, Y., Zhu, W., Li, H., Lou, H., & Zhai, G. (2009). Enhancement of oral absorption of curcumin by self-microemulsifying drug delivery systems. *International Journal of Pharmaceutics*, 371, 148-155.

de Folter, J. W. J., van Ruijven, M. W. M., & Velikov, K. P. (2012). Oil-in-water Pickering emulsions stabilized by colloidal particles from the water-insoluble protein zein. *Soft Matter*, 8, 6807-6815.

Devraj, R., Williams, H. D., Warren, D. B., Mullertz, A., Porter, C. J. H., & Pouton, C. W. (2013). *In vitro* digestion testing of lipid-based delivery systems: Calcium ions combine with fatty acids liberated from triglyceride rich lipid solutions to form soaps and reduce the solubilization capacity of colloidal digestion products. *International Journal of Pharmaceutics*, 441, 323-333.

Dickinson, E. (2009). Hydrocolloids as emulsifiers and emulsion stabilizers. *Food Hydrocolloids*, 23, 1473-1482.

Dickinson, E. (2012). Use of nanoparticles and microparticles in the formation and stabilization of food emulsions. *Trends in Food Science & Technology*, 24, 4-12.

- Dickinson, E. (2017). Biopolymer-based particles as stabilizing agents for emulsions and foams. *Food Hydrocolloids*, 68, 219-231.
- Fernández-García, E., Carvajal-Lérida, I., & Pérez-Gálvez, A. (2009). *In vitro* bioaccessibility assessment as a prediction tool of nutritional efficiency. *Nutrition Research*, 29, 751-760.
- Fu, T.-J., Abbott, U. R., & Hatzos, C. (2002). Digestibility of food allergens and nonallergenic proteins in simulated gastric fluid and simulated intestinal fluid comparative study. *Journal of Agricultural & Food Chemistry*, 50, 7154-7160.
- Fujisawa, S., Atsumi, T., Mariko Ishihara, & Yoshinori Kadoma. (2004). Cytotoxicity, ROS-generation Activity and Radical-scavenging Activity of Curcumin and Related Compounds. *Anticancer Research*, 24, 563-570.
- Goel, A., Kunnumakkara, A. B., & Aggarwal, B. B. (2008). Curcumin as “Curecumin”: From kitchen to clinic. *Biochemical Pharmacology*, 75, 787-809.
- Goh, K. K. T., Sarkar, A., & Singh, H. (2008). Chapter 12 - Milk protein–polysaccharide interactions. In *Milk Proteins* (pp. 347-376). San Diego: Academic Press.
- Goh, K. K. T., Sarkar, A., & Singh, H. (2014). Chapter 13 - Milk Protein–Polysaccharide Interactions. In *Milk Proteins* (Second edition) (pp. 387-419). San Diego: Academic Press.
- Gong, C., Wu, Q., Wang, Y., Zhang, D., Luo, F., Zhao, X., Wei, Y., & Qian, Z. (2013). A biodegradable hydrogel system containing curcumin encapsulated in micelles for cutaneous wound healing. *Biomaterials*, 34, 6377-6387.
- Hasan, M., Belhaj, N., Benachour, H., Barberi-Heyob, M., Kahn, C. J. F., Jabbari, E., Linder, M., & Arab-Tehrany, E. (2014). Liposome encapsulation of curcumin: Physico-chemical characterizations and effects on MCF7 cancer cell proliferation. *International Journal of Pharmaceutics*, 461, 519-528.
- Heger, M., Golen, R. F. v., Broekgaarden, M., & Michel, M. C. (2014). The molecular basis for the pharmacokinetics and pharmacodynamics of curcumin and its metabolites in relation to cancer. *Pharmacological Reviews*, 66, 222-307.
- Jagannathan, R., Abraham, P. M., & Poddar, P. (2012). Temperature-dependent spectroscopic evidences of curcumin in aqueous medium: A mechanistic study of its solubility and stability. *The Journal of Physical Chemistry B*, 116, 14533-14540.
- Joung, H. J., Choi, M.-J., Kim, J. T., Park, S. H., Park, H. J., & Shin, G. H. (2016). Development of food-grade curcumin nanoemulsion and its potential application to food beverage system: Antioxidant property and *in vitro* digestion. *Journal of Food Science*, 81, N745-N753.

Jovanovic, S. V., Steenken, S., Boone, C. W., & Simic, M. G. (1999). H-atom transfer is a preferred antioxidant mechanism of curcumin. *Journal of the American Chemical Society*, 121, 9677-9681.

Kakkar, V., Singh, S., Singla, D., & Kaur, I. P. (2011). Exploring solid lipid nanoparticles to enhance the oral bioavailability of curcumin. *Molecular Nutrition & Food Research*, 55, 495-503.

Khopde, S. M., Indira Priyadarsini, K., Palit, D. K., & Mukherjee, T. (2000). Effect of solvent on the excited state photophysical properties of curcumin. *Photochemistry and Photobiology*, 72, 625-631.

Kido, Y., Hiramoto, S., Murao, M., Horio, Y., Miyazaki, T., Kodama, T., & Nakabou, Y. (2003). ϵ -Polylysine inhibits pancreatic lipase activity and suppresses postprandial hypertriacylglyceridemia in rats. *The Journal of Nutrition*, 133, 1887-1891.

Kolev, T. M., Velcheva, E. A., Stamboliyska, B. A., & Spiteller, M. (2005). DFT and experimental studies of the structure and vibrational spectra of curcumin. *International Journal of Quantum Chemistry*, 102, 1069-1079.

Kumar, A., Kaur, G., Kansal, S. K., Chaudhary, G. R., & Mehta, S. K. (2016). (Cationic+nonionic) mixed surfactant aggregates for solubilisation of curcumin. *The Journal of Chemical Thermodynamics*, 93, 115-122.

Kurniawansyah, F., Mammucari, R., & Foster, N. R. (2017). Polymorphism of curcumin from dense gas antisolvent precipitation. *Powder Technology*, 305, 748-756.

Laguna, L., Picouet, P., Guàrdia, M. D., Renard, C. M. G. C., & Sarkar, A. (2017). *In vitro* gastrointestinal digestion of pea protein isolate as a function of pH, food matrices, autoclaving, high-pressure and re-heat treatments. *LWT - Food Science and Technology*, 84, 511-519.

Li, J., Hwang, I.-C., Chen, X., & Park, H. J. (2016). Effects of chitosan coating on curcumin loaded nano-emulsion: Study on stability and *in vitro* digestibility. *Food Hydrocolloids*, 60, 138-147.

Lin, C.-C., Lin, H.-Y., Chen, H.-C., Yu, M.-W., & Lee, M.-H. (2009). Stability and characterisation of phospholipid-based curcumin-encapsulated microemulsions. *Food Chemistry*, 116, 923-928.

Liu, J., Svärd, M., Hippen, P., & Rasmuson, Å. C. (2015). Solubility and crystal nucleation in organic solvents of two polymorphs of curcumin. *Journal of Pharmaceutical Sciences*, 104, 2183-2189.

Liu, Y., & Guo, R. (2008). pH-dependent structures and properties of casein micelles. *Biophysical Chemistry*, 136, 67-73.

Luo, Z., Murray, B. S., Ross, A.-L., Povey, M. J. W., Morgan, M. R. A., & Day, A. J. (2012). Effects of pH on the ability of flavonoids to act as Pickering emulsion stabilizers. *Colloids and Surfaces B: Biointerfaces*, 92, 84-90.

Ma, P., Zeng, Q., Tai, K., He, X., Yao, Y., Hong, X., & Yuan, F. (2017a). Preparation of curcumin-loaded emulsion using high pressure homogenization: Impact of oil phase and concentration on physicochemical stability. *LWT - Food Science and Technology*, 84, 34-46.

Malik, P., Ameta, R. K., & Singh, M. (2016). Physicochemical study of curcumin in oil driven nanoemulsions with surfactants. *Journal of Molecular Liquids*, 220, 604-622.

Marefati, A., Bertrand, M., Sjöö, M., Dejmek, P., & Rayner, M. (2017). Storage and digestion stability of encapsulated curcumin in emulsions based on starch granule Pickering stabilization. *Food Hydrocolloids*, 63, 309-320.

McClements, D. J. (2012a). Crystals and crystallization in oil-in-water emulsions: Implications for emulsion-based delivery systems. *Advances in Colloid and Interface Science*, 174, 1-30.

McClements. (2012b). 10 - Fabrication, characterization and properties of food nanoemulsions. In Q. Huang (Ed.), *Nanotechnology in the Food, Beverage and Nutraceutical Industries* (pp. 293-316): Woodhead Publishing.

McClements, D. J. (2015). *Food emulsions: Principles, practices, and techniques*: CRC press.

McClements, D. J., Decker, E. A., Park, Y., & Weiss, J. (2009). Structural design principles for delivery of bioactive components in nutraceuticals and functional foods. *Critical Reviews in Food Science and Nutrition*, 49, 577-606.

McClements, D. J., & Li, Y. (2010). Structured emulsion-based delivery systems: controlling the digestion and release of lipophilic food components. *Advances in Colloid Interface Sciences*, 159, 213-228.

McClements, D. J., & Rao, J. (2011). Food-grade nanoemulsions: Formulation, fabrication, properties, performance, biological fate, and potential toxicity. *Critical Reviews in Food Science and Nutrition*, 51, 285-330.

McClements, D. J., Saliva-Trujillo, L., Zhang, R., Zhang, Z., Zou, L., Yao, M., & Xiao, H. (2016). Boosting the bioavailability of hydrophobic nutrients, vitamins, and nutraceuticals in natural products using excipient emulsions. *Food Research International*, 88, 140-152.

Minekus, M., Alming, M., Alvito, P., Ballance, S., Bohn, T., Bourlieu, C., Carriere, F., Boutrou, R., Corredig, M., Dupont, D., Dufour, C., Egger, L., Golding, M., Karakaya,

S., Kirkhus, B., Le Feunteun, S., Lesmes, U., Macierzanka, A., Mackie, A., Marze, S., McClements, D. J., Menard, O., Recio, I., Santos, C. N., Singh, R. P., Vegarud, G. E., Wickham, M. S. J., Weitschies, W., & Brodkorb, A. (2014). A standardised static *in vitro* digestion method suitable for food - an international consensus. *Food & Function*, 5, 1113-1124.

Mishra, M. K., Sanphui, P., Ramamurty, U., & Desiraju, G. R. (2014). Solubility-hardness correlation in molecular crystals: Curcumin and sulfathiazole polymorphs. *Crystal Growth & Design*, 14, 3054-3061.

Pan, K., Zhong, Q., & Baek, S. J. (2013). Enhanced dispersibility and bioactivity of curcumin by encapsulation in casein nanocapsules. *Journal of Agricultural and Food Chemistry*, 61, 6036-6043.

Payton, F., Sandusky, P., & Alworth, W. L. (2007). NMR study of the solution structure of curcumin. *Journal of Natural Products*, 70, 143-146.

Pickering, S. U. (1907). CXCVI.-Emulsions. *Journal of the Chemical Society, Transactions*, 91, 2001-2021.

Pinheiro, A. C., Coimbra, M. A., & Vicente, A. A. (2016). *In vitro* behaviour of curcumin nanoemulsions stabilized by biopolymer emulsifiers – Effect of interfacial composition. *Food Hydrocolloids*, 52, 460-467.

Pinheiro, A. C., Lad, M., Silva, H. D., Coimbra, M. A., Boland, M., & Vicente, A. A. (2013). Unravelling the behaviour of curcumin nanoemulsions during *in vitro* digestion: Effect of the surface charge. *Soft Matter*, 9, 3147-3154.

PubChem-969516. PubChem Compound Database; CID=969516. National Centre for Biotechnology Information. <https://pubchem.ncbi.nlm.nih.gov/compound/969516> (accessed June 26, 2017). In.

Qi, J., Huang, C., He, F., & Yao, P. (2013). Heat-treated emulsions with cross-linking bovine serum albumin interfacial films and different dextran surfaces: Effect of paclitaxel delivery. *Journal of Pharmaceutical Sciences*, 102, 1307-1317.

Rachmawati, H., Edityaningrum, C. A., & Mauludin, R. (2013). Molecular inclusion complex of curcumin- β -cyclodextrin nanoparticle to enhance curcumin skin permeability from hydrophilic matrix gel. *AAPS PharmSciTech*, 14, 1303-1312.

Ramsden, W. (1903). Separation of solids in the surface-layers of solutions and 'suspensions' (observations on surface-membranes, bubbles, emulsions, and mechanical coagulation). -- Preliminary account. *Proceedings of the Royal Society of London*, 72, 156-164.

- Rao, P. J., & Khanum, H. (2016). A green chemistry approach for nanoencapsulation of bioactive compound – Curcumin. *LWT - Food Science and Technology*, 65, 695-702.
- Ravindranath, V., & Chandrasekhara, N. (1980). Absorption and tissue distribution of curcumin in rats. *Toxicology*, 16, 259-265.
- Sanphui, P., Goud, N. R., Khandavilli, U. B. R., Bhanoth, S., & Nangia, A. (2011). New polymorphs of curcumin. *Chemical Communications*, 47, 5013-5015.
- Sari, T. P., Mann, B., Kumar, R., Singh, R. R. B., Sharma, R., Bhardwaj, M., & Athira, S. (2015). Preparation and characterization of nanoemulsion encapsulating curcumin. *Food Hydrocolloids*, 43, 540-546.
- Sarkar, A., Goh, K. K. T., & Singh, H. (2009a). Colloidal stability and interactions of milk-protein-stabilized emulsions in an artificial saliva. *Food Hydrocolloids*, 23, 1270-1278.
- Sarkar, A., Goh, K. K. T., & Singh, H. (2010a). Properties of oil-in-water emulsions stabilized by β -lactoglobulin in simulated gastric fluid as influenced by ionic strength and presence of mucin. *Food Hydrocolloids*, 24, 534-541.
- Sarkar, A., Goh, K. K. T., Singh, R. P., & Singh, H. (2009b). Behaviour of an oil-in-water emulsion stabilized by β -lactoglobulin in an *in vitro* gastric model. *Food Hydrocolloids*, 23, 1563-1569.
- Sarkar, A., Horne, D. S., & Singh, H. (2010b). Interactions of milk protein-stabilized oil-in-water emulsions with bile salts in a simulated upper intestinal model. *Food Hydrocolloids*, 24, 142-151.
- Sarkar, A., Horne, D. S., & Singh, H. (2010c). Pancreatin-induced coalescence of oil-in-water emulsions in an *in vitro* duodenal model. *International Dairy Journal*, 20, 589-597.
- Sarkar, A., Murray, B., Holmes, M., Ettelaie, R., Abdalla, A., & Yang, X. (2016a). *In vitro* digestion of Pickering emulsions stabilized by soft whey protein microgel particles: Influence of thermal treatment. *Soft Matter*, 12, 3558-3569.
- Sarkar, A., & Singh, H. (2012). Oral behaviour of food emulsions. In J. Chen & L. Engelen (Eds.), *Food Oral Processing* (pp. 111-137): Wiley-Blackwell.
- Sarkar, A., & Singh, H. (2016). Emulsions and foams stabilised by milk proteins. In P. L. H. McSweeney & J. A. O'Mahony (Eds.), *Advanced Dairy Chemistry: Volume 1B: Proteins: Applied Aspects* (pp. 133-153). New York, NY: Springer New York.

Sarkar, A., Ye, A., & Singh, H. (2016b). On the role of bile salts in the digestion of emulsified lipids. *Food Hydrocolloids*, 60, 77-84.

Sarkar, A., Ye, A., & Singh, H. (2017a). Oral processing of emulsion systems from a colloidal perspective. *Food & Function*, 8, 511-521.

Sarkar, A., Zhang, S., Murray, B., Russell, J. A., & Boxal, S. (2017b). Modulating *in vitro* gastric digestion of emulsions using composite whey protein-cellulose nanocrystal interfaces. *Colloids and Surfaces B: Biointerfaces*, 158, 137-146.

Scanff, P., Savalle, B., Miranda, G., Pelissier, J. P., Guilloteau, P., & Toullec, R. (1990). *In vivo* gastric digestion of milk proteins. Effect of technological treatments. *Journal of Agricultural and Food Chemistry*, 38, 1623-1629.

Selvam, C., Jachak, S. M., Thilagavathi, R., & Chakraborti, A. K. (2005). Design, synthesis, biological evaluation and molecular docking of curcumin analogues as antioxidant, cyclooxygenase inhibitory and anti-inflammatory agents. *Bioorganic & Medicinal Chemistry Letters*, 15, 1793-1797.

Setthacheewakul, S., Mahattanadul, S., Phadoongsombut, N., Pichayakorn, W., & Wiwattanapatpee, R. (2010). Development and evaluation of self-microemulsifying liquid and pellet formulations of curcumin, and absorption studies in rats. *European Journal of Pharmaceutics and Biopharmaceutics*, 76, 475-485.

Shah, B. R., Li, Y., Jin, W., An, Y., He, L., Li, Z., Xu, W., & Li, B. (2016a). Preparation and optimization of Pickering emulsion stabilized by chitosan-tripolyphosphate nanoparticles for curcumin encapsulation. *Food Hydrocolloids*, 52, 369-377.

Shah, B. R., Zhang, C., Li, Y., & Li, B. (2016b). Bioaccessibility and antioxidant activity of curcumin after encapsulated by nano and Pickering emulsion based on chitosan-tripolyphosphate nanoparticles. *Food Research International*, 89, 399-407.

Shao, Y., & Tang, C.-H. (2016). Gel-like pea protein Pickering emulsions at pH3.0 as a potential intestine-targeted and sustained-release delivery system for β -carotene. *Food Research International*, 79, 64-72.

Sharma, R. A., Euden, S. A., Platton, S. L., Cooke, D. N., Shafayat, A., Hewitt, H. R., Marczylo, T. H., Morgan, B., Hemingway, D., Plummer, S. M., Pirmohamed, M., Gescher, A. J., & Steward, W. P. (2004). Phase I Clinical Trial of Oral Curcumin. *Biomarkers of Systemic Activity and Compliance*, 10, 6847-6854.

Sharma, R. A., Gescher, A. J., & Steward, W. P. (2005). Curcumin: The story so far. *European Journal of Cancer*, 41, 1955-1968.

Sharma, R. A., McLelland, H. R., Hill, K. A., Ireson, C. R., Euden, S. A., Manson, M. M., Pirmohamed, M., Marnett, L. J., A. J. Gescher, & W. P. Steward. (2001).

Pharmacodynamic and pharmacokinetic study of oral curcuma extract in patients with colorectal cancer. *Clinical Cancer Research*, 7, 1894-1900.

Singh, H., & Sarkar, A. (2011). Behaviour of protein-stabilised emulsions under various physiological conditions. *Advances in Colloid and Interface Science*, 165, 47-57.

Tapal, A., & Tikku, P. K. (2012). Complexation of curcumin with soy protein isolate and its implications on solubility and stability of curcumin. *Food Chemistry*, 130, 960-965.

Thorat, A. A., & Dalvi, S. V. (2014). Particle formation pathways and polymorphism of curcumin induced by ultrasound and additives during liquid antisolvent precipitation. *CrystEngComm*, 16, 11102-11114.

Thorat, A. A., & Dalvi, S. V. (2015). Solid-state phase transformations and storage stability of curcumin polymorphs. *Crystal Growth & Design*, 15, 1757-1770.

Tikekar, R. V., Pan, Y., & Nitin, N. (2013). Fate of curcumin encapsulated in silica nanoparticle stabilized Pickering emulsion during storage and simulated digestion. *Food Research International*, 51, 370-377.

Tokle, T., Mao, Y., & McClements, D. J. (2013). Potential biological fate of emulsion-based delivery systems: Lipid particles nanolaminated with lactoferrin and β -lactoglobulin coatings. *Pharmaceutical Research*, 30, 3200-3213.

Tønnesen, H. H., & Karlsen, J. (1985). Studies on curcumin and curcuminoids. *Zeitschrift für Lebensmittel-Untersuchung und Forschung*, 180, 402-404.

Tønnesen, H. H., Karlsen, J., & Mostad, A. (1982). Structural studies of curcuminoids. I. The crystal structure of curcumin. *Acta Chemica Scandinavica*, 36b, 475-479.

Tønnesen, H. H., Karlsen, J., & van Henegouwen, G. B. (1986). Studies on curcumin and curcuminoids. VIII. Photochemical stability of curcumin. *Zeitschrift für Lebensmittel-Untersuchung und Forschung*, 183, 116-122.

Tønnesen, H. H., Másson, M., & Loftsson, T. (2002). Studies of curcumin and curcuminoids. XXVII. Cyclodextrin complexation: solubility, chemical and photochemical stability. *International Journal of Pharmaceutics*, 244, 127-135.

Vecchione, R., Quagliariello, V., Calabria, D., Calcagno, V., De Luca, E., Iaffaioli, R. V., & Netti, P. A. (2016). Curcumin bioavailability from oil in water nano-emulsions: *In vitro* and *in vivo* study on the dimensional, compositional and interactional dependence. *Journal of Controlled Release*, 233, 88-100.

Wang, C., Liu, Z., Xu, G., Yin, B., & Yao, P. (2016). BSA-dextran emulsion for protection and oral delivery of curcumin. *Food Hydrocolloids*, 61, 11-19.

- Wang, X., Jiang, Y., Wang, Y.-W., Huang, M.-T., Ho, C.-T., & Huang, Q. (2008). Enhancing anti-inflammation activity of curcumin through O/W nanoemulsions. *Food Chemistry*, 108, 419-424.
- Wang, Y.-J., Pan, M.-H., Cheng, A.-L., Lin, L.-I., Ho, Y.-S., Hsieh, C.-Y., & Lin, J.-K. (1997). Stability of curcumin in buffer solutions and characterization of its degradation products. *Journal of Pharmaceutical and Biomedical Analysis*, 15, 1867-1876.
- Xiao, J., Li, C., & Huang, Q. (2015). Kafirin nanoparticle-stabilized Pickering emulsions as oral delivery vehicles: Physicochemical stability and *in vitro* digestion profile. *Journal of Agricultural and Food Chemistry*, 63, 10263-10270.
- Xiao, J., Wang, X., Gonzalez, A. J. P., & Huang, Q. (2016). Kafirin nanoparticles-stabilized Pickering emulsions: Microstructure and rheological behaviour. *Food Hydrocolloids*, 54, 30-39.
- Xiao, J., Wang, X. a., Perez Gonzalez, A. J., & Huang, Q. (2016). Kafirin nanoparticles-stabilized Pickering emulsions: Microstructure and rheological behaviour. *Food Hydrocolloids*, 54, Part A, 30-39.
- Xu, D., Zhang, J., Cao, Y., Wang, J., & Xiao, J. (2016). Influence of microcrystalline cellulose on the microrheological property and freeze-thaw stability of soybean protein hydrolysate stabilized curcumin emulsion. *LWT - Food Science and Technology*, 66, 590-597.
- Xu, G., Wang, C., & Yao, P. (2017). Stable emulsion produced from casein and soy polysaccharide compacted complex for protection and oral delivery of curcumin. *Food Hydrocolloids*, 71, 108-117.
- Yu, H., & Huang, Q. (2010). Enhanced *in vitro* anti-cancer activity of curcumin encapsulated in hydrophobically modified starch. *Food Chemistry*, 119, 669-674.
- Yusoff, A., & Murray, B. S. (2011). Modified starch granules as particle-stabilizers of oil-in-water emulsions. *Food Hydrocolloids*, 25, 42-55.
- Zhang, R., & McClements, D. J. (2016). Enhancing nutraceutical bioavailability by controlling the composition and structure of gastrointestinal contents: Emulsion-based delivery and excipient systems. *Food Structure*, 10, 21-36.
- Zhao, Z., Xie, M., Li, Y., Chen, A., Li, G., Zhang, J., Hu, H., Wang, X., & Li, S. (2015). Formation of curcumin nanoparticles via solution-enhanced dispersion by supercritical CO₂. *International Journal of Nanomedicine*, 10, 3171-3181.
- Zheng, B., Zhang, Z., Chen, F., Luo, X., & McClements, D. J. (2017). Impact of delivery system type on curcumin stability: Comparison of curcumin degradation in aqueous solutions, emulsions, and hydrogel beads. *Food Hydrocolloids*, 71, 187-197.

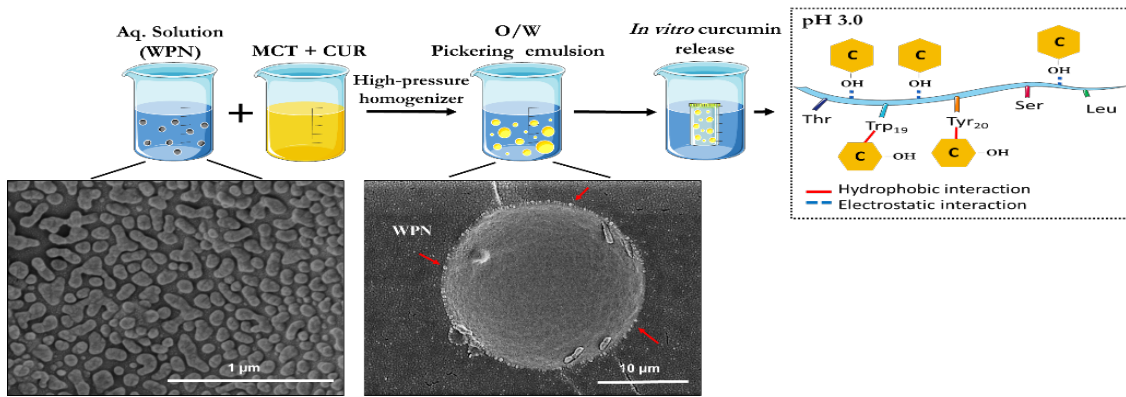
Zou, L., Liu, W., Liu, C., Xiao, H., & McClements, D. J. (2015a). Utilizing food matrix effects to enhance nutraceutical bioavailability: increase of curcumin bioaccessibility using excipient emulsions. *Journal in Agricultural Food Chemistry*, 63, 2052-2062.

Zou, L., Zheng, B., Liu, W., Liu, C., Xiao, H., & McClements, D. J. (2015b). Enhancing nutraceutical bioavailability using excipient emulsions: Influence of lipid droplet size on solubility and bioaccessibility of powdered curcumin. *Journal of Functional Foods*, 15, 72-83.

Zou, L., Zheng, B., Zhang, R., Zhang, Z., Liu, W., Liu, C., Zhang, G., Xiao, H., & McClements, D. J. (2016). Influence of lipid phase composition of excipient emulsions on curcumin solubility, stability, and bioaccessibility. *Food Biophysics*, 11, 213-225.

Chapter 3

Pickering emulsion stabilized by protein nanogel particles for delivery of curcumin: Effects of pH and ionic strength on curcumin retention²



Abstract

This study aimed to design whey protein nanogel particles (WPN)-stabilized Pickering emulsion as a delivery vehicle for curcumin (CUR). Firstly, the effectiveness of WPN to stabilize medium chain triglyceride (MCT) oil was assessed using droplet sizing, microscopy across scales, surface coverage calculations and interfacial viscosity measurements. Then, the ability of this delivery vehicle to encapsulate CUR and the effects of pH and ionic strengths on the retention of CUR were investigated in an *in vitro* release model at 37 °C. Results demonstrate that 1.0 wt% WPN was sufficient to create a monolayer of particles at the droplet surface resulting in ultra-stable droplets that were resistant to coalescence over a year. Addition of 500 µg/ mL of CUR did not result in any change in the droplet size of the Pickering emulsion droplets. The CUR was fully retained within the Pickering emulsions, which might be attributed to the nanometric size of the gaps (≈ 30 nm) at the interface that did not allow CUR to diffuse out into the release media. The partitioning of CUR to the dispersed phase was influenced by pH of the media. Increased binding affinities between CUR and WPN at the interface (binding affinity constant, $K_a = 1 \times 10^4$ M⁻¹) existed at pH 3.0 as compared to that at pH 7.0 ($K_a = 6.67 \times 10^1$ M⁻¹) owing to the

² Published as: Araiza-Calahorra, A., & Sarkar, A. (2019a). Pickering emulsion stabilized by protein nanogel particles for delivery of curcumin: Effects of pH and ionic strength on curcumin retention. *Food Structure*, 21, 100 – 113. DOI: <https://doi.org/10.1016/j.foostr.2019.100113>

electrostatic interactions between CUR and interfacial WPN in the former. Such binding affinities between CUR and interfacial WPN at pH 7.0 was further influenced by presence of ions.

3.1 Introduction

Over more than a century ago, in 1904, Walter Ramsden first mentioned that “solid matter has the power of forming persistent emulsions” (Ramsden, 1904). After three years, Pickering published an extensive experimental study on particle-stabilized emulsions for plant spray applications, from which the term "Pickering emulsions" was coined (Pickering, 1907). In an oil-in-water Pickering emulsion, particles are irreversibly adsorbed at the oil-in-water interface due to their high energy of adsorption (thousands of kT/particle). Irreversible adsorption of micro- or nano particles to the oil-water interface provides ultra-stability against coalescence and Ostwald ripening (Dickinson, 2012).

In recent years, there has been an upsurge of research efforts in designing Pickering emulsions to overcome stability issues in conventional emulsions (Araiza-Calahorra et al., 2018; Gupta and Rousseau, 2012; McClements., 2012). Moreover, in the research domain of delivery of bioactive lipophilic molecules, such as curcumin, Pickering emulsion stabilized by food-grade laboratory-synthesized particles have been recently recognized as promising templates (Araiza-Calahorra et al., 2018).

Curcumin (CUR), the main curcuminoid present in the *Curcuma longa* plant, has been used in traditional medicine for many centuries in Asian countries (Goel et al., 2008). More recently, its potent free-radical scavenging activity has been reported to play an important role on its multiple health-promoting properties such as anti-inflammatory, anti-carcinogenic, anti-diabetic, anti-aging and anti-oxidant activities (Wilken et al., 2011). The free-radical quenching properties of CUR is attributed to its chemical structure. The structure consists of two aromatic rings connected by seven carbons that hold two α , β -unsaturated carbonyl groups (Payton et al., 2007). However, the main drawbacks for the industrial applications of CUR as a nutraceutical or pharmaceutical ingredient are its low water-solubility, alkaline degradation and chemical instability, which reduces its bioavailability when orally administered (Araiza-Calahorra et al., 2018).

Recently, Pickering emulsions have been used to encapsulate CUR as the formation of a mechanical barrier by the particles can protect the encapsulated CUR against pro-oxidants and thus potentially enhance the physical and chemical stability of these bioactive compounds (Wang et al., 2015). For example, Pickering stabilizers that have been used in literature specifically for encapsulating CUR include silica (Tikekar et al.,

2013), chitosan-tripolyphosphate nanoparticles (CS/TPP NPs) (Shah et al., 2016a,b), zein-tannic acid complex colloidal particles (Zou et al., 2015), starch granules (Marefati et al., 2017), kafirin (Xiao et al., 2015a) and gliadin particles (Zhou et al., 2018). Particularly, CUR-loaded Pickering emulsions stabilized by biocompatible sub-micron sized CS/TPP NPs, ranging from 322 to 814 nm size have been recently demonstrated to be stable for 30 days (25 °C) with a CUR half-life degradation (50 wt%) of 120 hours (22 °C, in the dark) (Shah et al., 2016b). In another example of Pickering stabilizers used for encapsulating CUR, hydrophobically modified starch granule-stabilized Pickering emulsions were developed to assess the stability and loss of encapsulated CUR (Marefati et al., 2017). When samples were not subjected to a heat treatment, release of encapsulated CUR was higher during storage as compared to that of heat-treated emulsions. Authors suggested that the large particles size of starch granules (d_{43} of granules $\sim 1.8 \mu\text{m}$) allowed rather faster release of the CUR through the gaps at the oil-water interface between these micron-sized starch granules. On the contrary, heat-treated emulsions presented a rather fused barrier of partially gelatinized starch granules at the interface, most likely closing those interfacial gaps, which retained the encapsulated CUR more efficiently. An alternative approach to reduce the size of the interfacial gaps might be to reduce the size of the Pickering stabilizers to a nanometric size. Up until now, use of Pickering emulsions for delivering CUR is a relatively new field, and literature on the influence of interfacial properties on CUR retention is relatively scarce till date.

Besides polysaccharide-based particles, protein-based particles as Pickering stabilizers have attracted significant research attention as a potential formulation approach to develop functional food materials (Dickinson, 2012, 2017; Sağlam et al., 2014; Sarkar et al., 2019). Particularly, in case of protein, two classes of particles have been used by previous researchers, namely 'nanoparticles' and 'gel particles'. The protein-based nanoparticles are prepared by delicately balancing the attractive and repulsive forces of proteins. During such nanoparticle formation, change in pH, ions or solvent addition cause unfolding of dilute solutions of protein and exposure of functional groups (Liu et al., 2017; Peinado et al., 2010; Xiao et al., 2015b). Subsequent thermal or chemical crosslinking leads to the formation of cross-linked nanoparticles. The most common preparation methods for protein nanoparticles are coacervation, solvent extraction, electrospray etc. (Jain et al., 2018; Verma et al., 2018).

On the other hand, protein-based gel particles are new entrants to the food-based particle library, these can be either microgels (micron-sized) or nanogels or (nanometric-sized) (Matsumiya and Murray, 2016; Sarkar et al., 2018a; Sarkar et al., 2016). These protein microgels or nanogels are soft colloidal particles that are

produced by using a top-down technique of forming a physically cross-linked heat-set hydrogel prepared by using highly concentrated protein solutions, followed by breaking them down to gel particles under high shear forces. A combination of steric and electrostatic repulsions confers good colloidal stability to these particles in aqueous dispersions (Dickinson, 2017). Although protein microgels has been previously reported in the literature as Pickering stabilizers, controlled shearing to create protein nanogels and making Pickering emulsions with the latter has been rare until recently (Sarkar et al., 2018a). In particular, to our knowledge, this is the first study that reports the encapsulation and stability of bioactive compounds in emulsions stabilized by whey protein nanogel particles.

Therefore, in the present work, we aimed to design oil-in-water Pickering emulsions stabilized by nanometric-sized gel protein particle as a new encapsulation system for CUR. We have created protein-based nanogel particles, hereafter named as whey protein nanogel particles (WPN) with a mean hydrodynamic diameter of < 100 nm size. It was hypothesized that due to the formation of a closely packed mechanical barrier and reduced interstitial gap size, WPN-stabilized Pickering emulsion can serve as an effective template for allowing better retention of CUR within the emulsion system. The ability of the Pickering emulsions on preserving CUR was evaluated at different pH and ionic strengths. To our knowledge, this is the first study that has employed WPN-stabilized Pickering emulsion to encapsulate CUR and investigated the mechanisms behind pH/ ion-induced changes in CUR retention and advances the current state-of-the art on Pickering emulsion delivery vehicles for CUR. Although CUR is used in this study as a model lipophilic compound, the knowledge from this fundamental study can be used for rational designing of nanogel-stabilized oil-in-water Pickering emulsions for encapsulation of any lipophilic bioactive compound.

3.2 Materials and methods

3.2.1 Materials

Whey protein isolate (WPI) with $\geq 90\%$ protein content was gifted from Fonterra Co-operative Group Limited (Auckland, New Zealand). Curcumin, CUR ($\geq 65\%$ purity), methanol, sodium chloride, sodium hydroxide, sodium phosphate monobasic monohydrate, sodium phosphate dibasic anhydrous and hydrogen chloride were purchased from Thermo Fisher Scientific, Loughborough, UK. Heptane, acetic acid, sodium acetate, and calcium chloride were purchased from Sigma-Aldrich, Dorset, UK. The lipid phase consisted of medium-chain triglyceride (MCT-oil) Miglyol® 812 with a density of 945 kg m^{-3} at $20 \text{ }^\circ\text{C}$ (Cremer Oleo GmbH & Co, Germany). Dialysis

membranes of molecular weight cut off 3,500 Da were purchased from Thermo Scientific, Paisley, UK. All reagents were of analytical grade and used without further purification unless otherwise reported. All solutions were prepared with Milli-Q water with a resistivity of 18.2 M Ω cm at 25 °C (Milli-Q apparatus, Millipore, Bedford, UK). Sodium azide (0.02 wt %) was added as a preservative.

3.2.2 Preparation of whey protein nanogel particles

The nanogel particles were created based on modification of a previous top-down technique (Sarkar et al., 2018a; Sarkar et al., 2016). The WPI powder was dissolved in 10 mM phosphate buffer at pH 7.0 for 2 hours to prepare whey protein solution (10 wt%). The WPI solution was heated in a temperature-controlled water bath at 90 °C for 30 min to form a heat-set gel (quiescent), followed by cooling down for 15 min and storage at 4 °C overnight to form heat-set hydrogels. Obtained WPI gels were pre-homogenized with buffer (5 wt%) using a hand blender (HB724, Kenwood) for 1 minute. The resulting 5 wt% whey protein gel was passed two times through a high-pressure two-chamber homogenizer Jet homogenizer (University of Leeds, UK) at 300 bars. The resulting whey protein nanogel particles (WPN) were diluted with buffer and used as the continuous phase for the emulsion preparation. Emulsions were prepared in triplicate.

3.2.3 Preparation of whey protein nanogel-stabilized emulsions (E_{WPN}), CUR-loaded emulsions (CUR- E_{WPN}) and whey protein isolate-stabilized emulsions (E_{WPI})

Pickering emulsions (E_{WPN}) were prepared using fixed MCT oil concentration (20 wt%) and WPN of varying concentrations (0.1 - 3.0 wt%). The emulsifier concentration was changed by diluting the aqueous dispersion of WPN (5 wt% protein) with phosphate buffer (pH 7.0) to get the desired protein content in the final emulsion. Briefly, coarse WPN-stabilized emulsions (20:80 w/w) were prepared using Ultra Turrax T25 homogenizer (IKA-Werke GmbH & Co., Staufen Germany) at 13,500 rpm for 1 min. Following this, the coarse emulsions were homogenized using the Leeds Jet homogenizer at 300 bars using two passes to prepare fine E_{WPN} droplets. In case of CUR-loaded emulsions (CUR- E_{WPN}), CUR was added to the MCT-oil phase at 500 μ g/ mL and stirred at 200 rpm for 30 min at 60 °C to ensure maximum solubility before the coarse emulsion formation step. The choice of MCT-oil as the lipidic phase was to ensure maximum CUR solubility in the dispersed phase (Appendix A, Figure A1).

Emulsions stabilized by whey protein isolate solution (E_{WPI}) were prepared as controls to compare the difference in the microstructure between E_{WPN} and E_{WPI} emulsions. The E_{WPI} (20 wt% MCT oil, 1 wt% WPI) were prepared following the same protocol as described above for E_{WPN} . All emulsions samples were prepared in triplicates.

3.2.4 Transmission electron microscopy

Transmission electron microscopy (TEM) was employed to observe the microstructure of WPN, E_{WPI} and E_{WPN} samples using a previously reported method (Sarkar et al., 2018b; Sarkar et al., 2017). Briefly, 10 μ L of samples were fixed with 2.5% (v/v) glutaraldehyde and post-fixed in 0.1% (w/v) osmium tetroxide. The samples were then carefully exposed to serial dehydration in ethanol (20 - 100%) before being embedded in araldite. Ultra-thin sections (80 - 100 nm) were deposited on 3.05 mm grids and stained with 8% (v/v) uranyl acetate and lead citrate. The sections were cut on an “Ultra-cut” microtome. Images were recorded using a CM10 TEM microscope (Philips, Surrey, UK).

3.2.5 Cryogenic- Scanning Electron Microscopy

Cryogenic scanning electron microscopy (cryo-SEM) of the WPN, E_{WPI} , E_{WPN} and CUR- E_{WPN} were conducted. Particularly, for cryo-SEM of emulsion samples *i.e.* E_{WPI} , E_{WPN} and CUR- E_{WPN} , heptane was used as the dispersed rather than MCT oil, to avoid interference by crystallization of oil during the freezing step as used in a previous study involving Pickering emulsions stabilized by microgels (Destribats et al., 2014). Both the systems (heptane or MCT-oil emulsions) presented the same overall microstructural behaviour and therefore, the cryo-SEM images observed using heptane emulsions can be extrapolated to MCT-oil emulsions. The WPN, E_{WPI} , E_{WPN} or CUR- E_{WPN} were mounted on rivets attached to the sample stub. The samples were plunge-frozen in liquid nitrogen “slush” at -180 °C, then transferred to the cryo-preparation chamber on the SEM. The frozen protein nanogels or emulsion droplets were cleaved and then etched at -95 °C for 4 minutes. Next, the samples were coated with 5 nm of platinum (Pt). Finally, the Pt-coated samples were transferred to the SEM for imaging at -135 °C. The heptane emulsion sample was imaged in a FEI Quanta 200F ESEM with a Quorum Polar Prep 2000 cryo system.

3.2.6 Confocal scanning laser microscopy (CLSM)

The microstructures of the emulsions (20 wt% MCT oil) *i.e.* E_{WPI} , E_{WPN} and $CUR-E_{WPN}$ were characterized using a Zeiss LSM 880 inverted confocal microscope (Carl Zeiss MicroImaging GmbH, Jena, Germany). Also, the $CUR-E_{WPN}$ was characterized after the CUR retention experiments. A stock solution of Nile Red (1 mg/ mL in dimethyl sulfoxide, Sigma-Aldrich) was used to stain MCT-oil to a final concentration of 0.02 mg mL⁻¹ and a stock solution of Fast Green (1 mg mL⁻¹ in Milli-Q water) was used to stain the protein to a final concentration of 0.1 mg m⁻¹. The fluorescently labelled emulsion samples were placed on a concave confocal microscope slide, secured with a glass coverslip and finally imaged using an oil immersion 63× lens and the pinhole diameter maintained at 1 Airy Unit to filter out the majority of light scatter. Nile Red was excited at a wavelength of 488 nm and Fast Green at 633 nm. The emission filters were set at 555 - 620 nm for Nile Red and 660 - 710 nm for Fast Green (Ong et al., 2011).

In general, CUR is known to bind to certain hydrophobic domain of proteins. Hence, CUR binding to WPN was imaged by placing the $CUR-E_{WPN}$ emulsions directly in the slide and covered them with a glass coverslip using CUR auto-fluorescence. For imaging of CUR, the auto-fluorescence of CUR was recorded using the filters set for Nile Red dye, since CUR exhibits an excitation of 455 nm and an emission at 540 nm (Minear et al., 2011).

3.2.7 Determination of adsorption efficiency by WPN

To determine the amount of WPN at the interface of the emulsion droplets, E_{WPN} samples were centrifuged for 15 min at 1,770 g at 25 °C (Eppendorf 5702, Hamburg, Germany). Subnatants were carefully removed using a syringe and filtered through 0.45 μm filters (Perkin Elmer, Waltham, MA, USA). The process was repeated twice, and the absorbance of the filtrates was detected using a DC protein assay kit (Bio-Rad Laboratories, Watford, UK) and a UV-Vis Spectrophotometer. The protein concentration of the filtrates was determined with the Lowry method using BSA as the standard. The adsorption efficiency was calculated as the difference between the total amount of protein used for initial emulsion preparation and the amount of protein in the continuous phase as a percentage of total protein concentration.

3.2.8 Interfacial shear viscosity

The interfacial shear viscosity was measured using a two-dimensional Couette-type viscometer in presence of WPI or WPN. Details have been previously described (Murray and Dickinson, 1996; Sarkar et al., 2017). Briefly, a stainless steel biconical

disc (radius 14.5 mm) was suspended from a thin torsion wire with its edge in the plane of the oil-water interface of the solution contained within a cylindrical glass dish (radius 72.5 mm). The deflection of the disk was measured by reflection of a laser off a mirror on the spindle of the disc onto a scale at a fixed distance from the axis of the spindle. The interfacial viscometer was operated in a constant shear-rate mode, as described in a recent study (Zembyla et al., 2018). For the measurements, a layer of pure *n*-tetradecane was layered over an aqueous solution of whey protein isolate (WPI) or whey protein nanogel particles (WPN). A concentration of 0.5 wt% was used as the aqueous phase at pH 7.0. The constant shear rate apparent interfacial viscosity, η_i , is given by the following equation:

$$\eta_i = \frac{g_f}{\omega} K(\theta - \theta_0) \quad (3.1)$$

where, K is the torsion constant of the wire, θ is the equilibrium deflection of the disc in the presence of the film, θ_0 is the equilibrium deflection in the absence of the film, *i.e.* due to the drag force of the sub-phase on the disc, g_f is the geometric factor, and ω is the angular velocity of the dish. A fixed value of $\omega = 1.27 \times 10^{-3} \text{ rad s}^{-1}$ was used.

3.2.9 Droplet and particle size distribution

Droplet size distributions of the emulsion samples (E_{WPI} , E_{WPN} and $CUR-E_{WPN}$) were determined using static light scattering at 25 °C using a Malvern MasterSizer 3000 (Malvern Instruments Ltd, Malvern, Worcestershire, UK). The refractive index of the MCT-oil (Miglyol® 812 oil) and the dispersion medium were set at 1.445 and 1.33, respectively. The absorbance value of the emulsion droplets was 0.001. The mean droplet size distribution of the emulsions was reported as volume mean diameter d_{43} (De Brouckere mean diameter) and surface mean d_{32} (Sauter mean diameter). The d_{43} refers to the mean diameter of a sphere with the same volume, whereas the d_{32} is the diameter of a sphere that has the same volume/surface area ratio as the sphere of interest. Both are generally used to characterize an emulsion droplet. Particle size of the WPN was determined using dynamic light scattering (DLS) at 25 °C using a Zetasizer Nano-ZS (Malvern Instruments, Malvern UK) in a PMMA standard disposable cuvette. Particle size was measured after diluting the samples in phosphate buffer (pH 7.0). Each sample was analysed three times and the average value was reported in the result section.

3.2.10 ζ -potential

The ζ -potential of the WPN, E_{WPN}, and CUR-E_{WPN} was determined using a particle electrophoresis instrument (Zetasizer, Nano ZS series, Malvern Instruments, Worcestershire, UK). Samples were diluted in Milli-Q water (0.1 wt% particle or 0.002 wt% droplet concentration) and added to a folded capillary cell (Model DTS 1070, Malvern Instruments Ltd., Worcestershire, UK). Mean and standard deviation of the ζ -potential value of each sample was calculated from three individual measurements on triplicate samples.

3.2.11 Measurement of CUR retention in Pickering emulsions

To recover the encapsulated CUR from Pickering emulsion, the emulsions samples (200 μ L), were disrupted with methanol (1 mL). Sample-solvent mixtures were centrifuged at 1,770 g at ambient temperature for 10 min to precipitate the WPN (Marefati et al., 2017). Noteworthy, during extraction with methanol, a distinct orange-red colour was observed at neutral pH (pH 7.0) (Appendix A, Figure A2a), which can be attributed to pH-induced changes in the CUR structure. As a diarylheptanoid, CUR contains two aromatic rings joined by a seven carbons chain (heptane) with a α , β -unsaturated- β -diketone structure (Araiza-Calahorra et al., 2018). Depending on the solvent characteristics, electron delocalization and deprotonation when in neutral-alkaline environment alters the β -diketone structure undergoing *keto-enol* tautomerism (Khopde et al., 2000; Nardo et al., 2008). Alteration of the tautomerism of the structure causes the optical properties of CUR to change, causing a deviation of the spectral band position in the absorption or emission spectrum of the molecule to a longer wavelength (bathochromic shift) *i.e.* changing CUR's colour from yellow to red (Tønnesen and Karlsen, 1985). Visual appearance of CUR dilution (1:1 (v/v) methanol/buffer, 25 °C) as a function of different pH (2.0 - 7.0) can be observed in Appendix A, Figure A2b.

Hence, the supernatant of the centrifuged CUR-E_{WPN} samples at the two biologically relevant pH conditions (pH 3.0 and pH 7.0) were first diluted to appropriate concentrations for quantification of encapsulated CUR (Appendix A, Figure A3). The wavelength used was 425 nm and it was chosen based on a scan performed on methanol containing CUR ranging from 300 to 500 nm. Diluted samples were placed in a cuvette to measure the absorbance in a UV-VIS spectrophotometer (6715 UV/VIS Spectrophotometer, Jenway, UK). A standard curve of known concentrations of CUR in methanol was prepared to convert the absorbance measurements to CUR concentration.

3.2.12 CUR retention in Pickering emulsions

The capacity of the Pickering emulsions to retain CUR during short-term storage was measured based on the CUR concentration recovered from the emulsions after they were subjected to pH 3.0 or pH 7.0 in absence and presence of ions (50 mM NaCl or 10 mM CaCl₂). In brief, CUR-E_{WPN} was mixed with the appropriate buffer in a 1:0.5 w/w ratio and pH was adjusted to the desired value (pH 3.0 and 7.0) in absence or presence of 50 mM NaCl or 10 mM CaCl₂ and the mixture was placed in pre-soaked dialysis membrane (100 kDa molecular weight cut-off membrane, Spectrum Laboratories, USA). Subsequently, the membranes were suspended in buffers at corresponding pH and ionic strengths at 37 °C with agitation (90 rpm) for 30 minutes. The aqueous buffers used were sodium acetate buffer for pH 3.0, and phosphate buffer for pH 7.0. Since CUR is known to be hydrophobic with limited solubility in water, ethanol was added into the aqueous buffer solutions at a final concentration of 15 % (v/v) based on a previous study (Shah et al., 2016b). After 30 minutes, CUR-E_{WPN} samples within the dialysis membranes were taken out and CUR concentration in the emulsion sample and CUR released to the aqueous buffers was measured using the method described earlier.

3.2.13 Fluorescence measurements

Previously, ability of CUR to form complexes with numerous proteins, such as soy protein isolate or β -lactoglobulin has been reported (Chen et al., 2015; Sneharani et al., 2010). Thus, binding studies of CUR with WPN was conducted at pH 3.0 and pH 7.0 in presence or absence of ions and such interactions were measured using an adapted fluorescence emission spectroscopy method described by Sahu et al., (2008). Steady-state fluorescence measurements were carried out in a CLARIOstar microplate spectrofluorimeter reader (BMG Labtech). The fluorescence of CUR was measured by keeping its concentration constant (10 μ M) and by varying the WPN concentration (0 - 40 μ M) in either sodium acetate buffer (pH 3.0), and phosphate buffer (pH 7.0) in absence or presence of 50 mM NaCl or 10 mM CaCl₂. The emission spectra were recorded from 450 to 650 nm with an excitation wavelength of 420 nm. Solutions without WPN were used as controls for the fluorescence measurements. The binding constant was determined by the following equation (Sahu et al., 2008):

$$\frac{1}{\Delta FI} = \frac{1}{\Delta FI_{max}} + \frac{1}{K_d \Delta FI_{max} [WPN]} \quad (3.2)$$

where ΔFI is the change in the CUR fluorescence intensity in the presence and absence of WPN, ΔFI_{\max} is the maximal change in the CUR fluorescence intensity, K_a is the binding constant, and $[WPN]$ is the concentration of WPN. The intensity data were then used to plot the double-reciprocal plot $1/[CM]$ versus $1/\Delta FI$. The intercept of the double-reciprocal plot on the $1/\Delta FI$ axis is $1/\Delta FI_{\max}$, which was used to calculate the binding constant from the value of the slope in the plot.

3.2.14 Statistical analysis

The statistical software Minitab 16 (Minitab Inc. State College Pennsylvania) was used. The analysis was carried out with the three individual measurements on three individual emulsion samples (*i.e.* 9 measurements) and analysed with two-way analysis of variance (ANOVA) and Student's t-test; significance was accepted at $p < 0.05$.

3.3 Results and discussion

3.3.1 Characteristics of aqueous dispersions of WPN

The hydrodynamic diameter of WPN dispersion was determined by DLS and morphology was probed using cryo-SEM and TEM across scales (Figure 3.1). The particle size distribution was monomodal with a polydispersity index of 0.24, and a mean hydrodynamic radius of 83.05 nm (Figure 3.1a). As can be observed from the cryo-SEM image (Figure 3.1b), the size of WPN was in close agreement with DLS and WPN showed a tendency to aggregate in the observation grid (Figure 3.1b). It is difficult to comment with certainty on the sphericity of the particles because of the possible effects of preparation for cryo-SEM on particle morphology, as have been observed previously (Sarkar et al., 2017). Looking at lower length scale, the TEM image (Figure 3.1c) showed that WPN formed a hierarchical structure of aggregates of protein of different characteristic sizes as postulated by Schmitt et al. (2010) using small angle X-ray scattering experiments.

Previous researchers have shown the formation of microgel particles of spherical shape of about 200 - 500 nm (Destribats et al., 2014; Sarkar et al., 2016). Differences in size and aggregate morphology of WPN used in this study as compared to the previous reports can be attributed to the variation in the processing route, such as using the high-pressure homogeniser (Leeds Jet Homogeniser, University of Leeds, UK), which uses turbulent flow and extremely high localized pressures as compared to conventional homogenizers, as well as the initial protein concentration used to form

the hydrogel (Nicolai et al., 2011; Sarkar et al., 2017; Schmitt et al., 2011; Torres et al., 2017). The WPN exhibited an average ζ -potential value of -30.46 mV, which suggests that the electrostatic repulsion between the particles was high enough to ensure dispersion stability at pH 7.0 (Figure 3.1a). The negative charge was expected as WPN was above the isoelectric point (pI) and the value was within the range found in the literature (Destribats et al., 2014; Sarkar et al., 2016).

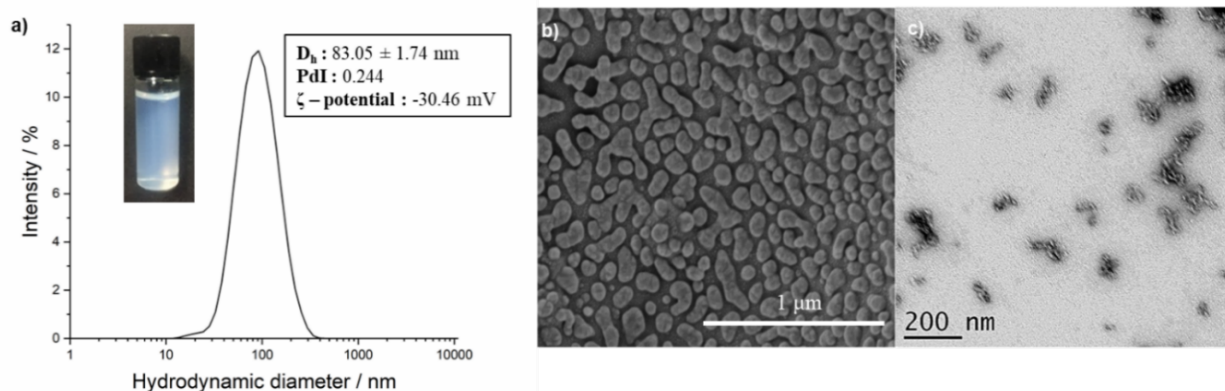


Figure 3.1. a) Intensity distribution of WPN with inset representing the visual image and physicochemical characteristics of the WPN, and micrographs of 1 wt% WPN at various length scales: b) Cryo-SEM, and c) TEM.

3.3.2 Characteristics of Pickering emulsions (EWPN)

Firstly, we conducted interfacial shear viscosity experiments and microstructural evaluation across scales to investigate whether the WPN were forming Pickering emulsions as compared to a conventional emulsion stabilized by WPI. Applying shear rheology deformation to the interfacial layers in E_{WPI} or E_{WPN} will give us information on the formation and structuring of adsorbed protein or particle layers, respectively. This method is particularly sensitive to differentiating proteins versus particles based on their interfacial flow behaviour, and consequently can give quantitative insight into difference between WPN and WPI (Murray et al., 2011; Sarkar et al., 2017). Surface shear viscosity (η_i) values for WPN were compared to those of WPI solution, both dispersed in phosphate buffer at pH 7.0. We present the measurements of η_i values at 'short' (2 and 3 h) and 'long' (24 h) adsorption time scales in Table 3.1. As expected, the value of η_s for WPI decreased from ~ 453 mN s m $^{-1}$ at 2 h to its quarter after 24 h, which in agreement with previous works with protein monolayers (Chen and Dickinson, 1995; Dickinson et al., 1990).

However, the value of η_i for WPN at the oil-water interface was twice as that of WPI in 2 h time scale. Of more interest is that the η_i became almost an order of magnitude higher than that of WPI in 24 h time scale (Table 3.1). The high values

obtained for WPN is indicative of strengthening of the interfacial films by the presence of adsorbed particles. These quantitative results perfectly corroborate with the qualitative observation of nanogel particles at the interface of the WPN-stabilized emulsions in the CLSM, cryo-SEM and TEM images (Figure 3.2).

Table 3.1. Interfacial shear viscosities (η_i / mN s m⁻¹) O/W interface in presence of whey protein isolate (WPI) and whey protein nanogel particles (WPN) at pH 7.0. Values represent mean \pm SD of at least three independent experiments (n \geq 3).

Adsorption time / h	0.5 wt% WPN	0.5 wt% WPI
2	916.13 \pm 100.83	453.22 \pm 112.46
3	969.62 \pm 75.78	334.19 \pm 55.87
24	1006.13 \pm 278.36	127.50 \pm 27.75

In particular, the sizing of the droplets (Figure 3.2) highlight that E_{WPI} droplets ($d_{43} = 0.89 \pm 0.08 \mu\text{m}$) were much smaller in size as compared to that of E_{WPN} droplets ($d_{43} = 10.29 \pm 2.31 \mu\text{m}$), which is expected owing to the larger size of WPN particles (~ 80 nm, Figure 3.1a) stabilizing the droplets in the latter as compared to protein molecule counterpart in the former (~ 2 nm). Also looking at the cryo-SEM and TEM images at different magnification (Figure 3.2), the interface of the E_{WPI} droplets did not present any visible protein molecules that is expected owing to the size of the protein molecules being smaller as compared to the microscopic resolution in agreement with previous studies (Sarkar et al., 2017). However, the particles are clearly evident at the interface of E_{WPN} droplets that confirms the Pickering stabilization by these particles providing ultra-stability to these droplets against coalescence over a year storage period (data not shown).

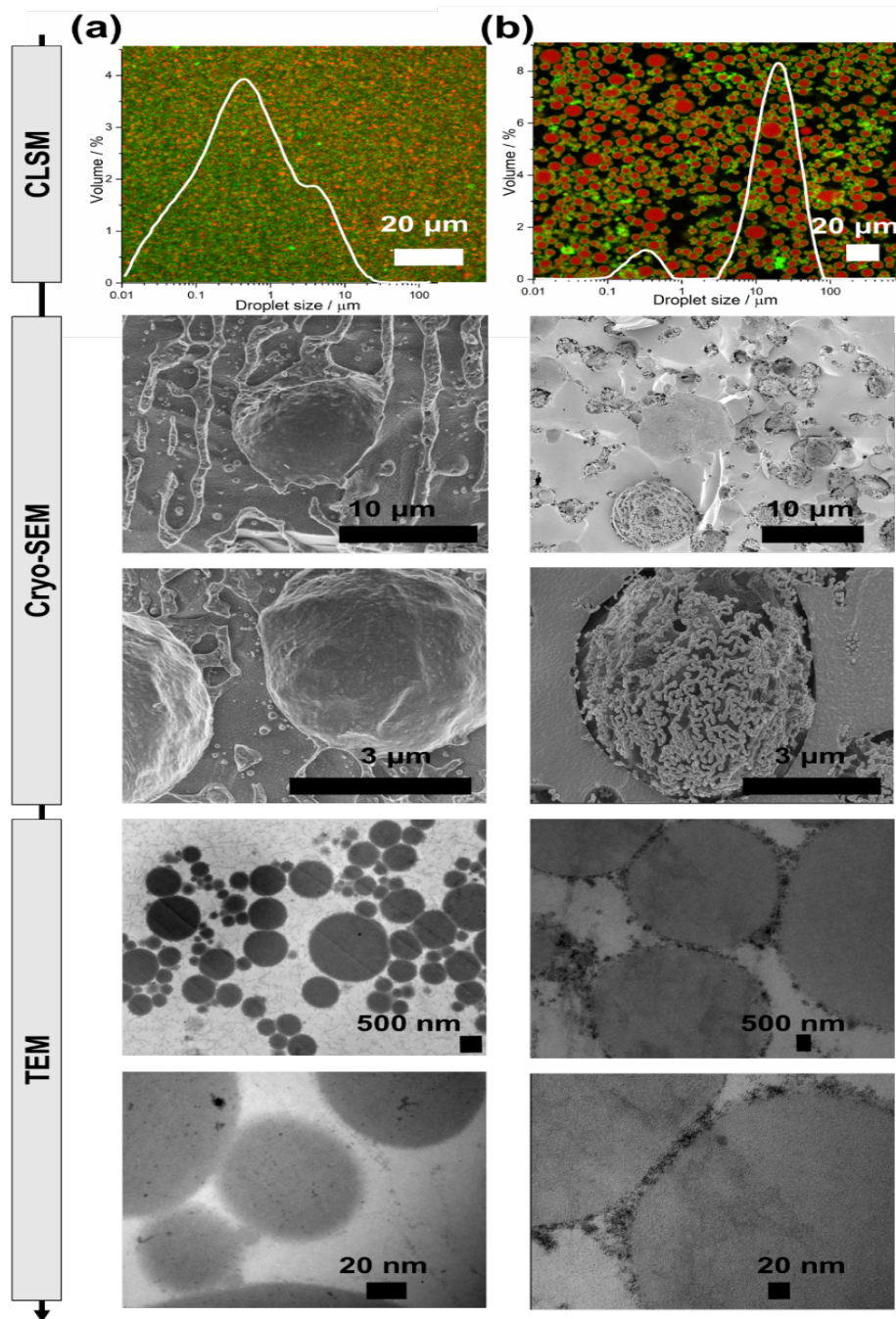


Figure 3.2. Micrographs of 20 wt% MCT-oil-in-water emulsion stabilised by a) 1 wt% WPI and b) 1 wt% WPN at pH 7.0 with superimposed droplet size distribution at multiple length scales. In Cryo-SEM, 20 wt% heptane-in-water emulsions was used.

The droplet size distribution, mean droplet size and charge of the Pickering emulsions (0.1 - 3 wt% WPN) are shown in Figures 3.3a, and b, respectively. In Figure 3.3a, it can be observed that the droplet size distribution of E_{WPN} was mostly bimodal

with two populations of droplets clearly identified except for emulsions stabilized by 0.1 - 0.5 wt% WPN. The signature peak in the area of 0.1 - 1 μm most likely corresponds to the unadsorbed WPN, which has been reported previously (Sarkar et al., 2018a; Sarkar et al., 2016), while the more prominent peak in the area of 5 to 50 μm represents the Pickering emulsion droplets. In case of 0.1 - 0.5 wt% WPN, a third peak was observed in 50 - 500 μm range highlighting either coalesced or flocculated droplets in these emulsions. When the concentrations of WPN was above 0.5 wt%, the third peak almost disappeared with increase of second peak suggesting more adsorption of particles to the droplet surface until 1.0 wt% (Figure 3.3a). However, above 1.0 wt% WPN, the percentage of the relative area of the first peak increased at the expense of the second peak, suggesting a gradual increase of unadsorbed WPN. No significant change in the mean oil droplet diameter occurred when varying the concentration of WPN, except for 0.1 - 0.25 wt% samples ($p < 0.01$) (Figure 3.3b).

The absolute magnitude of ζ -potential of all emulsions was higher as compared to that of the WPN present in the aqueous phase (Figure 3.3b) ($p < 0.05$). This increase in negative surface charge might be attributed to the concentration of WPN at the droplet surface as compared to being in the aqueous phase. Such magnitude $\geq \pm 30$ mV is generally indicative of strong electrostatic stabilization of droplets (McClements, 2004) in addition to the mechanical stabilization provided by the particles.

The maximum adsorption efficiency for these systems was calculated to be 100% (0.1 wt%) (Figure 3.3c). The absorption efficiency in emulsions prepared with higher concentrations of WPN gradually decreased to 58.34% for 3 wt% (Figure 3.3c) further supporting the unadsorbed particles seen in light scattering data (Figure 3.3b). Besides adsorption efficiency, surface coverage (C_s) was calculated to provide a useful indication of the density of the particles anchored at the oil-in-water interface for emulsions undergoing limited coalescence (Gautier et al., 2007). In principle, the percentage of interfacial area covered by the particles can be calculated using equation 3.3, as reported previously by Binks and Olusanya (2017). The simplest version of this equation assumes all the particles are adsorbed at the droplet surface and the non-adsorbed particles are neglected. Under these assumptions, equation 3.3 is defined as:

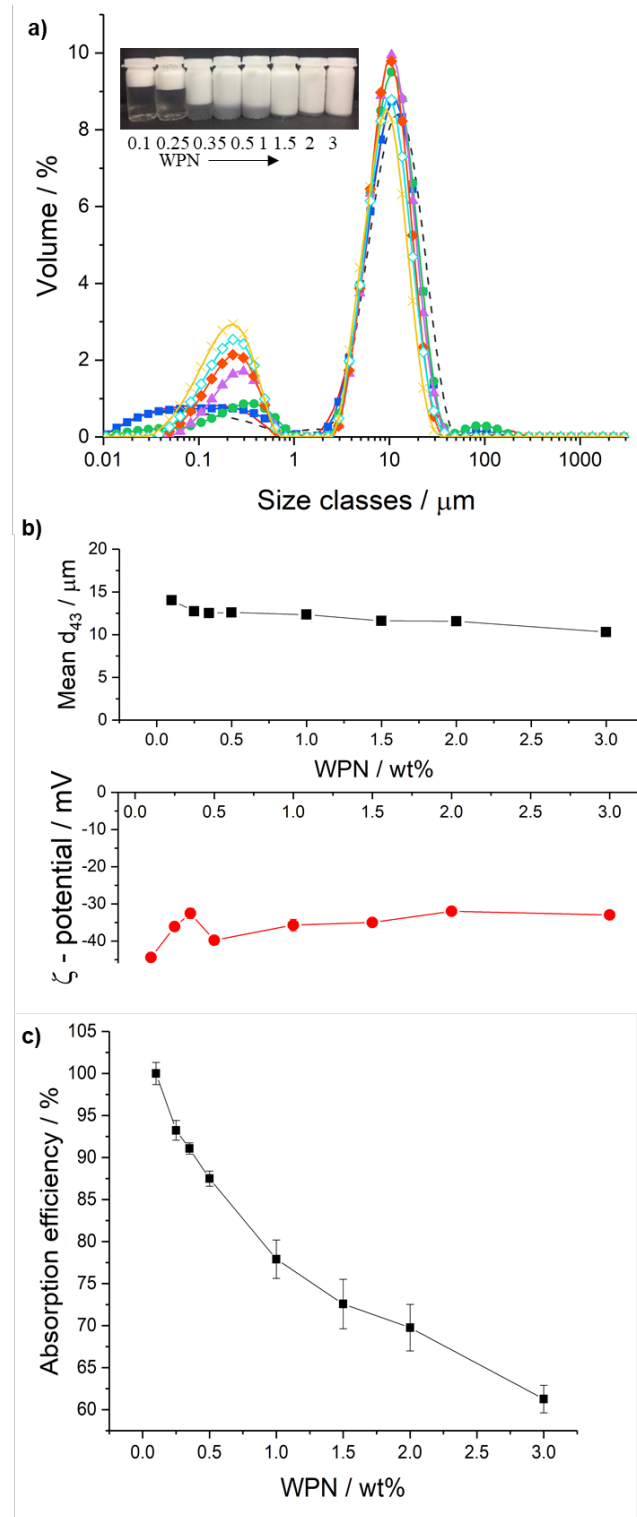


Figure 3.3. a) Droplet size distribution of 20 wt% MCT- oil-in-water emulsions stabilized by 0.1 wt% (black, dashed line), 0.25 wt% (red, solid circle), 0.35 wt% (blue, solid square), 0.5 wt% (green, solid circle), 1 wt% (purple, solid triangle), 1.5 wt% (orange, solid diamond), 2 wt% (turquoise, open diamond), 3 wt% (brown, cross) WPN, respectively, where insert represents the corresponding visual images of the Pickering emulsions, with b) mean d_{43} values (black, solid square), and ζ -potential values (red, solid circle) at pH 7, and c) corresponding absorption efficiency of WPN (black, solid square) at the droplet surface. Error bars represent standard deviation.

$$\frac{1}{d_{32}} = \frac{m_p}{4C_s V_d \rho_p d_p} \quad (3.3)$$

where, m_p is the mass of the particle, V_d the volume of the oil phase, ρ_d the density of the particle, d_d the particle radius and d_{32} is the mean droplet diameter. Assuming all particles were monodisperse and were adsorbed at the oil-water interface in a hexagonal close packing arrangement, the surface coverage should be equal to 0.907.

Below the critical concentration of the 1.0 wt%, the surface coverage obtained was significantly below 0.907 (Table 3.2). In this concentration range, it can be suggested that the droplet size was dictated by the particle concentration (Binks et al., 2005). This behaviour is typical of Pickering emulsions undergoing limited coalescence and has been reported for particles of a similar size range, such as coloured organic pigment particles, silica, and poly(glycerol monomethacrylate)-poly(2-hydroxypropyl methacrylate) (PGMA-PHPMA) diblock copolymer particles (Binks and Olusanya, 2017; Gautier et al., 2007; Thompson et al., 2014).

Table 3.2. Surface coverage of emulsion droplets by various concentrations of WPN.

WPN (wt%)	C _s
0.1	0.14
0.25	0.32
0.35	0.46
0.5	0.68
1	1.35
1.5	1.95
2	2.59
3	3.45

In the case of higher WPN concentrations (1 - 3 wt%), surface coverage was greater than 0.907, suggesting either formation of a multilayer or aggregates of WPN at the interface (Binks and Olusanya, 2017) or an excess of particles that were not adsorbed. In order to characterise the morphology of particles at the droplet surface, cryo-SEM imaging of heptane droplets covered by 1 wt% nanogel particles at pH 7.0 is shown in Figure 3.3b1. As can be clearly observed, the interface was covered by a network of particles where WPN adopted configurations of either individual particles

or a network of particle aggregates. These observations correspond to the high surface coverage as calculated and reported in Table 3.2. Such visual clarity of nanometric-sized aggregates versus nanometric sized-single particle at the droplet surface has been also previously observed in cryo-SEM images of Pickering droplets by previous authors (Destribats et al., 2014).

In summary, emulsions ≥ 0.5 wt% experienced limited coalescence in the particle-poor regime, whereas ≥ 1 wt% it transitioned towards a particle-rich regime. It is clear that within the explored concentration range, the addition of 1 wt% demonstrated to create stable droplets with complete coverage (~ 1.14 monolayers theoretically). Hence, this concentration was selected hereafter to create Pickering emulsion for encapsulation of CUR (CUR- E_{WPN}), and *in vitro* retention of CUR.

3.3.3 Characteristics of CUR-loaded Pickering emulsions

The CUR content in the CUR- E_{WPN} was 474 ± 29.4 $\mu\text{g}/\text{mL}$, which was close to the amount of 500 $\mu\text{g}/\text{mL}$ added to the oil. This suggests that CUR was not degraded or lost during the emulsification process. The size distribution of CUR- E_{WPN} was identical to the distribution of samples without the addition of CUR (E_{WPN}) (Figure 3.4a) with diameters in the former ranging between 5 and 50 μm ($p > 0.05$). This suggests that the addition of CUR did not negatively affect the droplet size of the CUR- E_{WPN} (Araiza-Calahorra et al., 2018).

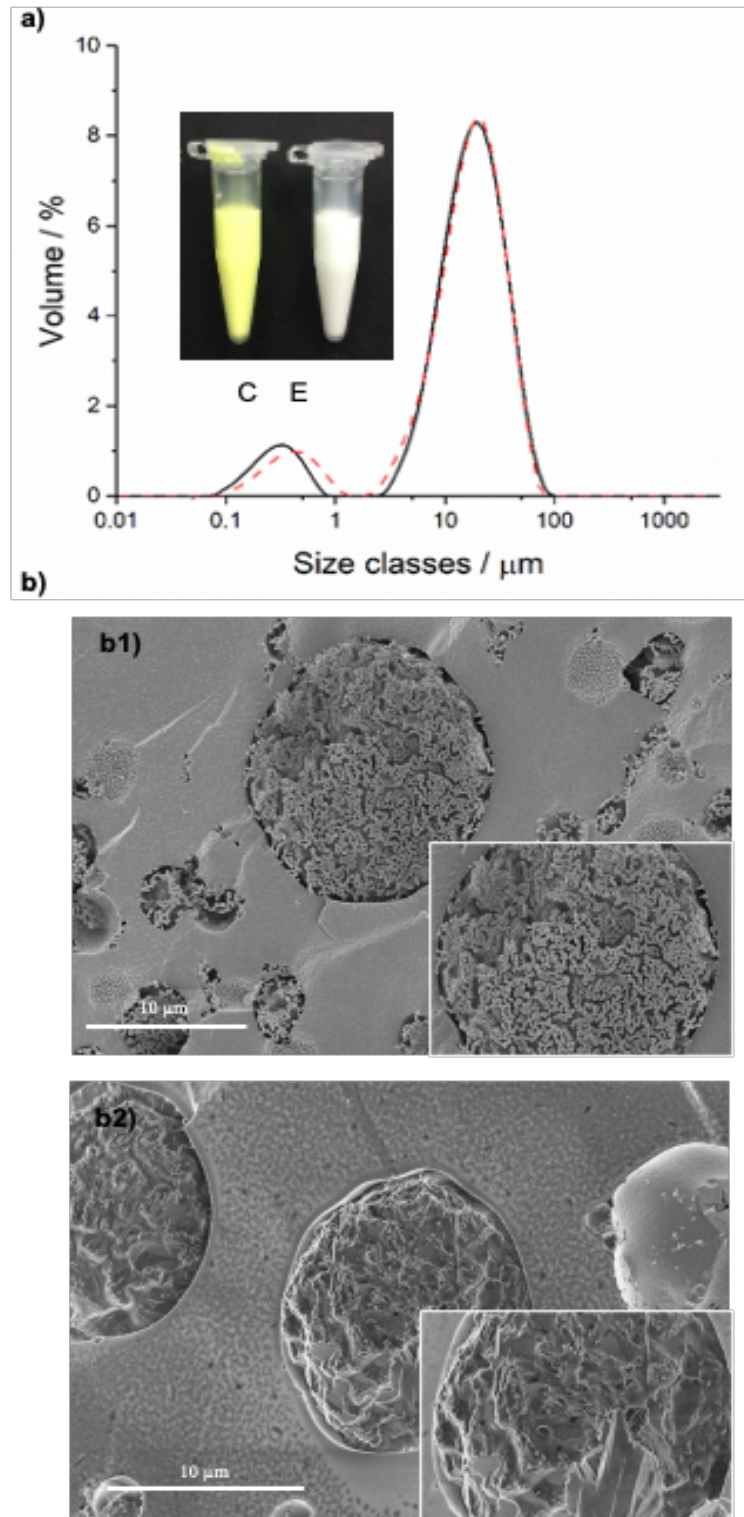


Figure 3.4. a) Droplet size distribution of emulsion-stabilized by 1 wt% WPN without curcumin (E_{WPN}) (black, solid line) or loaded with (red, dashed line) (CUR- E_{WPN}) curcumin with inset representing the corresponding emulsions, respectively *i.e.*. C and E are with and without curcumin, respectively. b) Cryo-SEM images of b1) 20 wt% heptane-in-water Pickering emulsion (E_{WPN}) stabilized by 1 wt% WPN and b2) CURE $_{\text{WPN}}$ stabilized by 1 wt% WPN.

Furthermore, the typical dimensions of empty spaces (Sarkar et al. 2016) between the WPN arranged on the triangular lattice ($((\sqrt{3}-1)d_{\text{WPN}})/2$) was calculated to be $\cong 30$ nm for the current study with a diameter (d_{WPN}) of the nanogel particle at 80 nm. Overall, Pickering emulsion stabilized by nanometric-sized WPN allowed loading high concentrations of CUR without any effect on the size distribution of the emulsions or CUR diffusing out of the empty spaces at the interfaces. The cryo-SEM analysis allowed to observe the morphology of CUR- E_{WPN} droplets (Figure 3.4b2) which was in agreement with the samples without CUR (Figure 3.3b) in terms of droplet size. However, it appears that the surface was not showing the same degree of WPN aggregates at the interface as observed in the samples without CUR (Figure 3.4b1). This suggests that there might have been some interactions between CUR in the dispersed phase and WPN in the adsorbed phase, which is discussed in detail in the next sections. However, one must be cautious with interpreting this cryo-SEM data as there might be interaction between CUR and heptane in the dispersed phase, causing some microstructural changes in these images that might be specific to these images.

3.3.4 CUR retention in the CUR- E_{WPN}

After characterizing the stability and surface coverage of the Pickering emulsions, the next aim was to assess the retention of CUR within the CUR- E_{WPN} droplets. The retention ability was assessed as a function of pH (pH 3.0 and 7.0) and ions *i.e.* 50 mM NaCl, and 10 mM CaCl₂. The choice of pH and ions were based on physiological relevance *i.e.* pH and ions that are commonly encountered in the gastric and duodenal regimes in human physiology. The retention of CUR in the Pickering emulsions was measured using a dialysis approach as described in the materials and methods section, based on the protocol previously used by Shah et al. (2016b). Ethanol was added to the aqueous buffer media in order to solubilize the CUR and create a 'force-release' environment to the aqueous buffer media because CUR is poorly soluble in aqueous phase.

The CLSM imaging was performed to characterize the microstructural changes (if any) in the Pickering emulsion droplets before and after the retention experiments (Figure 3.5a1-a3). As can be observed, the presence of a bright ring around the droplets indicates an adsorbed layer of nano-meter sized WPN at the interface at both acidic (gastric environment) and basic pH (duodenal environment). This indicates that the emulsions were stable with no pH-induced hydrolysis of the WPN at the interface. Noteworthy, a bright ring around the emulsion droplets were evident in the non-stained samples *i.e.* the samples where only auto-fluorescence of CUR could be observed (Figure 3.5b1-b3). It is well documented in literature that CUR binds to the hydrophobic

domain of numerous proteins such as bovine casein micelles, bovine serum albumin (BSA), human serum albumin (HAS), soy protein isolate and β -lactoglobulin (β -lg) through hydrophobic interactions (Chen et al., 2015; Sahoo et al., 2009; Sahu et al., 2008; Sneharani et al., 2010; Zsila et al., 2003). However, the observed intensities obviously need interpreting with caution since it is well documented in literature that CUR phosphorescence intensity strongly depends on the energy of the exciting photons applied (Chignell et al., 1994). Nonetheless, this observation of a bright auto-fluorescing ring at the particle-laden interface surrounding the CUR- E_{WPN} emulsion droplets with increased intensity and the intensity within the oil droplets might suggest that CUR was mainly retained within the emulsion. This CUR might be retained in two ways; either being bound to the interfacial WPN or were dispersed within the oil droplets. Indeed, CUR release into the aqueous buffer media was verified (less than 1% of CUR was the loss), which confirmed that in all cases CUR remained entrapped within the emulsion systems, either bound or solubilised within the oil phase. As WPN at the droplet surface might form a complex with CUR, the partitioning of CUR in the dispersed phase versus interface might be affected. Hence, CUR retention in CUR- E_{WPN} and further characterization of the interaction between CUR and WPN were performed using spectroscopic techniques, which is discussed in the following sections.

In the absence of ions, about 60.53% of CUR was found to be dispersed in the oil phase at acidic conditions (pH 3.0), which means that 39.47% of CUR was bound to the WPN. Figure 3.6a shows both, the amount of CUR retained within the Pickering emulsion, and the amount of CUR bound to the WPN as a function of pH. On the contrary, CUR retention within the oil droplets was statistically higher ($p < 0.05$) in neutral pH (76.85%). The CUR retention in CUR- E_{WPN} when subjected to different salt concentration are also plotted in Figure 3.6a. At pH 3.0, changes in retention parameters were not statistically significant ($p > 0.05$) on addition of ions. However, at pH 7.0, the CUR retention values were statistically significant ($p < 0.05$) in absence or presence of the divalent cations. These results points out the relevance of pH in CUR retention and binding, which was not obvious in the CLSM images (Figure 3.5). To understand this better, we measured changes in fluorescence intensity to quantify binding constants (K_a) (Figure 3.6b) between CUR and WPN (corresponding fluorescence spectra reported in Appendix B, Figure B4).

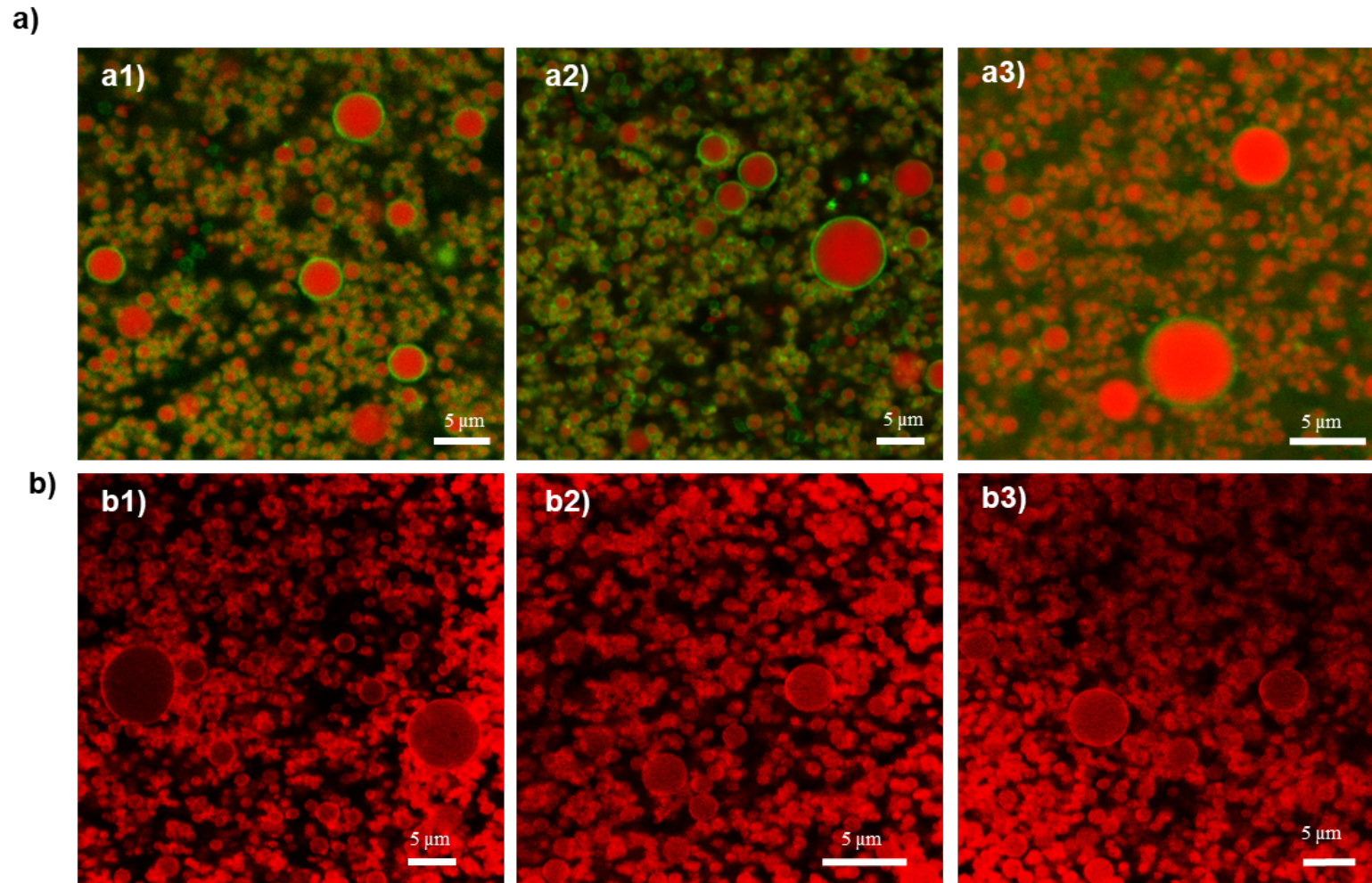


Figure 3.5. a1, b1) Confocal micrographs of original CUR-E_{WPN} droplets, a2, b2) after incubation at 37 °C in buffered solutions (15% v/v ethanol) at pH 3.0, and a3, b3) after incubation at 37 °C in buffered solutions (15% v/v ethanol) at pH 7.0 respectively. Top images a) represent staining oil by Nile Red and WPN by Fast Green, whereas b) images in bottom has no added stain but uses auto-fluorescence of CUR.

3.3.5 Binding of CUR and WPN

Figure 3.6b shows the double-reciprocal plot $1/[WPN]$ versus $1/\Delta FI$ that has been used to calculate the binding constant from the value of the slope in the plot. The binding constants were estimated to be in the range of $6.67 \times 10^1 - 1.33 \times 10^4 \text{ M}^{-1}$ (Figure 3.6b). Binding constants in the order of 10^4 show that there existed a strong affinity between WPN and CUR at pH 3.0. The K_a results obtained are in agreement with previous studies that have reported similar values for β -Ig and CUR (10^5 M^{-1}), and other dietary polyphenols, such as resveratrol (10^4 – 10^6 M^{-1}), epigallocatechin-3-gallate (10^4 – 10^5 M^{-1}), and catechin and epicatechin (10^3 M^{-1}) (Kanakis et al., 2011; Liang et al., 2008; Shpigelman et al., 2010; Sneharani et al., 2010). Nevertheless, this is the first study that provides binding constant values between CUR and WPN. Interestingly, the K_a at neutral pH was found to be $6.67 \times 10^1 \text{ M}^{-1}$, which is three orders of magnitude lower than that at acidic pH 3.0 ($1.00 \times 10^4 \text{ M}^{-1}$). Findings of our study are in close agreement with previous studies that have reported that at neutral pH, the K_a for CUR with denatured β -Ig was $7.0 \pm 0.2 \times 10^2 \text{ M}^{-1}$ (Sneharani et al., 2010), which might explain the increased partitioning of CUR to the oil phase as shown in Figure 3.6a.

The influence of ions on the K_a is also shown in Figure 3.6b. Interestingly, the K_a for the CUR/ WPN mixture at pH 3.0 was not significantly affected by addition of 50 mM NaCl and 10 mM CaCl_2 ($1.33 \times 10^4 \text{ M}^{-1}$). These results suggest that addition of ions did not alter the physical stability and solubility of CUR at pH 3.0. On the contrary, at pH 7.0, the presence of both, monovalent and multivalent ions enhanced the binding affinity between CUR and WPN (6.67×10^3 and $8.00 \times 10^3 \text{ M}^{-1}$, for 50 mM NaCl and 10 mM CaCl_2 , respectively), although these values were still one order of magnitude lower than the ones calculated at pH 3.0. These results can be explained in terms of pH-induced changes in CUR conformation and/or WPN charge distribution.

At acidic pH, CUR primarily exists in the open *enol* tautomeric form (Nardo et al., 2008). In the open conformation, the valence electrons of the carbonyl and enolic oxygen act as H-bond acceptors and the enolic proton as H-bond donor, with charges of -0.73, -0.70, and 0.50, respectively in water (Balasubramanian, 2006). The H-bond accepting and donating capabilities of the molecule expands the number of possible interaction sites that account for CUR's increased binding behaviour. A possible mechanism of the interaction between CUR and WPN, focusing on amino acid residues in βA sheet domain of β -Ig, at pH 3.0 is schematically shown in Figure 3.7a. The βA sheet domain of β -Ig was used since studies have indicated that, upon partial denaturation, Tyr₂₀, which is located close to the base of the that is generally considered to be the binding pocket, is highly accessible, and that Trp₁₉ is critical for

the interaction of β -Ig and CUR (Brownlow et al., 1997; Mohammadi et al., 2016). Here, the *enol* tautomeric form of CUR (Litwinienko and Ingold, 2004) allows hydrophobic interactions with aromatic residues of WPN, such as tyrosine (Tyr) and tryptophan (Trp). Also, worth noting that CUR possess a weak net negative charge (Figure 3.7a), whereas WPN undergoes protonation at pH 3.0 ($pI \sim 5.2$) and is strongly positively charged. Hence, at pH 3.0, both electrostatic and hydrophobic interactions play a role in CUR-WPN binding (Figure 3.7a) that support their high binding affinities (Figure 3.6b).

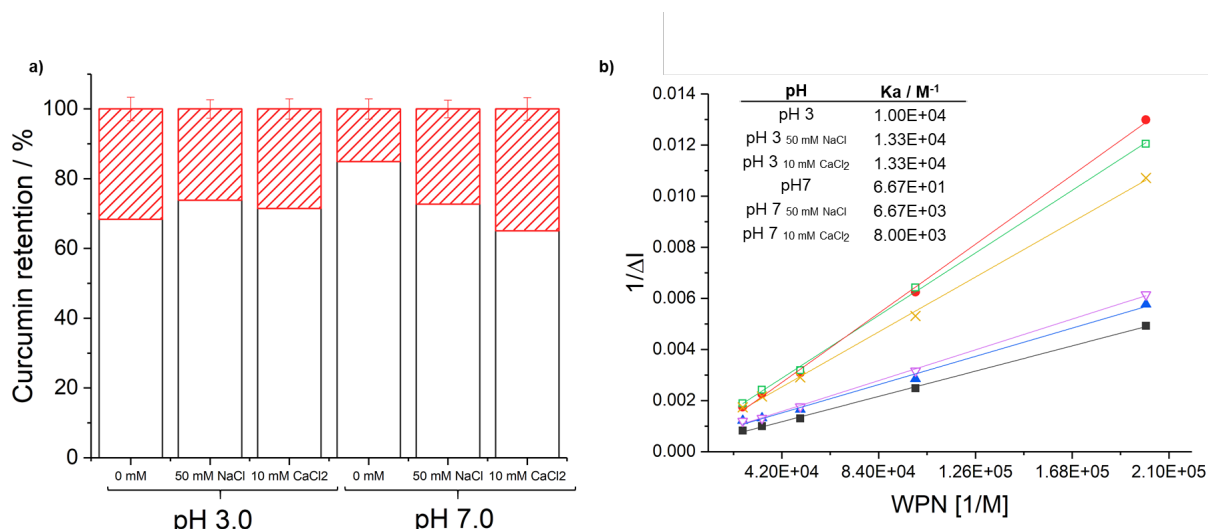
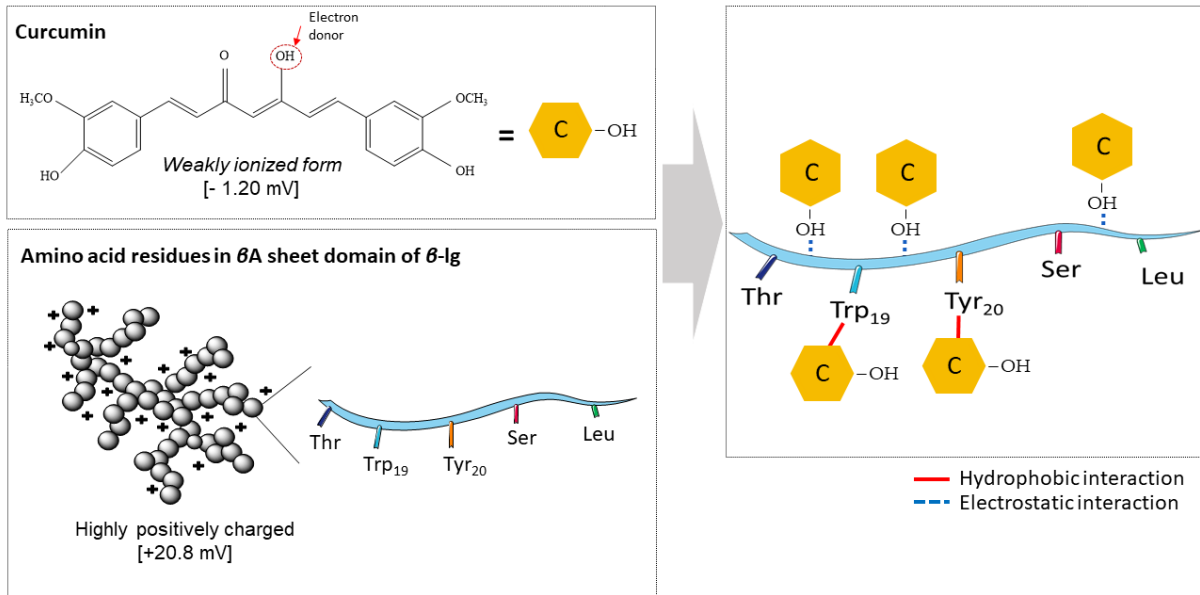


Figure 3.6. a) Percentage of CUR retained (black) in CUR-E_{WPN} droplets and bound (red, diagonal stripes) to WPN in the interface during incubation at 37 °C in buffered solutions (15% v/v ethanol) at 0 mM NaCl/ CaCl₂, 50 mM NaCl, and 10 mM CaCl₂, and b) double reciprocal plot 1/[CM] versus 1/ΔFI b). Error bars represent standard deviation.

Conformation of the β -diketone group in CUR is highly dependent on the chemical environment that successively dictates its intermolecular bonding behaviour (Heger et al., 2014). Upon changing the environment to pH 7.0 (Figure 3.7b), CUR adopts the *diketo* tautomeric conformation characterized by a visible red band or shoulder present in steady-state absorption spectra measurements (Khopde et al., 2000; Nardo et al., 2009; Nardo et al., 2008). Underscored by the fact that a red shift in the absorption spectrum of CUR was observed at neutral pH (Appendix B, Figure B2), it is suggested that changes in pH to neutral pH reduced CUR binding behaviour limiting its migration to the interfacial layer of WPN and increasing the CUR concentration in the dispersed phase (Figure 3.6a). It is also worth noting that WPN and CUR both possessed a net negative charge contributing to higher degree of repulsive interactions, further contributing to limited binding affinity as observed in

Figure 3.6b. Hence at pH 7.0, the binding between CUR and WPN might be attributed only to the hydrophobic interactions (Figure 3.7b) as well as higher solubility of CUR in the dispersed phase, all of which contributing to higher partitioning to the oil (Figure 3.6a).

a)



b)

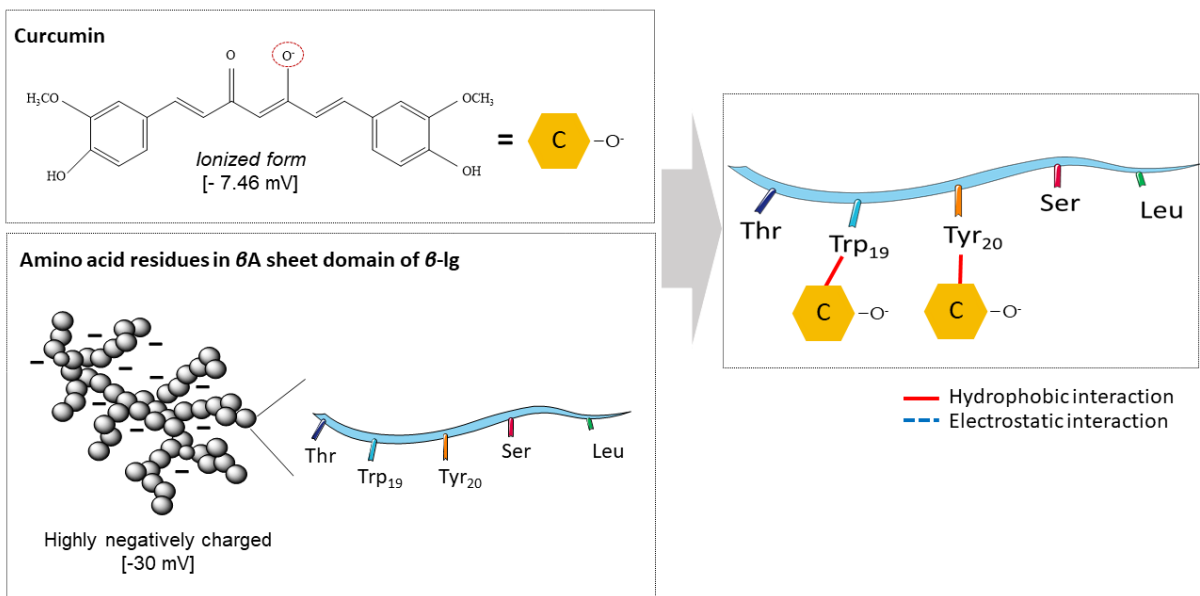


Figure 3.7. Schematic representation of the binding interaction of WPN with CUR at a) pH 3.0, and b) pH 7.0, respectively. The grey spheres represent WPN.

Retention of CUR in CUR-E_{WPN} was compared with similar measurements reported in the literature using other particle-laden interfaces. In Pickering emulsions stabilized by sub-micron sized chitosan-tripolyphosphate nanoparticles (CS/TPP NPs) ranging in size from 322 - 814 nm, 44% and 63% of the encapsulated CUR was retained after 24 hours at pH 2.0 and 7.4, respectively (Shah et al., 2016b), which is lower than the ranges observed in the current study. Overall, these results suggests that WPN-laden interface can be used to increase the retention of CUR, and such retention is largely associated with the mechanical barrier provided by the WPN at the droplet surface that are present either as particle or as network of aggregated particle reducing the gap size. In addition, the partitioning of the CUR retained within these emulsions might be dictated by electrostatic and/or hydrophobic interactions between CUR and interfacial WPN as well as solubility of the CUR in the oil phase, largely affected by the pH and ionic conditions of the medium.

3.4 Conclusions

In this study, whey protein nanogel particles were used to stabilize oil-in-water Pickering emulsions for encapsulation and controlled delivery of curcumin. We have investigated the influence of particle concentration on the structure and stability of emulsions containing 20 wt% MCT-oil stabilized by these nanogel particles. Comparing microstructure at multiple length scales, droplet size and interfacial rheology of emulsions stabilized by protein molecules and protein nanogel particles, we confirmed that the emulsions were Pickering stabilized ones in the latter case. Pickering emulsions presented a monolayer of particles at the droplet surface at a critical concentration of 1.0 wt% whey protein nanogel particles. Structural visualization (TEM and cryo-SEM) of emulsion stabilized by 1.0 wt% particle concentration revealed that whey protein nanogels adsorbed in two different conformations, as a closely packed layer of individual particles, and as network of aggregated particles.

Furthermore, whey protein nanogel-stabilized emulsions were used to encapsulate curcumin. The droplet size and stability of the curcumin-loaded Pickering emulsions were maintained after curcumin incorporation. It was demonstrated that curcumin retention in these Pickering emulsions were associated with the mechanical barrier provided by the whey protein nanogels at the interface and reduced interfacial gap size, latter associated with the nanometric size of these nanogel particles. Furthermore, the partitioning of curcumin in the dispersed phase varied as a function of pH in an *in vitro* release model with lower partitioning at pH 3.0 as compared to that

at pH 7.0. This was attributed to the electrostatic and hydrophobic interactions that allowed more binding of curcumin to whey protein nanogel particles at the interface at pH 3.0 as compared to that at pH 7.0. The binding of curcumin to whey protein nanogel particles at the interface at pH 7.0 was also affected by the presence of mono- and divalent cations. Overall, our study demonstrates the design principles for developing Pickering emulsions for controlled delivery of curcumin, with mechanisms unravelled behind curcumin binding to the interfacial whey protein nanogel particles as a function of pH and ionic strengths.

To understand the control release properties and its potential use as delivery systems for curcumin, the fate of the Pickering emulsions during gastric transit was studied in the following **Chapter 4**. In addition, to confer improved gastric stability characteristics to the emulsion might also be of great interest. This is now discussed in the next chapter where the formation of a thicker secondary layer facilitated by electrostatic interaction with dextran sulphate was employed.

3.5 References

- Araiza-Calahorra, A., Akhtar, M., & Sarkar, A. (2018). Recent advances in emulsion-based delivery approaches for curcumin: From encapsulation to bioaccessibility. *Trends in Food Science & Technology*, 71, 155-169.
- Balasubramanian, K. (2006). Molecular Orbital Basis for Yellow Curry Spice Curcumin's Prevention of Alzheimer's Disease. *Journal of Agricultural and Food Chemistry*, 54 (10), 3512-3520.
- Binks, B. P., & Olusanya, S. O. (2017). Pickering emulsions stabilized by coloured organic pigment particles. *Chemical Science*, 8 (1), 708-723.
- Binks, B. P., Philip, J., & Rodrigues, J. A. (2005). Inversion of silica-stabilized emulsions induced by particle concentration. *Langmuir*, 21 (8), 3296-3302.
- Brownlow, S., Cabral, J. H. M., Cooper, R., Flower, D. R., Yewdall, S. J., Polikarpov, I., North, A. C. T., & Sawyer, L. (1997). Bovine β -lactoglobulin at 1.8 Å resolution — still an enigmatic lipocalin. *Structure*, 5 (4), 481-495.
- Chen, F.-P., Li, B.-S., & Tang, C.-H. (2015). Nanocomplexation between Curcumin and Soy Protein Isolate: Influence on Curcumin Stability/Bioaccessibility and *in vitro* Protein Digestibility. *Journal of Agricultural and Food Chemistry*, 63 (13), 3559-3569.
- Chen, J., & Dickinson, E. (1995). Surface shear viscosity and protein-surfactant interactions in mixed protein films adsorbed at the oil-water interface. *Food Hydrocolloids*, 9 (1), 35-42.

- Chignell, C. F., Bilskj, P., Reszka, K. J., Motten, A. G., Sik, R. H., & Dahl, T. A. (1994). Spectral and photochemical properties of curcumin. *Photochemistry and Photobiology*, 59 (3), 295-302.
- Destribats, M., Rouvet, M., Gehin-Delval, C., Schmitt, C., & Binks, B. P. (2014). Emulsions stabilised by whey protein microgel particles: towards food-grade Pickering emulsions. *Soft Matter*, 10 (36), 6941-6954.
- Dickinson, E. (2012). Use of nanoparticles and microparticles in the formation and stabilization of food emulsions. *Trends in Food Science & Technology*, 24 (1), 4-12.
- Dickinson, E. (2017). Biopolymer-based particles as stabilizing agents for emulsions and foams. *Food Hydrocolloids*, 68, 219-231.
- Dickinson, E., Rolfe, S. E., & Dalgleish, D. G. (1990). Surface shear viscometry as a probe of protein-protein interactions in mixed milk protein films adsorbed at the oil-water interface. *International Journal of Biological Macromolecules*, 12 (3), 189-194.
- Gautier, F., Destribats, M., Perrier-Cornet, R., Dechezelles, J. F., Giermanska, J., Heroguez, V., Ravaine, S., Leal-Calderon, F., & Schmitt, V. (2007). Pickering emulsions with stimuable particles: from highly- to weakly-covered interfaces. *Physical Chemistry Chemical Physics*, 9 (48), 6455-6462.
- Goel, A., Kunnumakkara, A. B., & Aggarwal, B. B. (2008). Curcumin as "Curecumin": from kitchen to clinic. *Biochemical Pharmacology*, 75 (4), 787-809.
- Gupta, R., & Rousseau, D. (2012). Surface-active solid lipid nanoparticles as Pickering stabilizers for oil-in-water emulsions. *Food & Function*, 3 (3), 302-311.
- Heger, M., van Golen, R. F., Broekgaarden, M., & Michel, M. C. (2014). The molecular basis for the pharmacokinetics and pharmacodynamics of curcumin and its metabolites in relation to cancer. *Pharmacological Reviews*, 66 (1), 222-307.
- Jain, A., Singh, S. K., Arya, S. K., Kundu, S. C., & Kapoor, S. (2018). Protein Nanoparticles: Promising Platforms for Drug Delivery Applications. *ACS Biomaterials Science & Engineering*, 4 (12), 3939-3961.
- Kanakis, C. D., Hasni, I., Bourassa, P., Tarantilis, P. A., Polissiou, M. G., & Tajmir-Riahi, H.-A. (2011). Milk β -lactoglobulin complexes with tea polyphenols. *Food Chemistry*, 127 (3), 1046-1055.
- Khopde, S. M., Indira Priyadarsini, K., Palit, D. K., & Mukherjee, T. (2000). Effect of solvent on the excited state photophysical properties of curcumin *Photochemistry & Photobiology*, 72 (5), 625.

- Liang, L., Tajmir-Riahi, H. A., & Subirade, M. (2008). Interaction of β -lactoglobulin with resveratrol and its biological implications. *Biomacromolecules*, 9 (1), 50-56.
- Litwinienko, G., & Ingold, K. U. (2004). Abnormal solvent effects on hydrogen atom abstraction. 2. Resolution of the curcumin antioxidant controversy. The role of sequential proton loss electron transfer. *The Journal of Organic Chemistry*, 69, 5888-5896.
- Liu, F., Ou, S.-Y., & Tang, C.-H. (2017). Ca²⁺-induced soy protein nanoparticles as Pickering stabilizers: Fabrication and characterization. *Food Hydrocolloids*, 65, 175-186.
- Marefati, A., Bertrand, M., Sjöö, M., Dejmek, P., & Rayner, M. (2017). Storage and digestion stability of encapsulated curcumin in emulsions based on starch granule Pickering stabilization. *Food Hydrocolloids*, 63, 309-320.
- Matsumiya, K., & Murray, B. S. (2016). Soybean protein isolate gel particles as foaming and emulsifying agents. *Food Hydrocolloids*, 60, 206-215.
- McClements, D. J. (2004). *Food Emulsions: Principles, Practices, and Techniques* (Second Edition ed.): CRC Press, Taylor & Francis Group
- McClements. (2012). Advances in fabrication of emulsions with enhanced functionality using structural design principles. *Current Opinion in Colloid & Interface Science*, 17 (5), 235-245.
- Miner, S., O'Donnell, A. F., Ballew, A., Giaever, G., Nislow, C., Stearns, T., & Cyert, M. S. (2011). Curcumin inhibits growth of *Saccharomyces cerevisiae* through iron chelation. *Eukaryot Cell*, 10 (11), 1574-1581.
- Mohammadi, F., Mahmudian, A., Moeeni, M., & Hassani, L. (2016). Inhibition of amyloid fibrillation of hen egg-white lysozyme by the natural and synthetic curcuminoids. *RSC advances*, 6 (28), 23148-23160.
- Murray, B. S., & Dickinson, E. (1996). Interfacial rheology and the dynamic properties of adsorbed films of food proteins and surfactants. *Food Science & Technology International*, Tokyo, 2 (3), 131-145.
- Murray, B. S., Durga, K., Yusoff, A., & Stoyanov, S. D. (2011). Stabilization of foams and emulsions by mixtures of surface-active food-grade particles and proteins. *Food Hydrocolloids*, 25 (4), 627-638.
- Nardo, L., Andreoni, A., Bondani, M., Másson, M., & Tønnesen, H. (2009). Studies on curcumin and curcuminoids. XXXIV. Photophysical properties of a symmetrical, non-substituted curcumin analogue. *Journal of Photochemistry & Photobiology B: Biology*, 97 (2), 77-86.

- Nardo, L., Paderno, R., Andreoni, A., Másson, M., Haukvik, T., & Tønnesen, H. H. (2008). Role of H-bond formation in the photo reactivity of curcumin. *Spectroscopy*, 22, 187–198.
- Nicolai, T., Britten, M., & Schmitt, C. (2011). β -Lactoglobulin and WPI aggregates: Formation, structure and applications. *Food Hydrocolloids*, 25 (8), 1945-1962.
- Ong, L., Dagastine, R. R., Kentish, S. E., & Gras, S. L. (2011). Microstructure of milk gel and cheese curd observed using cryo scanning electron microscopy and confocal microscopy. *LWT - Food Science and Technology*, 44 (5), 1291-1302.
- Payton, F., Sandusky, P., & Alworth, W. L. (2007). NMR Study of the Solution Structure of Curcumin. *Journal of Natural Products*, 70 (2), 143-146.
- Peinado, I., Lesmes, U., Andrés, A., & McClements, D. J. (2010). Fabrication and Morphological Characterization of Biopolymer Particles Formed by Electrostatic Complexation of Heat Treated Lactoferrin and Anionic Polysaccharides. *Langmuir*, 26 (12), 9827-9834.
- Pickering, S. U. (1907). CXCVI.-Emulsions. *Journal of the Chemical Society, Transactions*, 91 (0), 2001-2021.
- Ramsden, W. (1904). Separation of solids in the surface-layers of solutions and 'suspensions' (observations on surface-membranes, bubbles, emulsions, and mechanical coagulation). —Preliminary account. *Proceedings of the Royal Society of London*, 72 (477-486), 156-164.
- Sağlam, D., Venema, P., van der Linden, E., & de Vries, R. (2014). Design, properties, and applications of protein micro- and nanoparticles. *Current Opinion in Colloid & Interface Science*, 19 (5), 428-437.
- Sahoo, B. K., Ghosh, K. S., & Dasgupta, S. (2009). Molecular interactions of isoxazolcurcumin with human serum albumin: Spectroscopic and molecular modelling studies. *Biopolymers*, 91 (2), 108-119.
- Sahu, A., Kasoju, N., & Bora, U. (2008). Fluorescence Study of the Curcumin-Casein Micelle Complexation and Its Application as a Drug Nanocarrier to Cancer Cells. *Biomacromolecules*, 9, 2905–2912.
- Sarkar, A., Ademuyiwa, V., Stublely, S., Esa, N. H., Goycoolea, F. M., Qin, X., Gonzalez, F., & Olvera, C. (2018a). Pickering emulsions co-stabilized by composite protein/ polysaccharide particle-particle interfaces: Impact on *in vitro* gastric stability. *Food Hydrocolloids*, 84, 282-291.

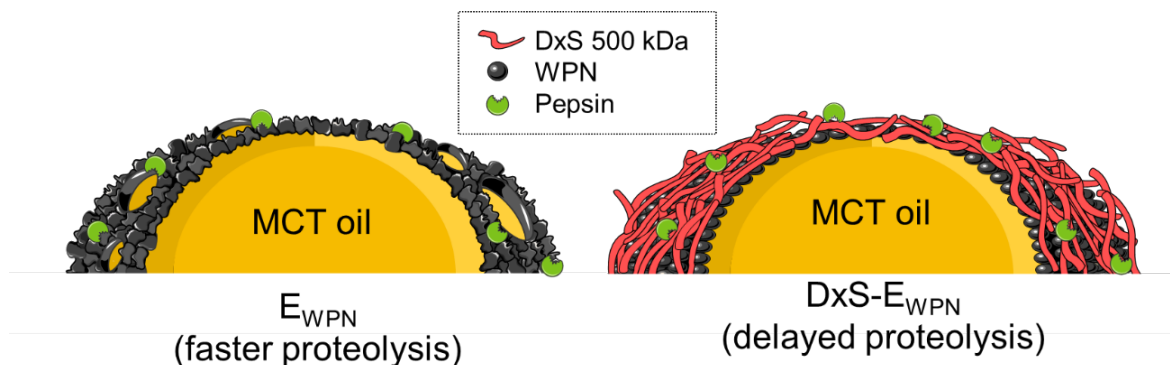
- Sarkar, A., Kanti, F., Gulotta, A., Murray, B. S., & Zhang, S. (2017). Aqueous Lubrication, Structure and Rheological Properties of Whey Protein Microgel Particles. *Langmuir*, 33 (51), 14699-14708.
- Sarkar, A., Li, H., Cray, D., & Boxall, S. (2018b). Composite whey protein–cellulose nanocrystals at oil-water interface: Towards delaying lipid digestion. *Food Hydrocolloids*, 77, 436-444.
- Sarkar, A., Murray, B., Holmes, M., Ettelaie, R., Abdalla, A., & Yang, X. (2016). *In vitro* digestion of Pickering emulsions stabilized by soft whey protein microgel particles: influence of thermal treatment. *Soft Matter*, 12 (15), 3558-3569.
- Sarkar, A., Zhang, S., Holmes, M., & Ettelaie, R. (2019). Colloidal aspects of digestion of Pickering emulsions: Experiments and theoretical models of lipid digestion kinetics. *Advances in Colloid & Interface Science*, 263, 195-211.
- Sarkar, A., Zhang, S., Murray, B., Russell, J. A., & Boxal, S. (2017). Modulating *in vitro* gastric digestion of emulsions using composite whey protein-cellulose nanocrystal interfaces. *Colloids and Surfaces B: Biointerfaces*, 158, 137-146
- Schmitt, C., Bovay, C., Vuilliomenet, A.-M., Rouvet, M., & Bovetto, L. (2011). Influence of protein and mineral composition on the formation of whey protein heat-induced microgels. *Food Hydrocolloids*, 25 (4), 558-567.
- Schmitt, C., Moitzi, C., Bovay, C., Rouvet, M., Bovetto, L., Donato, L., Leser, M. E., Schurtenberger, P., & Stradner, A. (2010). Internal structure and colloidal behaviour of covalent whey protein microgels obtained by heat treatment. *Soft Matter*, 6 (19), 4876-4884.
- Shah, B. R., Li, Y., Jin, W., An, Y., He, L., Li, Z., Xu, W., & Li, B. (2016a). Preparation and optimization of Pickering emulsion stabilized by chitosan-tripolyphosphate nanoparticles for curcumin encapsulation. *Food Hydrocolloids*, 52, 369-377.
- Shah, B. R., Zhang, C., Li, Y., & Li, B. (2016b). Bioaccessibility and antioxidant activity of curcumin after encapsulated by nano and Pickering emulsion based on chitosan-tripolyphosphate nanoparticles. *Food Research International*, 89 (Pt 1), 399-407.
- Shpigelman, A., Israeli, G., & Livney, Y. D. (2010). Thermally-induced protein–polyphenol co-assemblies: beta lactoglobulin-based nanocomplexes as protective nanovehicles for EGCG. *Food Hydrocolloids*, 24 (8), 735-743.
- Sneharani, A. H., Karakkat, J. V., Singh, S. A., & Rao, A. G. A. (2010). Interaction of Curcumin with β -Lactoglobulin—Stability, Spectroscopic Analysis, and Molecular Modelling of the Complex. *Journal of Agricultural & Food Chemistry*, 58 (20), 11130-11139.

- Thompson, K. L., Mable, C. J., Cockram, A., Warren, N. J., Cunningham, V. J., Jones, E. R., Verber, R., & Armes, S. P. (2014). Are block copolymer worms more effective Pickering emulsifiers than block copolymer spheres? *Soft Matter*, 10 (43), 8615-8626.
- Tikekar, R. V., Pan, Y., & Nitin, N. (2013). Fate of curcumin encapsulated in silica nanoparticle stabilized Pickering emulsion during storage and simulated digestion. *Food Research International*, 51 (1), 370-377.
- Tønnesen, H. H., & Karlsen, J. (1985). Studies on curcumin and curcuminoids. 6. Kinetics of curcumin degradation in aqueous solution. *Zeitschrift für Lebensmittel-Untersuchung und Forschung*, 180 (5), 402-404.
- Torres, O., Murray, B., & Sarkar, A. (2017). Design of novel emulsion microgel particles of tuneable size. *Food Hydrocolloids*, 71, 47-59.
- Verma, D., Gulati, N., Kaul, S., Mukherjee, S., & Nagaich, U. (2018). Protein based nanostructures for drug delivery. *Journal of pharmaceutics*, 2018, 9285854-9285854.
- Wang, L.-J., Hu, Y.-Q., Yin, S.-W., Yang, X.-Q., Lai, F.-R., & Wang, S.-Q. (2015). Fabrication and characterization of antioxidant Pickering emulsions stabilized by zein/chitosan complex particles (ZCPs). *Journal of Agricultural & Food Chemistry*, 63 (9), 2514-2524.
- Wilken, R., Veena, M. S., Wang, M. B., & Srivatsan, E. S. (2011). Curcumin: A review of anti-cancer properties and therapeutic activity in head and neck squamous cell carcinoma. *Molecular Cancer*, 10, 12-12.
- Xiao, J., Li, C., & Huang, Q. (2015a). Kafirin nanoparticle-stabilized Pickering emulsions as oral delivery vehicles: Physicochemical stability and *in vitro* digestion profile. *Journal of Agricultural & Food Chemistry*, 63 (47), 10263-10270.
- Xiao, J., Li, Y., Li, J., Gonzalez, A. P., Xia, Q., & Huang, Q. (2015b). Structure, morphology, and assembly behaviour of kafirin. *Journal of Agricultural & Food Chemistry*, 63 (1), 216-224.
- Zembyla, M., Murray, B. S., & Sarkar, A. (2018). Water-in-oil Pickering emulsions stabilized by water-insoluble polyphenol crystals. *Langmuir*, 34 (34), 10001-10011.
- Zhou, F. Z., Zeng, T., Yin, S. W., Tang, C. H., Yuan, D. B., & Yang, X. Q. (2018). Development of antioxidant gliadin particle stabilized Pickering high internal phase emulsions (HIPEs) as oral delivery systems and the *in vitro* digestion fate. *Food & Function*, 9 (2), 959-970.
- Zou, Y., Guo, J., Yin, S.-W., Wang, J.-M., & Yang, X.-Q. (2015). Pickering emulsion gels prepared by hydrogen-bonded zein/tannic acid complex colloidal particles. *Journal of Agricultural & Food Chemistry*, 63 (33), 7405-7414.

Zsila, F., Bikádi, Z., & Simonyi, M. (2003). Unique, pH-dependent biphasic band shape of the visible circular dichroism of curcumin–serum albumin complex. *Biochemical & Biophysical Research Communications*, 301 (3), 776-782.

Chapter 4

Designing biopolymer-coated Pickering emulsions to modulate *in vitro* gastric digestion: A static model study³



Abstract

The aim of this study was to restrict the degree of gastric destabilization of Pickering emulsions by using electrostatic deposition of a biopolymeric layer at the proteinaceous particle-laden oil-water interface. Pickering emulsions (20 wt% oil) were prepared using whey protein nanogel particles (WPN, $d_H \sim 91.5$ nm) (1 wt%) and the emulsions were coated by a layer of anionic polysaccharide, dextran sulphate (DxS) of molecular weight (MW) of 40 or 500 kDa, respectively. The hypothesis was that DxS coating on the protein nanogel particle-laden interface would act as a steric barrier against interfacial proteolysis of WPN by pepsin. During static *in vitro* gastric digestion, the droplet size, ζ -potential, microstructure (confocal microscopy with fluorescently labelled dextran) and protein hydrolysis were monitored. The ζ -potential measurements confirmed that 0.2 wt% DxS was sufficient to coat the WPN-stabilized emulsion droplets with clear charge reversal from +35.9 mV to -28.8 (40 kDa) and -46.2 mV (500 kDa). Protein hydrolysis results showed a significantly lower level of free amino groups upon addition of 0.2 wt% DxS of either 40 or 500 kDa MW to the WPN ($p \leq 0.05$). Emulsions coated with DxS-500 kDa presented stable droplets with lower degree of pepsin hydrolysis of the adsorbed layer as compared to those coated with DxS-40 kDa or uncoated protein nanogel-stabilized interface after 120 min of digestion, highlighting the importance of charge density and molecular weight of the

³ Published as: Araiza-Calahorra, A., & Sarkar, A. (2019b). Designing biopolymer-coated Pickering emulsions to modulate *in vitro* gastric digestion: a static model study. *Food & Function*, 10(9), 5498 – 5509. DOI: <https://doi.org/10.1039/C9FO01080G>

polymer coating. Insights from this study could enable designing gastric-stable emulsions for encapsulation of lipophilic compounds that require delivery to the intestine.

4.1. Introduction

The global prevalence of obesity has nearly tripled in the last 40 years (Organization 2018). Currently, one of the proposed strategies to attenuate this global epidemic is food structuring to increase satiety. Such strategies include designing food structures that delay the digestion of calorie-dense lipids to provoke generation of satiety hormones and enhance post-meal satiation *via* an 'ileal brake' mechanism (Holt et al., 1992; Maljaars et al., 2008; Pawlak et al., 2002). Although significant attempts have been made to delay the digestion of lipid-based food structures *i.e.* *via* designing model oil-in-water emulsions through interfacial engineering, many if not most of these interfacial layers, are competitively displaced by bio-surfactants *i.e.* bile salts, consequently preventing such delay (Mackie et al., 2000; Sarkar et al., 2010; Sarkar et al., 2016b). The key conclusion from these colloidal studies is that a more structurally complex and/ or thicker interfacial structure is needed that is resistant to this competitive displacement and at the same time not readily digested by human proteolytic enzymes (Chu et al., 2009; Reis et al., 2009; Sarkar et al., 2019; Wulff-Pérez et al., 2012).

Recently, colloidal particles have been used for the interfacial design of either oil-in-water or water-in-oil interfaces and these are referred to as Pickering emulsions (Dickinson 2012; Zembyla et al., 2018). An important reason why Pickering emulsions have gained significant interest is that as opposed to conventional emulsions stabilized by proteins or surfactants, Pickering emulsions are highly resilient to coalescence and Oswald ripening (Dickinson 2012). Such ultra-stability is given by the high desorption energies (thousands of kT / particle), which makes it practically impossible to desorb these particles once they are adsorbed at the interface. Thus, Pickering stabilizers are promising candidates for delaying lipid digestion as there is negligible possibilities of these particles to be displaced by bile salts once they have been adsorbed at the oil-water interface (Araiza-Calahorra et al., 2018; Sarkar et al., 2019). For example, protein microgel particles have been recently used as Pickering stabilizers for oil-in-water emulsions (Destribats et al., 2013). Such protein microgel particle-stabilized interfaces have been shown to delay lipolysis to a certain extent by providing a transient barrier to the access of bile salts and lipase (Sarkar et al., 2016a). However, such behaviour was only observed when the gastric phase of these Pickering emulsions was completely bypassed in a highly unrealistic condition and consequently

the effect of digestion of the protein microgel particles by pepsin was not taken into account. In other words, the main drawback of these protein particle-stabilized emulsions is that there is hydrolysis of the particle-laden interface by pepsin (Sarkar et al., 2016a) under simulated gastric digestion conditions (Mackie and Macierzanka 2010). Peptic hydrolysis of the adsorbed protein particle layer at the interface may lead to changes in emulsion microstructure and stability and thus might not be able to delay lipid digestion in the later phases. Thus, the unresolved challenge is to develop particle-stabilized emulsions that are protected against pepsin-induced hydrolysis in the gastric phase.

One approach to protect these emulsions from gastric destabilization might be biopolymer coatings through the layer-by-layer (LbL) deposition methodology. The LbL technique has been conventionally used to increase the stability of protein-stabilized emulsions against environmental stresses, such as changes in pH, ionic strength, temperature and spray-drying (Dickinson 2009; Fioramonti et al., 2015; Gharsallaoui et al., 2010; Liu et al., 2010; Qiu et al., 2015; Roudsari et al., 2006). This technique consists of electrostatic deposition of an ionic polysaccharide onto the surface of a mutually oppositely charged protein-stabilized emulsion droplet (Aoki et al., 2005). In addition, there has also been significant progress into the use of biopolymer coatings to improve the chemical stability of encapsulated components, such as digestion, release and absorption rates of lipid droplets within the gastrointestinal tract (GIT) (Gudipati et al., 2010; Hu et al., 2011; Klinkesorn and Julian McClements 2010; Lomova et al., 2015). In the domain of Pickering emulsions, one study reported a particle-particle interface, where negatively-charged inulin particles were electrostatically deposited on Pickering emulsions stabilized by positively-charged lactoferrin nanogel particles. In this study, it was shown that the electrostatic deposition of inulin particles decreased the rate and degree of hydrolysis of the lactoferrin nanogel particles at the oil-water interface during gastric digestion (Sarkar et al., 2018). Electrostatic adsorption of lactoferrin-based nanoparticles or nanogel particles with polysaccharides such as pectin, carrageenan and inulin nanoparticles has been previously reported (Sarkar et al., 2018; Togle et al., 2012; Togle et al., 2010). Nevertheless, use of biopolymer coating at particle-laden interfaces is a simple tool to delay the gastric destabilization in simulated gastric condition, which has not attracted much attention in literature (Togle et al., 2012).

In our previous study, we have comprehensively characterised the use of whey protein nanogel particle (WPN) as Pickering stabilizers for oil-in-water emulsions (E_{WPN}) (Araiza-Calahorra and Sarkar 2019). In this study we aimed to understand the influence of biopolymer coating on the gastric fate of whey protein nanogel-stabilized Pickering oil-in-water emulsions using the INFOGEST *in vitro* static gastric model

(Minekus et al., 2014). Whey protein isolate (WPI) was used to produce the soft solid particles *i.e.* whey protein nanogel particles (WPN), acting as the Pickering stabilizer. To coat the emulsion stabilized by WPN, dextran sulphate (DxS), which is a branched-chain polysaccharide with 1–6 and 1–4 glycosidic linkage with approximately 2.3 sulphate groups per glucosyl unit, of two molecular weights *i.e.* 40 and 500 kDa, was used. The DxS was selected due to the abundance of highly negatively charged sulphate groups that will allow electrostatic deposition to cationic WPN-stabilized droplets at gastric pH *i.e.* below the isoelectric point ($pI \sim 5.2$) of whey protein. We hypothesize that DxS coating on the protein nanogel particle-laden interface would act as a steric barrier against interfacial proteolysis by pepsin and the barrier properties will depend on the molecular weight of the DxS used. A combination of complementary techniques, such as light scattering, zeta-potential, confocal microscopy (with fluorescently-labelled DxS), protein hydrolysis using sodium dodecyl sulphate polyacryl amide gel electrophoresis (SDS-PAGE) of the adsorbed layer and standardized ortho-phthaldialdehyde (OPA) assay were used to test the above-stated hypothesis.

4.2 Materials and Methods

4.2.1 Materials

Whey protein isolate (WPI) with $\geq 90\%$ protein content was gifted from Fonterra Co-operative Group Limited (Auckland, New Zealand). Porcine pepsin (P7000, measured enzyme activity: 371 U mg^{-1} using haemoglobin as substrate), dextran sulphate sodium salt (DxS) of molecular weight (MW) 40 and 500 kDa containing 15–19% and 16 - 19% of sulphur content, respectively, and fluorescein isothiocyanate (FITC)-labelled dextran sulphate (MW 40 and 500 kDa) were purchased from Sigma-Aldrich Company Ltd, Dorset, UK. Sodium chloride, sodium hydroxide, sodium phosphate monobasic monohydrate, sodium phosphate dibasic anhydrous and hydrogen chloride were purchased from Thermo Fisher Scientific, Loughborough, UK. The lipid phase consisted of medium-chain triglyceride (MCT-oil) Miglyol[®] 812 with a density of 945 kg m^{-3} at $20 \text{ }^\circ\text{C}$ (Cremer Oleo GmbH & Co, Germany). Sodium dodecyl sulphate polyacrylamide gel electrophoresis (SDS-PAGE) reagents including Mini-Protean Precast TGX gels (8 - 16%) and Precision Plus Protein All Blue Standards were purchased from Bio-Rad (Bio-Rad Laboratories Ltd., Richmond, CA, USA). All reagents were of analytical grade and used without further purification unless otherwise reported. All solutions were prepared with Milli-Q water with a resistivity of $18.2 \text{ M}\Omega \text{ cm}$ at $25 \text{ }^\circ\text{C}$ (Milli-Q apparatus, Millipore, Bedford, UK). Sodium azide (0.02 wt %) was added as a preservative.

4.2.2 Preparation of whey protein nanogel particles (WPN)

The whey protein nanogel particles (WPN) were produced based on modification of a previously developed top-down technique (Sarkar et al., 2018; Sarkar et al., 2016a). The WPI powder (10 wt%) was dissolved in 10 mM phosphate buffer at pH 7.0 for 2 hours to ensure complete dispersion. The WPI solution was heated in a temperature-controlled water bath at 90 °C for 30 min to form a heat-set gel (quiescent), followed by cooling down for 15 min and storage at 4 °C overnight to form heat-set hydrogels. Obtained WPI gels were pre-homogenized with phosphate buffer (5 wt%) using a hand blender (HB724, Kenwood) for 1 minute and transferred to a vacuum box (John Fraser and Sons Ltd, London, UK) for degassing. The resulting 5 wt% whey protein gel was passed through a Leeds Jet homogenizer, a bespoke two-chamber homogenizer developed in the School of Food Science and Nutrition (University of Leeds, Leeds, UK) at 300 bars for two passes, respectively. Final whey protein nanogel particles (WPN) were diluted with buffer to the desired protein concentration for the emulsion preparation.

4.2.3 Preparation of Pickering oil-in-water emulsions

Whey protein nanogel-stabilized emulsions (EWPN). Pickering oil-in-water emulsions were prepared using MCT-oil (20 wt%) and a protein content of 1 wt% in the final emulsion. Briefly, coarse E_{WPN} (20:80 w/w) droplets were prepared using Ultra Turrax T25 homogenizer (IKA-Werke GmbH & Co., Staufen Germany) at 13,500 rpm for 1 min. Following this, the coarse emulsions were homogenized using Leeds Jet homogenizer (School of Food Science and Nutrition, University of Leeds, UK) at 300 bars using two passes to prepare fine E_{WPN} droplets.

Whey protein nanogel-stabilized emulsion coated with dextran sulphate (DxS-EWPN). Two types of emulsions of dextran sulphate (DxS)-coated Pickering emulsions (DxS- E_{WPN}) were produced by mixing E_{WPN} at pH 3.0 (40 wt% MCT, 2.5 wt% WPN in aqueous phase) produced using afore-mentioned method, with aqueous dispersions of DxS of 40 kDa or 500 kDa, while maintaining the pH at pH 3.0. For confocal laser scanning microscopy, another set of samples were prepared using Fluorescein isothiocyanate (FITC)-labelled DxS of 40 kDa or 500 kDa. The biopolymer solutions were prepared by dissolving the powdered DxS of desired MW into Milli-Q water (pH 3.0) and stirring overnight at 21 °C to ensure dissolution. The E_{WPN} and aqueous dispersions of DxS were mixed in 1:1 w/w to produce DxS- E_{WPN} (20 wt%

MCT, 1 wt% WPN) with different concentrations of DxS-40 kDa or DxS-500 kDa (0.05 -1 wt%), pH was readjusted to pH 3.0 using 1.0 M HCl and samples were stirred for 2 hours at 25 °C to allow electrostatic deposition of DxS to the E_{WPN} droplets. Hereafter, the emulsions named as DxS- E_{WPN} -40 and DxS- E_{WPN} -500 represent the polymer-coated emulsions containing DxS of MW, 40 kDa or 500 kDa, respectively.

4.2.4 *In vitro* gastric digestion of particles and emulsions

The aqueous dispersions of WPN, WPN+DxS-40 kDa and WPN+DxS-500 kDa, respectively and the corresponding emulsions *i.e.* E_{WPN} , DxS- E_{WPN} -40 and DxS- E_{WPN} -500 were digested using slightly adapted digestion protocol Minekus et al., (2014), *i.e.* without the simulated oral phase considering that neither WPN nor DxS are susceptible to α -amylase. Briefly, 10 mL of pre-incubated sample (37 °C, 1 h) at pH 3.0 was mixed with 10 mL of simulated gastric fluid (SGF), consisting of 0.257 g L⁻¹ of KCl, 0.061 g L⁻¹ of KH₂PO₄, 1.05 g L⁻¹ of NaHCO₃, 1.38 g L⁻¹ of NaCl, 0.0122 g L⁻¹ of MgCl₂(H₂O)₆, 0.024 g L⁻¹ of (NH₄)₂CO₃ and 2000 U/ mL pepsin at pH 3.0. The mixture was incubated for 2 h at 37 °C under agitation using a shaking water bath (Grant Instruments Ltd, Cambridge, UK). As control, samples were also subjected to SGF treatment without added pepsin *i.e.* SGF buffer. During the gastric phase, samples were periodically withdrawn from the sample-SGF mixture at 5, 30, 60, 90, 120 and 150 min for size, charge, microscopy and SDS-PAGE analysis. Proteolysis of the samples was terminated by neutralizing to pH 7.0 using freshly prepared 1 M NH₄HCO₃ except for size and charge measurements, in latter experiments, samples were characterized immediately after digestion.

4.2.5 Particle size and droplet size distribution

The physicochemical properties and stability of aqueous dispersions of WPN+DxS-40 kDa and WPN+DxS-500 kDa, respectively and their corresponding emulsions *i.e.* E_{WPN} , DxS- E_{WPN} -40 and DxS- E_{WPN} -500 before and after digestion were monitored using their particle size distribution, ζ -potential and microstructural changes as a function of gastric digestion time.

Particle size of the aqueous dispersions of WPN, WPN+DxS-40 kDa and WPN+DxS-500 kDa, respectively was determined using dynamic light scattering (DLS) at 25 °C using a Zetasizer Nano-ZS (Malvern Instruments, Malvern UK) in a PMMA standard disposable cuvette. Particle size of the samples before and after gastric digestion was measured after diluting the samples in SGF buffer (pH 3.0). Droplet size distributions of the three Pickering emulsion samples *i.e.* E_{WPN} , DxS- E_{WPN} -

40 and DxS-E_{WPN}-500 were determined using static light scattering at 25 °C using Malvern MasterSizer 3000 (Malvern Instruments Ltd, Malvern, Worcestershire, UK). The refractive index of the MCT (Miglyol® 812 oil) and the dispersion medium were set at 1.445 and 1.33, respectively. The absorbance value of the emulsion droplets was 0.001. The mean particle size distribution of the emulsions was reported as volume mean diameter (d_{43}) and surface mean diameter (d_{32}) based on five measurements on triplicate samples.

4.2.6 ζ -potential

The ζ -potential of aqueous dispersions of WPN, WPN+DxS-40 kDa and WPN+DxS-500 kDa, respectively and their corresponding emulsions *i.e.* E_{WPN}, DxS-E_{WPN}-40 and DxS-E_{WPN}-500 before and after digestion was determined using a particle electrophoresis instrument (Zetasizer, Nano ZS series, Malvern Instruments, Worcestershire, UK). Samples were diluted in SGF buffer (pH 3.0) (0.1 wt% particle or 0.002 wt% emulsion droplet concentration) and added to a folded capillary cell (Model DTS 1070, Malvern Instruments Ltd., Worcestershire, UK). Samples were equilibrated for 1 min and the data was processed using the Smoluchowski model. The ζ -potential results were reported as mean result of at least five reported readings made on triplicate samples.

4.2.7 Confocal scanning laser microscopy (CLSM)

The microstructure of the Pickering emulsions *i.e.* E_{WPN}, DxS-E_{WPN}-40 and DxS-E_{WPN}-500 was observed before and after the gastric digestion experiments using a Zeiss LSM 880 inverted confocal microscope (Carl Zeiss MicroImaging GmbH, Jena, Germany). A stock solution of Nile Red (1 mg/mL in dimethyl sulfoxide, Sigma-Aldrich) was used to stain the MCT-oil to a final concentration of 0.02 mg mL⁻¹ and a stock solution of Fast Green (1 mg mL⁻¹ in Milli-Q water) was used to stain the WPN to a final concentration of 0.1 mg mL⁻¹. Fluorescein isothiocyanate (FITC)-labelled-DxS of 40 kDa or 500 kDa was used to image DxS-E_{WPN}-40 and DxS-E_{WPN}-500, respectively, where FITC-DxS was used during the emulsion preparation process. The emulsion samples were placed on a concave confocal microscope slide, secured with a glass coverslip and finally imaged using an oil immersion 40× lens. The pinhole diameter was maintained at 1 Airy Unit to filter out majority of the light scattering. Nile Red was excited at a wavelength of 488 nm, Fast Green at 633 nm and FITC-DxS at 495 nm. The emission filters were set at 555 - 620 nm for Nile Red, 660 - 710 nm for Fast Green and 450 - 520 nm for FITC-DxS.

4.2.8 Quantification of protein hydrolysis

Protein hydrolysis was quantified using the standardized ortho-phthaldialdehyde (OPA) method, as described by Nielsen, Petersen, and Dambmann (2001) with minor modifications. Briefly, OPA reagent consisted of 3.81 g sodium tetraborate, 0.088 g dithiothreitol and 0.1 g sodium dodecyl sulphate (SDS). Exactly, 0.080 g OPA was dissolved in 2 mL ethanol and added to the above-mentioned solution and made up to 100 mL with Milli-Q water. The solution was kept in the dark. Absorbance at 340 nm was measured, using a UV-VIS spectrophotometer (6715 UV/VIS Spectrophotometer, Jenway, UK) blanked with OPA reagent and Milli-Q water. Quantification of protein hydrolysis was performed by using a reference calibration curve of L-leucine solution (0 - 200 μ M). Exactly, 160 μ L of standard solutions were added to 1200 μ L OPA reagent in a PMMA cuvette, mixed for 5 seconds and absorbance was measured after standing for 2 min. The same procedure was applied to the samples. The protein hydrolysis was expressed as a μ M free amino groups per mass of the total protein in sample.

4.2.9 Sodium dodecyl sulphate polyacrylamide gel electrophoresis (SDS-PAGE)

The protein composition of the aqueous dispersions of WPN, WPN+DxS-40 and WPN+DxS-500, respectively and corresponding adsorbed phases of the emulsion droplets (E_{WPN} , DxS- E_{WPN-40} and DxS- $E_{WPN-500}$) after gastric hydrolysis by pepsin was examined using SDS-PAGE under reducing conditions. The WPN-SGF, WPN+DxS-40 kDa-SGF or WPN+DxS-500 kDa-SGF mixtures (1.5 mL) after gastric digestion with pepsin were mixed with SDS buffer (0.5 M Tris, 2.0% SDS, 0.05% β -mercaptoethanol, pH 6.8), at a 1:2 ratio (sample : SDS buffer), heated at 95 °C for 5 min and 10 μ L was loaded into precast gels placed on a Mini-PROTEAN II system (Bio-Rad Laboratories, Richmond, CA, USA). 5 μ L of protein molecular weight marker was added in the first lane. After running the gel at 100 V for an hour, the gel was stained for 120 min with a Coomassie Brilliant Blue R-250 solution in 20% isopropanol. The gels were destained overnight in Milli-Q water and scanned using a ChemiDoc™ XRS + System with image Lab™ Software (Bio-Rad Laboratories, Richmond, CA, USA).

For measuring the composition of adsorbed phase in case of E_{WPN} , DxS- E_{WPN-40} or DxS- $E_{WPN-500}$, the emulsion-SGF mixtures (1.5 mL) after digestion and termination of the pepsin-induced hydrolysis were collected at specific time points and

centrifuged for 40 min at 4,000 g at 20 °C using an Eppendorf centrifuge (Thermo Scientific, Waltham, MA). The cream layer was collected carefully, and a certain amount of cream was then mixed with SDS buffer at a sample: SDS buffer ratio of 1:4, heated at 95 °C for 5 min with 10 μ L of sample loaded and the SDS-PAGE experiment was conducted. The intensities of the protein bands were quantified using Image Lab Software Version 6.0. Bands within the lanes was selected automatically by the software to cover the whole band. Background intensity was subtracted after scanning an empty lane. The percentage composition of each sample was determined by scanning the gradual reduction in peak volume intensity for each intact protein bands of WPI (β -lactoglobulin (β -lg), α -lactalbumin (α -la) and bovine serum albumin (BSA)). The SDS PAGE experiments were carried out in triplicates and band intensities was reported as an average of three reported readings.

4.2.10 Statistical analysis

Mean and standard deviation were calculated from three individual measurements performed on triplicate samples and analysed using the one-way analysis of variance (ANOVA) and Student's t-test where significance was accepted at $p < 0.05$.

4.3. Results and Discussion

4.3.1 Optimization of the biopolymer-coated Pickering emulsions

Firstly, the influence of pH on the ζ -potential of WPN, DxS-40 kDa and DxS-500 kDa was examined (Appendix C, Figure C1). The ζ -potential of the WPN went from being highly positive to highly negative as the pH was increased from 2.0 to 7.0 due to the protonation of the ionisable groups as they move from above to below the isoelectric point, respectively (Appendix C, Figure C1). On the other hand, the ζ -potential of the DxS was negative at all pH values examined within the experimental window (Appendix C, Figure C1). The magnitude of the negative charge of the low MW DxS-40 Da was smaller as compared to that of the high MW DxS-500 kDa ($p < 0.05$), which is expected owing to the charge densities of the sulphate groups per unit of the dextran molecule being proportional to the MW of the biopolymer.

Secondly, we examined the influence of MW and concentration of DxS on the droplet size and charge of emulsions stabilized by WPN (Figure 4.1). At pH 3.0, the ζ -potential of the E_{WPN} was highly positive since WPN is below its isoelectric point (Appendix C, Figure C1). As the biopolymers were added, there was a significant reduction in net ζ -potential values. Upon adding 0.1 wt% DxS-40 kDa or DxS-500 kDa,

the net charge almost reduced to zero particularly in case of DxS- E_{WPN} -40 (Figure 4.1a1) whilst some positive charge remained in case of DxS- E_{WPN} -500 (Figure 4.1a2). This suggests that the coverage by DxS was incomplete at such low concentration. When the DxS concentration was increased to 0.2 wt%, the ζ -potential values of the DxS- E_{WPN} -40 or DxS- E_{WPN} -500 droplets showed a charge reversal from positive to negative values, highlighting that electrostatic interaction was sufficient between WPN-laden interface and DxS, irrespective of the MW. This result was attributed to the electrostatic deposition of anionic groups of the biopolymers onto the cationic surface of the protein-stabilized droplets (Gu et al., 2004, 2005; Güzey and McClements 2006; Harnsilawat et al., 2006). The net charge reached a plateau at ≥ 0.2 wt% DxS, which suggests that the anionic DxS had fully saturated the surface of cationic E_{WPN} droplets, with DxS-40 having lower magnitude of ζ -potential as compared to DxS-500, as discussed before.

Droplet size measurements indicated that addition of DxS increased the volume-average mean diameter (d_{43}) of the DxS- E_{WPN} -40 droplets, which ranged from 6.84 to 98.4 μm (Figure 4.1b1), whereas for DxS- E_{WPN} -500 droplets, the d_{43} ranged from 6.84 to 58.9 μm (Figure 4.1b2). These observations suggest droplet flocculation due to the formation of polymeric bridges between anionic DxS adsorbed to WPN-laden interface and some cationic patches in the surface of the neighbouring uncoated E_{WPN} droplets (Tokle et al., 2010). In addition, these flocculated droplets were not easily disrupted by the dilution or shear effects within the static light scattering (SLS) equipment. Interestingly, at an optimum concentration of 0.2 wt% DxS (Figures 4.1c1 and 4.1c2), the droplet size distribution became smaller with shrinkage in the more prominent peak in the size range of 10 - 1000 μm to 1 - 100 μm . This suggests that on adding higher amounts of DxS, a reduction in the droplet flocculation and electrostatic stabilization of the droplets was observed, as corroborated by the charges on the electrical charge observed in Figure 4.1a1 and 4.1a2. Since 0.2 wt% of anionic DxS was the minimum concentration needed to completely coat the cationic E_{WPN} droplets at pH 3.0, irrespective of the MW of DxS, resulting in negatively charged DxS- E_{WPN} -40 or DxS- E_{WPN} -500 emulsion droplets (Figure 4.1a1 and 4.1a2), this concentration was selected for the preparation of the DxS- E_{WPN} -40 or DxS- E_{WPN} -500 droplets.

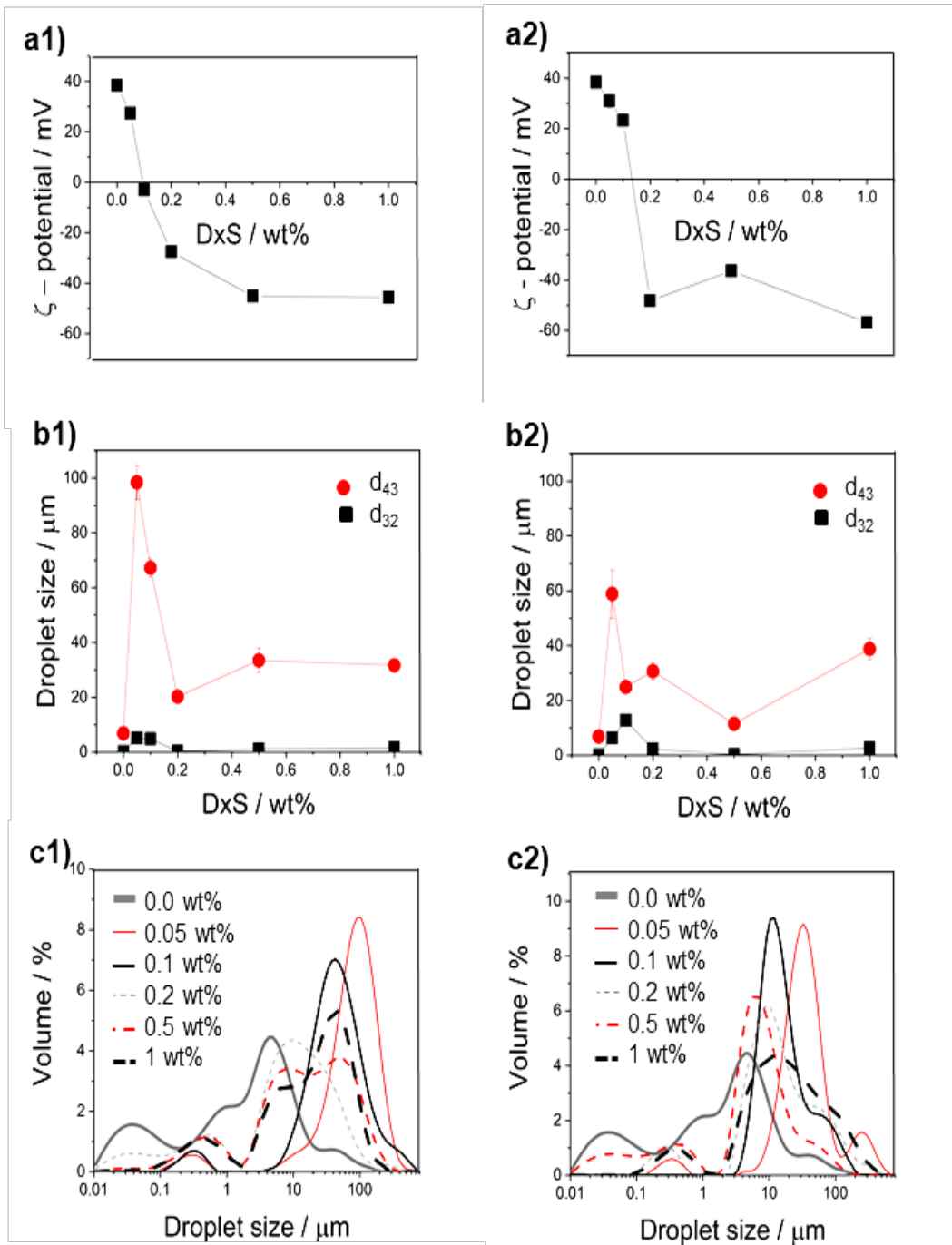


Figure 4.1. Change in a) mean ζ -potential values, b) mean droplet size (d_{43} and d_{32}) and c) mean droplet size distribution of 20 wt% MCT oil-in-water emulsions (DxS- E_{WPN}) at pH 3.0 containing 1 wt% WPN on addition of dextran sulphate (DxS) of (1) 40 kDa and (2) 500 kDa molecular weights, respectively. Error bars in figures a) and b) represent standard deviations, respectively.

4.3.2 *In vitro* gastric digestion of aqueous dispersions of WPN and DxS+WPN

Firstly, we determined the behaviour of the aqueous dispersions of WPN in absence and presence of 0.2 wt% DxS-40 kDa or DxS-500 kDa, respectively (Figure 4.2, 4.3 and Appendix C, Table C1 and Appendix C, Figure C2 and C3). This sets the scene to understand how the particles might behave when present in the continuous phase of the respective emulsions and compare it when they are present at the adsorbed phase. To determine the behaviour of the aqueous dispersion of WPN in presence or absence of DxS in the *in vitro* gastric digestion model, changes in their physicochemical properties and protein composition were examined as a function of digestion time. As controls, an aqueous dispersion of 1 wt% WPN and 1wt% WPN in presence of 0.2 wt% DxS-40 kDa or DxS-500 kDa in SGF without pepsin were also analysed (Appendix C, Table C2).

WPN. At pH 3.0, WPN had a hydrodynamic diameter of 91.5 nm and a ζ -potential of +30.2 mV (Appendix C, Table C1). Formation of WPN during the heat treatment is the result of the association of small aggregates *via* hydrophobic, electrostatic and disulphide bonds (Schmitt et al., 2010). After addition of SGF buffer (pH 3.0) without pepsin, changes in ζ -potential were not significant ($p > 0.05$) (see time zero in Appendix C, Figure C2). Upon gastric incubation in SGF containing pepsin, the size distribution of the particles became multi-modal and it was no longer possible to measure the hydrodynamic diameter using DLS as the particle size was too polydisperse to be considered for Rayleigh fitting (data not shown). This indicates that WPN was hydrolysed by pepsin and created different sizes of particle aggregates. As can be expected, a significant decrease in the ζ -potential value was also observed within the first 15 min of digestion, which remained fairly constant at $\sim +20$ mV even after 2 h (Appendix C, Figure C2).

The results are in agreement with the protein hydrolysis monitored using SDS-PAGE (Figure 4.2a1 and 4.2b1). It can be observed that, after just 5 min of incubation, the intensity of the bands corresponding to the major whey proteins *i.e.* β -lactoglobulin (β -lg), α -lactalbumin (α -la) as well as bovine serum albumin (BSA) bands was reduced considerably (remaining intact proteins were 24%, 19.27% and 0%, respectively), with simultaneous appearance of a mixture of peptides with molecular weights < 10 kDa after 2 h incubation (Figure 4.2a1). These results can be explained in terms of

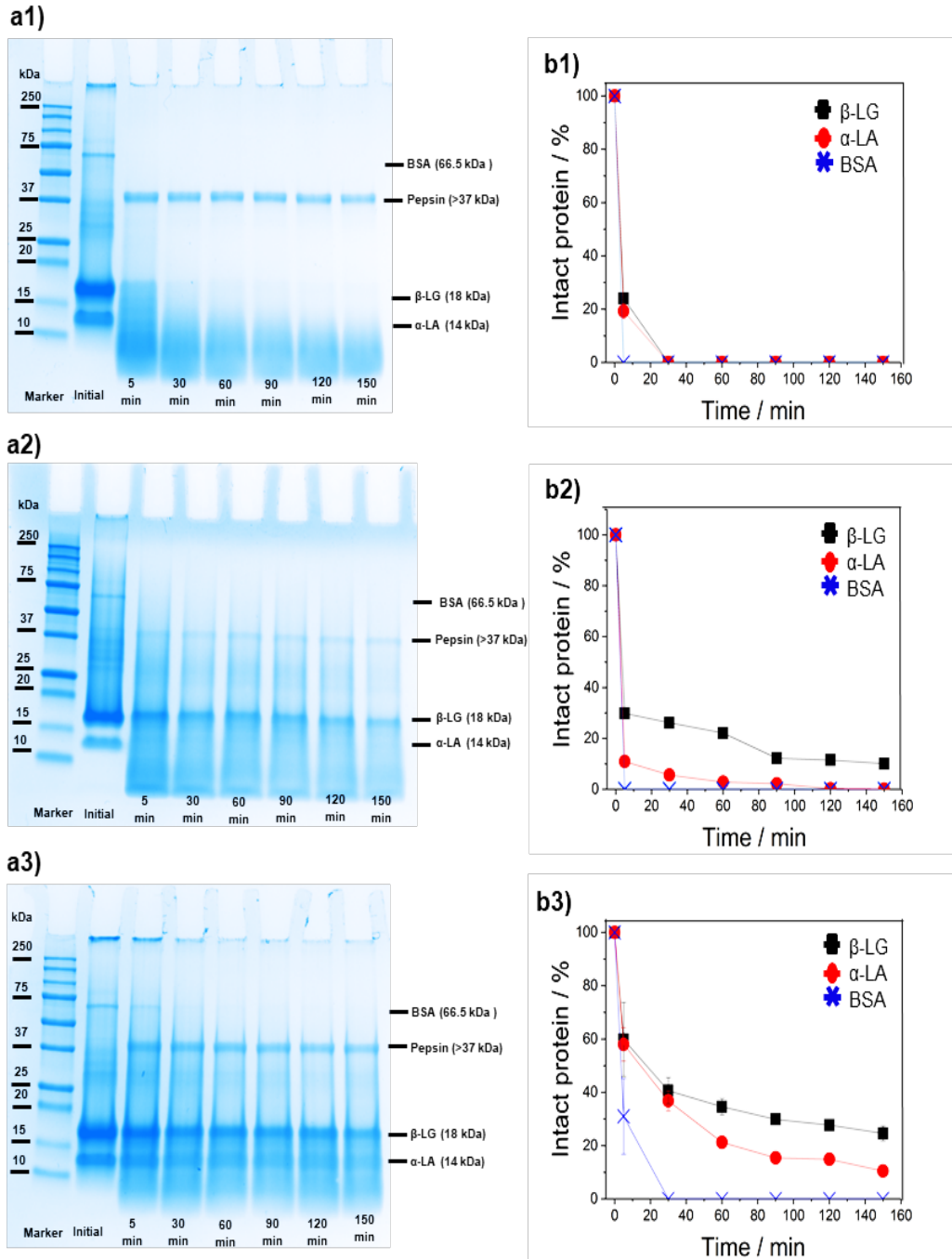


Figure 4.2. a) SDS-PAGE image and b) percentage of intact protein bands of (1) 1 wt% WPN and 1 wt% WPN with addition of 0.2 wt% DxS of (2) 40 kDa or (3) 500 kDa molecular weights, respectively, as a function of *in vitro* gastric digestion time. Error bars in figure b represent standard deviations.

temperature-induced conformational changes in the whey protein structure. In native state, β -lg (the major protein in whey protein isolate) has most of the hydrophobic amino acids buried inside the β -barrel structure making them not easily accessible to pepsin, which makes native β -lg resistant to pepsin hydrolysis (Sarkar et al., 2009).

Upon heating, unfolding of the protein molecule exposes the hydrophobic amino acids, making it highly susceptible to hydrolysis by pepsin (Reddy et al., 1988). From our results it is evident that the thermal treatment during WPN preparation exposed the hydrophobic amino acids, which were not refolded during the particle formation making them more accessible to pepsin hydrolysis during gastric incubation as compared to native WPI.

WPN+DxS. At pH 3.0, aqueous dispersions of WPN containing either DxS-40 kDa or DxS-500 kDa had highly negative ζ -potential values of -21.6 mV and -37.4 mV, respectively, which suggest that the DxS saturated the surface of cationic WPN (Appendix C, Table C1). Addition of DxS caused particle aggregation irrespective of the MW, and it was not possible to measure the hydrodynamic diameter using DLS (Appendix C, Figure C3b and C3c).

Presence of SGF without pepsin did not showed significant ($p < 0.05$) changes in the ζ -potential for both 40 and 500 kDa DxS (-37.7 and -40.5 mV, respectively) (see time zero in Appendix C, Figure C2). During gastric incubation with pepsin, the magnitude of ζ -potential of the particles was reduced from -37.7 mV to a constant value ranging between -4.4 and +2.2 mV for 40 kDa DxS samples (Appendix C, Figure C2). The ζ -potential of the WPN+DxS-500 kDa particles was more negative than that of the WPN+DxS-40 kDa and was reduced from -40.5 mV to a constant value ranging between -15.7 and -22.3 mV, during the 120 min of gastric incubation (Appendix C, Figure C2). The most likely explanation for this effect is that there was electrostatic screening of charge of the biopolymer-coated particles by the SGF buffer, as can be corroborated by the control samples subjected to the SGF without pepsin (Appendix C, Table C2).

The SDS-PAGE electrograms of WPN+DxS for both biopolymers are shown in Figures 4.2a2 and 4.2a3. It can be seen that for both biopolymers *i.e.* DxS-40 kDa or DxS-500 kDa, the β -lg bands remained relatively resistant to pepsin hydrolysis as compared to that of WPN alone (Figure 4.2a1). Particularly, it can be observed that the band corresponding to α -la protein remained resistant to pepsin hydrolysis for DxS-500 kDa, with a clear band still present after up to 2.5 h incubation in SGF (Figure 4.2a3). Quantification of the SDS-PAGE gel bands (Figures 4.2b2 and 4.2b3) suggests that in presence of DxS-40 kDa, the proportion of β -lg and α -la decreased to 11.47% and 0.25%, respectively after 2 h of incubation (Figure 4.2b2). As for DxS-500 kDa, the proportion of intact protein bands were much higher, with 27.70% of β -lg and 14.88% of α -la remaining after 2 h of incubation (Figure 4.2b3).

In addition, the free amino group (NH₂) content was determined by OPA method for the WPN and WPN after addition of 0.2 wt% DxS of 40 and 500 kDa before and after gastric digestion with added pepsin and shown in Figure 4.3.

The concentration of free NH₂ increased generally with digestion time for all samples. Results indicated that for WPN, there was an increase in the proteolysis profile in the first 30 min gastric digestion from 989.97 mM NH₂/ g to 3,747 mM NH₂/ g, after which it levelled off to values between 3,747 - 4088.66 mM NH₂/ g during the 120 min gastric digestion. These values are in agreement with previously reported hydrolysis of different whey proteins (Church et al., 1985; Lemieux et al., 1990). Levels of proteolysis were significantly ($p < 0.05$) lower after addition of DxS. For lower molecular weight DxS (40 kDa), after 30 min gastric digestion, the free NH₂/ g concentration was 3,105.88 mM NH₂/ g (as compared to 3,747 mM NH₂/ g in WPN) with a relatively constant value between 3,105.88 - 3,808.97 mM NH₂/ g during the 120 min (Figure 4.3). The proteolysis profile for DxS of higher molecular weight of 500 kDa was 771.01 mM NH₂/ g in the first 30 min with values between 771.01 - 2,752.21 mM NH₂/ g after the 120 min gastric digestion, clearly indicating the barrier effect of DxS-500 kDa on proteolysis of WPN.

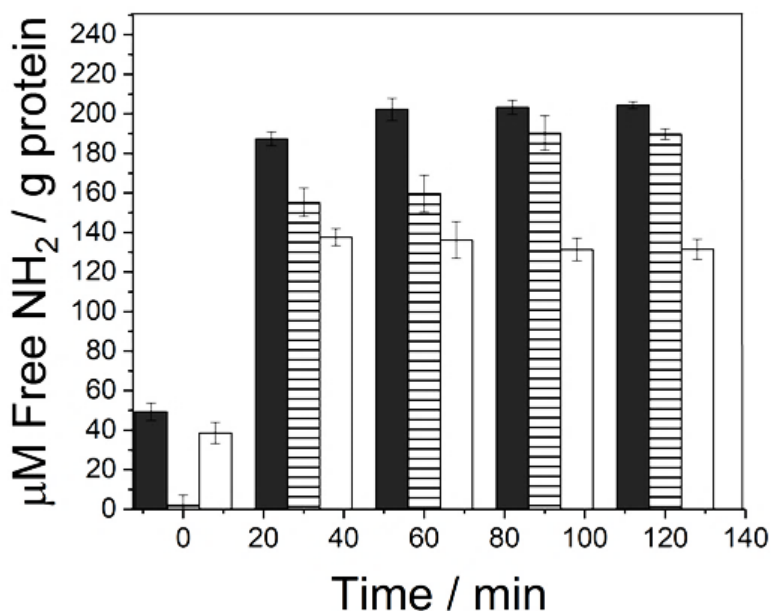


Figure 4.3. Free amino acid content of 1 wt% WPN (dark) and 1 wt% WPN with addition of 0.2 wt% DxS of 40 kDa (lined pattern) or 500 kDa (dotted pattern) molecular weights, respectively, as measured by OPA spectrophotometric and as a function of *in vitro* gastric digestion time. Error bars in figure represent standard deviations.

A possible explanation from the increased protection to WPN upon DxS addition might be related to the aggregation state of the particles, *i.e.* DxS was aggregating the WPN particles limiting the access of pepsin to the peptic cleave sites of WPN. In addition, the higher extent of protection to WPN against proteolysis by DxS-500 kDa as compared to that of DxS-40 kDa may arise from a combination of high ζ -potential values, and/ or the MW (degree of branching) that somehow physically inhibited the enzyme to reach the hydrophobic moieties of the protein nanogel particles. These results are in agreement with a previous study that have reported increased resistance to gastric proteolysis during first 10 min of simulated gastric conditions of lactoferrin nanoparticles, when coating these particles with low methoxyl pectins as compared to that of high methoxyl pectins. The increased gastric resistance was largely associated with the increased electro-kinetic charge of the former (Tokle et al., 2012). Overall, these results suggest that the extent of the protective effect of DxS-500 kDa was markedly higher than that of DxS-40 kDa in the bulk phase and it would be interesting to see whether such effects exist when DxS coats the WPN-stabilized droplets at the surface.

4.3.3 Physicochemical and microstructural characterization of E_{WPN} , DxS- E_{WPN} -40 and DxS- E_{WPN} -500 during *in vitro* gastric digestion

Pickering emulsion samples with or without the biopolymer coating of 0.2 wt% DxS were prepared at pH 3.0, subjected to *in vitro* gastric model (SGF, pH 3.0) at 37 °C and then the droplet size, charge, and microstructure were measured as a function of digestion time (Figures 4.4 and 4.5). In addition, as controls, E_{WPN} , DxS- E_{WPN} -40 and DxS- E_{WPN} -500 in SGF without pepsin were also analysed (Appendix C, Figure C3).

E_{WPN} . Freshly prepared E_{WPN} at pH 7.0 presented a bimodal droplet size distribution with the droplet population in the peak area of 0.1 - 1.0 μm corresponding to the unadsorbed WPN and the population in the peak area of 10-100 μm corresponding to the emulsion droplets (Figure 4.4a1). The mean droplet diameter (d_{43}) was 9.61 μm and the droplets presented a highly negative charge of -26.70 mV, because the adsorbed layer of WPN was above its pI (data not shown). Confocal images of the E_{WPN} shows the WPN particles (stained green by Fast Green) clearly adsorbed on the surface of the oil droplets (stained by Nile Red) (Figure 4.4a1). Upon decreasing the pH to gastric pH 3.0, the droplet size distribution and the volume average mean diameter (d_{43}) were not significantly changed ($p > 0.05$) (Figure 4.4a1 and Table 4.1), but the droplets presented a charge reversal to a highly positive charge

of +35.9 mV, as the pH was below the *pI* as previously discussed with respect to Figure 4.1a1 and 4.1a2.

Table 4.1. Droplet size and ζ -potential values for E_{WPN} , DxS- E_{WPN} -40 and DxS- E_{WPN} -500 at pH 3.0, respectively.

	E_{WPN}		DxS- E_{WPN} -40		DxS- E_{WPN} -500	
	$d_{43} / \mu\text{m}$	ζ -potential / mV	$d_{43} / \mu\text{m}$	ζ -potential / mV	$d_{43} / \mu\text{m}$	ζ -potential / mV
pH 3.0	11.50 ± 1.20	+35.9 ± 0.80	22.2 ± 0.98	-28.8 ± 1.30	38.8 ± 0.07	-46.2 ± 2.42

Incubation of E_{WPN} with SGF without pepsin did not significantly influence the droplet size distribution (Figure 4.4a1), mean droplet size (d_{43} 16.93 μm) and ζ -potential of the droplets (see time zero in Figure 4.4b1), indicating that E_{WPN} was stable to any aggregation under the ionic environment of the gastric conditions. From the confocal images, it can be seen that the emulsion droplets did not show significant aggregation (Fig. 5b1) as compared to initial emulsions (Figure 4.5a1). When E_{WPN} was incubated in SGF with pepsin, the mean droplet size decreased from 16.93 μm to 9.72 μm within the first 5 min of gastric digestion and remained fairly constant obtained over time (Figure 4.4b1). The droplet size distribution shows the appearance of a population of smaller droplet size (Figure 4.4a1), which was not observed in the control samples (Appendix C, Figure C3). Interestingly, the ζ -potential of the droplets remained fairly constant at +37.6 mV by the end of the gastric incubation (Figure 4.4b1) indicating the presence of enough WPN at the interface. Therefore, it can be suggested that the decrease in size of the E_{WPN} with smaller sized population might have been caused by pepsin hydrolysis either hydrolysing the protein at the surface of the emulsion droplets, or the particles bridging different droplets. This result is in agreement with previous studies that have reported decrease of d_{43} values after gastric digestion of whey protein microgel-stabilized Pickering emulsions (Sarkar et al., 2016a).

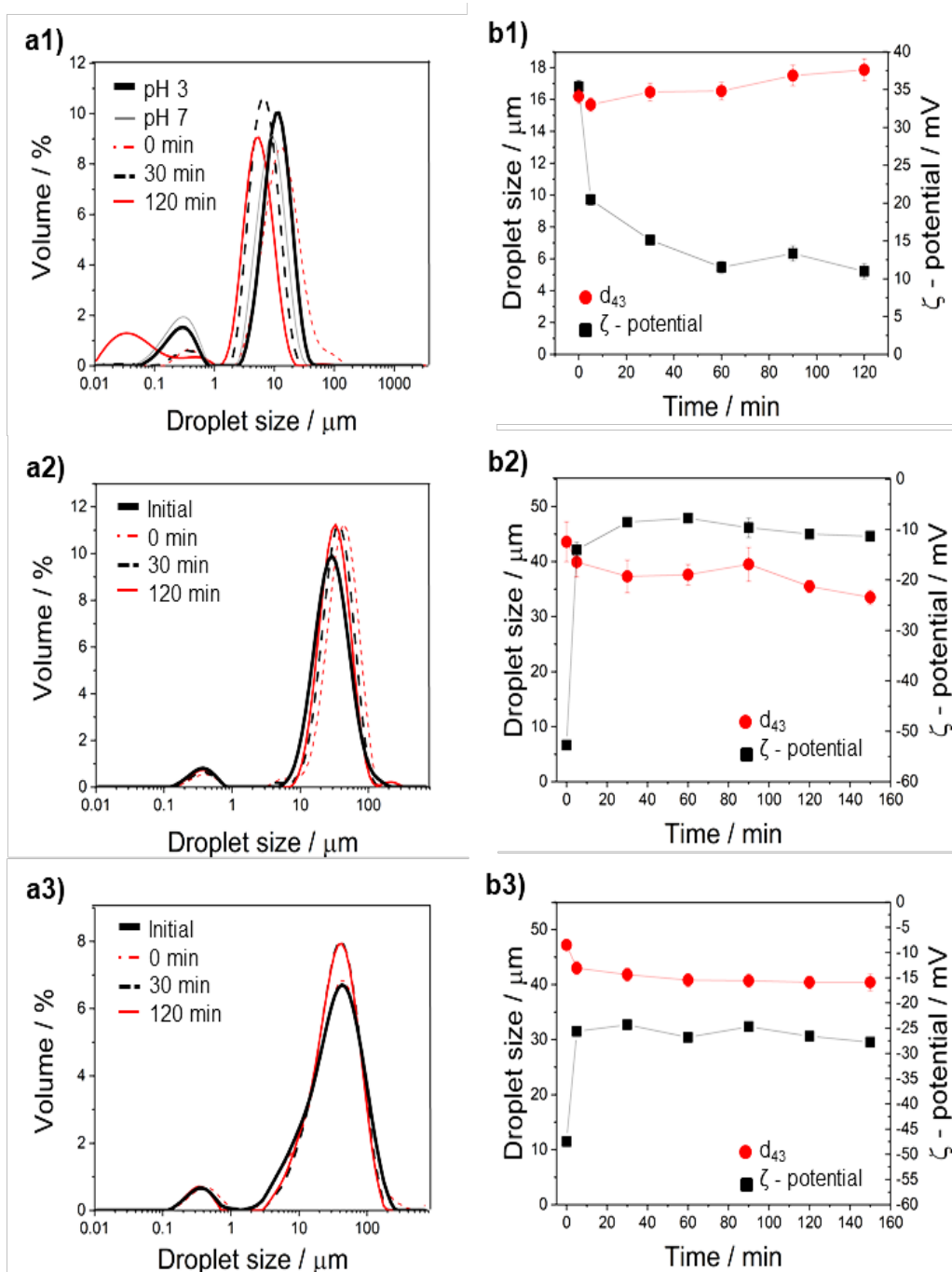


Figure 4.4. a) Droplet size distribution and b) mean droplet size (d_{43}) and ζ -potential values of (1) E_{WPN}, (2) DxS-E_{WPN}-40 and (3) DxS-E_{WPN}-500 after *in vitro* gastric digestion, respectively. Error bars in figure b represent standard deviations.

Looking at the confocal images, after 30 minutes incubation, the microstructure of the emulsion (Figure 4.4c1) changed dramatically showing very limited population of droplets. One might argue it is due to the dilution effect with SGF, however that can be negated by looking at the image at 0 min which had equivalent droplet concentration due to dilution with SGF buffer without any added pepsin. This suggests

that pepsin was hydrolysing the bridges between the WPN-coated droplets as well as was rupturing the particle-layer at the interface to a certain extent resulting in some degree of droplet coalescence. Such coalesced droplets were most likely rising to the top and thus were not visualized by the confocal microscopy resulting in reduction in droplet volume (Figures 4.5c1). Confocal micrographs of the emulsion after 120 min of gastric digestion provided further evidence of the appearance of individual droplets that appeared to be less aggregated emulsion droplets (Figures 4.5d1) than the ones in 0 min (Figures 4.4b1). A thin interfacial layer around the oil droplets even after 120 min was observed in the microscopic image (Figure 4.5d1) suggesting that either WPN or peptide network of WPN were still present in the emulsion droplets after the gastric digestion that were somehow protecting the droplets against coalescence.

DxS-E_{WPN}-40 and DxS-E_{WPN}-500. Before digestion, biopolymer-coated emulsions containing either of the two anionic DxS (40 or 500 kDa MW) had high negative charges (-28.8 and -46.2 mV for 40 kDa and 500 kDa, respectively) at pH 3.0 (Table 4.1), suggesting that the biopolymer had substantially adsorbed onto the cationic WPN-stabilized oil droplets at pH 3.0. Both 40 and 500 kDa DxS-E_{WPN} presented a bimodal particle size distributions (Fig. 4a2 and 4a3) with a mean droplet size (d_{43}) of 22.2 and 38.8 μm , respectively (Table 4.1). The increase of the droplet size might result from the aggregation of the E_{WPN} droplets after addition of DxS, as reflected by the confocal images (Figures 4.5a2 and 4.5a3). In addition, it can also be observed in Figures 4.5a2 and 4.5a3 that FITC-labelled DxS (stained in blue) is electrostatically adsorbed to the WPN particles (stained in green). At this point, it is worth mentioning that, Nile Red was not used to stain the oil droplets, since both Nile Red and FITC-labelled DxS possessed similar excitation wavelengths. For this reason, images were only acquired using Fast green (for WPN) and FITC-DxS for visualizing the biopolymer coating. Appendix C, Figure C4 shows a control image indicating that the presence of FITC-labelled DxS only records the DxS and not the WPN.

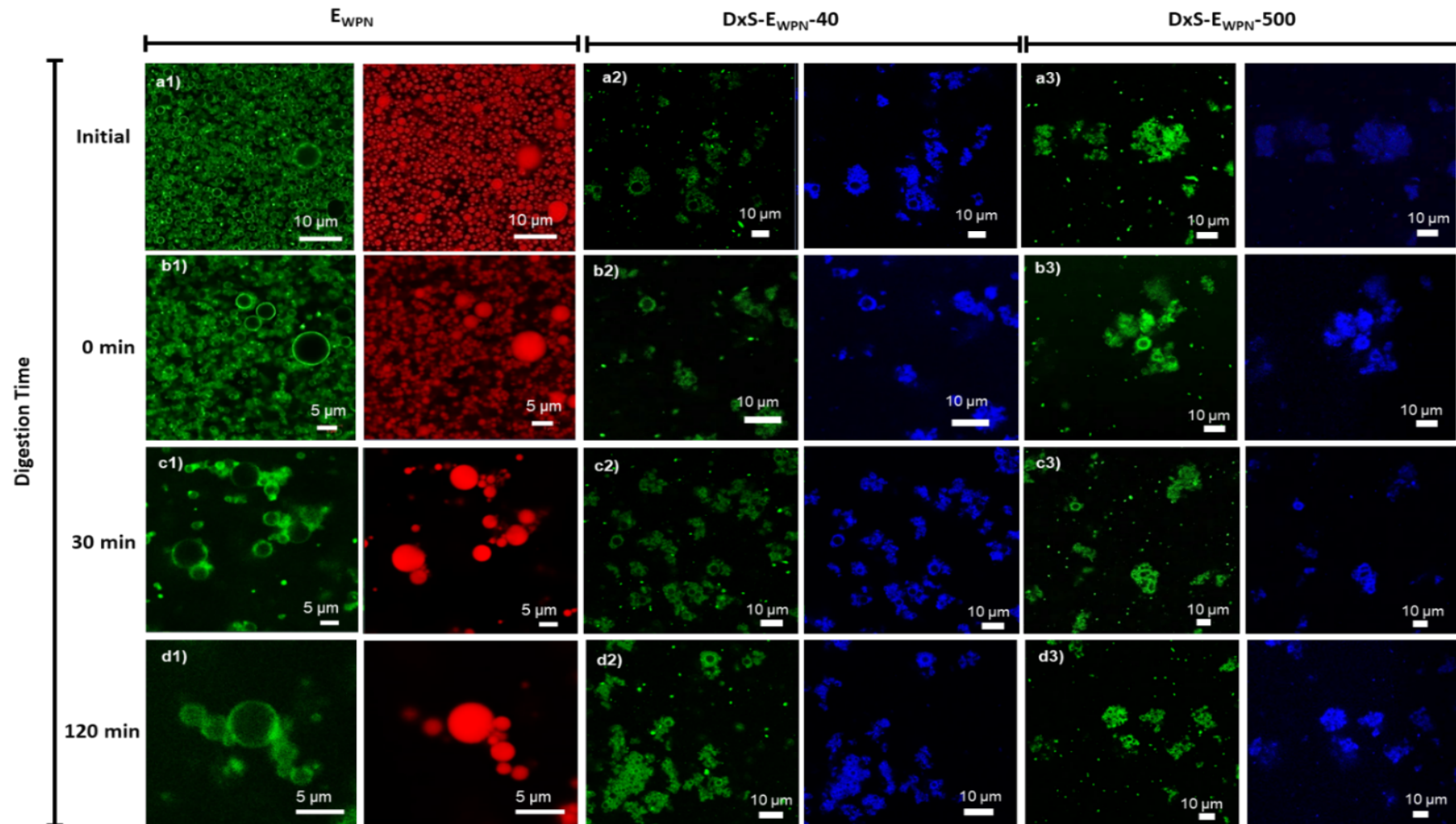


Figure 4.5. Confocal micrographs of (1) E_{WPN} , (2) $DxS-E_{WPN-40}$ and (3) $DxS-E_{WPN-500}$ at 0 min (a), after 30 min (b), and 120 min (c) of *in vitro* gastric digestion in presence of SGF containing pepsin, respectively. Note, 0 min represents the behavior in presence of SGF buffer without added pepsin. Green colour represents WPN stained by Fast Green; red colour represents the oil droplets stained by Nile Red, and the blue colour represents the FITC-labelled dextran sulfate.

Incubation in SGF without pepsin showed no significant ($p < 0.05$) changes in the ζ -potential values and d_{43} (see time zero for Figures 4.4b2 and 4b3) for DxS of both MW, confirming there was no SGF-induced effects on aggregation of the droplets. The confocal images (Figures 4.5b2 and 4.5b3) further confirms that the FITC-labelled DxS remained adsorbed to the WPN and that the emulsion droplets sizes are in agreement with the light scattering data. After addition of pepsin, there was a pronounced decrease in the magnitude of their negative charge within the first 5 min of digestion, reaching a fairly constant value at longer digestion time scales (Figures 4.4b2 and 4.4b3). This negative charge is in line with the anionic DxS being bound to the DxS- E_{WPN} droplets under SGF, as evidenced by the bright blue ring surrounding the emulsion droplets and indicating the presence of the FITC-labelled DxS (Figures 4.5c2-c3 and 4.5d2-d3). Emulsions were stable to the gastric conditions, since there was no increase in the mean particle diameter (d_{43}) (Figures 4.4b2 and 4.4b3), and there was no evidence of coalescence in the microscopy images (Figures 4.5c2-c3 and 4.5d2- d3). Irrespective of digestion times, DxS appeared to be in the same region as the WPN highlighting that the electrostatic complexation at the interface remained almost unaffected in presence of pepsin. These results clearly indicate that DxS- E_{WPN} -40 and DxS- E_{WPN} -500 emulsion droplets at gastric conditions exhibited resistance to any pepsin-induced microstructural changes.

4.3.4 Protein composition of adsorbed phase of E_{WPN} , DxS- E_{WPN} -40 and DxS- E_{WPN} -500 during *in vitro* gastric digestion

The SDS-PAGE of the adsorbed phases of all emulsion systems, *i.e.* E_{WPN} , DxS- E_{WPN} -40 and DxS- E_{WPN} -500 were compared (Figure 4.6). The SDS-PAGE electrograms revealed that in E_{WPN} , the major protein constituents, β -Ig and α -la, as well as BSA were identified in the initial undigested emulsion (Figure 4.6a1). However, upon incubation in SGF containing pepsin, within the first 5 min the BSA fraction almost completely disappeared, and the proportion of the β -Ig and α -la fractions decreased to 55.39% and 36.19%, respectively (Figure 4.6b1). These results suggest that the emulsification of the WPN slightly decreased the accessibility of pepsin as compared to that when WPN was freely available in aqueous dispersion (Figure 4.2a1). These results can be explained in terms of wetting of WPN by the oil phase that consequently reduced its accessibility to pepsin. However, after 120 min of gastric incubation, both β -Ig and α -la bands completely disappeared, indicating complete hydrolysis of these proteins. At the end of the gastric phase (2.5 h), a fuzzy thick band representing a mixture of peptides with molecular weights < 10 kDa was observed in the gels (Figure 4.6a1). This supports the thin particle-laden interface observed in the

micrographs even after 2 hours of digestion, which might be the peptide remnants of nanogel particles or peptides (Figure 4.5d1).

In contrast, the digestion pattern of the DxS-E_{WPN} emulsion during gastric proteolysis was very different from that E_{WPN} (Figures 4.6a1 and 4.6a3). In addition, it should be noted that some interfacial material remained in the stacking gel. It is possible that the protein nanogel aggregates present in the adsorbed phase were too large (>250 kDa) to enter the resolving gel. The hydrolysis pattern for DxS-E_{WPN}-40 emulsions after 5 minutes of gastric incubation revealed that the proportion of BSA decreased to 17.4%, whereas significant proportion of β -lg and α -la fractions remained with intact fractions of about 48.4% and 40.3%, respectively (Figure 4.6b2). After 120 min, the quantity of BSA, β -lg and α -la remaining undigested was 0.12%, 11.62% and 11.88%, respectively (Figure 4.6b2). Confocal fluorescent microscopy images of the emulsions after 120 min digestion indicated the aggregated microstructure arrangement of the droplets, which may also contribute to the slowed pepsin hydrolysis, since pepsin would have to diffuse through the outer parts of these aggregates before it could reach the protein sites underneath these DxS coating (Figures 4.5c2-d2). These results suggested that the polysaccharide coating decreased the digestibility of the WPN located at the interface of E_{WPN}.

In the case of 500 kDa DxS-E_{WPN}, a considerable amount of interfacial material was also observed to remain in the stacking gel (Figure 4.6a3). However, within the first 5 min of gastric incubation, the BSA fraction was reduced to 95.27%, whereas the proportion of the β -lg and α -lg fractions decreased to 89.70% and 94.518%, respectively (Figures 4.6b3). At the end of the 2.5 h gastric digestion, around 83.42%, 67.50% and 73.75% of the BSA, β -lg and α -la fractions remained still intact. These result are in agreement with previous studies that have reported that the presence of a polysaccharide coating reduced the activity of pepsin for protein-stabilized emulsions after 2 h gastric incubation (Tokle et al., 2012; Li et al., 2011).

A possible explanation for this effect could be that the formation of a more complex structure increased the barrier properties of DxS+WPN and reduced the pepsin diffusion to the underneath WPN-stabilized interface. Previous proteolytic studies on casein-stabilized emulsions with an adsorbed dextran sulphate layer have suggested that there may be an associative interaction of the enzyme (trypsin) with the adsorbed DxS layer, as a large increase in the interfacial shear viscosity was observed (Jourdain et al., 2009). Thus, it seems reasonable to suppose that, pepsin may be trapped or co-adsorbed within the DxS coatings, reducing the availability of pepsin in the close vicinity of hydrophobic groups of WPN for potential proteolysis. Consequently, we can reasonably infer that, a bigger molecular structure may impart

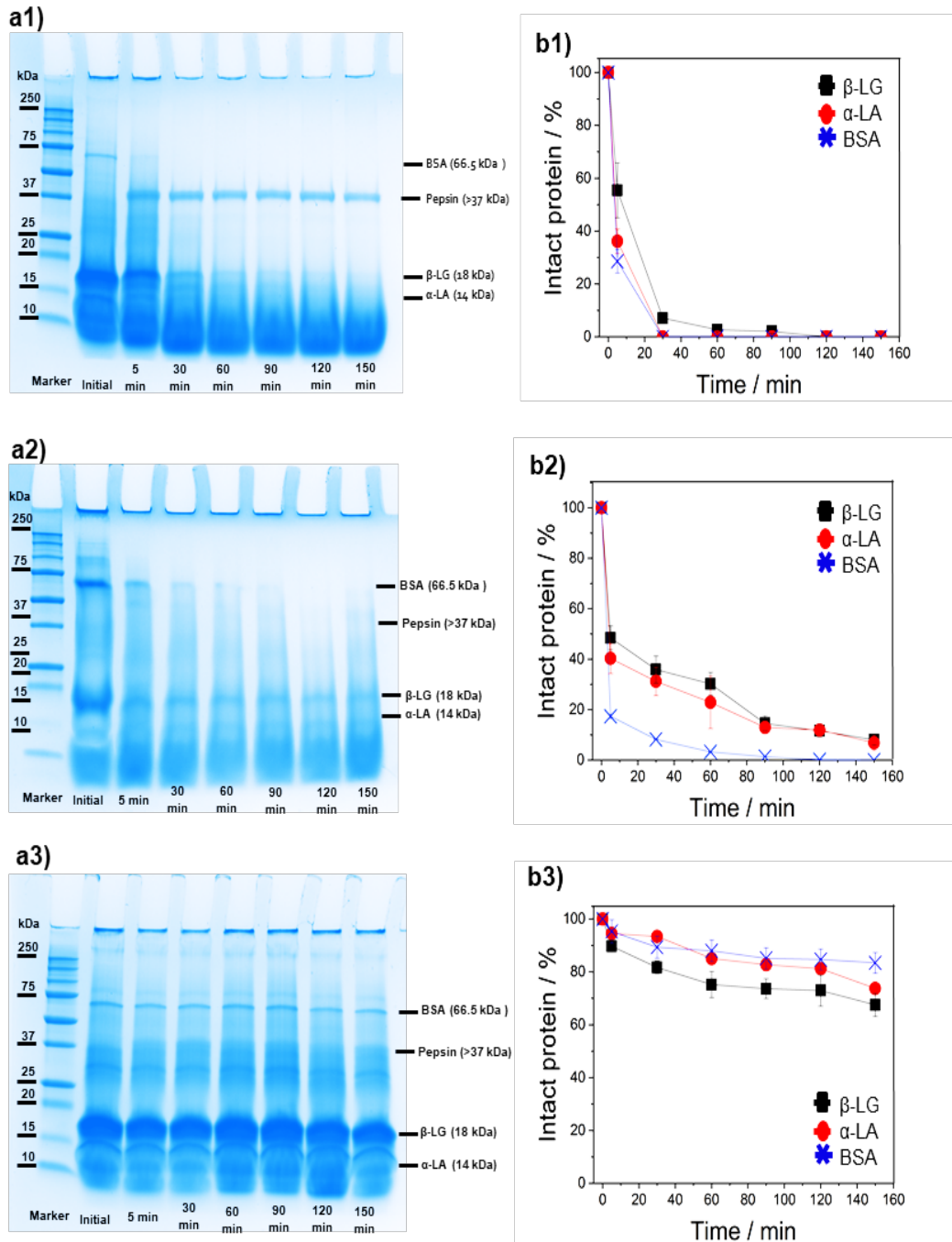


Figure 4.6. a) SDS-PAGE image and b) percentage of intact protein bands of the adsorbed phase of (1) E_{WPN}, (2) DxS-E_{WPN}-40, and (3) DxS-E_{WPN}-500 as a function of *in vitro* gastric digestion time. Error bars in figure b represent standard deviations.

a greater barrier effects to WPN substrate against pepsin attack, which is consistent with the differences in extent of hydrolysis between the two different MW of DxS used. A schematic diagram to illustrate the physical state of the DxS-E_{WPN} when it is exposed to *in vitro* gastric conditions is presented in Figure 4.7.

The E_{WPN} is stable in presence of SGF in absence of enzymes, but when pepsin is added to the system, hydrolysis of the interfacial protein layer occurs producing remnants of nanogel particle or peptides. On the contrary, hydrolysis of the interfacial protein layer on the $DxS-E_{WPN}$ is delayed by the presence of a physical barrier provided by a biopolymer either by providing an electrostatically repelling layer or simply providing a steric hindrance to pepsin, thus preventing gastric destabilization of the emulsion droplets.

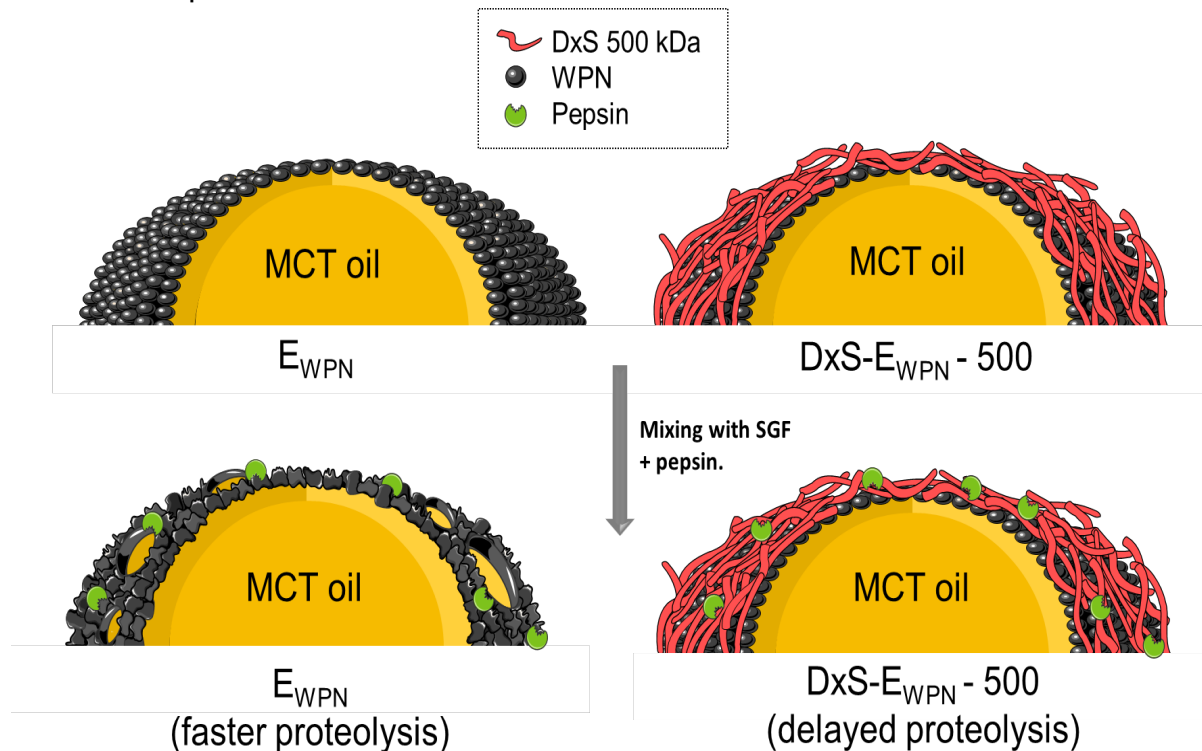


Figure 4.7. Schematic diagram of interaction of E_{WPN} and $DxS-E_{WPN}-500$ on digestion with SGF. The grey shaded circles represent the WPN particles, the long coil red structures represent the DxS-500 kDa electrostatically attached at the interfacial layer and the smaller green structures represent the pepsin.

4.4 Conclusions

In this study, we have studied the influence of coating of anionic dextran sulphate on the physicochemical properties and digestibility of whey protein nanogel particle-coated droplets under *in vitro* gastric conditions. Findings from this study report that the stability and degree of pepsin hydrolysis of the whey protein nanogel particles at the interface is restricted in presence of a secondary coating of dextran sulphate, latter could provide a steric and electrostatic barrier. In addition, the molecular weight of the coating had an appreciable effect on the degree of pepsin hydrolysis, with dextran sulphate of a molecular weight of 500 kDa presenting a better barrier to pepsin-hydrolysis of the underlying protein nanogel particle-laden interface

as compared to that of the 40 kDa molecular weight within the simulated gastric phase. Such results are mainly attributed to the higher negative charge density associated with higher degree of sulphate groups in the higher molecular weight system or the higher order molecular structure that trapped pepsin protecting the protein-laden interface against complete enzymatic hydrolysis. Insights from this study could enable creating future gastric-stable emulsions for food and pharmaceutical applications targeting altered lipid digestion profile in the intestinal phase or encapsulation of lipophilic bioactive compounds that need to be delivered to intestines without any gastric destabilization.

Both polymer-coated emulsions showed good *in vitro* gastric stability as compared to uncoated ones. However, such electrostatic interaction might not be relevant at pH 6.8 (intestinal pH), as both the protein nanogel particles and dextran sulphate will be negatively charged. Therefore, Maillard conjugation between whey protein isolate and dextran was employed to develop microgel particles to stabilize Pickering emulsions. Hence, in the following chapter (**Chapter 5**), the design of conjugated microgel particles and stability of O/W conjugated microgel-stabilized Pickering emulsions will be evaluated. In addition, behaviour during *in vitro* gastric digestion is of great importance to appreciate their potential application as oral delivery system for lipophilic compounds.

4.5 References

- Aoki, T., Decker, E. A., & McClements, D. J. (2005). Influence of environmental stresses on stability of O/W emulsions containing droplets stabilized by multi-layered membranes produced by a layer-by-layer electrostatic deposition technique. *Food Hydrocolloids*, 19(2), 209-220.
- Araiza-Calahorra, A., Akhtar, M., & Sarkar, A. (2018). Recent advances in emulsion-based delivery approaches for curcumin: From encapsulation to bioaccessibility. *Trends in Food Science & Technology*, 71, 155-169.
- Araiza-Calahorra, A., & Sarkar, A. (2019). Pickering emulsion stabilized by protein nanogel particles for delivery of curcumin: Effects of pH and ionic strength on curcumin retention. *Food Structure*, 21, 100113.
- Chu, B.-S., Rich, G. T., Ridout, M. J., Faulks, R. M., Wickham, M. S. J., & Wilde, P. J. (2009). Modulating pancreatic lipase activity with galactolipids: effects of emulsion interfacial composition. *Langmuir*, 25(16), 9352-9360.

- Church, F. C., Porter, D. H., Catignani, G. L., & Swaisgood, H. E. (1985). An o-phthalaldehyde spectrophotometric assay for proteinases. *Analytical Biochemistry*, 146(2), 343-348.
- Destribats, M., Wolfs, M., Pinaud, F., Lapeyre, V., Sellier, E., Schmitt, V., & Ravaine, V. (2013). Pickering emulsions stabilized by soft microgels: influence of the emulsification process on particle interfacial organization and emulsion properties. *Langmuir*, 29(40), 12367-12374.
- Dickinson, E. (2009). Hydrocolloids as emulsifiers and emulsion stabilizers. *Food Hydrocolloids*, 23(6), 1473-1482.
- Dickinson, E. (2012). Use of nanoparticles and microparticles in the formation and stabilization of food emulsions. *Trends in Food Science & Technology*, 24(1), 4-12.
- Fioramonti, S. A., Arzeni, C., Pilosof, A. M. R., Rubiolo, A. C., & Santiago, L. G. (2015). Influence of freezing temperature and maltodextrin concentration on stability of linseed oil-in-water multilayer emulsions. *Journal of Food Engineering*, 156, 31-38.
- Gharsallaoui, A., Saurel, R., Chambin, O., Cases, E., Voilley, A., & Cayot, P. (2010). Utilisation of pectin coating to enhance spray-dry stability of pea protein-stabilised oil-in-water emulsions. *Food Chemistry*, 122(2), 447-454.
- Gu, Y. S., Decker, E. A., & McClements, D. J. (2004). Influence of pH and κ -carrageenan concentration on physicochemical properties and stability of β -lactoglobulin-stabilized oil-in-water emulsions. *Journal of Agricultural and Food Chemistry*, 52(11), 3626-3632.
- Gu, Y. S., Decker, E. A., & McClements, D. J. (2005). Influence of pH and carrageenan type on properties of β -lactoglobulin stabilized oil-in-water emulsions. *Food Hydrocolloids*, 19(1), 83-91.
- Gudipati, V., Sandra, S., McClements, D. J., & Decker, E. A. (2010). Oxidative stability and *in vitro* digestibility of fish oil-in-water emulsions containing multi-layered membranes. *Journal of Agricultural and Food Chemistry*, 58(13), 8093-8099.
- Güzey, D., & McClements, D. J. (2006). Influence of environmental stresses on O/W emulsions stabilized by β -lactoglobulin-pectin and β -lactoglobulin-pectin-chitosan membranes produced by the electrostatic layer-by-layer deposition technique. *Food Biophysics*, 1(1), 30-40.
- Harnsilawat, T., Pongsawatmanit, R., & McClements, D. J. (2006). Influence of pH and ionic strength on formation and stability of emulsions containing oil droplets coated by β -lactoglobulin-alginate interfaces. *Biomacromolecules*, 7(6), 2052-2058.

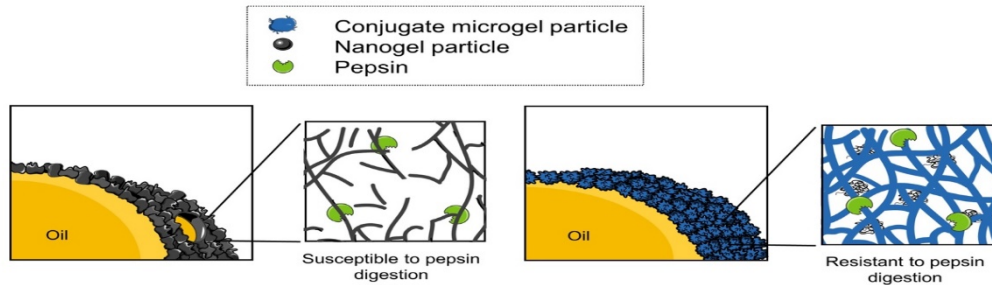
- Holt, S., Brand, J., Soveny, C., & Hansky, J. (1992). Relationship of satiety to postprandial glycaemic, insulin and cholecystokinin responses. *Appetite*, 18(2), 129-141.
- Hu, M., Li, Y., Decker, E. A., Xiao, H., & McClements, D. J. (2011). Impact of layer structure on physical stability and lipase digestibility of lipid droplets coated by biopolymer nanolaminated coatings. *Food Biophysics*, 6(1), 37-48.
- Jourdain, L. S., Schmitt, C., Leser, M. E., Murray, B. S., & Dickinson, E. (2009). Mixed layers of sodium caseinate + dextran sulphate: influence of order of addition to oil–water interface. *Langmuir*, 25(17), 10026-10037.
- Klinkesorn, U., & Julian McClements, D. (2010). Impact of lipase, bile salts, and polysaccharides on properties and digestibility of tuna oil multilayer emulsions stabilized by lecithin–chitosan. *Food Biophysics*, 5(2), 73-81.
- Lemieux, L., Puchades, R., & Simard, R. E. (1990). Free Amino Acids in Cheddar Cheese: Comparison of Quantitation Methods. 55(6), 1552-1554.
- Li, Y., Hu, M., Du, Y., & McClements, D. J. (2011). Controlling lipid nanoemulsion digestion using nanolaminated biopolymer coatings. *Journal of Microencapsulation*, 28(3), 166-175.
- Liu, S., Elmer, C., Low, N. H., & Nickerson, M. T. (2010). Effect of pH on the functional behaviour of pea protein isolate–gum Arabic complexes. *Food Research International*, 43(2), 489-495.
- Lomova, M. V., Brichkina, A. I., Kiryukhin, M. V., Vasina, E. N., Pavlov, A. M., Gorin, D. A., Sukhorukov, G. B., & Antipina, M. N. (2015). Multilayer capsules of bovine serum albumin and tannic acid for controlled release by enzymatic degradation. *ACS Applied Materials & Interfaces*, 7(22), 11732-11740.
- Mackie, A., & Macierzanka, A. (2010). Colloidal aspects of protein digestion. *Current Opinion in Colloid & Interface Science*, 15(1), 102-108.
- Mackie, A. R., Gunning, A. P., Wilde, P. J., & Morris, V. J. (2000). Orogenic displacement of protein from the oil/water interface. *Langmuir*, 16(5), 2242-2247.
- Maljaars, P. W. J., Peters, H. P. F., Mela, D. J., & Masclee, A. A. M. Ileal brake: (2008). A sensible food target for appetite control. A review. *Physiology & Behaviour*, 95(3), 271-281.
- Minekus, M., Alming, M., Alvito, P., Ballance, S., Bohn, T., Bourlieu, C., Carrière, F., Boutrou, R., Corredig, M., Dupont, D., Dufour, C., Egger, L., Golding, M., Karakaya, S., Kirkhus, B., Le Feunteun, S., Lesmes, U., Macierzanka, A., Mackie, A., Marze, S., McClements, D. J., Ménard, O., Recio, I., Santos, C. N., Singh, R. P., Vegarud, G. E.,

- Wickham, M. S. J., Weitschies, W., & Brodkorb, A. (2014). A standardised static *in vitro* digestion method suitable for food – an international consensus. *Food & Function*, 5(6), 1113-1124.
- Nielsen, P. M., Petersen, D., & Dambmann, C. (2001). Improved Method for Determining Food Protein Degree of Hydrolysis. 66(5), 642-646.
- Organization, W. H. (2018). Obesity and overweight. In (Vol. 2019). <https://www.who.int/news-room/fact-sheets/detail/obesity-and-overweight>.
- Pawlak, D. B., McMillan, J., Holt, S. H. A., & Brand-Miller, J. (2002). Glycaemic index and obesity. *The American Journal of Clinical Nutrition*, 76(1), 281S-285S.
- Qiu, C., Zhao, M., & McClements, D. J. (2015). Improving the stability of wheat protein-stabilized emulsions: Effect of pectin and xanthan gum addition. *Food Hydrocolloids*, 43, 377-387.
- Reddy, I. M., Kella, N. K. D., & Kinsella, J. E. (1988). Structural and conformational basis of the resistance of β -lactoglobulin to peptic and chymotryptic digestion. *Journal of Agricultural and Food Chemistry*, 36(4), 737-741.
- Reis, P., Holmberg, K., Watzke, H., Leser, M. E., & Miller, R. (2009). Lipases at interfaces: a review. *Advances in Colloid and Interface Science*, 147-148, 237-250.
- Roudsari, M., Nakamura, A., Smith, A., & Corredig, M. (2006). Stabilizing behaviour of soy soluble polysaccharide or high methoxyl pectin in soy protein isolate emulsions at low pH. *Journal of Agricultural and Food Chemistry*, 54(4), 1434-1441.
- Sarkar, A., Ademuyiwa, V., Stublely, S., Esa, N. H., Goycoolea, F. M., Qin, X., Gonzalez, F., & Olvera, C. (2018). Pickering emulsions co-stabilized by composite protein/ polysaccharide particle-particle interfaces: Impact on *in vitro* gastric stability. *Food Hydrocolloids*, 84, 282-291.
- Sarkar, A., Goh, K. K. T., Singh, R. P., & Singh, H. (2009). Behaviour of an oil-in-water emulsion stabilized by β -lactoglobulin in an *in vitro* gastric model. *Food Hydrocolloids*, 23(6), 1563-1569.
- Sarkar, A., Horne, D. S., & Singh, H. (2010). Interactions of milk protein-stabilized oil-in-water emulsions with bile salts in a simulated upper intestinal model. *Food Hydrocolloids*, 24(2), 142-151.
- Sarkar, A., Murray, B., Holmes, M., Ettelaie, R., Abdalla, A., & Yang, X. (2016a). *In vitro* digestion of Pickering emulsions stabilized by soft whey protein microgel particles: influence of thermal treatment. *Soft Matter*, 12(15), 3558-3569.

- Sarkar, A., Ye, A., & Singh, H. (2016b). On the role of bile salts in the digestion of emulsified lipids. *Food Hydrocolloids*, 60, 77-84.
- Sarkar, A., Zhang, S., Holmes, M., & Ettelaie, R. (2019). Colloidal aspects of digestion of Pickering emulsions: experiments and theoretical models of lipid digestion kinetics. *Advances in Colloid and Interface Science*, 263, 195-211.
- Schmitt, C., Moitzi, C., Bovay, C., Rouvet, M., Bovetto, L., Donato, L., Leser, M. E., Schurtenberger, P., & Stradner, A. (2010). Internal structure and colloidal behaviour of covalent whey protein microgels obtained by heat treatment. *Soft Matter*, 6(19), 4876.
- Tokle, T., Lesmes, U., Decker, E. A., & McClements, D. J. (2012). Impact of dietary fibre coatings on behaviour of protein-stabilized lipid droplets under simulated gastrointestinal conditions. *Food & Function*, 3(1), 58-66.
- Tokle, T., Lesmes, U., & McClements, D. J. (2010). Impact of electrostatic deposition of anionic polysaccharides on the stability of oil droplets coated by lactoferrin. *Journal of Agricultural and Food Chemistry*, 58(17), 9825-9832.
- Wulff-Pérez, M., de Vicente, J., Martín-Rodríguez, A., & Gálvez-Ruiz, M. J. (2012). Controlling lipolysis through steric surfactants: New insights on the controlled degradation of submicron emulsions after oral and intravenous administration. *International Journal of Pharmaceutics*, 423(2), 161-166.
- Zembyla, M., Murray, B. S., & Sarkar, A. (2018). Water-In-Oil Pickering Emulsions Stabilized by Water-Insoluble Polyphenol Crystals. *Langmuir*, 34(34), 10001-10011.

Chapter 5

Conjugate microgel-stabilized Pickering emulsions: Role in delaying gastric digestion⁴



Abstract

In this study, a new class of microgels called 'conjugate microgels' was designed, where whey protein isolate (WPI) was conjugated with dextran (Dx, 500 kDa) (WPI-Dx) *via* Maillard reaction before fabricating the microgel particles. Such microgel particles were assessed for their abilities to act as Pickering stabilizers for oil-in-water emulsions and also checked if they offered gastric stability to the Pickering emulsions during *in vitro* digestion against interfacial pepsinolysis. WPI-Dx conjugates were obtained by controlled dry heating (60 °C, 79% RH, 24 - 48 h incubation). Sodium dodecyl sulphate polyacrylamide gel electrophoresis (SDS-PAGE) and ortho-phthaldialdehyde (OPA) profile revealed that the degree of conjugation ranged from 11.6 to 28.1%. The WPI-Dx conjugates were re-dispersed and heat-treated to form heat-set gels with moduli ranging from ~45 to 250 kPa. Microgel particles (hydrodynamic diameters of 130 - 150 nm, ζ -potentials of -4.5 to -8.0 mV) were created by controlled shearing of these heat-set gels. Interfacial shear rheology measurements and microscopic examination confirmed that conjugated microgel particles with lower degree of conjugation (WPDx₁₀M) were effective as Pickering stabilizers. When present in an aqueous dispersion, WPDx₁₀M had reduced the degree of gastric proteolysis (120 - 130 μ M free NH₂) as compared to non-conjugated counterparts (187 - 205 μ M free NH₂). When present at the droplet surface, cross-

⁴ Published as: Araiza-Calahorra, A., Glover, Z.J., Akhtar, M., and Sarkar, A. (2020). Conjugate microgel-stabilized Pickering emulsions: Role in delaying gastric digestion. *Food Hydrocolloids*, 105, 105794. DOI: <https://doi.org/10.1016/j.foodhyd.2020.105794>

correlation image analysis revealed that WPD_{X10M} was successful in delaying interfacial gastric proteolysis. Insights from this study suggest that conjugate microgel particles might be useful to design gastric-stable Pickering emulsions in the future for effective delivery of lipophilic compounds to the intestines.

5.1. Introduction

Proteins are widely used as ingredients in complex colloidal systems to bring microstructural functionality to the food products such as the stabilization of emulsions and foams, thickening and gelation. Numerous attempts have been made in literature to further improve the functional properties of proteins to provide resilience to environmental stresses such as pH, ions and heat treatments for applications in food, pharmaceutical and cosmetic industries. Such modifications to proteins have been obtained through physical, chemical and/ or enzymatic treatments (Akhtar and Ding, 2017; Rodríguez-Patino and Pilosof, 2011). Chemical modifications have not been widely used due to associated safety issues or lack of acceptance by consumers, while enzymatic cross-linking is time consuming and often not affordable (Chevalier et al., 2002). Nevertheless, covalent linkage (or glycation) with polysaccharides via the Maillard reaction, has been widely used to improve the functional properties of proteins (Akhtar and Dickinson, 2003; Dickinson and Semenova, 1992; Goh et al., 2014; Kato et al., 1989; Wong et al., 2011).

Covalent conjugation between proteins and polysaccharides is formed through the condensation of the reducing sugar of the polysaccharide and the deprotonated ϵ -amino group of a lysine residue, which are the primary source of reactive amino groups in proteins (Kato, 2002). An important reason why Maillard conjugation between proteins and polysaccharides has gained significant interest is that, as opposed to other methods of conjugation such as acetylation, amidation, and succinylation, the Maillard reaction occurs naturally during thermal processing, which means it does not require additional chemical reactants other than the naturally present reducing sugar and the lysine residues in the proteins (Oliver et al., 2006). More importantly, through a well-controlled Maillard reaction, the protein functionality can be significantly improved for novel food applications. For example, numerous studies have investigated the use of different proteins and polysaccharides, such as β -casein-glucose (Darewicz and Dziuba, 2001), soy protein-dextran (Diftis and Kiosseoglou, 2004), β -lactoglobulin-dextran (Dickinson et al., 1991), whey and egg white protein-glucose 6-phosphate (Aoki et al., 1994), casein-maltodextrins (Shepherd et al., 2000). Most of these studies were oriented towards improving protein solubility, emulsifying

and foaming capacity, or to improve the resilience of the colloidal systems against environmental stresses (pH, ions etc.).

Most food proteins have a well-defined secondary and tertiary structure such that they aggregate spontaneously and irreversibly depending on the degree and rate of heat-treatment applied. It has been observed that Maillard conjugation of proteins with polysaccharides tends to influence the final textural properties of heat, cold or acid-induced gels (Cabodevila et al., 1994; Matsudomi et al., 2002; Meydani et al., 2019; Spotti, et al., 2019; Spotti, et al., 2013a, 2013b; Sun, et al., 2011; Sun et al., 2004). For example, studies on the gelation properties of soy protein isolate-xylose of glucono- δ -lactone, dried egg white-galactomannan and ovalbumin-ketohexose conjugated gels have shown that enhanced fracture properties and reduced syneresis can be achieved by the Maillard reaction, as compared to their controls. Nevertheless, there is paucity of studies focusing on the influence of the Maillard reaction on the gelation of whey protein isolate-dextran conjugated systems (Spotti, et al., 2019; Spotti, et al., 2013a, 2013b; Sun, et al., 2011). Dextran is widely used to conjugate proteins since they are reductive in nature and their neutral character inhibits the formation of any electrostatic complex with proteins. In addition, they are suitable for protein gelation studies since they are unable to form gel-like structures (Sun, et al., 2011). Nevertheless, the use of such conjugated heat-set gels to create microgel particles and use them as Pickering stabilizer has not been investigated so far.

In our previous study, we have developed and characterised whey protein nanogel particles (WPN) as Pickering stabilizers for oil-in-water emulsions (Araiza-Calahorra and Sarkar, 2019b). Furthermore, we have demonstrated that electrostatic deposition of dextran sulphate of a molecular weight of 500 kDa, to the cationic WPN can decrease the rate and extent of gastric proteolysis of the WPN-interfacial layer and prevent gastric coalescence of the Pickering emulsion droplets in simulated gastric conditions at pH 3.0 (Araiza-Calahorra and Sarkar, 2019a). However, it is well known that human physiology has a complex milieu of pH, ionic conditions and bio-surfactants and therefore, electrostatic complexation between proteinaceous particles and polysaccharide might not provide sufficient barrier to droplets against physiologically-driven coalescence (Sarkar et al., 2019; Singh and Sarkar, 2011).

Hence, this study aims to design, for the first time, oil-in-water Pickering emulsions stabilized by whey protein isolate (WPI) – dextran (Dx) conjugated micrometric-sized gel particles as a Pickering stabilizer, and test its efficacy in delaying gastric proteolysis of the interfacial material. The mechanical properties of heat-induced WPI-Dx conjugate gels obtained *via* Maillard reaction was investigated and the gastric fate of the microgel particles designed by a top-down shearing approach of

these conjugate heat-set gels and corresponding Pickering emulsions was studied. In addition, we introduced a proof-of-concept cross-correlation image analysis of the emulsion systems to quantify and analyse the protein hydrolysis caused by pepsin. We hypothesize that conjugation of proteins with polysaccharide creates a tortuous network in the microgel particles that is capable of delaying the digestibility of the proteinaceous microgel particles by pepsin during simulated gastric digestion.

5.2 Materials and Methods

5.2.1 Materials

Whey protein isolate (WPI) with $\geq 90\%$ protein content was gifted by Fonterra Co-operative Group Limited (Auckland, New Zealand). Dextran (Dx) of molecular weight (MW) 500 kDa and porcine pepsin (P7000, measured enzyme activity: 371 U mg^{-1} using haemoglobin as the substrate) were purchased from Sigma-Aldrich Company Ltd (Dorset, UK). Medium-chain triglyceride (MCT-oil) Miglyol[®] 812 with a density of 945 kg m^{-3} at 20 °C was used as the lipid phase (Cremer Oleo GmbH & Co, Germany). Sodium dodecyl sulphate polyacrylamide gel electrophoresis (SDS-PAGE) reagents including Bolt[™] 4 - 12% Bis-Tris Plus gels, 20x Bolt[™] MES SDS Running Buffer, 4 x Bolt[™] LDS Sample Buffer and PageRuler[™] Plus Pre-stained Protein Ladder were purchased from Thermo Fisher Scientific (Loughborough, UK). All reagents were of analytical grade and used without further purification unless otherwise reported. All solutions were prepared with Milli-Q water with a resistivity of 18.2 $\text{M}\Omega \text{ cm}$ at 25 °C (Milli-Q apparatus, Millipore, Bedford, UK). Sodium azide (0.02 wt %) was added as a preservative.

5.2.2 Preparation of whey protein isolate - dextran conjugate

Maillard conjugates of WPI and Dx (WPI-Dx) were prepared using the method described by Ding et al., (2017). Briefly, WPI and Dx were completely dissolved in a 1:2 w/w ratio in 100 mL Milli-Q water with gentle stirring under room temperature. The pH of the solution was adjusted to either pH 7.0 or 11.0 as shown in Table 5.1. The solutions were stored in the refrigerator at 4 °C overnight and then frozen at -20 °C for 6 h. These were then freeze dried for a period of 24 h. After freeze drying, Maillard reaction of the resulting WPI and Dx mixture was promoted by incubating the powder in a desiccator pre-heated at 60 °C for 24 to 48 hours, with a relative humidity (79%) controlled by saturated potassium bromide (KBr) solution. The WPI-Dx conjugates of different degrees of conjugation (DC) were stored in a dark and dry place for further

characterization. An untreated WPI-Dx mixture *i.e.* non-conjugated WPI-Dx, without any modification was similarly prepared as a control.

Table 5.1. Nomenclature, conjugation conditions and characterization of conjugates obtained *via* OPA analysis.

Sample nomenclature	Ratio of WPI to Dx (w:w)	Maillard reaction conditions	DC (%)
WPI-Dx ₁₀	1:2	pH 7.0, 24 h, 60 °C	11.58 ± 3.07
WPI-Dx ₂₀	1:2	pH 11.0, 24 h, 60 °C	19.32 ± 1.68
WPI-Dx ₃₀	1:2	pH 11.0, 48 h, 60 °C	28.14 ± 2.91

5.2.3 Determination of free amino groups

The DC of the conjugates and degree of hydrolysis during gastric digestion of samples were quantified by detecting the content of free amino groups using a standardized ortho-phthaldialdehyde (OPA) method, as described by Nielsen et al., (2001) with minor modifications. Briefly, the OPA reagent was prepared using 3.81 g sodium tetraborate, 0.088 g dithiothreitol and 0.1 g sodium docecyl sulphate (SDS). Exactly 0.080 g OPA was dissolved in 2 mL ethanol and added to the above-mentioned solution and made up to 100 mL with Milli-Q water and the solution was kept in the dark. Each of the WPI-Dx conjugates prepared with different DC was dissolved in Milli-Q water with gentle stirring at a concentration corresponding to a WPI content of 1.0 mg/ mL. For each prepared sample, 160 µL was added to 1200 µL OPA reagent in a PMMA cuvette, mixed for 5 s and the absorbance was measured at 340 nm using a UV-VIS spectrophotometer (6715 UV/VIS Spectrophotometer, Jenway, UK), using blank prepared with OPA reagent and Milli-Q water. The baseline was established by using non-conjugated WPI-Dx solution. The degree of conjugation can thus be calculated as follows:

$$\text{Degree of conjugation (DC) \%} = \frac{(C_{\text{untreated}} - C_{\text{conjugate}})}{C_{\text{untreated}}} \times 100\%$$

where, $C_{\text{untreated}}$ is the concentration in the non-conjugated WPI-Dx mixture and $C_{\text{conjugate}}$ is the concentration of the conjugated samples. The analysis of each sample was carried out in triplicate.

The same OPA procedure was applied for quantification of protein hydrolysis. A reference calibration curve of L-leucine solution (0 - 200 μM) was used and the protein hydrolysis was expressed as a μM free amino groups per mass of the total protein in sample.

5.2.4 Preparation of heat-induced gels and microgel particles

The WPI-Dx Maillard conjugate and non-conjugated powders described in section 2.2 were dispersed in phosphate buffer for 2 h to ensure complete dissolution and to maintain the final pH of the dispersion at pH 7.0. Protein concentration was 11.57 wt% for non-conjugated and ~10% DC samples, and the protein concentration was 8.02 wt% for ~20 and 30% DC samples. The aqueous solutions of the non-conjugated and three conjugate samples were heated at 65 °C in a temperature-controlled water bath for 1 h to form a heat-set gel (quiescent), followed by cooling down for 15 min and stored at 4 °C for 24 h before further analysis. The gel formation was induced by heat-induced protein aggregation. When aqueous dispersions of WPI are heated at ≥ 65 °C, heat treatment causes unfolding of the globular proteins causing the exposure of the free sulfhydryl group and the inner hydrophobic amino acids. Protein aggregation is caused initially by hydrophobic interactions followed by formation of intramolecular disulphide-bonds. Large aggregates are formed by further sulfhydryl-catalysed disulphide-bond interchange and non-covalent interactions between the dimers (Croguennec et al., 2004; Nicolai, et al., 2011).

To obtain microgel particles, the afore-mentioned non-conjugated and conjugate heat-set gels were pre-homogenized with phosphate buffer at pH 7.0 (2 wt% protein) using a hand blender (HB724, Kenwood) for 1 min and transferred to a vacuum box (John Fraser and Sons Ltd, London, UK) for degassing. The resulting microgel particles were passed twice through a Jet homogenizer (a bespoke two-chamber homogenizer developed in the School of Food Science and Nutrition, University of Leeds, Leeds, UK) at 300 bar for two passes. Final non-conjugated microgels particles and conjugate microgel particles are referred to as N-WPDxM and WPDxM, respectively, and were diluted with phosphate buffer to the desired protein concentration for the preparation of Pickering emulsions.

5.2.5 Mechanical properties of heat-induced WPI-Dx gels

Uniaxial single compression tests on the gel samples (10.10 mm diameter × 8.30 mm height) were performed with a TA-TX2 Texture Analyser Micro Systems Ltd., (Surrey, UK) using a cylindrical probe (diameter 59 mm), attached with a 50 kg load cell. The tests were carried out at room temperature at a constant speed of 1 mm/ s and the gels were compressed until rupture (80% strain with respect to their initial height). The parameters calculated from the uniaxial compression test were true fracture stress, which is the load at the point of the fracture divided by the cross-section area during fracture and the Young's modulus, which is calculated as the slope of the initial linear region of maximum stress versus the Henky strain. Measurements were performed in triplicate and mean values and standard deviations were calculated.

5.2.6 Preparation of Pickering oil-in-water emulsions

Pickering oil-in-water emulsions (E_{WPDxM}) were prepared using MCT-oil (20 wt%) and WPDxM gel particles to give a final protein content of 1 wt% in the final emulsion. Briefly, coarse E_{WPDxM} droplets were prepared using Ultra Turrax T25 homogenizer (IKA-Werke GmbH & Co., Staufen Germany) at 13,500 rpm for 1 min. Following this, the coarse emulsions were homogenized twice using a Jet homogenizer (School of Food Science and Nutrition, University of Leeds, UK) at 300 bar to prepare fine emulsion droplets.

5.2.7 Interfacial shear viscosity

The interfacial shear viscosity was measured as previously described by Murray and Dickinson (1996) and Sarkar et al., (2017) using a two-dimensional Couette-type viscometer. Briefly, a stainless steel biconical disc (radius 14.5 mm) was suspended from a thin torsion wire with its edge in the plane of the oil-water interface of the solution contained within a cylindrical glass dish (radius 72.5 mm). The deflection of the disc was measured by reflection of a laser off a mirror on the spindle of the disc onto a scale at a fixed distance from the axis of the spindle. The interfacial viscometer was operated in a constant shear-rate mode, as described in a recent study (Zembyla et al., 2018). For the measurements, a layer of pure *n*-tetradecane was layered over an aqueous solution of microgel particles at a concentration of 0.5 wt% in phosphate buffer at pH 7.0. The constant shear rate apparent interfacial viscosity, η_i , is given by the following equation:

$$\eta_i = \frac{g_f}{\omega} K(\theta - \theta_0) \quad (5.1)$$

where, K is the torsion constant of the wire, θ is the equilibrium deflection of the disc in the presence of the film, θ_0 is the equilibrium deflection in the absence of the film, *i.e.* due to the drag force of the sub-phase on the disc, g_f is the geometric factor, and ω is the angular velocity of the dish. A fixed value of $\omega = 1.27 \times 10^{-3} \text{ rad s}^{-1}$ was used.

5.2.8 *In vitro* gastric digestion of conjugate microgel particles

The aqueous dispersions of the non-conjugate and conjugate microgel particles and the corresponding selected emulsion *i.e.* E_{WPDxM} were digested using slightly adapted digestion protocol from Minekus, et al. (2014). Briefly, 10 mL of pre-incubated sample (37 °C, 1 h) at pH 3.0 was mixed with 10 mL of simulated gastric fluid (SGF), consisting of 0.257 g L⁻¹ of KCl, 0.061 g L⁻¹ of KH₂PO₄, 1.05 g L⁻¹ of NaHCO₃, 1.38 g L⁻¹ of NaCl, 0.0122 g L⁻¹ of MgCl₂(H₂O)₆, 0.024 g L⁻¹ of (NH₄)₂CO₃ and 2000 U/ mL pepsin at pH 3.0 without using any oral processing step. The mixture was incubated for 2.5 h at 37 °C under agitation using a shaking water bath (Grant Instruments Ltd, Cambridge, UK). During the gastric phase, samples were periodically withdrawn from the sample-SGF mixture at 5, 30, 60, 90, 120 and 150 min for size, charge, microscopy and SDS-PAGE analysis. Proteolysis of the samples was terminated by neutralizing to pH 7.0 using freshly prepared 1 M NH₄HCO₃ except for size and charge measurements, in latter experiments, samples were characterized immediately after digestion.

5.2.9 Particle size and droplet size distribution

The physicochemical properties and stability of aqueous dispersions of N-WPDxM and WPDxM prepared using the non-conjugated and conjugated gels and their corresponding emulsions *i.e.* E_{WPDxM} before and after digestion were monitored using their particle size distribution, ζ -potential and microstructural changes as a function of gastric digestion time as previously described (Araiza-Calahorra, et al., 2019a). The particle size of the conjugate microgel particles was also investigated as a function of pH (pH 2.0 - 7.0) and in presence of ions (50 mM NaCl, 10 mM CaCl₂) to understand their behaviour in simulated physiological fluids in the absence of any physiological enzymes (Araiza-Calahorra, et al., 2019b). Briefly, the particle size of the aqueous dispersions of WPDxM was determined using dynamic light scattering (DLS) at 25 °C using a Zetasizer Ultra (Malvern Instruments Ltd., Malvern, Worcestershire,

UK) in a PMMA standard disposable cuvette. Particle size of the samples before and after gastric digestion was measured after diluting the samples in SGF buffer (pH 3.0). Droplet size distributions of the emulsion samples (were determined using static light scattering at 25 °C using Malvern MasterSizer 3000 (E_{WPDxM}) Malvern Instruments Ltd., Malvern, Worcestershire, UK). The mean particle size distribution of the emulsions was reported as volume mean diameter (d_{43}) and surface mean diameter (d_{32}) based on five measurements on triplicate samples.

5.2.10 ζ -potential

The ζ -potential of aqueous dispersions of the conjugate microgel particles (WPDxM) and emulsion samples (E_{WPDxM}) before and after digestion was determined using a particle electrophoresis instrument (Zetasizer Ultra, Malvern Instruments Ltd, Malvern, Worcestershire, UK). Samples were diluted in SGF buffer (pH 3.0) (0.1 wt% particle or 0.002 wt% emulsion droplet concentration) and added to a folded capillary cell (Model DTS 1070, Malvern Instruments Ltd., Malvern, Worcestershire, UK). Samples were equilibrated for 1 min and the data was processed using the Smoluchowski model. The ζ -potential results were reported as mean result of at least five reported readings made on triplicate samples.

5.2.11 Cryogenic-Scanning Electron Microscopy

Cryogenic scanning electron microscopy (cryo-SEM) of the emulsion was conducted using heptane as the dispersed phase. Preliminary analysis on heptane or MCT-oil emulsions revealed that both systems presented the same overall microstructural behaviour. Nevertheless, heptane was used as the dispersed phase, to avoid interference by crystallization of oil during the freezing step as described by Destribats, et al. (2013) and Araiza-Calahorra, et al. (2019b). The emulsion sample was mounted on rivets attached to the sample stub. The samples were plunge-frozen in liquid nitrogen “slush” at -180 °C, then transferred to the cryo-preparation chamber on the SEM. The frozen emulsion droplets were cleaved and then etched at -95 °C for 4 min. Next, the samples were coated with 5 nm of platinum (Pt). Finally, the Pt-coated samples were transferred to the SEM for imaging at -135 °C. The heptane emulsion sample was imaged in a FEI Quanta 200F ESEM with a Quorum Polar Prep 2000 cryo system.

5.2.12 Confocal scanning laser microscopy (CLSM) and cross-correlation analysis

Microstructural observations were made using a Zeiss LSM 880 inverted confocal microscope (Carl Zeiss MicroImaging GmbH, Jena, Germany) using an oil immersion 63× lens and the pinhole diameter maintained at 1 Airy Unit to filter out the majority of the scattered light. A stock solution of Nile Red (1 mg/ mL in dimethyl sulfoxide) was used to stain the MCT-oil to a final concentration of 0.02 mg/ mL and a stock solution of Fast Green (1 mg/ mL in Milli-Q water) was used to stain the protein particles to a final concentration of 0.1 mg/ mL. Nile Red and Fast Green were excited at wavelengths of 488 and 633 nm, respectively. The emission filters were set at 555 - 620 nm for Nile Red and at 660 - 710 nm for Fast Green. Samples were placed on a concave confocal microscope slide and secured with a glass coverslip before imaging.

In addition, a combination of confocal microscopy and cross-correlation image analysis was applied to two channel microscopy images of emulsion samples stabilized by conjugate microgel particles (E_{WPDxM}) and emulsion samples stabilized by whey protein-based nanogel particles (E_{WPN}) before and after digestion with SGF containing pepsin. Briefly, fresh emulsion samples were stained and mixed with SGF containing pepsin. Samples were imaged after 5 - 10 min of incubation and z-stacks images were obtained using a scan rate of 400 Hz in sequential scan mode to avoid cross-talk between fluorophores. Images were accepted for analysis if they were part of 3 or more image planes within an image stack and of sufficient technical quality to discern discrete particles at the droplet interface. Image analysis was conducted using MATLAB R2018b (Mathworks, US), details have been previously described (Glover, et al., 2019b). Briefly, a region of interest around an oil droplet channel was selected and the largest circle in that image crop was found using the function 'imfindcircle' in MATLAB. The centre point and the radius of the circle was determined, and a cropped image was created from the original image with the droplet at the centre. The cropped images were 3.5× the diameter of the droplet in width and height to ensure no overlap with other droplets and protein structures occurred.

For the cross-correlation analysis, each pixel in the image was given a polar co-ordinate and the image was split into 20 radial segments. A threshold was applied to the red channel using the function 'graythresh', based on Otsu's method. For every radial segment, the intensity of the fat and protein was radially averaged using the MATLAB function 'accumarray' and a 1D cross-correlation was performed between the fat and the protein using the function 'xcorr'. The cross-correlation intensity was integrated for every radial segment using the function 'trapz' and the integrated values were scaled to the radius of the droplet in the selected region of interest to avoid

artifacts caused by minor changes in z-position over time. The cross-correlation analysis was performed for pairs of images at different time points where the same droplet was selected each time. Microscopy images were optimized for publication using Fiji, ImageJ.

5.2.13 Sodium dodecyl sulphate polyacrylamide gel electrophoresis (SDS-PAGE)

The protein composition of the aqueous dispersions of WPI and Dx conjugate solutions and the peptides generated in the N-WPDxM and WPDxM particles after gastric hydrolysis by pepsin was examined using sodium dodecyl sulphate polyacrylamide gel electrophoresis (SDS-PAGE) under reducing conditions. The WPI-Dx sample and N-WPDxM and WPDxM-SGF, mixtures (1.5 mL) after gastric digestion with pepsin were mixed with SDS buffer (0.5 M Tris, 2.0% SDS, 0.05% β -mercaptoethanol, pH 6.8), at a 1:2 ratio (sample : SDS buffer), heated at 95 °C for 5 min and 10 μ L was loaded into the precast gels placed on an Invitrogen™ Mini Gel Tank system (Thermo Fisher Scientific, Loughborough, UK). Exactly, 5 μ L of the protein molecular weight marker was added in the first lane. After running the gel at 200 V for 22 min, the gel was fixed in a Milli-Q: Methanol: Acetic acid (50:40:10 vol%) solution for 1 h and stained for 2 hrs with a Coomassie Brilliant Blue R-250 solution in 20% isopropanol. The gels were destained overnight in Milli-Q water and scanned using a ChemiDoc™ XRS + System with image Lab™ Software (Bio-Rad Laboratories, Richmond, CA, USA). The intensities of the protein bands were quantified using Image Lab Software Version 6.0. Bands within the lanes was selected automatically by the software to cover the whole band. Background intensity was subtracted after scanning an empty lane, which served as the blank. The percentage composition of each sample was determined by scanning the gradual reduction in peak volume intensity for each intact protein bands of WPI (β -lactoglobulin (β -lg), α -lactalbumin (α -la) and bovine serum albumin (BSA)). The SDS-PAGE experiments were carried out in triplicates and band intensities was reported as an average of three reported readings.

5.2.14 Statistical analysis

Means and standard deviations were calculated from three individual measurements performed on triplicate samples and analysed using the one-way analysis of variance (ANOVA) and Student's t-test where significance was accepted at $p < 0.05$.

5.3. Results and Discussion

5.3.1 Identifying the degree of conjugation (% DC)

To confirm the covalent conjugation of the carbonyl group of the reducing sugar with the free amino groups in the proteins, many studies have focused on the quantification of free amino groups (Wooster and Augustin, 2006). Thus, to estimate the extent of the Maillard reaction in the conjugate samples designed in this study, the loss of free amino groups of WPI was estimated using the OPA method taking the non-conjugated WPI-Dx mixture as the reference and the DC was calculated and shown in Table 5.1. Additionally, covalent coupling of WPI and Dx after dry heating was qualitatively established using SDS-PAGE patterns (Figure 5.1). Based on the DC obtained (see Table 5.1), the following nomenclature was followed henceforth, WPI-Dx₁₀ denotes the sample that presented a DC of 11.57%, WPI-Dx₂₀ refers to the sample with a DC of 19.32%, and WPI-Dx₃₀ refers to the sample that presented a DC of 28.14%. Accordingly, the same subscripts will be used henceforth to refer to the corresponding microgel particles (WPDx₁₀M, WPDx₂₀M and WPDx₃₀M).

Table 5.1 presents the Maillard reaction conditions used for the conjugation of Dx to WPI as a function of pH and reaction times. The pH of the solutions and the heating conditions are based on those commonly used for preparing Maillard conjugates using dextran (Akhtar, et al., 2003; Fechner et al., 2007; Ho et al., 2000; Liu et al., 2016; Liu et al., 2016). As shown in Table 5.1, the DC increased with increasing the pH of the protein-polysaccharide solution dispersion from pH 7.0 to pH 11.0. This behaviour might be expected considering that browning reaction is known to be promoted at higher pH levels (Kato, 1956). For example, it has been observed that a greater Maillard reaction was produced at pH above 7.0, as compared to pH 5.0 and 6.0 in solutions containing glucose and amino acids (Willits et al., 1958). Additionally, it has been observed that during the Maillard reaction, pH often decreases leading to a slowing down of the reaction (Mikami et al., 2015; Wolfrom et al., 1953). It should be noted that no buffer was used to control the pH of the solutions, as it has been suggested to influence the nature and quantity of the Maillard reaction products by catalysing the conversion of glycosylamine into the Amadori product during the first stage of the reaction (Potman and van Wijk, 1989). Thus, at pH 7.0, it is likely that a decrease of the pH, naturally caused during the Maillard reaction, may have led to the slowing down of the reaction, as compared to pH 11.0. In previous studies, it has been observed that, in the absence of buffer, changes in the pH of 3 - 4 units may occur (Madruga and Mottram, 1995).

The degree of conjugation was increased by increasing the reaction time from 24 to 48 h (Table 5.1) in line with a previous study (Wooster et al., 2006). The levels

of conjugation are similar to those reported in other studies using WPI and Dx (Spotti et al., 2013a, 2013b). However, slight discrepancies might arise from the fact that a bigger molecular weights of the Dx used in our study may have been less reactive with the free amino groups of the proteins due to a less open chain as compared to a biopolymer containing a shorter carbonic chain length (Chevalier et al., 2001).

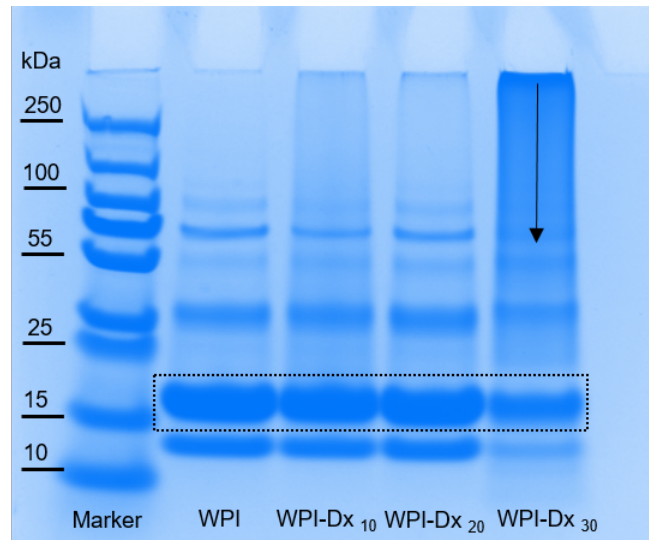


Figure 5.1. SDS-PAGE patterns of the protein marker (first lane), WPI solution and WPI-Dx conjugates with different degrees of conjugation, respectively. The dotted region represents the β -lactoglobulin band in 2nd - 5th lane and the arrow in the 5th lane represents the oligomers that was not efficiently resolved in the resolving gel.

In order to assess the level of reacted materials in WPI-Dx solutions, SDS-PAGE was used. As shown in Figure 5.1, for native WPI solution (lane 2), the intensities of bands at about 66 kDa, 18 kDa and 14 kDa that correspond to bovine serum albumin (BSA), β -lactoglobulin (β -lg) and α -lactalbumin (α -la), respectively, are clearly identified. For WPI-Dx₁₀, WPI-Dx₂₀ and WPI-Dx₃₀ (lanes 3 to 5), the intensities of the two major bands corresponding to β -lg and α -la were reduced as compared to that of the WPI solution (lane 2) (Figure 5.1). For β -lg, the remaining intact protein was 82.19%, 59.99% and 54.03%, and for α -la was 66.73%, 47.52% and 18.24%, respectively. In addition, in WPI-Dx₃₀ solution, an intense drag at the loading end of the gel was observed (shown by arrow in Figure 5.1). This indicates that WPI and Dx are conjugated into larger oligomers that could not migrate into the resolving gel. Similar results have been reported previously in WPI-Dx conjugate systems, where smearing of bands and reduced intensity of the characteristics proteins bands in the resolving gel have been observed (Akhtar, et al., 2003; Sun, et al., 2011; Zhu et al.,

2010). Although it is not possible to determine the exact molecular weights of the oligomers generated in the conjugate, it can be concluded that there were significant changes in the WPI-Dx systems upon conjugation and that the Maillard reaction was carried out successfully. The optical images of the freeze-dried non-conjugated and conjugate powders can be seen in Appendix C, Figure C1, where the conjugated powder clearly showed increased levels of visual brown coloration with increased DC in line with the SDS-PAGE results (Figure 5.1) and the DC reported in Table 5.1.

5.3.2 Mechanical properties of the conjugate WPI-Dx heat-set gels

In order to prepare the microgel particles, a heating step was required at first to convert the protein solution into heat-set hydrogel before shearing these gels into microscopic gel particles. The fracture properties of the parent gels were characterized to give an indication of the large deformation properties of the resultant microgel particles. To study the influence of glycosylation on the mechanical properties of the heat-set protein gels, the WPI-Dx conjugate gels with different DC were compared with WPI systems (*i.e.* no dextran added). The mechanical properties of WPI and WPI-Dx conjugate gels incubated for different reaction times are shown in Figure 5.2.

The appearance of the 10 wt% WPI gel was translucent and brittle, which indicates that a fine-stranded microstructure was formed (Figure 5.2a) (Clark et al., 1981). The gels formed by WPI presented an average fracture stress of 175.40 kPa (Figure 5.2), which is slightly higher than that previously reported for WPI gels of 8 - 20 wt% protein concentration (11.2 - 171.2 kPa) formed at pH 7.0 (Foegeding, 1992). This could be explained by the differences in heat-treatment conditions and presence of ions. Upon addition of Dx (non-conjugated WPI-Dx gels), the fracture stress increased to ~950 kPa (Appendix C, Figure C2), which indicates that addition of Dx had a pronounced effect on the gelation behaviour of proteins. This is in agreement with previous studies where presence of dextran, a neutral polysaccharide, has been shown to increase the modulus of whey protein isolate gels (Spotti, et al., 2013a; Spotti et al., 2012). It was proposed that other molecular interactions such as hydrogen bonds can be promoted by the addition of dextran, which caused the increased strength of the heat-set induced gel (Spotti, et al., 2013b).

For the heat-set conjugate gels with different DCs (WPI-Dx₁₀, WPI-Dx₂₀, WPI-Dx₃₀), a significant contribution of the Maillard conjugation to the fracture mechanics of the gels was observed ($p < 0.05$) (Figure 5.2), though all the DC levels resulted in self-supporting gels (Figure 5.2b-d). It is noteworthy that even under carefully replicated experiments there was incorporation of air into the WPI-Dx₃₀ samples subjecting the fracture measurements to some error (Figure 5.2d). Fracture stress was

significantly lower for sample WPI-Dx₃₀ with values of 272.56 kPa (Figure 5.2) as compared to 770.48 and 905.39 for WPI-Dx₁₀ and WPI-Dx₂₀, respectively. It is possible that due to the loss of native structure of the protein due to conjugation, groups that are primarily responsible for the gel network such as sulfhydryl groups were not freely available for covalent interaction (Spotti, et al., 2013b). Although the Young's modulus of WPI-Dx₁₀ increased as compared to that of WPI counterparts ($p < 0.05$), it was lower as compared to that of the non-conjugated WPI-Dx gels (see Appendix C, Figure C2) and it decreased by four-fold with increasing DC from 448.55 kPa for non-conjugated WPI-Dx gels to 92.15 kPa for the WPI-Dx₃₀ gels (Figure 5.2). Similar trends were observed by Spotti, et al. (2013a) who reported that increased Maillard reaction time decreased the Young's modulus values obtained for WPI-Dx conjugate gels irrespective of the dextran molecular weight studied (6 - 70 kDa). However, the discrepancies in Young's modulus values between our study and that of Spotti, et al. (2013a) could be due to differences in molecular weight of dextran used in our study (500 kDa), which is an order of magnitude higher as compared to the ones used by Spotti, et al. (2013a).

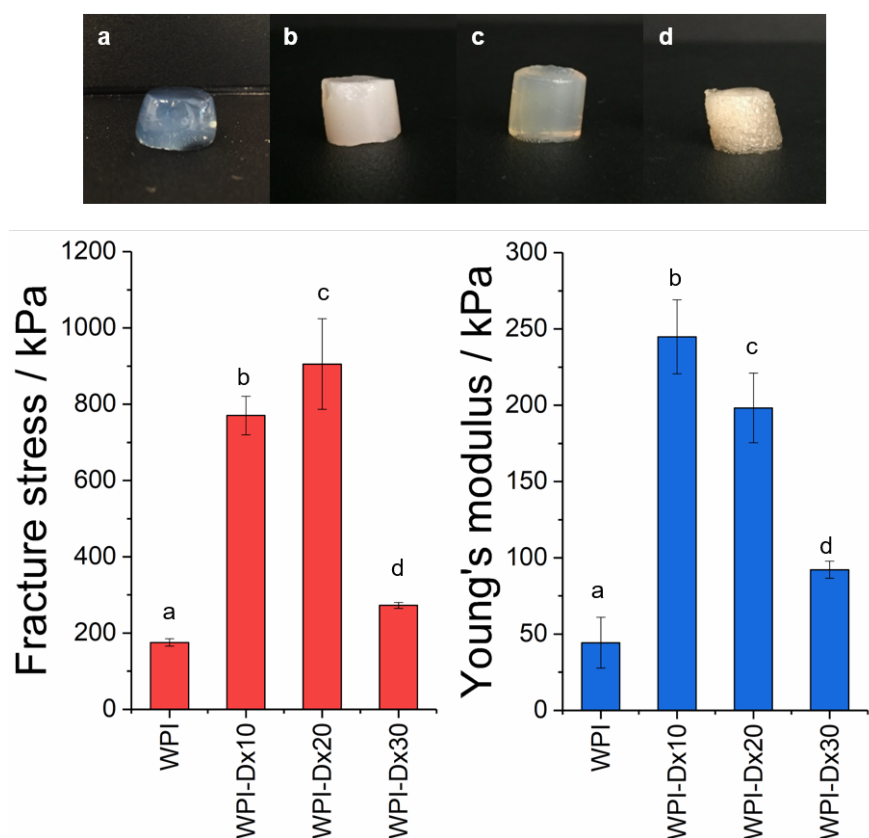


Figure 5.2. Fracture stress and Young's modulus of heat-treated WPI gels and heat-treated WPI-Dx conjugate gels and corresponding images of the thermo-set hydrogels of a) WPI, b) WPI-Dx₁₀, c) WPI-Dx₂₀ and d) WPI-Dx₃₀ (top).

Differences on the observed mechanical properties of conjugated gels could be caused by changes in the structure of the protein due to either the heat treatment or the coupling of dextran during Maillard reaction (Spotti, et al., 2013b). Such changes to the structure could affect the protein unfolding and further thermal denaturation and aggregation reactions altering the mechanism of gelation of the WPI-Dx conjugate gels. In addition, conjugation of Dx may also suppress the intermolecular association between neighbouring proteins in aqueous solutions due to possible steric hindrance effect caused by Dx (Sun, et al., 2011).

5.3.3 Characteristics of conjugate microgel particles

Conjugate microgel particles (WPDxM) were prepared by controlled shearing of the afore-mentioned WPI-Dx₁₀, WPI-Dx₂₀ and WPI-Dx₃₀ gels using a top down approach developed previously (Araiza-Calahorra, et al., 2019a, 2019b). For control purposes, an aqueous dispersion of mixed particles (*i.e.* non-conjugated N-WPDxM) was analysed (Appendix C, Figure C3). Aqueous dispersions of WPDx₁₀M, WPDx₂₀M, and WPDx₃₀M particles at pH 7.0 presented monomodal particle size distributions (Figure 5.3) with polydispersity index ranging from 0.2 - 0.3 and hydrodynamic diameters ranging from 136 to 146 nm (Table 5.2). The microgel particles were slightly negatively-charged at pH 7.0 (Table 5.2). The negative charge of the particle dispersions might be attributed to the fact that WPI was above its isoelectric point.

When compared to whey protein nanogel and microgel particles as previously described by Araiza-Calahorra, et al. (2019b) and Sarkar, et al. (2016), respectively, a decrease in the magnitude of the negative charge was observed in these conjugate microgel particles. This may be attributed to the addition of the neutral dextran molecule, which might have saturated the surface of these conjugated microgel particles. In addition, if we compare the ζ -potential of conjugate microgel particles, such as WPDx₁₀M and WPDx₂₀M (Table 5.2) with that of non-conjugated N-WPDxM systems (Appendix C, Figure C3), a similar ζ -potential values ($p > 0.05$) can be observed, suggesting that conjugation did not directly affect the charge groups of the proteins.

The colloidal stability of 1 wt% of aqueous dispersions of conjugate microgel particles (WPDx₁₀M, WPDx₂₀M, and WPDx₃₀M) at various pH and three different salinities (50 mM NaCl and 10 mM CaCl₂) was investigated (Appendix C, Figure C4 and C5). Changes in hydrodynamic diameter were measured since the stability of the microgel particles largely depends on the attractive and repulsive interactions between

the constituent proteins, which dictates the swelling behaviour of the microgel particles. From Appendix C, Figure C5, it can be observed that in the absence of added electrolytes (NaCl or CaCl₂), dispersions of WPDx₁₀M conjugate particles were found to aggregate within the pH range of 4.0 < pH < 5.5 as revealed by the turbidity (Appendix C, Figure C4) and size evolution of the microgel particles that increased drastically to several micrometres (Appendix C, Figure C5). The size evolution of WPDx₁₀M was found to corroborate with the near zero ζ -potential (data not shown),

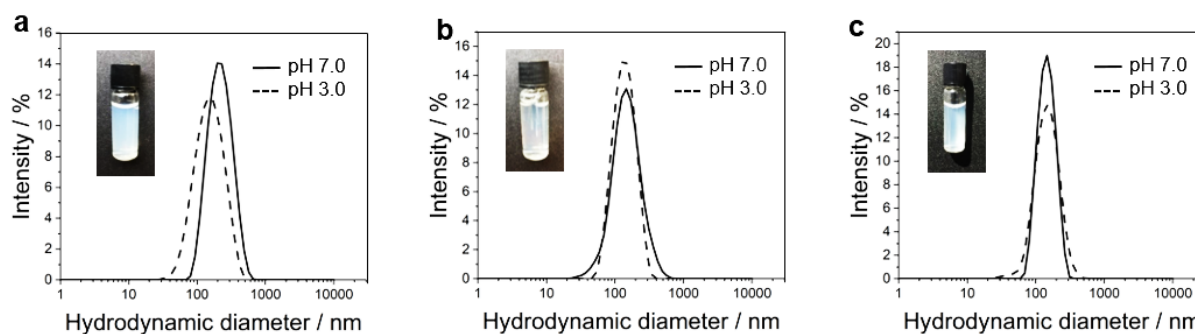


Figure 5.3. Particle size distribution of a) WPDx₁₀M, b) WPDx₂₀M, c) WPDx₃₀M particles (black full line: freshly prepared samples in phosphate buffer at pH 7.0, black dashed line: in SGF buffer at pH 3.0 without added pepsin) with inset representing the visual aspect of the particles.

suggesting that a low degree of conjugation did not significantly affected the isoelectric point (*pI*) of WPI (Sarkar, et al., 2016). Interestingly, on increasing DC to 20 and 30% (*i.e.* WPDx₂₀M, and WPDx₃₀M particles), the particles formed a slightly more stable dispersion within the same pH range of 4.0 < pH < 5.5. Especially for higher degree of conjugated particles *i.e.* WPDx₃₀M, the increase on the hydrodynamic diameter was not as large as compared to WPDx₁₀M samples in the same pH range (Appendix C, Figure C5).

In the presence of 50 mM NaCl, WPDx₁₀M particles presented a slight shift of the *pI* towards pH 5.0. Furthermore, in the presence of 10 mM CaCl₂, an observable shift of the instability domain towards neutral pH was also observed (Appendix C, Figure C5). With increased DC, the WPDx₂₀M, and WPDx₃₀M particles showed less responsiveness to pH and ions as opposed to WPDx₁₀M. Reduction in responsiveness to pH and ions upon increased degree of dextran attachment may be attributed to major conformational modification induced by the glycation (Chevalier et al., 2001) or electrostatic screening of the protein structure by the neutral dextran molecule (Wooster et al., 2006). In summary, physicochemical characterization of the conjugated microgel particles suggests that increased DC reduces the responsiveness of the particle to physiologically relevant ionic conditions and thus, might be more stable as opposed to non-conjugated WPI-based microgel particles.

5.3.4 Characteristics of conjugated microgel particles during *in vitro* gastric digestion

Besides pH and electrolytes, proteolysis by pepsin in the gastric regime is a major determining factor for breakdown of protein-based particles (Araiza-Calahorra et al., 2019a; David-Birman et al., 2013; Sarkar et al., 2019). Hence, changes in the physicochemical properties and protein composition of aqueous dispersions of conjugate particles were examined as a function of gastric digestion time. This sets the scene to understand the influence of polysaccharide conjugation on the gastric behaviour of aqueous dispersions of microgel particles and their behaviour when present at the oil-in-water interface.

Upon addition of SGF buffer without pepsin at pH 3.0, the particles presented a monomodal size distribution (Figure 5.3) with no significant difference in polydispersity index (0.21 - 0.28) and the hydrodynamic diameter ranging from 125 - 133 nm (Table 5.2). As might be expected, the ζ -potential became slightly positive since the WPI is now below its isoelectric point. After 5 min of incubation in SGF containing pepsin at pH 3.0, different sizes of particle aggregates were generated, and the polydispersity was too high to be measured using dynamic light scattering.

Figure 5.4 describes the protein composition of the microgel particles as a function of gastric incubation time as determined by SDS-PAGE. As controls, SDS-PAGE patterns of whey protein nanogel particles (Araiza-Calahorra et al., 2019a) and an aqueous dispersion of mixed whey protein-dextran microgel particles (*i.e.* non-conjugated N-WPDxM, particles without any Maillard reaction) are shown in Appendix C, Figure C6. It can be observed that for WPDx₁₀M after 30, 60 and 120 min in SGF containing pepsin, 17.09 ± 4.34 , 13.34 ± 4.62 and $1.47 \pm 0.08\%$ of β -lg and 6.45 ± 2.49 , 2.81 ± 0.61 and $0.17 \pm 0.12\%$ of α -la remained, respectively (Figure 5.4a). However, the control sample of mixed microgel particles without conjugation or WPN did not protect β -lg or α -la from immediate gastric proteolysis, as the intact bands were not detectable even after 5 min of digestion (Appendix C, Figure C6). This result indicates that conjugation with Dx (10% DC) increased the resistance of the microgel particles to gastric proteolysis. In contrast, digestion of microgels particles with higher DC *i.e.* both WPDx₂₀M and WPDx₃₀M did not even show traces of intact β -lg or α -la bands within the first 5 min of gastric proteolysis (Figures 5.4b and 5.4c).

Table 5.2. Mean hydrodynamic diameter (d_H , nm), polydispersity index and ζ -potential values of freshly prepared conjugated microgel particles in phosphate buffer at pH 7.0 and after addition of SGF at pH 3.0.

pH	WPD _{x₁₀} M			WPD _{x₂₀} M			WPD _{x₃₀} M		
	d_H / nm	Pdl	ζ -potential / mV	d_H / nm	Pdl	ζ -potential / mV	d_H / nm	Pdl	ζ -potential / mV
7.0	136 ± 2.2	0.22	-4.6 ± 0.23	131 ± 1.8	0.27	-5.6 ± 0.16	146 ± 3.9	0.278	-8.1 ± 0.18
3.0	130 ± 0.3	0.21	+9.6 ± 0.24	125 ± 2.5	0.22	+8.6 ± 0.07	133 ± 0.9	0.30	+6.01 ± 0.29

It is possible that a greater degree of conjugation was caused by the exposure of the hydrophobic amino acids naturally generated by increased conjugation of a high molecular weight polysaccharide making the particles highly susceptible to hydrolysis by pepsin (Nooshkam and Varidi, 2019). However, this needs to be further investigated in a future study.

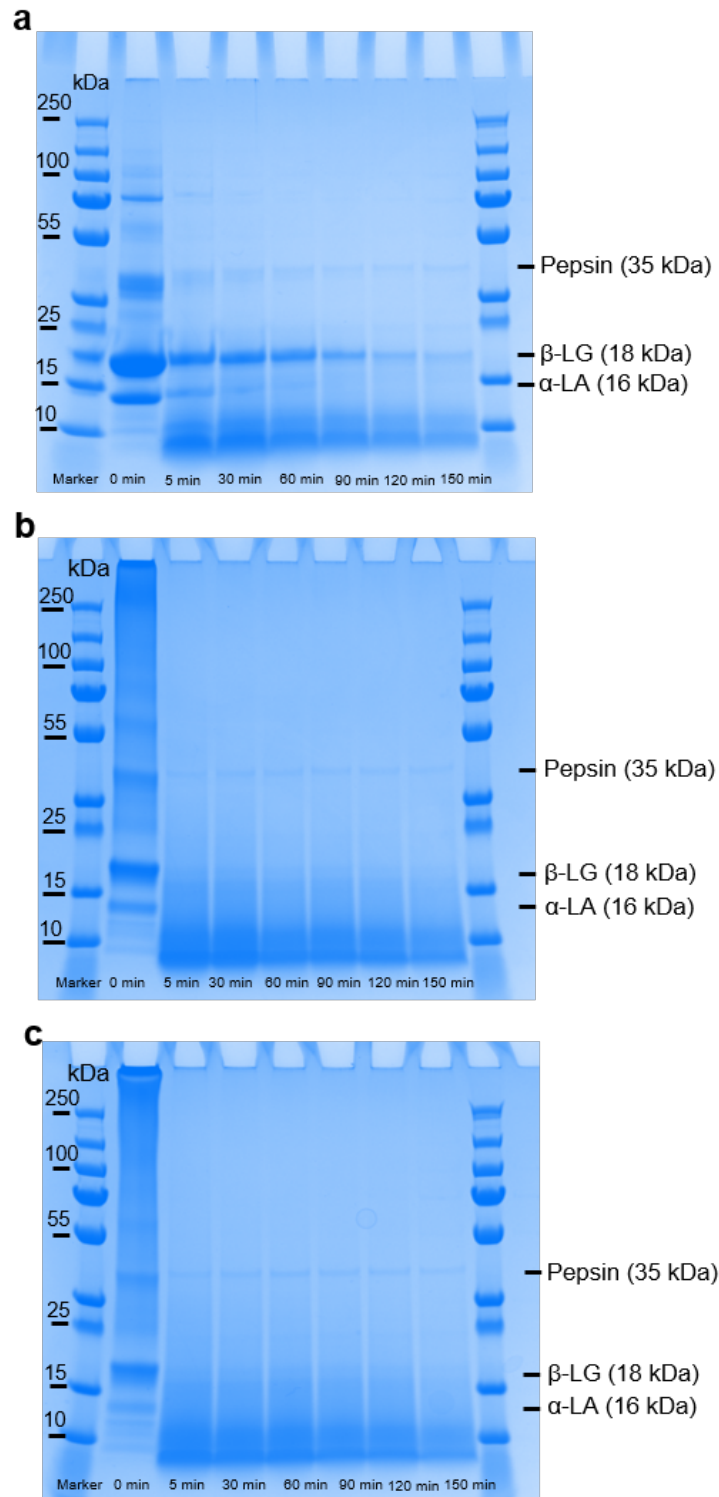


Figure 5.4. SDS-PAGE patterns of a) WPD_{x10M}, b) WPD_{x20M}, c) WPD_{x30M} particles as a function of *in vitro* gastric digestion time.

To investigate more quantitatively, the levels of free amino group (NH_2) were determined using OPA method for the different microgel particles during the gastric digestion. Figure 5.5 shows that at 0 min, all the three conjugate microgel particles ($\text{WPD}_{\text{x}10\text{M}}$, $\text{WPD}_{\text{x}20\text{M}}$, and $\text{WPD}_{\text{x}30\text{M}}$) had 29.3 - 33.1 μM of free NH_2 per g of protein, which is lower than that found previously in heat-induced whey protein nanogel particles (WPN) ($\sim 50 \mu\text{M}$ of free NH_2 per g of protein) (Araiza-Calahorra, et al., 2019a) before any digestion had begun. This can be expected as the free NH_2 acids from the protein was used in the conjugation process in case of the conjugate microgel particles. Of more importance here is the behaviour of these conjugate microgel particles as the gastric digestion commenced (Figure 5.5). The free pepsin hydrolysis presented relatively constant values ranging from 120.1 ± 7.0 to $130.7 \pm 9.9 \mu\text{M}$ NH_2 per g of protein after 120 min of gastric digestion with no significant difference between the microgel particles with different DC ($p > 0.05$). This is 36% lower than that of the previously studied WPN (Araiza-Calahorra et al., 2019a), that showed an increase in the proteolysis in the first 30 min gastric digestion to 187.4 - 204.4 μM NH_2 per g when subjected to the same 120 min of simulated *in vitro* gastric digestion. This proteolysis profile in WPN in the previous study (Araiza-Calahorra et al., 2019a) was directly correlated with heat-induced conformational changes in the whey protein structure that exposed the hydrophobic amino acids making it highly susceptible to hydrolysis by pepsin. Comparing with this previous study, it can be inferred that covalent conjugation with dextran (500 kDa) in the present study would be the only reason why the free amino group profile of all conjugated microgel particles was much lower than the WPN profile during 5 - 120 minutes of digestion ($p < 0.05$). In summary, OPA and SDS-PAGE patterns suggests that a low degree of conjugation was sufficient to delay pepsinolysis of the microgel particles during gastric digestion. Hence, $\text{WPD}_{\text{x}10\text{M}}$ particles were selected for the preparation of the whey protein microgel particle-stabilized Pickering emulsion droplets, which is referred to as $\text{E}_{\text{WPD}_{\text{x}10\text{M}}}$ henceforth.

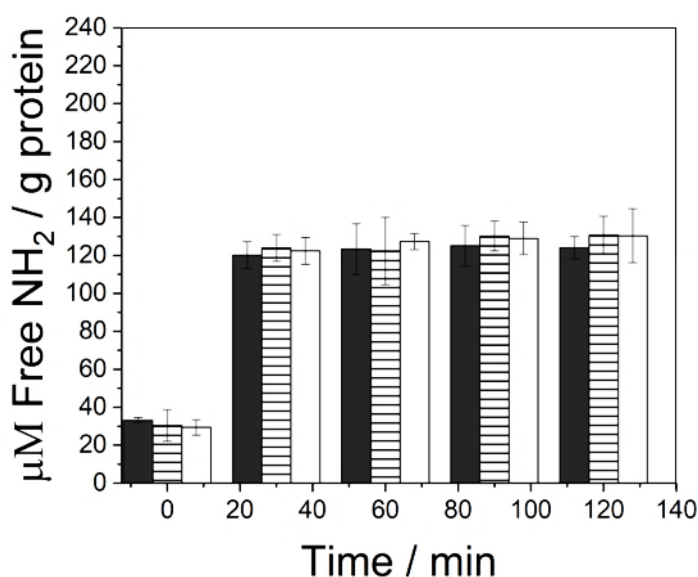


Figure 5.5. Free amino acid content of 1 wt% WPD_{x10}M (dark), WPD_{x20}M (lined pattern) and WPD_{x30}M (white), respectively, as measured by OPA spectrophotometric as a function of *in vitro* gastric digestion time. Error bars represent standard deviations.

5.3.5 Characteristics of Pickering emulsions stabilized by WPD_{x10}M (E_{WPDx10M})

Oil-in-water emulsions were prepared using high-pressure homogenization to determine if the WPD_{x10}M could successfully be used as Pickering stabilizers. Figure 6a shows the droplet size distribution of the 20 wt% MCT oil emulsion stabilised by WPD_{x10}M (1 wt% protein concentration). Droplet size distribution showed a bimodal distribution with oil droplet ranging from 1 to 50 μm (which does not change over one week), and the peak in the area of 0.1 - 1 μm most likely corresponding to unabsorbed WPD_{x10}M. Similar results have been reported previously where unadsorbed particles tend to form a smaller peak in static light scattering results (Araiza-Calahorra et al., 2019b; Du et al., 2020). As can be expected from the charge of the aqueous dispersion of microgel particles (Table 5.2), the emulsion droplets were slightly negatively-charged with a ζ -potential value of -5.39 mV (Figure 5.6a). Interestingly, no notable emulsion instability was observed over several months (data not shown), which indicates that only high adsorption energies via particle-stabilization by the microgel particles was governing the stability of the conjugate microgel-stabilized emulsions as opposed to any electrostatic contribution, the latter has been important contributor to droplet stability in cases of previously reported Pickering emulsions stabilized by whey protein-based microgel or nanogel particles (Araiza-Calahorra et al., 2019b; Destribats

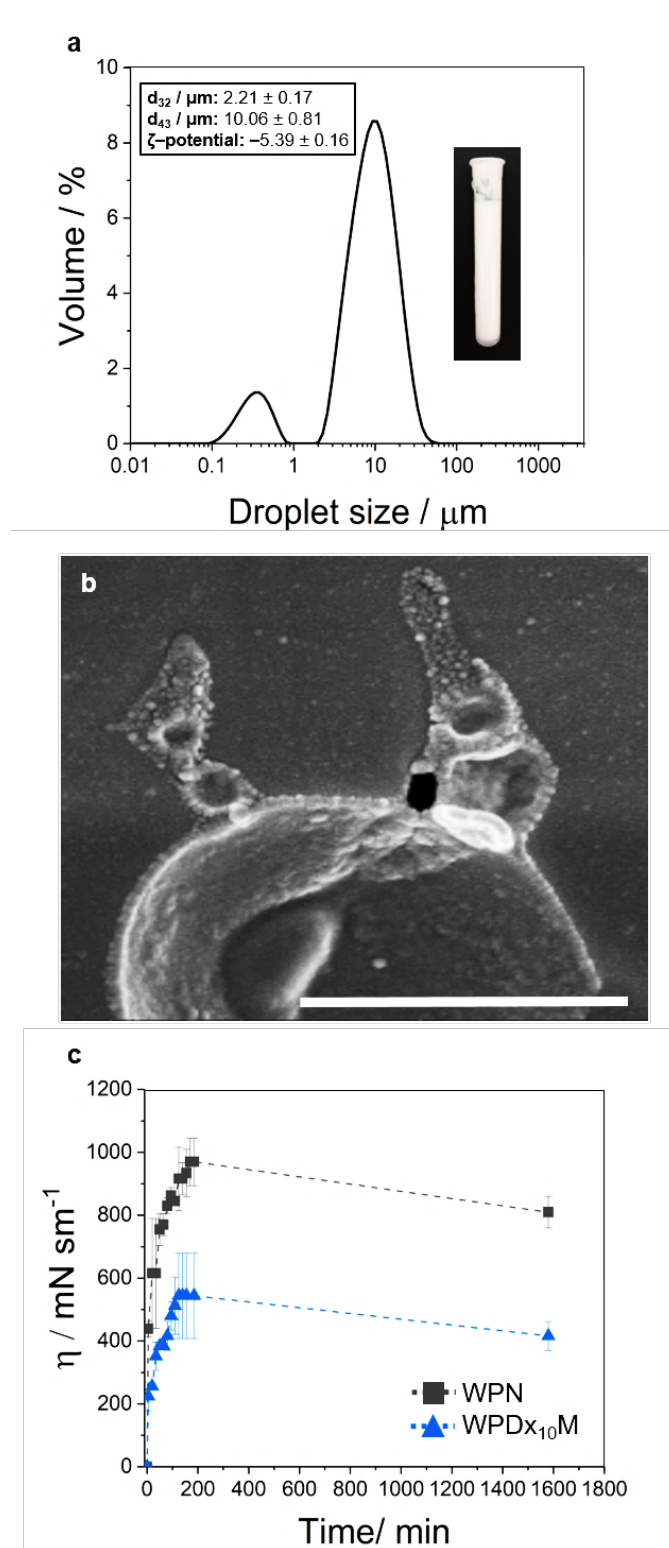


Figure 5.6. a) Droplet size distribution of E_{WPDx10M} , with inset representing the visual image and physicochemical characteristics and b) cryo-SEM micrographs at $150,000\times$ magnifications of Pickering Emulsions stabilized by 1 wt% WPD_{x10M} (scale bar $1 \mu\text{m}$) and c) interfacial shear viscosity at *n*-tetradecane-water interface against time of 0.5 wt% WPD_{x10M} (blue triangle) and WPN (dark square) as control after 24 hrs of adsorption. Error bars represent standard deviation.

et al., 2013; Sarkar et al., 2016). The cryo-SEM image (Figure 5.6b) clearly demonstrates the presence of a monolayer of spherical microgel particles at the interface of the WPD_{x10}M-stabilized emulsions further confirming the Pickering stabilization.

In order to quantitatively determine the mechanical performance of the adsorbed microgel particles at the O/W interface, interfacial shear viscosity (η_i) measurements were undertaken. Interfacial shear viscosity experiments can give powerful insights into structural characteristics of the adsorbed layer and relate the interfacial properties to aspects of the formation and stability of the emulsion (Murray et al., 2011; Zembyla et al., 2019; Zembyla et al., 2019). Figure 5.6c shows the time-dependent shear viscosity data of adsorbed films of WPN (used as control) (Araiza-Calahorra, et al., 2019b) and WPD_{x10}M particles at the n-tetradecane-water interface (0.5 wt%, pH 7.0, 25°C). For the first 3 h, η_i increased by approximately two folds for both particles reaching 970 mN s m⁻¹ for WPN, and 540 mN s m⁻¹ for WPD_{x10}M. After 24 h, the highest value (ca. 800 mN s m⁻¹) was obtained by WPN, whereas the lowest value obtained by WPD_{x10}M was ca. 400 mN s m⁻¹. This decrease in η_i in WPD_{x10}M versus WPN can be surprising considering that the fracture stress and Young's modulus of the parent conjugate gels with 10% DC being four-five folds higher than that of the whey protein counterparts (Figure 5.2). It is possible that the increased shear viscosity values in WPN may be due to stronger interactions between closely packed WPN particles adsorbed at the interface. On the contrary, because of the altered structural conformation of the WPD_{x10}M particles caused by the conjugation and/ or the presence of a high molecular weight polysaccharide, the interactions among WPD_{x10}M particles adsorbed at the interface were probably weakened, which decreased the interfacial shear viscosity values of the resultant conjugate particle. This can be further corroborated by the control samples (mixed non-conjugated N-WPD_xM particles) subjected to interfacial shear viscosity measurements (Appendix C, Figure C7), where it can be observed that an increase in η_i values was obtained in mixed non-conjugated N-WPD_xM microgel particles as compared to WPD_{x10}M but lower than WPN. This suggest that addition of a high molecular weight polysaccharide might have prevent protein-protein interactions between particles, or that the changes on the molecular structure caused by the conjugation altered the structure weakening the strength of the particle-laden film at the interface.

5.3.6 Characteristics of E_{WPD_{x10}M} during *in vitro* gastric digestion

The Pickering emulsion samples stabilized by WPD_{x10}M was exposed to an *in vitro* gastric digestion model to analyse whether the conjugate microgel particles had

any slowing down effect on proteolysis of the particle-laden interface and protected the Pickering emulsions against coalescence during simulated gastric conditions. The droplet size, charge, and microstructure as a function of time were recorded and a combination of confocal laser scanning microscopy and cross-correlation image analysis (Glover et al., 2019a; Glover et al., 2019b) was performed to quantify the amount of proteinaceous microgel particles located at the droplet interface (Figures 5.7-5.9).

5.3.6.1 Stability under simulated gastric conditions

As can be observed in Figure 5.7, the droplet size distribution of $E_{WPDx10M}$ and the volume-average mean diameter ($d_{43} = 7.61 \mu\text{m}$) were not significantly influenced by incubation in SGF without pepsin (Figure 5.7a, see Figure 5.6a for sample at pH 7.0), although the ζ -potential became positive (+8.54 mV) due to the protonation of the WPI (see time 0 min in Figure 5.7b). From the confocal images, it is noticeable that $WPDx_{10M}$ (stained in green) are stabilizing the emulsion droplets (stained in red) with no discernible coalesced oil droplets either before (Figure 5.8a) or after incubation in SGF without pepsin (Figure 8b). This indicates that $E_{WPDx10M}$ was stable to any aggregation under the ionic environment of the gastric conditions.

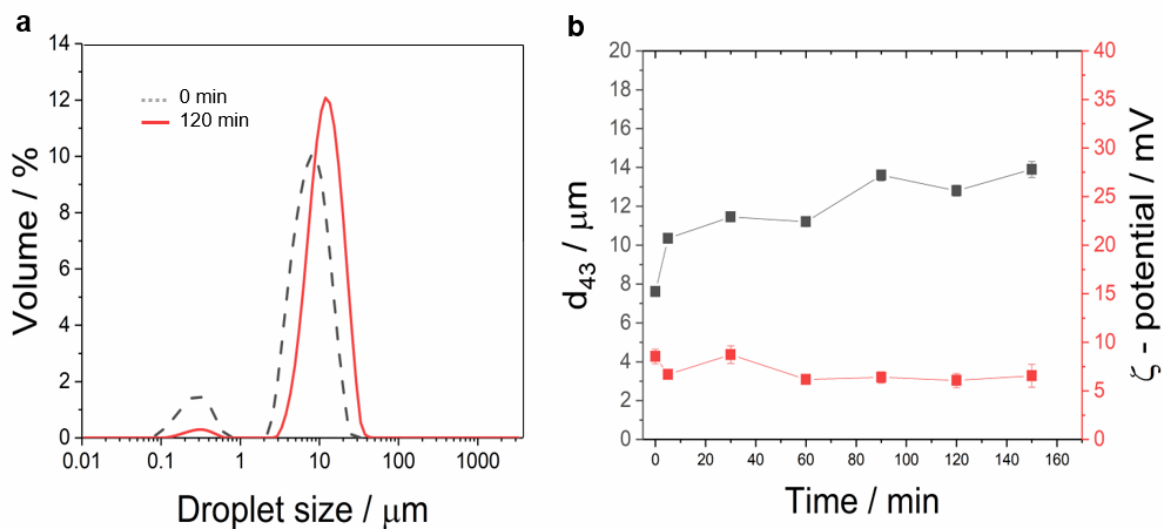


Figure 5.7. Change in a) mean droplet size distribution, b) mean droplet size (d_{43}) and mean ζ -potential values of 20 wt% MCT oil-in-water emulsions ($E_{WPDx10M}$) containing 1 wt% $WPDx_{10M}$ as a function of *in vitro* gastric digestion time. Error bars represent standard.

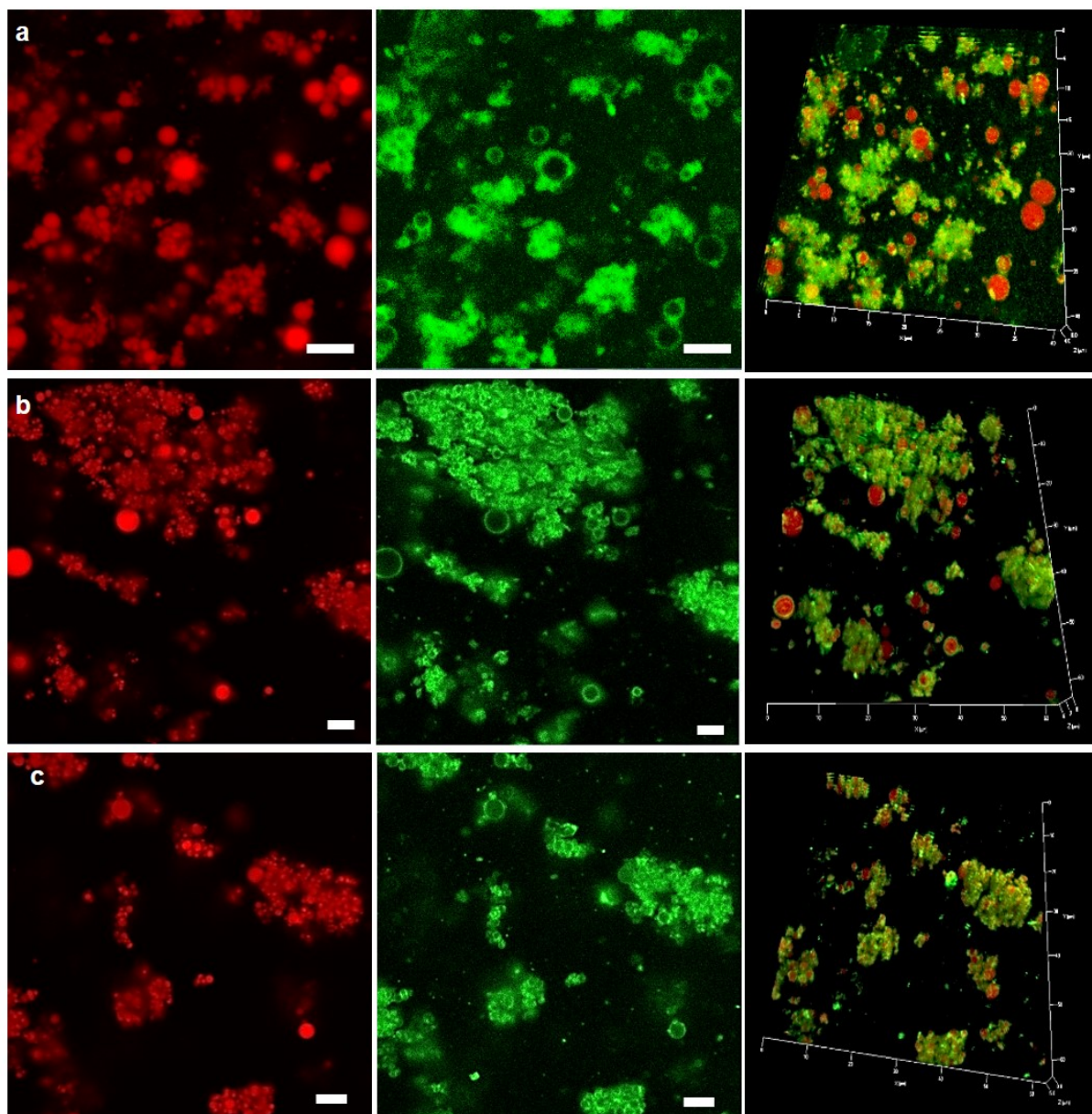


Figure 5.8. Confocal micrographs of $E_{WPDx10M}$ (a) initially without addition of SGF, (b) after addition of SGF at 0 min and (c) after 120 min of *in vitro* gastric digestion in presence of SGF containing pepsin, respectively. Note, 0 min represents the behavior in presence of SGF buffer without added pepsin. The left column with red filled colour represents the oil droplets stained by Nile Red, middle column with green outline represents $WPDx_{10M}$ stained by Fast Green; and the right column represent both the Nile Red and Fast Green channels. Scale bar is $5 \mu\text{m}$.

Interestingly, after addition of pepsin in the SGF, the emulsion exhibited a decrease in the magnitude of surface charge and the d_{43} values increased to a certain extent but remained bimodal after the 120 min (Figure 5.7a). It is worth noting that the first peak height diminished owing to digestion of the unadsorbed microgel particles, which can be expected from the discussion in the previous sections on digestion of aqueous dispersion of particles after 120 min (see Figure 5.4a). But the second peak

showed very similar peak height but shifted slightly towards larger droplet size indicating aggregation of droplets. The decrease in ζ -potential might suggest that the increase in droplet size arose from the aggregation of the droplets during gastric digestion. From the confocal images, emulsion droplets did not seem to have coalesced and no large oil droplets were noticeable even after 120 min (Figure 5.8c). Results indicate that a steric barrier was provided by the neutral conjugate microgel particles which was retained at the interface and played an important role in stabilizing the emulsions in simulated gastric conditions.

5.3.6.2 Cross-correlation image analysis of confocal microscopy images

To assess the impact of conjugation on the gastric destabilization, two channel microscopy images (protein and fat droplets) of two emulsion samples, control Pickering emulsion stabilized by whey protein nanogel particles (WPN) (Araiza-Calahorra et al., 2019b) and whey protein-dextran conjugated microgel particles (WPD_{X10M}) were obtained during simulated gastric conditions. Each image contained a distribution of Pickering emulsion droplets from which smaller regions containing individual emulsion droplets were analysed to extract local information. To analyse the amount of protein around the oil droplet, the droplet of interest was segmented into 20 radial segments ($\pi/10$) and the cross-correlation analysis was performed as a function of angle. Figure 5.9 shows the overlaying radial plot of the treated fat droplets and protein particles and the mean cross-correlation intensity distributed around the fat droplet within each segment of E_{WPN} (a) and E_{WPD_{X10M}} (b) after 0 min (t₁) to 5 - 10 min (t₂) of simulated gastric digestion. By overlaying the radial plots of the two different digestion time points (see Figure 9), it is clear that the changes in the maximal protein distribution from the oil droplet vary between samples. For E_{WPN}, it can be showed that the radial distribution of the maximal protein intensity at time t₂ was on average smaller compared to t₁ (Figure 5.9a). These results corroborate with previous results by Sarkar et al. (2016) and Araiza-Calahorra et al. (2019a) where whey protein-based microgel- as well as nanogel-stabilized Pickering emulsions show interfacial proteolysis by pepsin during *in vitro* gastric step. Nevertheless, the emulsion droplets did not seem to coalesce possibly due to fragments of peptides still present at the interface. As for E_{WPD_{X10M}}, a subtle change on the average distribution between t₁ and t₂ was observed (Figure 5.9b). Whilst there might be some protein interference in the same pixel from particles localized in a nearby emulsion droplet, which was due to the imaging procedure, the observed subtle changes in the protein concentration around the oil droplet is still a good indication of a reduced pepsin hydrolysis of the conjugate microgel particles located at the interface in line with the delayed behaviour observed in the aqueous dispersion (Figure 5.4a). Recent studies have shown that glycation alters the susceptibility of food proteins to gastrointestinal digestion. For example,

Corzo-Martínez et al., (2010) reported a decreased in the proteolytic susceptibility after simulated gastrointestinal digestion of β -lactoglobulin after conjugation with dextran (10 kDa). According to this study, steric hindrance caused by the molecules of dextran attached to β -lg contributed to the lower susceptibility of digestive enzymes toward the

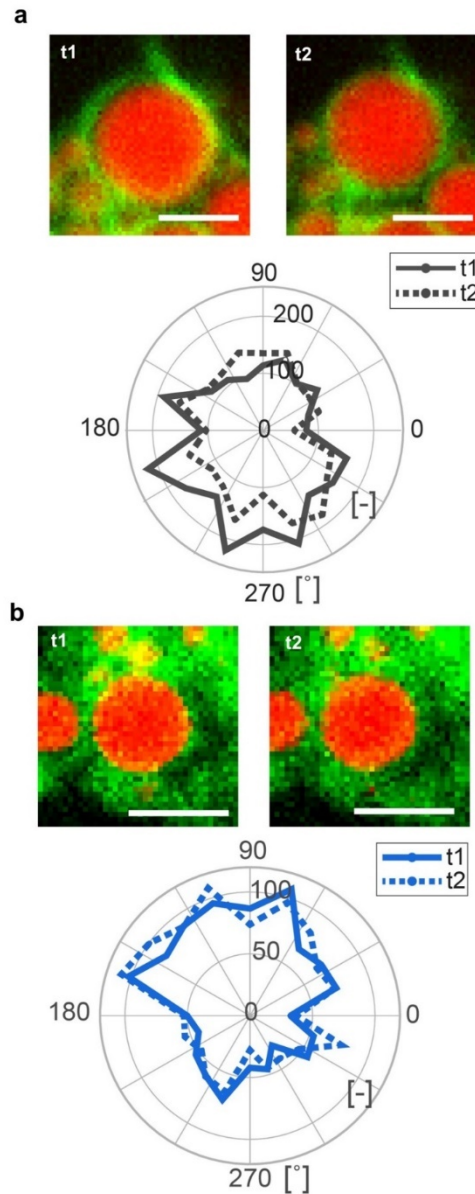


Figure 5.9. a) Pickering emulsion droplet (a) E_{WPN} and (b) $E_{WPDx10M}$ at time 0 min (t1) and at time 5 -10 min (t2) and corresponding mean integrated cross-correlation intensity around the droplet as a function of angle at time points t1 and t2. Cross-correlation intensities are scaled to the radius of the droplet in the image to account of minor changes in z-position over time. Scale bar is 2 μ m.

protein. In addition, Lesmes and McClements (2012) and Xu et al. (2014) have also shown an increased stability under gastric conditions of β -lg-dextran and whey protein-beet pectin conjugate emulsions, respectively. In the former, it was also reported that increasing molecular weight of the conjugated dextran from 10 kDa to 400 kDa rendered emulsion more stable to pepsin-induced instability. Therefore, as depicted schematically in Figure 5.10, we propose that a restricted access of digestive enzyme to potential cleavage sites of the protein in case of the conjugate microgel particles was possibly due to the tortuosity of network structure created during conjugation and parent thermo-set gel formation process. Hence, the conjugate microgel protected the emulsion droplets from destabilization by a physical mechanism caused by steric hindrance effects due to the high molecular weight of the dextran.

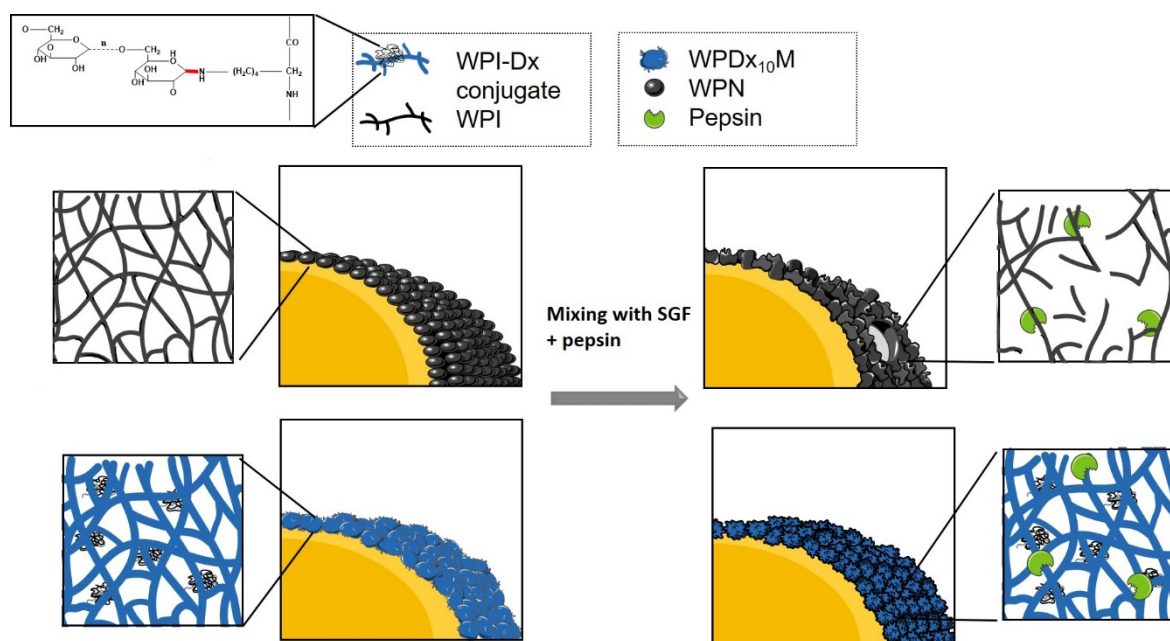


Figure 5.10. Schematic representation of the protective properties of the conjugated microgel particles-stabilized emulsion ($E_{WPDx10M}$) as compared to non-conjugated counterparts against complete *in vitro* gastric digestion by pepsin.

5.4 Conclusions

This study shows that whey protein was covalently linked to dextran via Maillard reaction as determined by OPA and SDS-PAGE, later shown by a gradual disappearance in the intrinsic characteristic band pattern of the WPI fractions. Changes in pH and reaction time increased the degree of conjugation. It was found that the degree of conjugation during Maillard reaction greatly influenced the large deformation properties of the heat-set gels fabricated using these conjugates, such

heat-set gels were used to create conjugate microgel particles for the first time by controlled shearing process. These protein-polysaccharide conjugate microgel particles had different responsiveness to pH, ions (NaCl/ CaCl₂) and pepsin depending on the degree of conjugation. The conjugation of whey protein isolate with dextran delayed the gastric digestion of conjugate microgel particles, which might be attributed to the steric hindrance effect that limits pepsin access to the proteinaceous group with the particles. Conjugate microgel particles with a low degree of conjugation of ~10% effectively acted as Pickering stabilizers for oil-in-water emulsions and by using a proof-of-concept cross-correlation analysis of confocal images it was demonstrated that such conjugate microgel particle-stabilized Pickering emulsions exhibited decreased pepsin digestibility kinetics as compared to droplets stabilized by non-conjugated whey protein-based nanogel particles. The novel insights generated in this study may be applied to rationally design Maillard-based conjugate microgel particle-stabilized emulsions to improve emulsion stability in the human gastric regime for effective delivery of lipophilic ingredients in the human intestines.

In summary, three different interfaces have been used to form Pickering emulsion in **Chapters 3 – 5**. Hence, it is important to compare these three systems as a function of their gastrointestinal digestion fate. More importantly, it is crucial to understand the behaviour of curcumin-loaded emulsions in the gastrointestinal regime. Therefore, in the next chapter (**Chapter 6**) targeted release in the gastrointestinal regime was investigated and the bioaccessibility and cellular uptake for curcumin was assessed.

5.5 References

- Akhtar, M., & Dickinson, E. (2003). Emulsifying properties of whey protein–dextran conjugates at low pH and different salt concentrations. *Colloids and Surfaces B: Biointerfaces*, 31(1-4), 125-132.
- Akhtar, M., & Ding, R. (2017). Covalently cross-linked proteins & polysaccharides: Formation, characterisation and potential applications. *Current Opinion in Colloid & Interface Science*, 28, 31-36.
- Aoki, T., Fukumoto, T., Kimura, T., Kato, Y., & Matsuda, T. (1994). Whey protein- and egg white protein-glucose 6-phosphate conjugates with calcium phosphate-solubilizing properties. *Bioscience, Biotechnology, and Biochemistry*, 58(9), 1727-1728.

- Araiza-Calahorra, A., & Sarkar, A. (2019a). Designing biopolymer-coated Pickering emulsions to modulate *in vitro* gastric digestion: a static model study. *Food & Function*, 10(9), 5498-5509.
- Araiza-Calahorra, A., & Sarkar, A. (2019b). Pickering emulsion stabilized by protein nanogel particles for delivery of curcumin: Effects of pH and ionic strength on curcumin retention. *Food Structure*, 21, 100113.
- Cabodevila, O., Hill, S. E., Armstrong, H. J., Sousa, I., & Mitchell, J. R. (1994). Gelation enhancement of soy protein isolate using the Maillard reaction and high temperatures. *Journal of Food Science*, 59(4), 872-875.
- Chevalier, F., Chobert, J.-M., Popineau, Y., Nicolas, M. G., & Haertlé, T. (2001). Improvement of functional properties of β -lactoglobulin glycosylated through the Maillard reaction is related to the nature of the sugar. *International Dairy Journal*, 11(3), 145-152.
- Clark, A.H., Judge, F. J., Richards, J. B., Stubbs, J. M., & Suggett, A. (1981). Electros microscopy of networks structures in thermally-induced globular protein gels. *International Journal of Peptide and Protein Research*, 17(3), 380-392.
- Corzo-Martínez, M., Soria, A. C., Belloque, J., Villamiel, M., & Moreno, F. J. (2010). Effect of glycation on the gastrointestinal digestibility and immunoreactivity of bovine β -lactoglobulin. *International Dairy Journal*, 20(11), 742-752.
- Darewicz, M., & Dziuba, J. (2001). The effect of glycosylation on emulsifying and structural properties of bovine β -casein. *Die Nahrung*, 45(1), 15-20.
- David-Birman, T., Mackie, A., & Lesmes, U. (2013). Impact of dietary fibres on the properties and proteolytic digestibility of lactoferrin nanoparticles. *Food Hydrocolloids*, 31(1), 33-41.
- Destribats, M., Wolfs, M., Pinaud, F., Lapeyre, V., Sellier, E., Schmitt, V., & Ravaine, V. (2013). Pickering emulsions stabilized by soft microgels: influence of the emulsification process on particle interfacial organization and emulsion properties. *Langmuir*, 29(40), 12367-12374.
- Dickinson, E., & Galazka, V. B. (1991). Emulsion stabilization by ionic and covalent complexes of β -lactoglobulin with polysaccharides. *Food Hydrocolloids*, 5(3), 281-296.
- Dickinson, E., & Semenova, M. G. (1992). Emulsifying properties of covalent protein—dextran hybrids. *Colloids and Surfaces*, 64(3), 299-310.
- Diftis, N., & Kiosseoglou, V. (2004). Competitive adsorption between a dry-heated soy protein—dextran mixture and surface-active materials in oil-in-water emulsions. *Food Hydrocolloids*, 18(4), 639-646.

- Ding, R., Valicka, E., Akhtar, M., & Ettelaie, R. (2017). Insignificant impact of the presence of lactose impurity on formation and colloid stabilising properties of whey protein–maltodextrin conjugates prepared via Maillard reactions. *Food Structure*, 12, 43-53.
- Du Le, H., Loveday, S. M., Singh, H., & Sarkar, A. (2020). Pickering emulsions stabilised by hydrophobically modified cellulose nanocrystals: Responsiveness to pH and ionic strength. *Food Hydrocolloids*, 99, 105344.
- Fechner, A., Knoth, A., Scherze, I., & Muschiolik, G. (2007). Stability and release properties of double-emulsions stabilised by caseinate–dextran conjugates. *Food Hydrocolloids*, 21(5-6), 943-952.
- Foegeding, E. A. (1992). Rheological properties of whey protein isolate gels determine by torsional fracture and stress relaxation 1. *Journal of Texture Studies*, 23(3), 337-348.
- Glover, Z. J., Bisgaard, A. H., Andersen, U., Povey, M. J., Brewer, J. R., & Simonsen, A. C. (2019a). Cross-correlation analysis to quantify relative spatial distributions of fat and protein in super-resolution microscopy images of dairy gels. *Food Hydrocolloids*, 97, 105225.
- Glover, Z. J., Ersch, C., Andersen, U., Holmes, M. J., Povey, M. J., Brewer, J. R., & Simonsen, A. C. (2019b). Super-resolution microscopy and empirically validated autocorrelation image analysis discriminates microstructures of dairy derived gels. *Food Hydrocolloids*, 90, 62-71.
- Goh, K. K. T., Sarkar, A., & Singh, H. (2014). Chapter 13 - Milk protein–polysaccharide interactions In H. Singh, M. Boland & A. Thompson (Eds.), *Milk Proteins* (Second Edition) (pp. 387-419). San Diego: Academic Press.
- Ho, Y.-T., Ishizaki, S., & Tanaka, M. (2000). Improving emulsifying activity of ϵ -polylysine by conjugation with dextran through the Maillard reaction. *Food Chemistry*, 68(4), 449-455.
- Kato, A. (2002). Industrial applications of Maillard-type protein-polysaccharide conjugates. *Food Science and Technology Research*, 8(3), 193-199.
- Kato, A., Sato, T., & Kobayashi, K. (1989). Emulsifying properties of protein–polysaccharide complexes and hybrids. *Agricultural and Biological Chemistry*, 53(8), 2147-2152.
- Kato, H. (1956). Studies on browning reactions between sugars and amino compounds: Part ii. Significance of n-glycosides for browning reactions. *Bulletin of the Agricultural Chemical Society of Japan*, 20, 279-283.

- Lesmes, U., & McClements, D. J. (2012). Controlling lipid digestibility: Response of lipid droplets coated by β -lactoglobulin-dextran Maillard conjugates to simulated gastrointestinal conditions. *Food Hydrocolloids*, 26(1), 221-230.
- Liu, F., Ma, C., McClements, D. J., & Gao, Y. (2016). Development of polyphenol-protein-polysaccharide ternary complexes as emulsifiers for nutraceutical emulsions: Impact on formation, stability, and bioaccessibility of β -carotene emulsions. *Food Hydrocolloids*, 61, 578-588.
- Liu, F., Wang, D., Sun, C., & Gao, Y. (2016). Influence of polysaccharides on the physicochemical properties of lactoferrin-polyphenol conjugates coated β -carotene emulsions. *Food Hydrocolloids*, 52, 661-669.
- Madruga, M. S., & Mottram, D. S. (1995). The effect of pH on the formation of Maillard-derived aroma volatiles using a cooked meat system. *Journal of the Science of Food and Agriculture*, 68(3), 305-310.
- Matsudomi, N., Nakano, K., Soma, A., & Ochi, A. (2002). Improvement of gel properties of dried egg white by modification with galactomannan through the Maillard reaction. *Journal of Agricultural and Food Chemistry*, 50(14), 4113-4118.
- Meydani, B., Vahedifar, A., Askari, G., & Madadlou, A. (2019). Influence of the Maillard reaction on the properties of cold-set whey protein and maltodextrin binary gels. *International Dairy Journal*, 90, 79-87.
- Mikami, Y., & Murata, M. (2015). Effects of sugar and buffer types, and pH on formation of Maillard pigments in the lysine model system. *Food Science and Technology Research*, 21(6), 813-819.
- Minekus, M., Alminger, M., Alvito, P., Ballance, S., Bohn, T., Bourlieu, C., Carrière, F., Boutrou, R., Corredig, M., Dupont, D., Dufour, C., Egger, L., Golding, M., Karakaya, S., Kirkhus, B., Le Feunteun, S., Lesmes, U., Macierzanka, A., Mackie, A., Marze, S., McClements, D. J., Ménard, O., Recio, I., Santos, C. N., Singh, R. P., Vegarud, G. E., Wickham, M. S. J., Weitschies, W., & Brodkorb, A. (2014). A standardised static *in vitro* digestion method suitable for food – an international consensus. *Food & Function*, 5(6), 1113-1124.
- Murray, B. S., & Dickinson, E. (1996). Interfacial rheology and the dynamic properties of adsorbed films of food proteins and surfactants. *Food Science and Technology International*, Tokyo, 2(3), 131-145.
- Murray, B. S., Durga, K., Yusoff, A., & Stoyanov, S. D. (2011). Stabilization of foams and emulsions by mixtures of surface-active food-grade particles and proteins. *Food Hydrocolloids*, 25(4), 627-638.

- Nielsen, P. M., Petersen, D., & Dambmann, C. (2001). Improved Method for Determining Food Protein Degree of Hydrolysis. *Food Chemistry and Toxicology*, 66(5), 642-646.
- Nooshkam, M., & Varidi, M. (2019). Maillard conjugate-based delivery systems for the encapsulation, protection, and controlled release of nutraceuticals and food bioactive ingredients: A review. *Food Hydrocolloids*, 105389.
- Oliver, C. M., Melton, L. D., & Stanley, R. A. (2006). Creating proteins with novel functionality via the Maillard reaction: A review. *Critical Reviews in Food Science and Nutrition*, 46(4), 337-350.
- Potman, R. P., & van Wijk, T. A. (1989). Mechanistic studies of the Maillard reaction with emphasis on phosphate-mediated catalysis In *Thermal Generation of Aromas. American Chemical Society*, 409, 182-195.
- Rodríguez Patino, J. M., & Pilosof, A. M. R. (2011). Protein–polysaccharide interactions at fluid interfaces. *Food Hydrocolloids*, 25(8), 1925-1937.
- Sarkar, A., Murray, B., Holmes, M., Ettelaie, R., Abdalla, A., & Yang, X. (2016). *In vitro* digestion of Pickering emulsions stabilized by soft whey protein microgel particles: influence of thermal treatment. *Soft Matter*, 12(15), 3558-3569.
- Sarkar, A., Zhang, S., Holmes, M., & Ettelaie, R. (2019). Colloidal aspects of digestion of Pickering emulsions: Experiments and theoretical models of lipid digestion kinetics. *Advances in Colloid and Interface Science*, 263, 195-211.
- Sarkar, A., Zhang, S., Murray, B., Russell, J. A., & Boxal, S. (2017). Modulating *in vitro* gastric digestion of emulsions using composite whey protein-cellulose nanocrystal interfaces. *Colloids and Surfaces B: Biointerfaces*, 158, 137-146.
- Shepherd, R., Robertson, A., & Ofman, D. (2000). Dairy glycoconjugate emulsifiers: casein–maltodextrins. *Food Hydrocolloids*, 14(4), 281-286.
- Singh, H., & Sarkar, A. (2011). Behaviour of protein-stabilised emulsions under various physiological conditions. *Advances in Colloid and Interface Science*, 165(1), 47-57.
- Spotti, M. J., Loyeau, P. A., Marangón, A., Noir, H., Rubiolo, A. C., & Carrara, C. R. (2019). Influence of Maillard reaction extent on acid induced gels of whey proteins and dextrans. *Food Hydrocolloids*, 91, 224-231.
- Spotti, M. J., Perduca, M. J., Piagentini, A., Santiago, L. G., Rubiolo, A. C., & Carrara, C. R. (2013a). Does dextran molecular weight affect the mechanical properties of whey protein/dextran conjugate gels? *Food Hydrocolloids*, 32(1), 204-210.

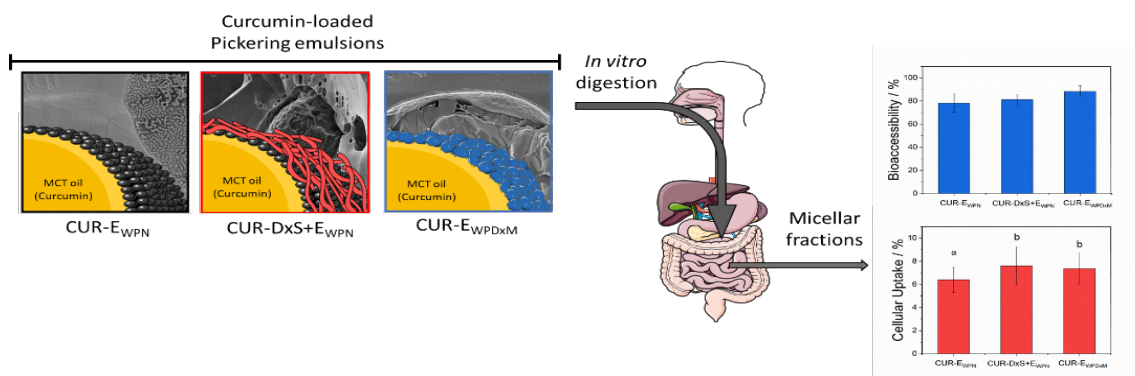
- Spotti, M. J., Perduca, M. J., Piagentini, A., Santiago, L. G., Rubiolo, A. C., & Carrara, C. R. (2013b). Gel mechanical properties of milk whey protein–dextran conjugates obtained by Maillard reaction. *Food Hydrocolloids*, 31(1), 26-32.
- Spotti, M. J., Santiago, L. G., Rubiolo, A. C., & Carrara, C. R. (2012). Mechanical and microstructural properties of milk whey protein/espina corona gum mixed gels. *LWT - Food Science and Technology*, 48(1), 69-74.
- Sun, W. W., Yu, S. J., Yang, X. Q., Wang, J. M., Zhang, J. B., Zhang, Y., & Zheng, E. L. (2011). Study on the rheological properties of heat-induced whey protein isolate–dextran conjugate gel. *Food Research International*, 44(10), 3259-3263.
- Sun, Y., Hayakawa, S., & Izumori, K. (2004). Modification of ovalbumin with a rare ketohexose through the Maillard reaction: Effect on protein structure and gel properties. *Journal of Agricultural and Food Chemistry*, 52(5), 1293-1299.
- van Beilen, J. B., & Li, Z. (2002). Enzyme technology: an overview. *Current opinion in biotechnology*, 13(4), 338-344.
- Willits, C. O., Underwood, J. C., Lento Jr., H. G., & Riccuti, C. (1958). Browning of sugar solutions. I. Effect of pH and type of amino acid in dilute sugar solutions. *Journal of Food Science*, 23(1), 61-67.
- Wolfrom, M. L., Kolb, D. K., & Langer, A. W. (1953). Chemical interactions of amino compounds and sugars. VII.1 pH dependency². *Journal of the American Chemical Society*, 75(14), 3471-3473.
- Wong, B. T., Day, L., & Augustin, M. A. (2011). Deamidated wheat protein–dextran Maillard conjugates: Effect of size and location of polysaccharide conjugated on steric stabilization of emulsions at acidic pH. *Food Hydrocolloids*, 25(6), 1424-1432.
- Wooster, T. J., & Augustin, M. A. (2006). Beta-lactoglobulin-dextran Maillard conjugates: their effect on interfacial thickness and emulsion stability. *Journal of Colloid Interface Science*, 303(2), 564-572.
- Xu, D., Yuan, F., Gao, Y., Panya, A., McClements, D. J., & Decker, E. A. (2014). Influence of whey protein–beet pectin conjugate on the properties and digestibility of β -carotene emulsion during *in vitro* digestion. *Food Chemistry*, 156, 374-379.
- Zembyla, M., Lazidis, A., Murray, B. S., & Sarkar, A. (2019). Water-in-oil Pickering emulsions stabilized by synergistic particle–particle interactions. *Langmuir*, 35(40), 13078-13089.
- Zembyla, M., Murray, B. S., Radford, S. J., & Sarkar, A. (2019). Water-in-oil Pickering emulsions stabilized by an interfacial complex of water-insoluble polyphenol crystals and protein. *Journal of Colloid and Interface Science*, 548, 88-99.

Zembyla, M., Murray, B. S., & Sarkar, A. (2018). Water-In-Oil Pickering Emulsions Stabilized by Water-Insoluble Polyphenol Crystals. *Langmuir*, 34(34), 10001-10011.

Zhu, D., Damodaran, S., & Lucey, J. A. (2010). Physicochemical and emulsifying properties of whey protein isolate (WPI)-dextran conjugates produced in aqueous solution. *Journal of Agricultural Food Chemistry*, 58(5), 2988-2994.

Chapter 6

Pickering emulsions stabilized by protein gel particles complexed and conjugated with biopolymers to enhance bioaccessibility and cellular uptake of curcumin⁵



Abstract

The aim of this study was to investigate the fate of curcumin (CUR)-loaded Pickering emulsions with complex interfaces during in vitro gastrointestinal transit and test the efficacy of such emulsions on improving the bioaccessibility and cellular uptake of CUR. CUR-loaded Pickering emulsions tested were whey protein nanogel particle-stabilized Pickering emulsions (CUR-E_{WPN}) and emulsions displaying complex interfaces included 1) layer-by-layer dextran sulphate-coated nanogel-stabilized Pickering emulsions (CUR-DxS+E_{WPN}) and 2) protein+dextran-conjugated microgel-stabilized Pickering emulsions (CUR-E_{WPDxM}). The hypothesis was that the presence of complex interfacial material at the droplet surface would provide better protection to the droplets against physiological degradation, particularly under gastric conditions and thus, improve the delivery of CUR to Caco-2 intestinal cells. The emulsions were characterized using droplet sizing, apparent viscosity, confocal and cryo-scanning electron microscopy, zeta-potential, lipid digestion kinetics, bioaccessibility of CUR as well as cell viability and uptake by Caco-2 cells. Emulsion droplets with modified complex interfacial composition (i.e. CUR-DxS+E_{WPN} and CUR-E_{WPDxM}) provided enhanced kinetic stability to the Pickering emulsion droplets against coalescence in the gastric regime as compared to droplets having unmodified interface (i.e. CUR-

⁵ Submitted as: Araiza-Calahorra, A., Wang, Y., Boesch, C., Zhao, Y., and Sarkar, A. Pickering emulsions stabilized by protein gel particles complexed and conjugated with biopolymers to enhance bioaccessibility and cellular uptake of curcumin. *Current Research in Food Science* (3, pp. 178 –188). DOI: <https://doi.org/10.1016/j.crf.2020.05.001>

E_{WPN}), whereas droplet coalescence occurred in intestinal conditions irrespective of the initial interfacial materials. A similar rate and extent of free fatty acid release occurred in all the emulsions during intestinal digestion ($p > 0.05$), which correlated with the bioaccessibility of CUR. Striking, CUR-DxS+ E_{WPN} and CUR- E_{WPDxM} significantly improved cellular CUR uptake as compared to CUR- E_{WPN} ($p < 0.05$). These results highlight a promising new strategy of designing gastric-stable Pickering emulsions with complex interfaces to improve the delivery of lipophilic bioactive compounds to the cells for the future design of functional foods.

6.1. Introduction

Curcumin (CUR), a natural polyphenol, is the major curcuminoid (70 – 80%) present in the rhizomes of turmeric plant *Curcuma longa* (Goel et al., 2008). Due to its potential health-promoting properties such as anti-tumor, anti-oxidant, anti-microbial and anti-inflammatory, the incorporation of CUR into functional foods has been of major interest in recent years to both functional food and pharmaceutical industries (Anand et al., 2007). However, significant research challenges exist with the incorporation of CUR and its use as a bioactive ingredient due to limited aqueous solubility, high rate of metabolism and low bioavailability with rapid clearance of CUR (Tønnesen et al., 2002).

To address these delivery challenges of CUR, several colloidal approaches such as liposomes, vesicles, protein-based complexes and emulsion-based delivery systems have surfaced in the literature (Amani et al., 2019; Araiza-Calahorra et al., 2018; Kolter et al., 2019). In particular, emulsion-based delivery systems have been increasingly used to encapsulate CUR due to their simple processing technique, the fact that they can be made entirely from bio-based materials, and that they are suitable for incorporation into a variety of food matrices (Kharat and McClements 2019). Nonetheless, emulsion-based delivery vehicles are mostly designed in isolation and often the fate of the encapsulated CUR within these emulsified lipid-based delivery systems during the physiological transit remain poorly understood. In particular, the bioaccessibility of CUR after passing through the gastrointestinal (GI) tract and permeability of CUR across the intestinal epithelium are crucial to understand the efficacy of these delivery vehicles, which have been given rare attention in literature to date (Zou et al., 2015).

Among the emulsion-based delivery vehicles, Pickering emulsions have attracted significant recent scientific and industrial interests since they possess many advantages in terms of high stability against coalescence and Oswald ripening (Rayner et al., 2012, Tzoumaki et al., 2014), and controlled digestibility of lipids by

preventing competitive displacement by bio-surfactants (bile salts) (Dickinson 2012; Ruiz-Rodriguez et al., 2014; Sarkar et al., 2016; Sarkar et al., 2019; Shimoni et al., 2013; Xiao et al., 2015). More specifically, Pickering emulsions stabilized by a wide range of particles, such as protein nanogels, modified starch granules, chitosan-tripolyphosphate complexes, silica, kafirin, ovotransferrin fibrils, nanocellulose and kaolinite (Araiza-Calahorra and Sarkar 2019; Asabuwa Ngwabebhoh et al., 2018; Lu et al., 2019; Marefati et al., 2017; Shah et al., 2016a, 2016b; Tang et al., 2019; Tikekar et al., 2013; Wei et al., 2019) have been recently used as delivery vehicles for CUR. However, only few studies have investigated the biofunctionalities of the encapsulated CUR in these Pickering emulsions after *in vitro* digestion (Lu et al., 2019; Marefati et al., 2017; Shah et al., 2016b; Tikekar et al., 2013; Wei et al., 2019). Many of these emulsions have been prepared using inorganic particles, restricting their application in edible formats (Asabuwa et al., 2018; Shah et al., 2016a; Shah et al., 2016b; Tang et al., 2019; Tikekar et al., 2013). In addition, literature is scarce on CUR bioaccessibility and potential cell toxicity as well as uptake of CUR by the cells when CUR is encapsulated in such Pickering emulsions (Lu et al., 2019). In our previous study, we demonstrated the capacity of whey protein nanogel-stabilized Pickering emulsions to encapsulate CUR under different conditions of physiologically relevant different pHs and ionic strengths (Araiza-Calahorra et al., 2019b).

In addition, Pickering emulsions stabilized by complex interfaces such as dextran sulphate (DxS)-coated nanogel particles (Araiza-Calahorra and Sarkar 2019a) or conjugate microgels in which dextran (Dx) was covalently conjugated to protein before micro-gelation process (Araiza-Calahorra et al., 2020) have successfully demonstrated higher kinetic stability to coalescence in the gastric phase as compared to that of non-modified simple nanogel-stabilized emulsions. The aim of this work was therefore to compare Pickering emulsions with complex interfaces (electrostatically-driven protein gel particles + biopolymer or covalently-conjugated protein-biopolymer gel particles at the interfaces) over nanogel particles as delivery vehicles for CUR for the first time. To test the efficacy of these delivery vehicles for curcumin, the fate of these Pickering emulsions loaded with CUR in simulated *in vitro* gastrointestinal digestion environment was investigated followed by assessment of curcumin bioaccessibility and cellular uptake. To our knowledge, the bioaccessibility and efficacy for delivering CUR to Caco2-cells after *in vitro* static simulated digestion when encapsulated in complex particle-stabilized Pickering emulsions has not been studied to date. Our hypothesis was that complex interfacial materials can provide better barrier to the droplets in the gastric environment and thus allow efficient release in the intestinal phase and therefore enhance the cellular uptake of CUR. Thus, novel insights from this study would advance the fundamental understanding of how

interfacial design of emulsions can be tailored to alter gastrointestinal release and increase intestinal uptake of CUR.

6.2 Materials and Methods

6.2.1 Materials

Curcumin (CUR) (1,7-bis(4-hydroxy-3-methoxyphenyl)-1,6-heptadiene-3,5-dione) ($\geq 65\%$ purity), dextran (Dx) as well as dextran sulphate (DxS) of molecular weight (MW) 500 kDa were purchased from Sigma-Aldrich Company Ltd (Dorset, UK) and used without any further purification. Powdered whey protein isolate (WPI) with $\geq 90\%$ protein content was a kind gift from Fonterra Co-operative Group Limited (Auckland, New Zealand). Miglyol[®] 812 medium-chain triglyceride (MCT) oil with a density of 945 kg m^{-3} at $20 \text{ }^\circ\text{C}$ was purchased from Cremer Oleo GmbH & Co (Germany) and was used as the dispersed phase without any further purification. All enzymes *i.e.* porcine pepsin (P7000, 526 U mg^{-1} using haemoglobin as a substrate), porcine pancreatin (P7545, $8 \times \text{USP}$ and trypsin activity of 6.48 U mg^{-1} using TAME, N-p-Tosyl-L-arginine methyl ester hydrochloride, as a substrate) and porcine bile extract B8631 (total bile salt content $49 \text{ wt}\%$ with $10\text{--}15\%$ glycodeoxycholic acid, $3\text{--}9\%$ taurodeoxycholic acid, $0.5\text{--}7\%$ deoxycholic acid, $5 \text{ wt}\%$ phospholipids) were purchased from Sigma-Aldrich Company Ltd. For cell culture experiments, human colon adenocarcinoma (Caco-2) cells were purchased from the European Collection of Authenticated Cell Culture (ECACC). Cell culture media and supplements *i.e.* Dulbecco's Modified Eagle Medium (DMEM), fetal bovine serum (FBS), Dulbecco's Phosphate-Buffered Saline (DPBS), non-essential amino acids (NEAA), trypsin EDTA, and penicillin-streptomycin mixture (5000 U mL^{-1}) were obtained from Gibco Cell Culture Products, Thermo Fisher Scientific (UK). Neutral red powder, HPLC-grade methanol, ethanol, and analytical-grade glacial acid, were acquired from Sigma-Aldrich Company Ltd. All solutions were prepared with Milli-Q water (resistivity of $18.2 \text{ M}\Omega \text{ cm}$ at $25 \text{ }^\circ\text{C}$) (Milli-Q apparatus, Millipore, Bedford, UK).

6.2.2 Methods

6.2.2.1 Preparation of CUR-loaded Pickering emulsion systems

6.2.2.1.1 Preparation of whey protein nanogel particles (WPN) and whey protein isolate+dextran conjugate microgel particles (WPDxM).

Whey protein nanogel particles (WPN) were produced based on a previously developed top-down technique (Araiza-Calahorra et al., 2019). Briefly, WPI powder ($10 \text{ wt}\%$) was dissolved in 20 mM phosphate buffer at $\text{pH } 7.0$ for 2 hours and the

solution was heated in a temperature-controlled water bath at 90 °C for 30 min to form a heat-set gel (quiescent). The resultant WPI gels were pre-homogenized with phosphate buffer (5 wt% protein) using a hand blender (HB724, Kenwood) for 1 min and the resulting whey protein macrogel dispersion (5 wt% protein) was passed through a high-pressure homogenizer at 300 bars for two passes to create WPN. The resultant WPN was diluted with buffer to the desired protein concentration for the Pickering emulsion preparation.

Whey protein isolate+Dx conjugate powder was prepared as described previously (Araiza-Calahorra et al., 2020). The pH of WPI+Dx solution (1:2 w/w ratio) was adjusted to pH 7.0 and gently stirred for 2 h at 25 °C. The WPI+Dx solution was stored at 4 °C overnight and then frozen at -20 °C for 6 h. Samples were then freeze-dried for 24 h and Maillard reaction of the resulting WPI+Dx was promoted by incubating the powder in a pre-heated desiccator at 60 °C for 24 hours, with relative humidity (79%) controlled by saturated KBr solution.

Whey protein isolate+Dx conjugated microgels (WPDxM) with a degree of conjugation of 10% were produced using the afore-mentioned method used for creating WPN with minor modifications. Briefly, conjugate powder was dispersed for 2 h in phosphate buffer at pH 7.0 to ensure complete dissolution to a final protein concentration of 11.6 wt%. The conjugate solution was heated in a temperature-controlled water bath at 65 °C for 1 hour to form a heat-set gel (quiescent), followed by cooling down for 15 min and stored at 4 °C. The obtained gels were pre-homogenized with phosphate buffer (2 wt%) to create macrogel particles using a hand blender (HB724, Kenwood) for 1 min and then passed through a high-pressure homogenizer at 300 bars twice to create microgel particles. Obtained conjugate microgel particles (WPDxM) were diluted with buffer to the desired protein concentration for the Pickering emulsion preparation.

6.2.2.1.2 CUR-loaded Pickering oil-in-water emulsion preparation.

The oil phase was prepared by dissolving 2 wt% CUR into heated MCT-oil (60 °C), by magnetically stirring for 30 min, and centrifuging for 10 min at 4 °C to remove any undissolved CUR (Araiza-Calahorra and Sarkar, 2019a). Oil-in-water Pickering emulsions (80:20 w/w) containing CUR *i.e.* CUR-E_{WPN} or CUR-E_{WPDxM} were prepared using WPN or WPDxM as Pickering stabilizers, respectively. Coarse emulsions were prepared by homogenizing the MCT-oil containing CUR with fresh WPN or WPDxM aqueous suspension at pH 7.0 (1 wt% final protein concentration in all emulsions) using a Ultra Turrax T25 homogenizer (IKA-Werke GmbH & Co., Staufen Germany) at 13, 500 rpm for 1 min. Fine CUR-E_{WPN} or CUR-E_{WPDxM} droplets were prepared by passing the coarse emulsions twice through a high-pressure homogenizer at 300 bars.

For the biopolymer-coated Pickering emulsions, CUR- E_{WPN} (40 wt% MCT-oil) and aqueous dispersions of DxS of 500 kDa Mw (0.4 wt%) were mixed in 1 : 1 w/w at pH 3.0 to allow mutually attractive interaction between the cationic WPN and anionic DxS at the interface, as previously described by Araiza-Calahorra et al. (2019b) and produce CUR-DxS- E_{WPN} (20 wt% MCT, 1 wt% WPN). For comparison purposes, all emulsions contained the same amount of oil and protein.

6.2.2.2 Particle and droplet size measurements

Light scattering was used to measure the size distribution of the initial nanogel/microgel particles (dynamic light scattering, DLS) and fresh emulsion droplets (static light scattering, SLS) undergoing *in vitro* gastrointestinal digestion. Aqueous dispersions of WPN and WPDxM was measured using DLS at 25 °C using a Zetasizer Nano-ZS (Malvern Instruments, Malvern UK) after 100× dilution in phosphate buffer (pH 7.0) at room temperature. Droplet size distributions before and after *in vitro* digestion of the emulsion samples were determined using SLS at 25 °C using Malvern MasterSizer 3000 (Malvern Instruments Ltd, Malvern, Worcestershire, UK). The mean particle size of the emulsions was reported as volume mean diameter (d_{43}) as it is more sensitive to droplet aggregation with systems showing bimodal size distribution. Results are based on three measurements on triplicate samples.

6.2.2.3 ζ -potential measurements

The ζ -potential values of aqueous dispersions of the nanogel and microgel particles and the three Pickering emulsion samples were determined using Zetasizer, Nano ZS series, Malvern Instruments, Worcestershire, UK. Samples before and after *in vitro* digestion were diluted to 0.01% particle or 0.004 wt% oil in 100× in phosphate buffer (pH 7.0) or SGF buffer (pH 3.0) or SIF buffer (pH 7.0) depending upon the condition, and added to a folded capillary cell (Model DTS 1070, Malvern Instruments Ltd., Worcestershire, UK). The ζ -potential measurements were performed for duplicate samples with three readings for each of them.

6.2.2.4 Apparent viscosity

The apparent viscosity of the freshly-prepared Pickering emulsions were measured using a rheometer (Kinexus Ultra⁺, Malvern Instruments Ltd, Worcestershire, UK) equipped with a cone-and-plate geometry (diameter 40 mm, model: CP4/40 SS017SS). About 1.4 mL of the emulsion sample was placed onto the

sample plate. Apparent viscosities were obtained for all the emulsion samples as a function of shear rates ranging from 1 to 1000 s⁻¹ at 37 °C. Data from the flow curves were fitted to Ostwald de Waele fit as shown in equation (6.1):

$$\eta_a(\dot{\gamma}) = K\dot{\gamma}^{n-1} \quad (6.1)$$

where, η_a is the apparent viscosity, $\dot{\gamma}$ is the shear rate, K is the consistency index and n is the flow behaviour index. Linear regression analysis was applied to the data in order to calculate the flow behaviour index and the consistency coefficient.

6.2.2.5 *In vitro* gastrointestinal digestion (static model)

A static digestion model was used in the *in vitro* digestion experiment employing a slightly adapted version from Minekus et al., (2014) omitting the oral step. Exactly 5 mL of the CUR-loaded Pickering emulsions at pH 3.0 (pre-incubated at 37 °C, 1 h) were mixed with 5 mL of simulated gastric fluid (SGF), consisting of 0.257 g L⁻¹ of KCl, 0.061 g L⁻¹ of KH₂PO₄, 1.05 g L⁻¹ of NaHCO₃, 1.38 g L⁻¹ of NaCl, 0.0122 g L⁻¹ of MgCl₂(H₂O)₆, 0.024 g L⁻¹ of (NH₄)₂CO₃ and 2000 U/ mL pepsin at pH 3.0. The mixture was incubated for 2 hours at 37 °C under agitation using a shaking water bath (Grant Instruments Ltd, Cambridge, UK) at 100 rpm.

To allow sequential gastrointestinal digestion, after 2 h of incubation, the pH of the sample + SGF (10 mL) was adjusted to pH 6.8 with 1 M NaOH and mixed with 7.73 mL of simulated intestinal fluid (SIF) electrolyte stock solution consisting of 0.254 g L⁻¹ of KCl, 0.054 g L⁻¹ of KH₂PO₄, 3.570 g L⁻¹ of NaHCO₃, 1.123 g L⁻¹ of NaCl and 0.335 g L⁻¹ of MgCl₂(H₂O)₆, 1.25 mL fresh bile (10 mM in the final digesta), 20 µL of 0.3 M CaCl₂ and 1 mL of a pancreatin solution (100 U mL⁻¹ based on trypsin activity in the final digesta) made up in SIF electrolyte stock solution. The *in vitro* intestinal digestion was carried out over 3 hours at pH 6.8 and 37 °C.

During this 5 hours *in vitro* digestion period, samples (sample+SGF and sample+SGF+SIF) were periodically collected for characterization. Samples were also prepared where CUR was dispersed in MCT-oil without any added protein gel particles and without employing any emulsification process (no vehicle) and also digested using similar SGF and SIF buffer. To stop the pepsin activity at specific time points, 0.2 M sodium bicarbonate was added to the samples to reach a final pH of 7.0. The pancreatin activity was stopped by adding 0.1 M of 4-(2-aminoethyl)benzenesulfonyl

fluoride hydrochloride (Pefabloc[®]) to the sample (5 mM final concentration). Experiments were performed in triplicate and mean values were calculated.

6.2.2.6 Free fatty acid release

After passing through simulated gastric and intestinal conditions, the free fatty acids (FFAs) released from the CUR-loaded emulsions were measured by using an automatic pH-stat titration unit (TIM 856 titration manager, Titralab, Radiometer analytical). Noteworthy that for doing the pH stat analysis of FFA release, this was a separate experiment where no aliquots were removed during the sequential gastrointestinal digestion. The pH-stat was used to monitor and control the pH at pH 6.8 for 3 hours. The volume of added NaOH (0.25 M) was assumed to be equal to the amount of free fatty acids generated by the lipolysis of emulsified triacylglycerols. The amount of free fatty acids released was calculated from the titration curves as described by Sarkar et al. (2016). Using a nonlinear regression model, the kinetic parameters for the initial stages of FFA release were derived as described previously (Sarkar et al., 2016; Sarkar et al., 2019) using equations (6.2) and (6.3).

$$\Phi_t = \Phi_{max} \left[1 - \exp\left(\frac{-6kMwDnt^2}{\rho_0 d_0^2 \Gamma^{max}}\right) \right] \quad (6.2)$$

where, t is the lipid digestion time in the intestine (min), Φ_{max} is the maximum total FFA level (%), k ($\text{mol s}^{-1} \text{m}^{-2}$) is the conversion rate of the lipid per unit area of the emulsion droplet surface, occurring at the maximum lipase surface coverage, Mw is the molecular weight of MCT-oil, d_0 is the initial average diameter of the emulsions (d_{32}) and ρ_0 is the density of the MCT-oil. Γ^{max} is the maximum coverage of the surface by the enzyme, D is the diffusion coefficient of the enzyme in the continuous aqueous phase and n donates the molar concentration of the lipase in SIF solution. In addition, the lipolysis half time ($t_{1/2}$) (min) *i.e.* the time required to achieve half of the maximum extent of lipid digestion was obtained from equation (6.3) (Sarkar et al., 2016; Sarkar et al., 2019):

$$t_{1/2} = \ln(2) \left(\frac{d_0 \rho_0}{6kMw} \right) \quad (6.3)$$

6.2.2.7 Bioaccessibility of CUR

The bioaccessibility of CUR in the Pickering emulsions was determined after 5 hours of sequential *in vitro* gastrointestinal digestion. The digesta obtained at the end of the sequential gastrointestinal digestion process was centrifuged at 3,000× g for 50 min at 5 °C. The middle layer was considered to be the “micellar fraction”, in which the CUR was solubilized. The concentration of CUR in the micelles was analysed using high-performance liquid chromatography (HPLC) analysis. An Agilent 1200 series HPLC instrument coupled with DAD detector was used for the analysis of CUR. The measurement wavelength was 425 nm, and the separation column was Agilent XDS-C18 (150 mm × 4.6 mm, 5 μm). The mobile phase A was 0.2% of acetic acid aqueous, and the mobile phase B was acetonitrile, with a flow rate of 1 mL/min. The gradient elution program was: 0 min, 60% of A; 4-10 min: 20% of A. The column temperature was maintained at 25 °C. The injection volume was 20 μL and an external CUR standard was used for quantitative analysis. A calibration curve was prepared with standard CUR in acetonitrile in concentrations ranging from 0.1 μM to 20.0 μM. Bioaccessibility (%) of CUR was calculated by dividing the amount of solubilized CUR in the micellar phase by the amount of CUR in the emulsion.

6.2.2.8 Microstructural characterization

6.2.2.8.1 Confocal scanning laser microscopy (CLSM).

The microstructure of the samples before and after *in vitro* digestion was imaged using a Zeiss LSM 700 CLSM (Carl Zeiss MicroImaging GmbH, Jena, Germany) confocal microscope using an oil immersion 63× lens and the pinhole diameter maintained at 1 Airy Unit to filter out majority of the light scattering. A stock solution of Fast Green (1 mg mL⁻¹ in Milli-Q water) was used to stain the protein particles to a final concentration of 0.1 mg mL⁻¹, which was excited at a wavelength of 633 nm. The emission filter was set at 660 - 710 nm. Samples were placed on a concave confocal microscope slide, secured with a glass coverslip and imaged.

6.2.2.8.2 Cryogenic-scanning electron microscopy.

Cryogenic scanning electron microscopy (cryo-SEM) of the fresh CUR-loaded emulsion samples *i.e.* CUR-E_{WPN}, CUR-DxS+E_{WPN}, and CUR-E_{WPDxM} were conducted. Cryo-SEM images were acquired using heptane as the dispersed rather than MCT oil to avoid interference by crystallization of oil during the freezing step as used in a previous studies by Destribats et al., (2014) and Araiza-Calahorra et al., (2019a). The CUR-E_{WPN}, CUR-DxS+E_{WPN}, and CUR-E_{WPDxM} were mounted on rivets attached to the sample stub. The samples were plunge-frozen in liquid nitrogen “slush” at -180 °C and

then transferred to the cryo-preparation chamber in the SEM. The frozen Pickering emulsion droplets were cleaved and then etched at $-95\text{ }^{\circ}\text{C}$ for 4 min. Next, the samples were coated with 5 nm of platinum (Pt). Finally, the Pt-coated samples were transferred to the SEM for imaging at $-135\text{ }^{\circ}\text{C}$. The heptane-based emulsion samples were imaged in a FEI Quanta 200 F ESEM with a Quorum Polar Prep 2000 cryo system.

6.2.2.9 Cell based assays

6.2.2.9.1 Cell culture.

Human colon adenocarcinoma cells, Caco-2, were cultivated in high glucose DMEM medium with pyruvate, supplemented with 10% FBS, 1% NEAA, 100 U mL^{-1} penicillin and $100\text{ }\mu\text{g mL}^{-1}$ streptomycin. Cells were grown under standard conditions at $37\text{ }^{\circ}\text{C}$ with 5% CO_2 in humidified atmosphere and medium was changed every 2 - 3 days. Cells were used for experiments within 10 in-house passages.

6.2.2.9.2 Cytotoxicity assay.

The cytotoxicity of the micellar phases of the Pickering emulsions was assessed by neutral red assay as described previously (Perez-Hernandez et al., 2020). Briefly, Caco-2 cells were seeded in 24-well plates at a density of 1×10^5 cells cm^{-2} and, upon reaching min 90% confluence, they were treated with CUR dissolved in DMSO (0.5 - 6.0 μM), micellar phase of digested CUR-encapsulated emulsion sample or micellar phase of digested emulsion sample without CUR. Medium was removed after 2.5 h and replaced by DMEM containing $40\text{ }\mu\text{g mL}^{-1}$ neutral red dye which was incubated for 2 hours. Subsequently, cells were washed with DPBS and the intracellular dye extracted by destain solution (AcOH/ H_2O /glacial acid, 50:49:1, v/v/v) for 10 -15 min. Absorbance of the neutral red dye was measured at 540 nm using a microplate reader (Tecan Spark 10M, Switzerland). Viability of the Caco-2 cells was calculated as percentage of control cells (DMEM medium only). DMSO (5%) was included as control which lowered the cell viability to 67%. Experiments were conducted over three independent passages and performed in triplicates per experiment.

6.2.2.9.3 Cellular curcumin uptake.

The cellular uptake of CUR from the micellar phase of digested CUR-encapsulated Pickering emulsions was determined using HPLC. Caco-2 cells were seeded at a density of 2×10^6 cells per 10 cm petri dish. When reaching confluence (min 90%), the cells were exposed to different micellar phase digesta containing $1\text{ }\mu\text{M}$ CUR for 2 hours under standard conditions. Subsequently, cells were washed twice

with ice-cold DPBS and lysed with methanol. The cell pellets were collected and subjected to extraction, which involved vortex (1 min), sonication (4 °C, 5 min) and centrifugation (10,000× g, 4 °C, 10 min). The supernatant was filtered through a 0.2 μm PTFE syringe and prepared for the subsequent curcumin HPLC analysis. Experiments were conducted in triplicate in subsequent cell passages.

6.2.3 Statistical analysis

Significant differences between samples were determined by one-way ANOVA and multiple comparison test and Tukey's adjustment was performed using SPSS software (IBM, SPSS statistics, version 24) and the level of confidence was 95%. Experiments were conducted at least in triplicate. Results in tables are expressed as mean ± standard deviation. Error bars in figures represent standard deviation.

6.3. Results and Discussion

6.3.1 Characteristics of curcumin Pickering emulsions

Initially, we evaluated the characteristics of the Pickering emulsion systems (CUR-E_{WPN}, CUR-DxS+E_{WPN} and CUR-E_{WPDxM}) using droplet size, size distribution, microstructure, surface morphology and electrical characteristics (ζ) before and after gastric and intestinal digestion steps. Apparent viscosity of the emulsions was also evaluated to understand how bulk properties might impact digestion behaviour. Figure 6.1 shows the surface morphology of the freshly-prepared Pickering emulsion samples with particle-laden interfaces probed using cryo-SEM. Figure 6.1a1 shows several CUR-E_{WPN} emulsion droplets homogeneously distributed throughout the micrograph with a woolly jacket of WPN attached to the droplet surface giving a raspberry-like surface appearance. At higher magnification (Figure 6.1a2), WPN seem to have an end-to-end aggregation at the droplet surface, which might be associated with nanogel merging with each other at interface. Also sample preparation process (*e.g.* freeze-fracturing) during the cryo-SEM might also result in such aggregation. Similar morphology has been also previously observed in cryo-SEM images of Pickering droplets in WPN-stabilized oil droplets without containing CUR (Araiza-Calahorra et al., 2019a). This suggested that addition of CUR had limited effects on the surface morphology of the droplets.

Pickering emulsion droplets stabilized by a more complex interface *i.e.* with WPN electrostatically-coated with DxS of 500 kDa MW were spherical with an average diameter of ~15 μm (Figure 6.1b1). Looking at the surface of such droplets at higher magnification, it can be observed that individual spherical WPN seem to be

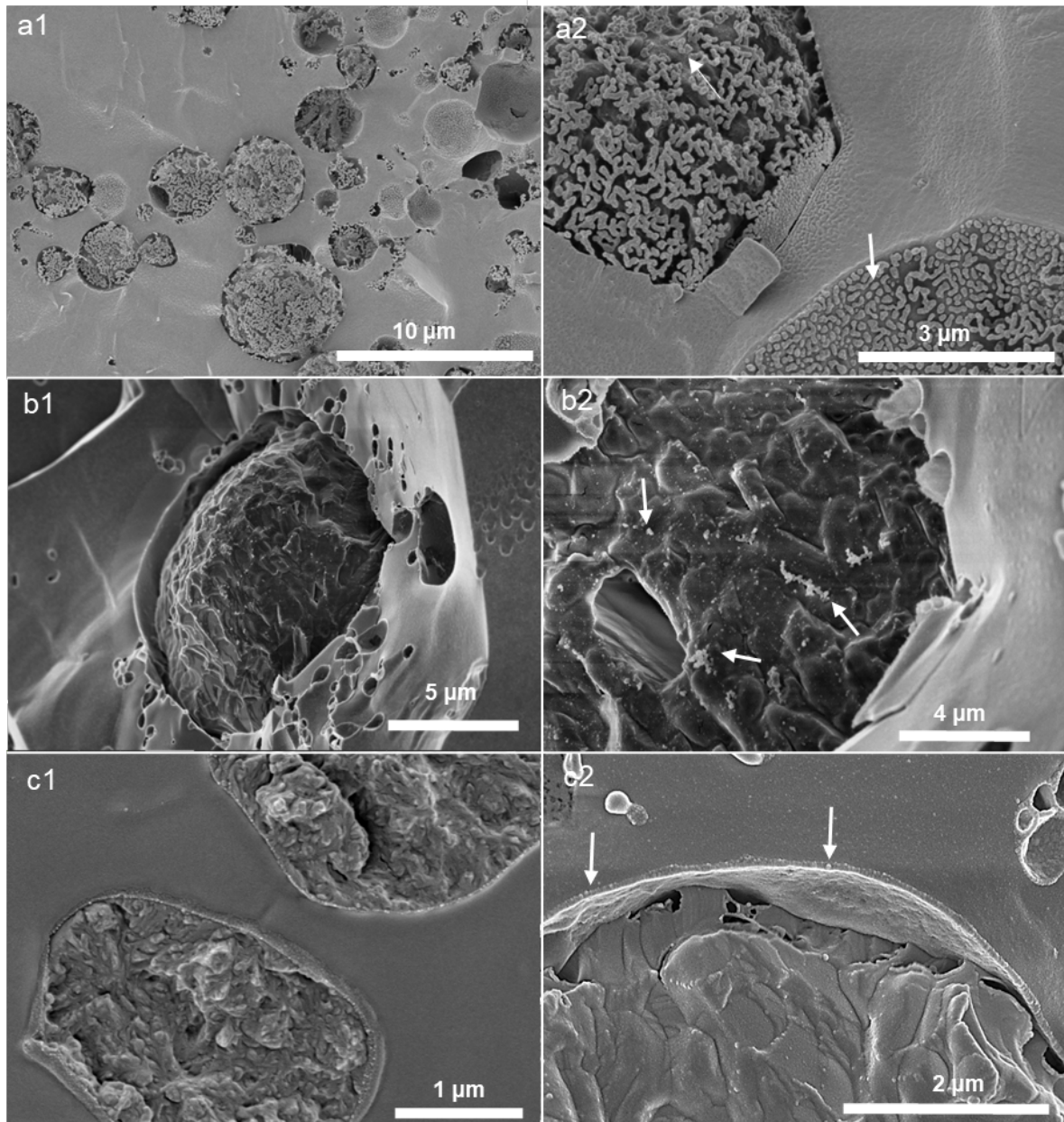


Figure 6.1. Cryo-SEM images of the three Pickering emulsions used for delivering curcumin *i.e.* a) CUR- E_{WPN} emulsion (magnification of 15,000 \times (a1), and 50,000 \times (a2), respectively), b) CUR-DxS+ E_{WPN} (magnification of 25,000 \times (b1), and 50,000 \times (b2), respectively) and c) CUR- E_{WPDxM} (magnification of 10,000 \times (c1), and 20,000 \times (c2), respectively). Arrows indicate the nanogel particle in a2, nanogel particle aggregated with dextran sulphate in b2, and conjugate microgel particles in c2.

aggregated, which can be an effect of DxS coating electrostatically attracting multiple neighbouring WPN within a thread-like network (Figure 6.1b2). The other Pickering emulsion with complex interface *i.e.* CUR- E_{WPDxM} samples showed the presence of conjugated microgel particles formed a thin surface layer adopting a more discrete configuration of individual microgel particles (Figures 6.1c1 and c2).

The droplet size distribution and mean diameters with representative confocal images of the three freshly-prepared Pickering emulsion systems are shown in Table 6.1 and Figure 6.2. The initial droplet size distribution of the three emulsions, CUR- E_{WPN} , CUR-DxS+ E_{WPN} and CUR- E_{WPDxM} presented bimodal distributions where the peak in the area of 0.1 - 1 μm in all systems corresponds to unadsorbed particles in line with the systems previously studied without loaded CUR (Araiza-Calahorra et al., 2019a, 2019b) and small emulsion droplets, while the peak in the area of 1 - 100 μm corresponds to the bigger emulsion droplets (Figure 6.2). The CUR- E_{WPN} presented oil droplet ranging in size from 1 to 50 μm and an average droplet diameter (d_{43}) of 14.93 μm (Table 6.1), whereas CUR-DxS+ E_{WPN} system presented oil droplets ranging in size from 3 to 100 μm and an average droplet diameter (d_{43}) of 54.56 μm (Table 6.1). This can be expected as the electrostatic coating with DxS resulted in droplet flocculation with DxS not only binding to individual droplets but also connecting two or more adjacent droplets as can be clearly observed as flocs in the confocal images (Figure 6.2). On the other hand, the conjugated microgel-laden system *i.e.* CUR- E_{WPDxM} presented a d_{43} of 7.9 μm (Table 6.1). From the confocal images in Figure 6.2, it is noticeable that all three systems had proteinaceous particles (stained in green) adsorbed at the interface acting as a barrier against oil droplet coalescence.

Table 6.1. Mean droplet size and ζ -potential of initial emulsions.

Emulsions	$d_{43} / \mu\text{m}$	ζ -potential / mV
CUR- E_{WPN}	14.93 \pm 3.3	-26.9 \pm 0.5
CUR-DxS+ E_{WPN}	54.56 \pm 6.1	-32.33 \pm 4.8*
CUR- E_{WPDxM}	7.9 \pm 0.2	-15.36 \pm 1.1

*Note that the initial emulsion CUR-DxS+ E_{WPN} was at pH 3.0 to allow electrostatic attraction between WPN and DxS, unlike the other two emulsions, which were at pH 7.0.

All the Pickering emulsions studied were negatively-charged (Table 6.1). CUR- E_{WPN} presented a high negative charge because the initial pH of the emulsions was appreciably above the isoelectric point (pI) of the whey protein isolate ($pI \sim 5.2$), whereas the decreased magnitude of negative charge for CUR- E_{WPDxM} , as compared to CUR- E_{WPN} may be attributed to the covalently attachment of the neutral dextran molecule (Araiza-Calahorra et al., 2020). For CUR-DxS+ E_{WPN} , the initial pH of the solution was at pH 3.0 to allowed electrostatic deposition of the dextran sulphate to the WPN-stabilized interface (Table 6.1). Hence, the negative charge of the droplets

suggested that the negatively charge biopolymer was successfully adsorbed onto the cationic WPN-stabilized oil droplets at pH 3.0 (Araiza-Calahorra and Sarkar 2019).

Figure 6.3 shows the apparent viscosity (η_a) versus shear rate of the initial emulsions before *in vitro* digestion. The apparent viscosity decreased as the shear rate increased for the emulsion samples with complex interfaces and the shear-sweep

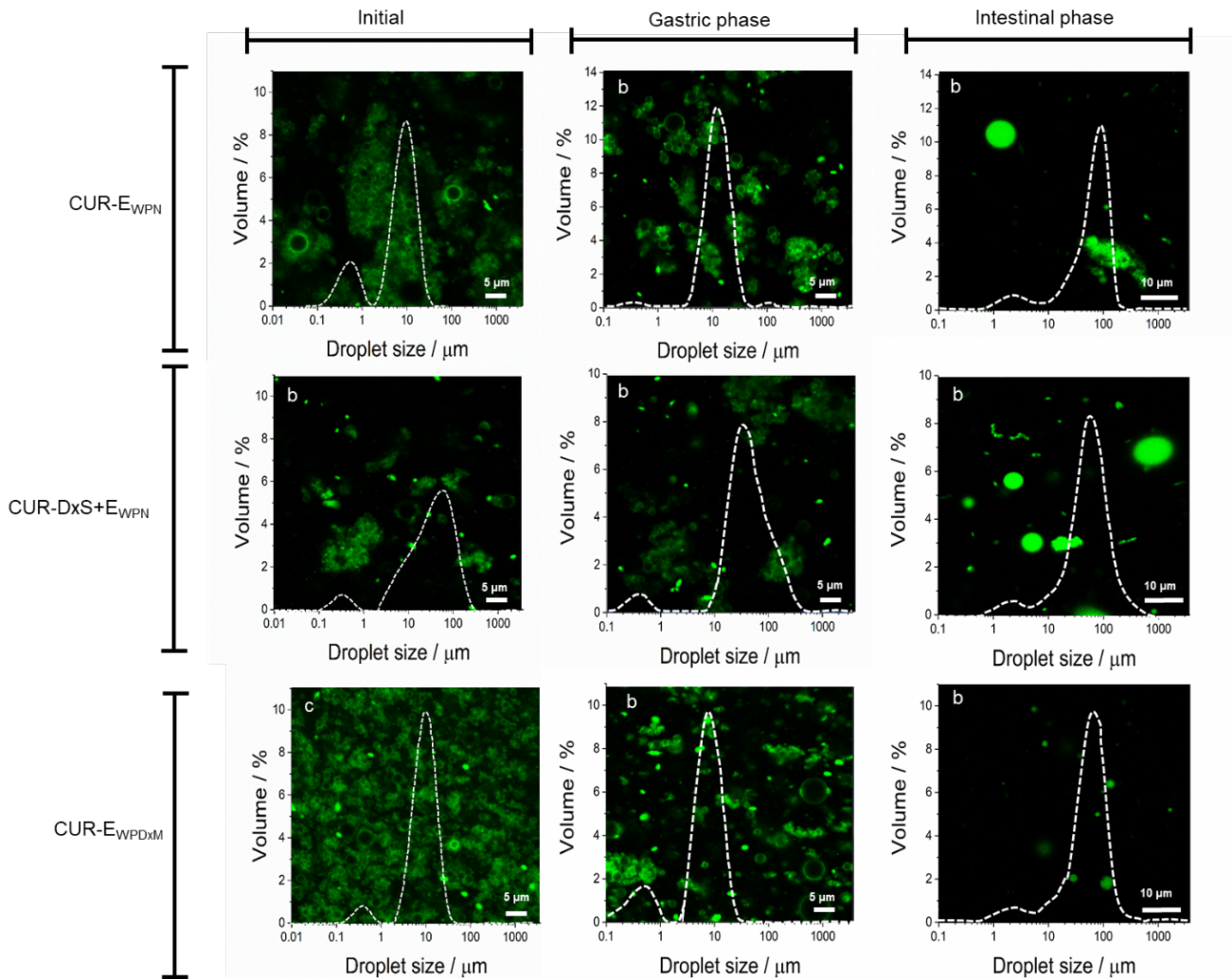


Figure 6.2. Confocal images with superimposed droplet size distribution of the freshly-prepared Pickering emulsions *i.e.* CUR- E_{WPN} , CUR-DxS+ E_{WPN} and CUR- E_{WPDxM} and after their exposure to 120 min of *in vitro* gastric or 180 min of *in vitro* sequential gastrointestinal digestion conditions.

data were satisfactorily fitted to the Ostwald de Waele model (R^2 ranging from 0.993 - 0.997). In other words, CUR-DxS+ E_{WPN} and CUR- E_{WPDxM} showed shear thinning behaviour, with flow behaviour index (η) ranging from 0.43-0.49, whilst CUR- E_{WPN} emulsions showed a Newtonian behaviour.

Additionally, the magnitude of η_a was orders of magnitude higher at shear rate ranging from 1 to 100 s^{-1} for CUR-DxS+E_{WPN} and CUR-E_{WPDxM} samples as compared to CUR-E_{WPN}, which suggested that the η_a increased with the addition of dextran by either conjugation or electrostatic complexation approaches. For CUR-DxS+E_{WPN}, the presence of unbound high MW DxS (500 kDa) remaining in the continuous phase might have increased the η_a of the emulsions. Also, the inter-droplet flocculation as observed in the confocal micrograph of CUR-DxS+E_{WPN} (Figure 6.2) might have contributed to higher viscosity and eventual thinning when the flocs were broken down into individual droplets as a function of increasing shear rate to allow subsequent flow. Even for CUR-E_{WPDxM}, the inter-droplet flocculation shown in Figure 6.2 appeared to be the most plausible reason for such high shear thinning behaviour where droplets aggregated owing to limited repulsive interactions (see ζ -potential values in Table 6.1). In summary, the η_a obtained for the systems containing dextran were not significantly different, while the η_a of CUR-E_{WPN} was significantly lower irrespective of the shear rates, which might play an important role in degree of FFA release during the gastrointestinal conditions and consequently bioaccessibility and cellular uptake of CUR.

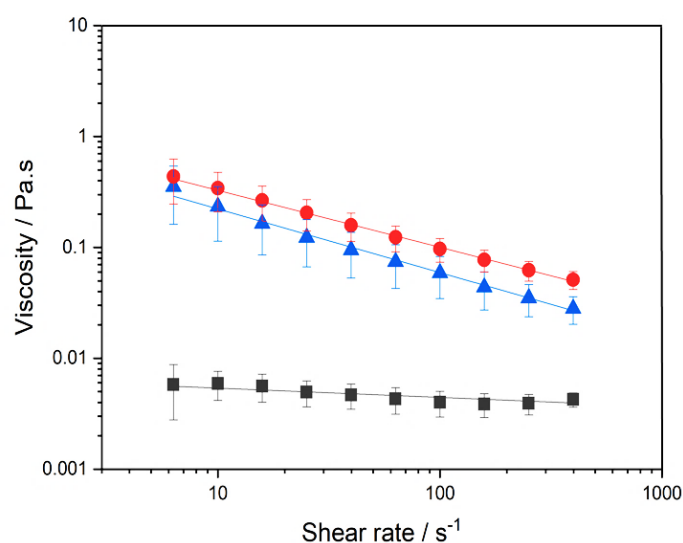


Figure 6.3. Flow curves of freshly prepared Pickering emulsions *i.e.* CUR-E_{WPN} (black squares) CUR-DxS+E_{WPN} (blue triangles) and CUR-E_{WPDxM} (red circles) at 37 °C. Data points represent the average of at least three measurements on triplicate sample. Error bars indicate the standard deviations. Solid lines are the best fits to the experimental data predicted using the Ostwald de Waele model (Equation 6.1).

6.3.2 Characteristics of CUR-loaded Pickering emulsions during *in vitro* gastrointestinal digestion

The kinetic stability and responsiveness of the three Pickering emulsions was accessed at gastric conditions without pepsin (*i.e.* SGF without pepsin, 37 °C) (see time 0 min in Fig. 4). Droplet size distribution did not change and consequently d_{43} of the systems remained similar to those of the freshly prepared samples (d_{43} 15.75, 59.6 and 7.60 μm for CUR- E_{WPN} , CUR-DxS- E_{WPN} and CUR- E_{WPM} , respectively) (Table 6.1), confirming there was no SGF-induced effects when no pepsin was employed. This phenomenon of stable emulsions after addition of gastric buffer (SGF) without pepsin was supported by the ζ -potential measurements where both CUR- E_{WPN} and CUR- E_{WPDxM} presented a charge reversal from negative to positive due to the protonation of the ionisable groups as they move from above to below the isoelectric point (Figure 6.4b). Interestingly, there were no significant differences in the ζ -potential of CUR-DxS+ E_{WPN} after addition of gastric buffer ($p > 0.05$).

After being exposed to 120 minutes of *in vitro* gastric digestion stage in the presence of pepsin, d_{43} values significantly decreased ($p > 0.05$) for CUR-DxS+ E_{WPN} from 59.6 μm to 52.75 μm , (Figure 6.4a), which explains the slight shift to smaller values observed in the droplet distribution with the breakdown of the droplet flocs (Figure 6.2). For CUR- E_{WPN} , the droplet size distribution evidenced some coalescence phenomena, which is clearly shown by a rise in a third peak in the range of 100-1000 μm size range (Figure 6.2), whereas the d_{43} and droplet size distribution remained unchanged for CUR- E_{WPDxM} . This behaviour in CUR- E_{WPN} might be related to the peptic hydrolysis of the proteinaceous nanogel particles at the surface of the emulsion droplets, which might have caused some coalescence of the droplets, whereas CUR- E_{WPDxM} presented good physical stability after the gastric stage. The complex interfaces were indeed successful in providing gastric stability to the droplets. Such desirable results in case of CUR-DxS+ E_{WPN} and CUR- E_{WPDxM} might be attributed to the polysaccharide coating/conjugation, which restricted the access of pepsin to potential cleavage sites of the protein (Araiza-Calahorra et al., 2020; Araiza-Calahorra et al., 2019). On the other hand, the high bulk viscosity of the CUR-DxS+ E_{WPN} and CUR- E_{WPDxM} (Figure 6.3) may have also hindered the diffusion of pepsin to the proteinaceous sides of the particle (Sarkar et al., 2017).

Upon subjecting the emulsions to gastric conditions with pepsin, the ζ -potential became less positive for all the samples, with CUR- E_{WPN} presenting significant differences from +31.7 to +16.1 mV after 120 minutes of gastric digestion (Figure 6.4b). This reduction in the absolute magnitude of ζ -potential after *in vitro* gastric conditions further supported the pepsin-induced hydrolysis of WPN particles when

absorbed at the E_{WPN} interface. However, such changes were not seen in the emulsions stabilized by complex interfaces supporting the confocal images and size distribution data (Figure 6.2), highlighting the kinetic stability of these emulsions with complex interfaces to droplet coalescence in the gastric conditions.

Under small intestinal conditions, all samples studied exhibited a significant increase in the d_{43} ranging between 60.25 and 69.25 μm corresponding to droplet coalescence irrespective of the initial interfacial material (Figure 6.2 and 6.4c). From the microscopic analysis, it became clear that the larger droplets measured by laser diffraction corresponded to the coalesced oil droplets of similar size after 180 minutes of intestinal conditions (Figure 6.2). Also, noteworthy that considerable amount of such coalesced oil droplets might have not been captured during confocal imaging due to migration of the oil to the top of the microscopic slide caused by the density gradient, which might explain why the images in the intestinal phase showed such lower number of droplets and largely empty regions, irrespective of the interfacial material.

Such increase of droplet diameter (Figure 6.4c) was more likely caused by digestion of lipids and proteins by pancreatic lipase and trypsin, respectively. In the intestinal phase, the particles at the droplet surface were most likely hydrolysed by trypsin creating peptide residues or particle fragments at the interface, thus making them incapable of providing coalescence stability can be expected in case of 'enzyme-responsive' particle-laden interfaces (Sarkar et al., 2019). Particularly, one might expect CUR-DxS+ E_{WPN} to behave similar to E_{WPN} because at intestinal pH (pH 6.8), both DxS and WPN are negatively-charged hindering any electrostatic attraction of the DxS to the WPN-coated surface and hence this particular complex interface *i.e.* the WPN+DxS did not even exist at near alkaline pH. To our surprise, even CUR- E_{WPDxM} behaved similarly to E_{WPN} highlighting that trypsin was somehow more capable of hydrolysing the proteinaceous parts of the conjugated microgel particles as compared to pepsin (Figure 6.2). Also, the dilution occurring in the emulsions by addition of SGF and SIF might have reduced any anticipated viscosity-induced benefits in these emulsions with complex interfaces (Figure 6.3). Finally, the lipid digestion products such as free fatty acids (FFAs), monoglycerides and diglycerides were also not capable of forming viscoelastic films to provide stability to the droplets against coalescence (Salvia-Trujillo et al., 2013b; Sarkar et al., 2019; Singh and Sarkar 2011; Torres et al., 2019). The electrical charges on the emulsion samples after intestinal phase significantly decreased for all samples indirectly highlighting the presence of lipid digestion products such as mono- and/or di-glycerides and FFA at the droplet surface (Figure 6.4d). In summary, CUR-DxS+ E_{WPN} and CUR- E_{WPDxM} systems were more stable under gastric conditions, however, with the addition of the intestinal

components (*i.e.* pancreatin, bile salts, CaCl_2), all the Pickering systems behaved similarly irrespective of the initial interfacial material.

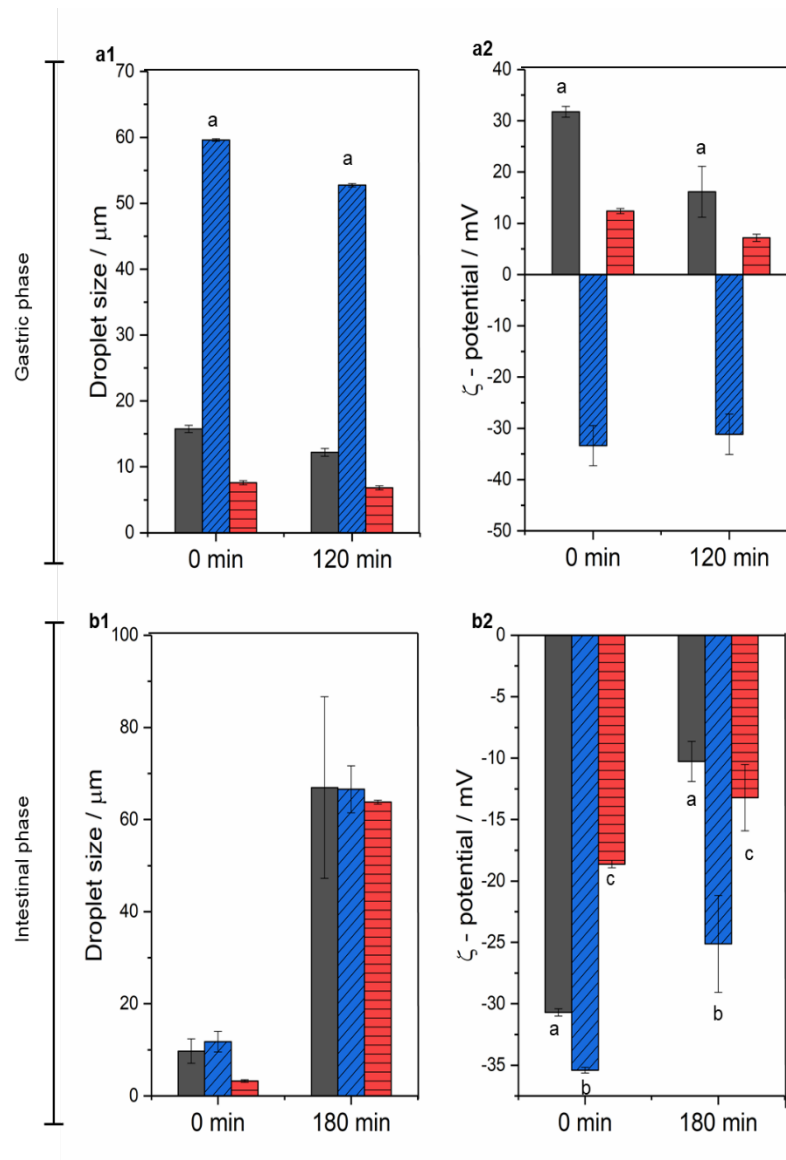


Figure 6.4. Average droplet diameter (d_{43}) (1) and ζ -potential value (2) of CUR-E_{WPN} (black bars) CUR-DxS+E_{WPN} (blue bars with diagonal lines) and CUR-E_{WPDxM} (red bars with horizontal lines) after *in vitro* gastric digestion (a) and *in vitro* intestinal digestion (b). 0 min in each case indicates the behaviour of the emulsions in presence of SGF (a) and SIF (b) buffer without any added enzymes. Error bars represent the standard deviations. (For interpretation of the references to colour in this figure legend, the reader is referred to the Web version of this article).

6.3.3 Influence of emulsion type on lipid digestion kinetics

It was important to understand whether such gastric stability has any influence on the rate and degree of %FFA release as the latter is known to be related to the droplet size. All emulsions presented a steep increase in the amount of %FFA released within the first 5 minutes after exposure to neutral pH (pH 6.8), ions, bile salts and pancreatin. It was followed by a more gradual increase at longer times, until a relatively constant final value of %FFA was reached (Figure 6.5a). Using equations 6.2 and 6.3, the time required for completion of 50% digestion ($t_{1/2}$), and the digestion rate (k) were calculated (inset table in Figure 6.5a). Interestingly, there was no significant difference between emulsion samples in terms of the rate (k) and extent (Φ_{max}) of %FFA release ($p > 0.05$). This supports the droplet size results, where no significant difference on the final d_{43} between samples was observed in the intestinal stage, suggesting that the addition of dextran either by complexation or conjugation approaches had no influence on the lipolysis rate and extent of the Pickering emulsions. However, the time required for 50% of digestion ($t_{1/2}$) was slight but significantly different between samples ($p < 0.05$). Similar results were reported on employment of dietary fibres on the digestion rate of emulsified lipids. A slight decrease in lipolysis rate with increasing concentrations of polysaccharides (chitosan, pectin or methylcellulose) was attributed to the interaction of the polysaccharides with digestion metabolites, such as bile salts, lipases, etc. (Espinal-Ruiz et al., 2014). Lipolysis of Pickering emulsions stabilized by lactoferrin nanoparticles electrostatically coated with iota-carrageenan rendered elevated rate and extent of lipolysis, whereas the use of alginate as a secondary coating significantly reduced both the aforementioned parameters (Meshulam and Lesmes, 2014). Changes in the emulsion lipolysis dynamics was explained by the physical changes in emulsion properties such as droplet size, and organization state (e.g. aggregation versus coalescence) due to the addition of the dietary fibre.

These results suggest that both, electrostatically or covalently attached dextran were able to control the initial rate of lipid digestion within a simulated in vitro system validating the hypothesis. However, the encapsulated lipid irrespective of the interfacial material were digested and released to the same extent.

6.3.4 Influence of emulsion type on CUR bioaccessibility

CUR bioaccessibility of the three CUR-loaded Pickering emulsions as well the non-emulsified MCT-oil are shown in Figure 6.5b. It was found that curcumin bioaccessibility was 46.67 ± 4.19 , 78.18 ± 7.97 , 81.22 ± 4.38 and $88.42 \pm 4.77\%$ for CUR in non-emulsified MCT-oil, CUR-E_{WPN}, CUR-DxS+E_{WPN} and CUR-E_{WPDxM},

respectively. This suggests that CUR bioaccessibility increased when CUR was delivered in Pickering emulsion format in comparison to the non-emulsified bulk system. Between Pickering samples, the conjugation with Dx or the electrostatic deposition of DxS had no significant benefit over the WPN-stabilized emulsions ($p > 0.05$) on the bioaccessibility of CUR, which is in agreement with the FFA release results showing no significant difference ($p > 0.05$) (Figure 6.5a). In addition, the *in vitro* bioaccessibility correlated positively with the total amount of FFAs produced at the end of the lipid digestion process of the three emulsion systems (Pearson correlation coefficient 0.981, $p = 0.0182$).

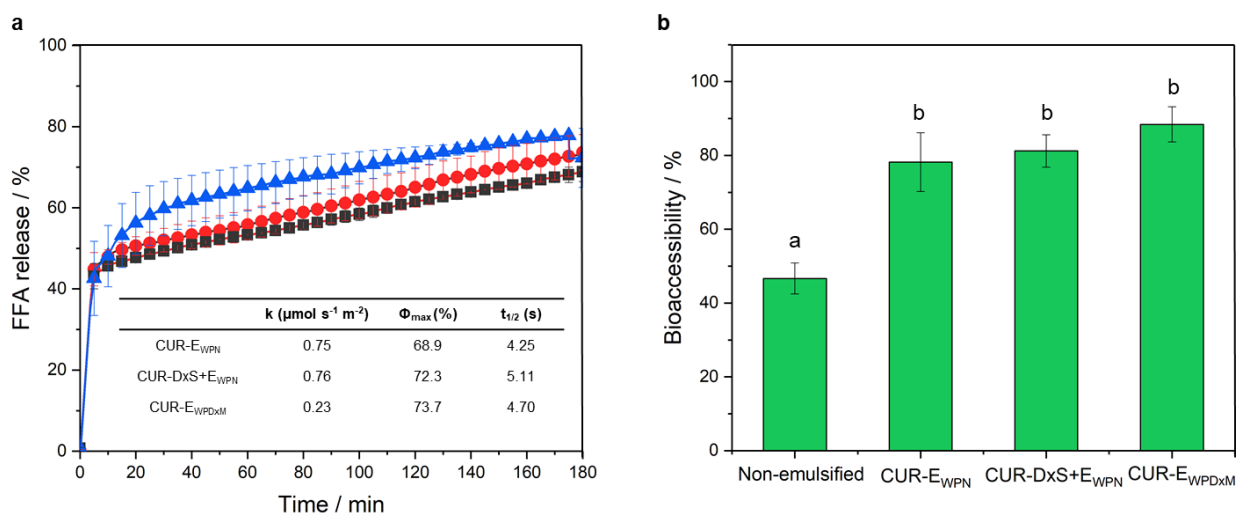


Figure 6.5. Percentage of free fatty acid (% FFA) released (a) from CUR-E_{WPN} (black squares), CUR-DxS+E_{WPN} (blue triangles) and CUR-E_{WPDxM} (red circles) with insets representing maximum FFA release (Φ_{max} , %), lipolysis rate constant (k , $\mu\text{mol s}^{-1} \text{m}^{-2}$) and the time to achieve 50% digestion ($t_{1/2}$, s), and bioaccessibility (b) of CUR after *in vitro* gastrointestinal digestion from the micellar phase of the aforementioned emulsions. The solid lines connecting the data points in the %FFA curves (a) are the best fits to the experimental data predicted using the mathematical model (Equation (6.2)). Data presented are mean with standard deviation of three independent experiments. Different letters indicate significant differences. (For interpretation of the references to colour in this figure legend, the reader is referred to the Web version of this article).

The lack of differences in the bioaccessibility (Figure 6.5b) among the different delivery systems can be attributed to the fact that all of the emulsion systems had similar droplet characteristics (Figures 6.2 and 6.4) and consequently similar %FFA release (Figure 6.5a) after the small intestinal digestion phase. In contrast, CUR in bulk MCT-oil (*i.e.* non-emulsified sample) presented significantly lower bioaccessibility under simulated intestinal conditions ($p < 0.05$) as compared to those of the emulsion counterparts (Figure 6.5b). This result suggests that there was a more efficient transfer of CUR into the mixed micelles when incorporated into a Pickering emulsion-based

delivery vehicle. The reduced surface area of the bulk oil prevented efficient access to the triglyceride to the lipase. Thus, the CUR remained dissolved within this oil phase and was not extracted effectively into the micellar phase reducing the bioaccessibility (Salvia-Trujillo et al., 2013a).

Previous studies on Pickering emulsions for CUR delivery have reported a bioaccessibility of 8.8% for kafirin-, 21% and 53% for chitosan tripolyphosphate- in medium and long chain triglyceride, respectively, and 25.3% and 80.8% in modified and un-modified kaolite nanoparticle-stabilized Pickering emulsions (Shah et al., 2016b; Tang et al., 2019; Xiao et al., 2015). This confirms an improved effect of the Pickering emulsion systems designed in this study on the bioaccessibility of CUR over previous studies and thus support the hypothesis that effective particle design and Pickering emulsion formation can enhance the total amount of CUR that can be made available into the micellar phase after digestion. Interestingly, there were no clear relationship between improved gastric stability of the emulsions and bioaccessibility of CUR. In other words, gastric-stable emulsions with complex interfaces (CUR-DxS+E_{WPN}, CUR-E_{WPDxM}) were not advantageous over the simple nanogel-particles (CUR-E_{WPN}) in terms of bioaccessibility.

6.3.5 Cell viability and uptake in presence of CUR

Next, we aimed to understand whether the increased gastric stability of the emulsions designed with complex interfaces had any impact on viability of Caco-2 cells and benefit in terms of cellular CUR uptake. From Figures 6.6a, it can be observed that CUR-encapsulated Pickering emulsion formulations, as well as CUR concentration had a significant effect on cell viability of Caco-2 cells. It has been previously reported that incubation of bile acids with Caco-2 cells reversibly decreases the molecular diffusion across the intestinal epithelium (Münch et al., 2007; Raimondi et al., 2008). Hence, a control experiment was conducted to evaluate toxicity of bile salts in the *in vitro* digestion medium (*i.e.* SGF + SIF) (Appendix D, Figure D1). In addition, CUR in non-emulsified MCT-oil (Figure 6.6a) and digested Pickering emulsions without added CUR (blank) were also investigated as controls (Figure 6.6a). Digested blank-Pickering emulsions without CUR exhibited some cytotoxicity to the cells in E_{WPN} and E_{WPDxM} systems with cell viability below 80% at an equivalent CUR concentration of 0.50 μ M (Figure 6.6a). This might be attributed to the gradual decrease in cell viability with increasing bile salt concentration (Appendix D, Figure D1) which suggests that possibly the digestion medium (SGF and SIF) resulted in some degree of cytotoxicity, which might be attributed to bile salt-mediated disruption

of lipidic cell membranes *via* its surfactant-like activity and consequently necrosis and cellular injury (Perez and Briz, 2009).

In Figure 6.6a, it is shown that more than 80% cell viability was retained for all Pickering emulsion systems from 0.5 to 2 μM CUR concentration after 2 hours of incubation but was below 80% for the non-emulsified sample at 2 μM . With increasing CUR concentration to 4 and 6 μM , the viability of Caco-2 cells decreased to below 80%, especially for the non-emulsified and CUR- E_{WPN} , which clearly suggests that CUR-DxS+ E_{WPN} and CUR- E_{WPDxM} were significantly less toxic at higher CUR concentrations (4 and 6 μM) as compared to non-emulsified CUR dissolved in MCT oil. In other words, Pickering emulsion systems with complex interfaces were more effective in reducing digestion-medium associated alteration of the encapsulated CUR and consequently toxicity to the Caco-2 cells. Given the effects of CUR on cell viability, a concentration of 1 μM was used for the cell uptake study.

As shown in Figure 6.6b, the use of biopolymer by complexation significantly increased the cellular uptake from $6.3 \pm 1.09\%$ for CUR- E_{WPN} to $7.6 \pm 1.66\%$ for CUR-DxS+ E_{WPN} , whereas conjugation did not increase the cellular uptake ($7.36 \pm 1.34\%$ for CUR- E_{WPDxM}) significantly. Previous literature that have assessed the cellular uptake

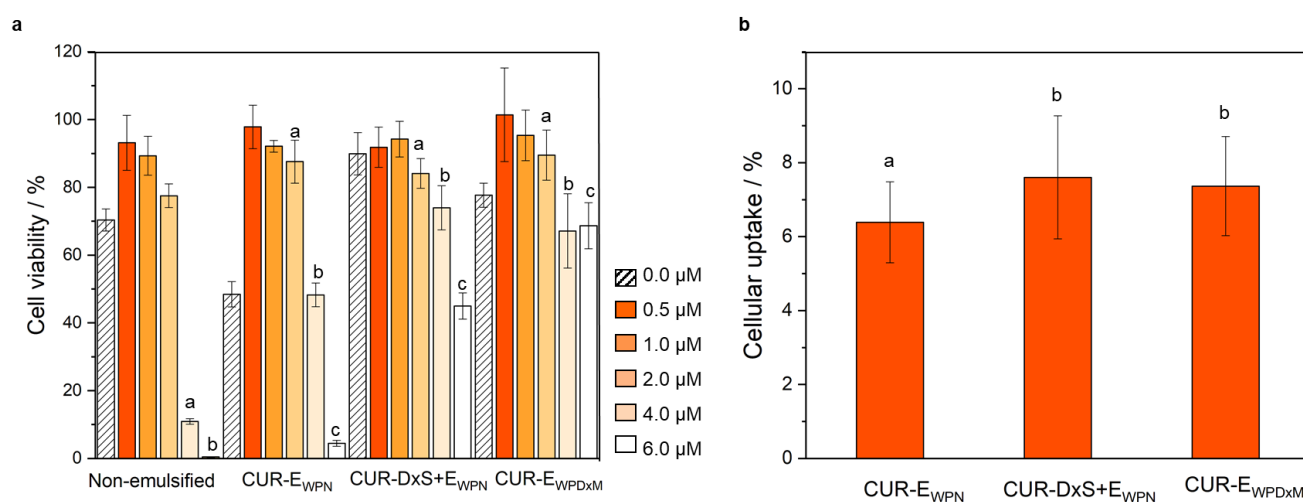


Figure 6.6. Cell viability (a) of MCT-dissolved CUR (non-emulsified) systems and the three Pickering emulsion-based delivery vehicles (CUR- E_{WPN} , CUR-DxS+ E_{WPN} and CUR- E_{WPDxM}) at different concentrations of CUR against Caco-2 cells incubated for 2 h along with the digested blank emulsion without any curcumin (blank bars with diagonal lines), and cellular uptake (b) of CUR by the Caco-2 cells in the three Pickering emulsion-based delivery vehicles. Data presented are mean with standard deviation of three independent experiments. Different letters indicate mean significant differences between CUR concentrations (0.5 μM – 6.0 μM) for cell viability, and significant differences between emulsion types (CUR- E_{WPN} , CUR-DxS+ E_{WPN} and CUR- E_{WPDxM}) for cellular uptake.

of CUR in Caco-2 cells after *in vitro* digestion, have reported an increased cellular uptake from 4.44 ± 0.11 to $10.5 \pm 0.15\%$ when using whey protein isolate and whey protein isolate-coated with chitosan nanoemulsions, respectively (Silva et al., 2019). Other studies have recently demonstrated intracellular uptake in Caco-2 cells of CUR encapsulated in different nanocarriers such as polymer micelles, nanoemulsion and liposome (Yan et al., 2019). The maximum cellular uptake reported for these systems at a CUR concentration of $100 \mu\text{M}$ was 3.67 ± 0.10 , 5.55 ± 0.13 , 3.36 ± 0.51 and $6.46 \pm 0.18\%$ for free CUR, polymer micelles, liposomes and nanoemulsions, respectively. In this study by Yan et al. (2019), the increased uptake was attributed to the positively-charged multilayer nanoemulsion, which was hypothesized to be more effectively internalized into the Caco-2 cells.

Our results clearly suggest that the cellular uptake for CUR encapsulated in Pickering emulsions was significantly increased as compared to free CUR, polymer micelles, liposomes and nanoemulsions reported in previous studies, and that DxS-coated nanogel-stabilized or Dx-conjugated microgel-stabilized Pickering emulsions (7.4 - 7.6% uptake) were more effective vehicles to deliver CUR to Caco-2 cells. This might be explained by an increase in colonic mucosal permeability caused by dextran (Kitajima et al., 1999). In addition, it is worth reminding that both these emulsions with complex interfaces were gastric stable and offered increased cell viability. Therefore, at this stage, we hypothesize that reduced physiological degradation of CUR in the gastric phase (Kharat et al., 2017, Tønnesen and Karlsen, 1985, Wang et al., 1997) obtained by gastric-stable emulsions using complex particle-biopolymer interfaces, can be a potential mechanism contributing to the reduced cellular toxicity at an increased concentration of CUR and enhanced cellular internalization of CUR, however, the exact mechanism needs further investigation in the future.

6.4 Conclusions

The purpose of this study was to evaluate Pickering emulsion systems with complex interfaces for delivery, bioaccessibility and cellular uptake of curcumin after *in vitro* simulated gastric and small intestinal digestion phase. Results show that all curcumin-loaded Pickering emulsions systems can increase the bioaccessibility of curcumin as compared to non-emulsified curcumin dissolved in bulk oil. Also, curcumin-loaded Pickering emulsions were significantly less toxic at higher curcumin concentrations as compared to non-emulsified curcumin dissolved in bulk oil, indicating the importance of delivering curcumin using a delivery vehicle. Cellular uptake results showed that Pickering emulsions with complex interfaces which provided kinetic stability to coalescence in the gastric conditions can enhance the

cellular uptake of curcumin in Caco-2 cells. This study suggests that the development of Pickering emulsions with suitable interfacial engineering can be used as effective templates to increase bioaccessibility and cellular uptake of curcumin. Further studies are needed to clearly understand the mechanism behind better cellular internalization of curcumin in the Pickering emulsions designed with complex interfaces and whether or not gastric stability has a direct correlation with cell viability.

6.7 References

- Amani, S., Mohamadnia, Z., & Mahdavi, A. (2019). pH-responsive hybrid magnetic polyelectrolyte complex based on alginate/BSA as efficient nanocarrier for curcumin encapsulation and delivery. *International Journal of Biological Macromolecules*, 141, pp. 1258-1270.
- Anand, P., Kunnumakkara, A. B., Newman, R. A., & Aggarwal, B., B. (2007). Bioavailability of Curcumin: Problems and Promises. *Molecular Pharmaceutics*, 4(6), pp. 807-818.
- Araiza-Calahorra, A., Akhtar, M., & Sarkar, A. (2018). Recent advances in emulsion-based delivery approaches for curcumin: From encapsulation to bioaccessibility. *Trends in Food Science & Technology*, 71, pp. 155-169.
- Araiza-Calahorra, A., Glover, Z. J., Akhtar, M., & Sarkar, A. (2020). Conjugate microgel-stabilized Pickering emulsions: Role in delaying gastric digestion. *Food Hydrocolloids*, 105, pp. 105794.
- Araiza-Calahorra, A., & Sarkar, A. (2019a). Pickering emulsion stabilized by protein nanogel particles for delivery of curcumin: Effects of pH and ionic strength on curcumin retention. *Food Structure*, 21, pp. 100113.
- Araiza-Calahorra, A., & Sarkar, A. (2019b). Designing biopolymer-coated Pickering emulsions to modulate *in vitro* gastric digestion: a static model study. *Food & Function*, 10(9), pp. 5498-5509.
- Asabuwa Ngwabebhoh, F., Ilkar Erdagi, S., & Yildiz, U. (2018). Pickering emulsions stabilized nanocellulosic-based nanoparticles for coumarin and curcumin nanoencapsulations: *In vitro* release, anticancer and antimicrobial activities. *Carbohydrate Polymers*, 201, pp. 317-328.
- Destribats, M., Rouvet, M., Gehin-Delval, C., Schmitt, C., & Binks, B. P. (2014). Emulsions stabilised by whey protein microgel particles: towards food-grade Pickering emulsions. *Soft Matter*, 10(36), pp. 6941-6954.

- Dickinson, E. (2012). Use of nanoparticles and microparticles in the formation and stabilization of food emulsions. *Trends in Food Science & Technology*, 24(1), pp. 4-12.
- Espinal-Ruiz, M., Parada-Alfonso, F., Restrepo-Sánchez, L. P., Narváez-Cuenca, C. E., & McClements, D. J. (2014). Impact of dietary fibres [methyl cellulose, chitosan, and pectin] on digestion of lipids under simulated gastrointestinal conditions. *Food & Function*, 5(12), pp. 3083-3095.
- Goel, A., Kunnumakkara, A. B., & Aggarwal, B. B. (2008). Curcumin as “Curecumin”: From kitchen to clinic. *Biochemical Pharmacology*, 75(4), pp. 787-809.
- Kharat, M., & McClements, D. J. (2019). Recent advances in colloidal delivery systems for nutraceuticals: A case study – Delivery by Design of curcumin. *Journal of Colloid and Interface Science*, 557, pp. 506-518.
- Kharat, M., Du, Z., Zhang, G., McClements, D.J., 2017. Physical and chemical stability of curcumin in aqueous solutions and emulsions: impact of pH, temperature, and molecular environment. *J. Agric. Food Chem.* 65 (8), 1525–1532.
- Kitajima, S., Takuma, S., & Morimoto, M. (1999). Changes in Colonic Mucosal Permeability in Mouse Colitis Induced with Dextran Sulfate Sodium. *Experimental Animals*, 48(3), pp. 137-143.
- Kolter, M., Wittmann, M., Köll-Weber, M., & Süß, R. (2019). The suitability of liposomes for the delivery of hydrophobic drugs – A case study with curcumin. *European Journal of Pharmaceutics and Biopharmaceutics*, 140, pp. 20-28.
- Lu, X., Li, C., & Huang, Q. (2019). Combining *in vitro* digestion model with cell culture model: Assessment of encapsulation and delivery of curcumin in milled starch particle stabilized Pickering emulsions. *International Journal of Biological Macromolecules*, 139, pp. 917-924.
- Marefati, A., Bertrand, M., Sjöö, M., Dejmek, P., & Rayner, M. (2017). Storage and digestion stability of encapsulated curcumin in emulsions based on starch granule Pickering stabilization. *Food Hydrocolloids*, 63, pp. 309-320.
- Meshulam, D., Lesmes, U., 2014. Responsiveness of emulsions stabilized by lactoferrin nano-particles to simulated intestinal conditions. *Food Funct.* 5 (1), 65–73.
- Minekus, M., Alming, M., Alvito, P., Ballance, S., Bohn, T., Bourlieu, C., Carrière, F., Boutrou, R., Corredig, M., Dupont, D., Dufour, C., Egger, L., Golding, M., Karakaya, S., Kirkhus, B., Le Feunteun, S., Lesmes, U., Macierzanka, A., Mackie, A., Marze, S., McClements, D. J., Ménard, O., Recio, I., Santos, C. N., Singh, R. P., Vegarud, G. E., Wickham, M. S. J., Weitschies, W., & Brodkorb, A. (2014). A standardised static *in*

in vitro digestion method suitable for food – an international consensus. *Food & Function*, 5(6), pp. 1113-1124.

Münch, A., Ström, M., & Söderholm, J. D. (2007). Dihydroxy bile acids increase mucosal permeability and bacterial uptake in human colon biopsies. *Scandinavian Journal of Gastroenterology*, 42(10), pp. 1167-1174.

Perez-Hernandez, L. M., Nugraheni, K., Benohoud, M., Sun, W., Hernández-Álvarez, A. J., Morgan, M. R. A., Boesch, C., & Orfila, C. (2020). Starch Digestion Enhances Bioaccessibility of Anti-Inflammatory Polyphenols from Borlotti Beans (*Phaseolus vulgaris*). *Nutrients*, 12(295).

Perez, M. J., ., & Briz, O. (2009). Bile-acid-induced cell injury and protection. *World journal of gastroenterology*, 15(14), pp. 1677-1689.

Raimondi, F., Santoro, P., Barone, M. V., Pappacoda, S., Barretta, M. L., Nanayakkara, M., Apicella, C., Capasso, L., & Paludetto, R. (2008). Bile acids modulate tight junction structure and barrier function of Caco-2 monolayers via EGFR activation. 294(4), pp. G906-G913.

Rayner, M., Sjöo, M., Tingren, A., Dejmek, P., 2012. Quinoa starch granules as stabilizing particles for production of Pickering emulsions. *Faraday Discuss* 158, 139–155.

Ruiz-Rodriguez, P. E., Meshulam, D., & Lesmes, U. (2014). Characterization of Pickering O/W Emulsions Stabilized by Silica Nanoparticles and Their Responsiveness to *In vitro* Digestion Conditions. *Food Biophysics*, 9(4), pp. 406-415.

Salvia-Trujillo, L., Qian, C., Martín-Belloso, O., & McClements, D. J. (2013a). Influence of particle size on lipid digestion and β -carotene bioaccessibility in emulsions and nanoemulsions. *Food Chemistry*, 141(2), pp. 1472-1480.

Salvia-Trujillo, L., Qian, C., Martín-Belloso, O., & McClements, D. J. (2013b). Modulating β -carotene bioaccessibility by controlling oil composition and concentration in edible nanoemulsions. *Food Chemistry*, 139(1), pp. 878-884.

Sarkar, A., Mackie, A.R., 2020. Engineering oral delivery of hydrophobic bioactives in real-world scenarios. *Curr. Opin. Colloid Interface Sci.* 48, 40–52.

Sarkar, A., Murray, B., Holmes, M., Ettelaie, R., Abdalla, A., & Yang, X. (2016). *In vitro* digestion of Pickering emulsions stabilized by soft whey protein microgel particles: influence of thermal treatment. *Soft Matter*, 12(15), pp. 3558-3569.

Sarkar, A., Zhang, S., Holmes, M., & Ettelaie, R. (2019). Colloidal aspects of digestion of Pickering emulsions: Experiments and theoretical models of lipid digestion kinetics. *Advances in Colloid & Interface Science*, 263, pp. 195-211.

- Sarkar, A., Zhang, S., Murray, B., Russell, J. A., & Boxal, S. (2017). Modulating *in vitro* gastric digestion of emulsions using composite whey protein-cellulose nanocrystal interfaces. *Colloids & Surfaces B: Biointerfaces*, 158, pp. 137-146.
- Shah, B. R., Li, Y., Jin, W., An, Y., He, L., Li, Z., Xu, W., & Li, B. (2016a). Preparation and optimization of Pickering emulsion stabilized by chitosan-tripolyphosphate nanoparticles for curcumin encapsulation. *Food Hydrocolloids*, 52, pp. 369-377.
- Shah, B. R., Zhang, C., Li, Y., & Li, B. (2016b). Bioaccessibility and antioxidant activity of curcumin after encapsulated by nano and Pickering emulsion based on chitosan-tripolyphosphate nanoparticles. *Food Research International*, 89, pp. 399-407.
- Shimoni, G., Shani Levi, C., Levi Tal, S., & Lesmes, U. (2013). Emulsions stabilization by lactoferrin nanoparticles under *in vitro* digestion conditions. *Food Hydrocolloids*, 33(2), pp. 264-272.
- Silva, H. D., Beldíková, E., Poejo, J., Abrunhosa, L., Serra, A. T., Duarte, C. M. M., Brányik, T., Cerqueira, M. A., Pinheiro, A. C., & Vicente, A. A. (2019). Evaluating the effect of chitosan layer on bioaccessibility and cellular uptake of curcumin nanoemulsions. *Journal of Food Engineering*, 243, pp. 89-100.
- Singh, H., & Sarkar, A. (2011). Behaviour of protein-stabilised emulsions under various physiological conditions. *Advances in Colloid & Interface Science*, 165(1), pp. 47-57.
- Tang, Q., Xie, X., Li, C., Zhen, B., Cai, X., Zhang, G., Zhou, C., & Wang, L. (2019). Medium-chain triglyceride/water Pickering emulsion stabilized by phosphatidylcholine-kaolinite for encapsulation and controlled release of curcumin. *Colloids & Surfaces B: Biointerfaces*, 183, pp. 110414.
- Tikekar, R. V., Pan, Y., & Nitin, N. (2013). Fate of curcumin encapsulated in silica nanoparticle stabilized Pickering emulsion during storage and simulated digestion. *Food Research International*, 51(1), pp. 370-377.
- Tønnesen, H.H., Karlsen, J., 1985. Studies on curcumin and curcuminoids. VI. Kinetics of curcumin degradation in aqueous solution. *Z. Lebensm. Unters. Forsch.* 180 (5), 402–404.
- Tønnesen, H. H., Másson, M., & Loftsson, T. (2002). Studies of curcumin and curcuminoids. XXVII. Cyclodextrin complexation: solubility, chemical and photochemical stability. *International Journal of Pharmaceutics*, 244(1), pp. 127-135.
- Torres, O., Murray, B. S., & Sarkar, A. (2019). Overcoming *in vitro* gastric destabilisation of emulsion droplets using emulsion microgel particles for targeted intestinal release of fatty acids. *Food Hydrocolloids*, 89, pp. 523-533.

- Tzoumaki, M.V., Moschakis, T., Kiosseoglou, V., Biliaderis, C.G., 2011. Oil-in-water emulsions stabilized by chitin nanocrystal particles. *Food Hydrocolloids* 25 (6), 1521–1529.
- Wang, Y.-J., Pan, M.-H., Cheng, A.-L., Lin, L.-I., Ho, Y.-S., Hsieh, C.-Y., Lin, J.-K., 1997. Stability of curcumin in buffer solutions and characterization of its degradation products. *J. Pharmaceut. Biomed. Anal.* 15 (12), 1867–1876.
- Wei, Z., Zhu, J., Cheng, Y., & Huang, Q. (2019). Ovotransferrin fibril–stabilized Pickering emulsions improve protection and bioaccessibility of curcumin. *Food Research International*, 125, pp. 108602.
- Xiao, J., Li, C., & Huang, Q. (2015). Kafirin Nanoparticle-Stabilized Pickering Emulsions as Oral Delivery Vehicles: Physicochemical Stability and *in Vitro* Digestion Profile. *Journal of Agricultural and Food Chemistry*, 63(47), pp. 10263-10270.
- Yan, X., Cao, S., Li, Y., Xiao, P., Huang, Z., Li, H., & Ma, Y. (2019). Internalization and subcellular transport mechanisms of different curcumin loaded nanocarriers across Caco-2 cell model. *Journal of Drug Delivery Science & Technology*, 52, pp. 660-669.
- Zou, L., Zheng, B., Liu, W., Liu, C., Xiao, H., & McClements, D. J. (2015). Enhancing nutraceutical bioavailability using excipient emulsions: Influence of lipid droplet size on solubility and bioaccessibility of powdered curcumin. *Journal of Functional Foods*, 15, pp. 72-83.

Chapter 7

General discussion

7.1 Introduction

Lipid-based delivery systems are being developed in both pharmaceutical and food industries to protect and modulate the release of bioactive compounds to increase its bioavailability. The knowledge of the stability and efficiency of these lipid-based delivery systems can be useful to develop functional foods that deliver bioactive compounds to specific locations of the gastrointestinal (GI) tract where they function. In this PhD, the overarching goal was to understand the delivery of a highly potent bioactive compound, curcumin. Although curcumin has been widely investigated in literature due to its therapeutic properties, its poor water solubility, rapid metabolism and early clearance without being optimally bioavailable makes its unsuitable for pharmaceutical or functional food applications with validated “European Food Safety Authority” (EFSA) health claims to date. Many emulsion-based delivery systems have been investigated in the last two decades attempting targeted delivery of curcumin in intestinal sites.

In recent years, there has been a resurgence of interest in emulsions that are stabilized by solid particles (Pickering emulsions) due to its irreversible adsorption, which results in a higher energy barrier conferring them with long-term stability. Higher stability of Pickering emulsions compared to protein or surfactant-stabilized emulsions make them more suitable for encapsulation of bioactive compounds. Furthermore, the interests in encapsulating bioactive compounds using Pickering emulsions also arise from their properties such as that, once adsorbed, the particles are not competitively displaced by bile salts in the intestine, thus allowing precise control over the lipid digestion kinetics (Sarkar et al., 2019).

As discussed in the literature review in **Chapter 2**, Pickering emulsions for the delivery of curcumin have been designed in the recent years using different particles fabricated from polysaccharide origin (modified starch granules, chitosan-tripolyphosphate complexes, nanocellulose), protein origin (kafirin, ovotransferrin fibrils), and other materials (silica, kaolinite) (Asabuwa Ngwabebhoh et al., 2018; Lu et al., 2019; Marefati et al., 2017; Shah et al., 2016a; Shah et al., 2016b; Tang et al.,

2019; Tikekar et al., 2013; Wei et al., 2019). However, many of these Pickering systems cannot be considered as food-grade emulsions, which restricts their application in formats allowed for oral administration route. In addition, only few of these rather limited studies have investigated the stability of the encapsulated curcumin in these Pickering emulsions after passing through *in vitro* gastrointestinal digestion route (Lu et al., 2019; Marefati et al., 2017; Shah et al., 2016b; Wei et al., 2019; Tikekar et al., 2013). Therefore, the aim of this thesis was to engineer novel bio-compatible and bio-degradable Pickering stabilizers to design emulsions encapsulating curcumin with controlled release properties at specific physiological sites while increasing curcumin's bioaccessibility after gastrointestinal transit and eventually check the effects of such design on cellular internalization (Figure 7.1).

Three Pickering emulsions containing curcumin were developed; whey protein nanogel-stabilized, dextran sulphate coated-whey protein nanogel-stabilized, and conjugated whey protein-dextran microgel-stabilized Pickering emulsions. The innovative aspects of the Pickering systems developed in this PhD, was that it involved valorising two types of interactions (*i.e.* electrostatic and covalent) between whey protein and polysaccharides (dextran sulphate or dextran) to create complex particulate interfaces.

In view of the above, size, degree of aggregation, microstructure and adsorption efficiency were first analysed (Figure 7.1, **Chapter 3**). O/W emulsions were then prepared using whey protein nanogel particles and were evaluated as delivery systems for curcumin and the effect of different physiologically relevant pHs and ionic strengths on curcumin retention was assessed (Figure 7.1 **Chapter 3**). The gastric protection of this whey protein nanogel stabilized-Pickering emulsions was achieved by engineering a biopolymeric coating by electrostatic deposition of a negatively-charged dextran sulphate of two molecular weights (40 kDa and 500 kDa) (Figure 7.1 **Chapter 4**) to positively charged whey protein nanogel particle-coated oil-in-water emulsions at gastric pH. Emulsions coated with dextran sulphate of 500 kDa showed increased mechanical stability compared to 40 kDa against pepsinolysis of the underlying proteinaceous particle layer. Since electrostatic complexation can be highly susceptible to complex pH and ionic conditions present in human conditions, to further improve the resistance of the proteinaceous part of the interface from pepsinolysis, conjugation between whey protein isolate and dextran was undertaken by using Maillard reaction between whey protein and dextran (**Chapter 5**).

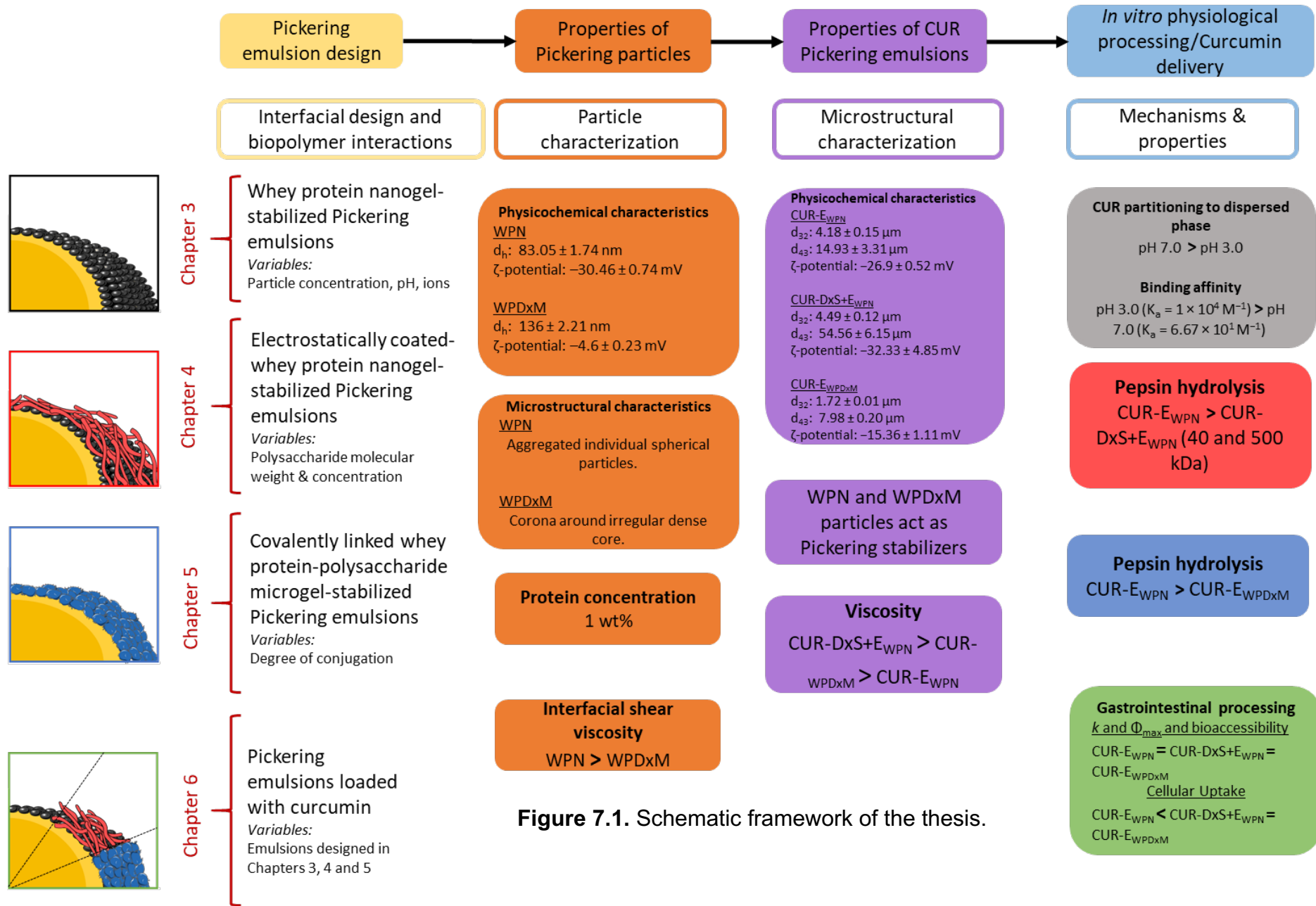


Figure 7.1. Schematic framework of the thesis.

Therefore, conjugated whey protein microgel particles with different degree of conjugation were engineered using a top-down technique after thermal gelation of whey protein-dextran conjugate of specific degree of conjugation. The resistance to gastric digestion as a function of the degree of conjugation was evaluated and selected microgel particles were used to stabilize O/W emulsions. This mechanism of complex particulate stabilization further improved the gastric stability of O/W emulsions and the characterization was undertaken using cross-correlation confocal image analysis for the first time to have quantitative estimation of the protein concentration at the interface post gastric digestion (Figure 7.1, **Chapter 5**). This additionally indicated that both these electrostatically-deposited or covalently-conjugated complex interfaces in **Chapters 4** and **5** were capable in providing gastric stability to the droplets. These two novel Pickering emulsions (**Chapters 4** and **5**) along with the emulsions stabilized by whey protein nanogel particles (**Chapter 3**) were then loaded with curcumin and subjected to gastrointestinal digestion and the micellar fraction was examined for bioaccessibility of curcumin. In addition, cellular uptake of curcumin released from these three Pickering systems were investigated in Caco-2 cells (**Chapter 6**).

7.2 Summary of main results

7.2.1 Assessment of curcumin solubility in different types of oil

Before the Pickering emulsions could be formulated, the maximum curcumin solubility in different oil types was determined (**Chapter 2**). Figure 7.2 summarizes the maximum solubility of curcumin dispersed in different types of edible oils. Oils with long chain lengths (LCT) (*i.e.*, sunflower oil, soybean oil and oleic acid) presented lower ability to solubilize curcumin as compared to medium chain triglycerides (MCT) (Figure 7.2) under all the conditions applied (*i.e.* temperature and stirring time). This difference in solubility behaviour might be attributed to the fact that, at a given mass, there are more available oxygen molecules in shorter chain length triglycerides to allow hydrogen bonding between the triglyceride molecule and curcumin (Ahmed et al., 2012). From this simple approach, MCT oil was chosen as the oil phase throughout this thesis and as the carrier oil for developing curcumin emulsions (**Chapter 2** and **6**).

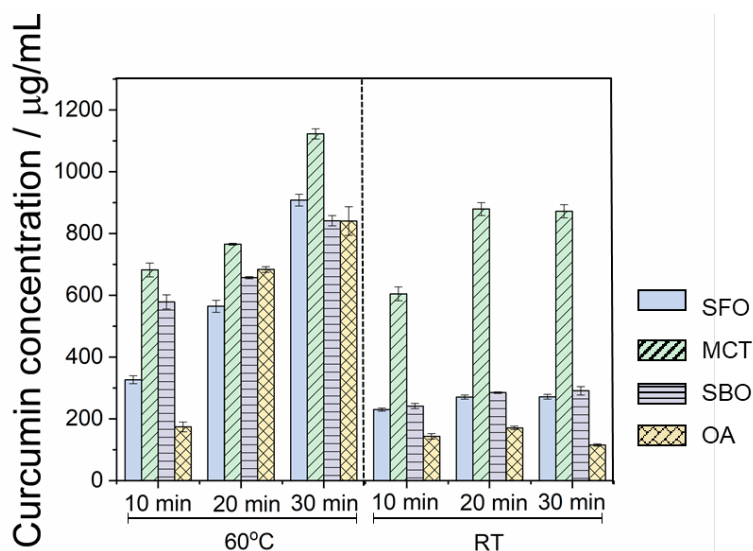


Figure 7.2. Solubility ($\mu\text{g}/\text{mL}$) of curcumin in various edible oils. SFO: sunflower oil, MCT: medium chain triacylglycerol, SBO: soybean oil, OA: oleic acid, RT: room temperature.

7.2.3 Assessment of nanogel and microgel particles

The detailed physicochemical characterization of whey protein nanogel (WPN) with respect to its suitability for use as Pickering stabilizer was performed in **Chapter 3**. To establish the effect of Maillard reaction between whey protein isolate and dextran (500 kDa) and conjugation degrees, the ability of the conjugates to form microgel particles, and the emulsifying capacity and stability of the corresponding emulsions was then evaluated in **Chapter 5**. The main findings on this section are related to the development of these nanogel and microgel particles. Whey protein nanogel (WPN) and conjugated whey protein-dextran microgel particles (WPDxM) were fabricated based on the principle of heat-induced gel protein formation. When aqueous dispersions of whey protein isolate are heated at $\geq 65\text{ }^{\circ}\text{C}$, it caused the proteins to unfold and expose its hydrophobic and sulfhydryl groups to the aqueous phase. Hydrophobic interactions followed by formation of intramolecular disulphide-bonds between neighbour protein molecules caused aggregation of protein chains into a three-dimensional network gel (Croguennec et al., 2004; Nicolai, et al., 2011). High-pressure homogenization of the heat-induced gels allowed formation of the nanogel or microgel particles.

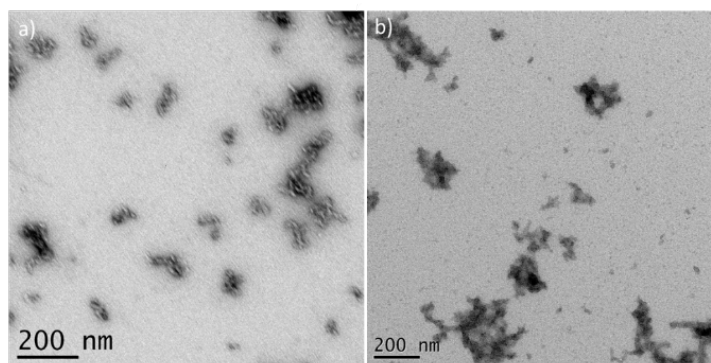


Figure 7.3. TEM micrographs of 1 wt% a) WPN and b) WPD_{x10M}.

Whey protein isolate and dextran (500 kDa) conjugates with different degrees of conjugation (10, 20 and 30%) were obtained by controlled dry heating (60°C, 79% RH, 24 - 48 hrs). Conjugate microgel particles (WPD_{x10, 20, 30M}) were prepared by controlled shearing of WPI-Dx₁₀, WPI-Dx₂₀ and WPI-Dx₃₀ gels using a top down approach (**Chapter 5**). Mixed non-conjugated whey protein-dextran particles (N-WPD_{xM}) were also created for control purposes. Table 7.1 summarizes the different characteristics of whey protein nanogel and conjugated whey protein-dextran microgel particles based on their mean hydrodynamic diameters (d_H) and ζ -potential values dispersed in water at pH 7.0 (**Chapter 3** and **5**). All nanogel and microgel particles produced by high-pressure homogenization had 1 wt% final whey protein content. WPN presented a small mean hydrodynamic size (d_H : ~83.05, ζ -potential: ~ -30.46, Table 7.1), whereas WPD_{x10,20,30M} and N-WPD_{xM} presented a bigger mean hydrodynamic size (d_H : ~136 - 146 nm, and ~265 nm, respectively, Table 7.1). Difference in size might be attributed to the addition of the large molecular weight dextran (500 kDa), which might have affected protein unfolding during heat-treatment, cold-set gelation and particle formation during high-pressure homogenization process as discussed in **Chapter 5**. Micro-structural evaluation of WPN and WPD_{x10M} revealed that WPN presented a more aggregated morphology of individual spherical particles, whereas WPD_{x10M} presented a corona around irregular dense core (Figure 7.3).

Table 7.1. Comparison of the characteristics of 1 wt% protein-based particles on their size (d_H) and ζ -potential at pH 7.0.

Characteristics	WPN	WPDx ₁₀ M	WPDx ₂₀ M	WPDx ₃₀ M	N-WPDxM
d_H / nm	83.05 ± 1.7	136 ± 2.21	131 ± 1.8	146 ± 3.9	262 ± 0.82
Pdl	0.244	0.22	0.27	0.278	0.269
ζ – potential / mV	-30.46 ± 0.74	-4.6 ± 0.23	-5.6 ± 0.16	-8.1 ± 0.18	-4.9 ± 0.30

In the case of the ζ -potential, there was a significant difference ($p < 0.05$) between WPN and particles with added dextran either in a conjugated or non-conjugated state (Table 7.1). The negative charge was expected for WPN as they were above the isoelectric point of whey protein isolate and a ζ -potential value of ≤ 30 mV was high enough to ensure dispersion stability at pH 7.0 (**Chapter 2**). The reduced ζ -potential was attributed to the addition of the neutral dextran molecule, which might have saturated the surface of these conjugated microgel particles (**Chapter 5**). In addition, it was observed that reducing the pH of the aqueous dispersion of particles from 7.0 to 3.0 did not play a significant effect on the stability and morphology of the particles (**Chapter 2 and 5**), with just the ζ -potential going from negative to positive as the pH was reduced from above to below the isoelectric point. Since the emphasis of this PhD was to develop protein-based microgel particles that can be less sensitive to hydrolysis during physiological conditions, WPDx₁₀M particles were chosen as Pickering stabilizers due to their ability to delay pepsinolysis of the microgel particles during gastric digestion (Figure 5.4, **Chapter 5**).

7.2.4 O/W emulsions

The effect of emulsification on morphological properties of Pickering emulsions using the previously designed WPN particles (E_{WPN}) was studied in **Chapter 3**. Electrostatic interactions between WPN-stabilized interface and selected dextran sulphate ($DxS+E_{WPN}$) to improve the barrier properties of the proteinaceous interface against gastric hydrolysis was studied in **Chapter 4**. In this chapter, development of layer-by-layer Pickering emulsions with DxS of 40 and 500 kDa were evaluated and their resistance to gastric condition was assessed using an *in vitro* static gastric model.

Chapter 5 considered the development of Pickering emulsions using conjugated (10% DC) whey protein-dextran microgel particles ($E_{WPDx10M}$) to study the influence of covalent interactions on the morphological and stability properties after to gastric conditions in an *in vitro* static gastric model. The main results on the emulsions physicochemical characteristics are summarized below.

When considering emulsification, emulsion stability and droplet size strongly depends on the particle concentration (McClements, 2004). Hence, to be able to design stable Pickering emulsions, a series of emulsions with 20 wt% oil phase and 80 wt% aqueous phase was prepared with different concentrations of WPN particles (0.1 - 3.0 wt%) (**Chapter 2**).

Laser diffraction, protein absorption and surface coverage calculations (Table 7.2) revealed that at low concentration of WPN (0.1 - 0.5 wt%), the oil-in-water interface was not sufficiently covered. At higher WPN concentration (1 - 3 wt%), particles were able to completely cover the surface of the droplet either as a multilayer or aggregates of WPN at the interface with an excess of particles remaining unabsorbed. An optimum protein concentration where samples presented fewer particles in the continuous phase and the surface coverage value suggested a hexagonal close packing arrangement was identified to be 1 wt% final protein concentration. Hence, this concentration was selected hereafter for design of all subsequent Pickering emulsion samples used throughout this thesis.

Interfacial shear viscosity experiments were used to give an insight on interfacial properties of the particle-laden interface (Murray et al., 2011; Zembyla et al., 2019; Zembyla et al., 2019). Hence, the mechanical performance of the adsorbed nanogel and microgel particles (*i.e.*, WPN and $WPDx_{10M}$) at the O/W interface was assessed using interfacial shear viscosity. Interfacial shear viscosity results showed that WPN presented the strongest film formation when compared to WPI, $WPDx_{10M}$ and N- $WPDxM$ (see Table 2.1, **Chapter 2** and Figures 5.6c and supplementary Figure 5S7, **Chapter 5**). Such high interfacial shear viscosity is indicative of the strong mechanical film formed by the presence of adsorbed particles which indicates strong interactions between closely packed WPN particles adsorbed at the interface, as compared to WPI-stabilized emulsions and $WPDx_{10M}$ and N- $WPDxM$.

Table 7.2. Summary of surface coverage, absorption efficiency, mean d_{43} and ζ -potential values of Pickering emulsions stabilized with different concentrations of WPN at pH 7.0.

WPN concentration / wt%	Surface coverage	Absorption efficiency / %	Mean d_{43} / μm	ζ -potential / mV
0.1	0.14	100 ± 1.31	14.00 ± 0.19	44.43 ± 1.04
0.25	0.32	93.23 ± 1.17	12.73 ± 0.17	36.13 ± 1.02
0.35	0.46	91.08 ± 0.60	12.50 ± 0.37	32.56 ± 1.39
0.5	0.68	87.49 ± 0.89	12.59 ± 0.21	39.80 ± 1.20
1	1.35	77.91 ± 2.28	12.34 ± 0.28	35.73 ± 1.57
1.5	1.95	72.57 ± 2.94	11.61 ± 0.20	35 ± 0.7
2	2.59	69.77 ± 2.76	11.56 ± 0.52	32 ± 0.66
3	3.45	61.27 ± 1.64	10.29 ± 0.07	32.96 ± 1.04

Possibly, the altered structural conformation caused by the conjugation and/or the presence of a high molecular weight polysaccharide reduced the interactions among adjacent WPD_{x10M} and N-WPD_{xM} particles adsorbed at the interface.

Table 7.3. Comparison of the characteristics of Pickering emulsions (without curcumin) based on their size (d_{43} , d_{32}) and ζ -potential at pH 7.0.

Characteristics	E_{WPN}	$DxS+E_{WPN}^*$	$E_{WPDx10M}$
d_{43} / μm	12.34 ± 0.28	37.4 ± 2.07	10.06 ± 0.81
d_{32} / μm	0.98 ± 0.43	4.21 ± 0.04	2.21 ± 0.17
ζ – potential / mV	-35.73 ± 1.15	-48.2 ± 0.80	-5.39 ± 0.16

* $DxS+E_{WPN}$ was at pH 3.0 to allow electrostatic attractions between WPN and DxS.

CLSM and cryo-SEM images (Figure 7.4) show the adsorbed particles at the O/W interface proving the ability of these engineered nanogel and microgel particles to act as effective Pickering stabilizers. The use of WPN or WPD_{x10}M for the formation of Pickering emulsions barely influenced the emulsion droplet size, which was around

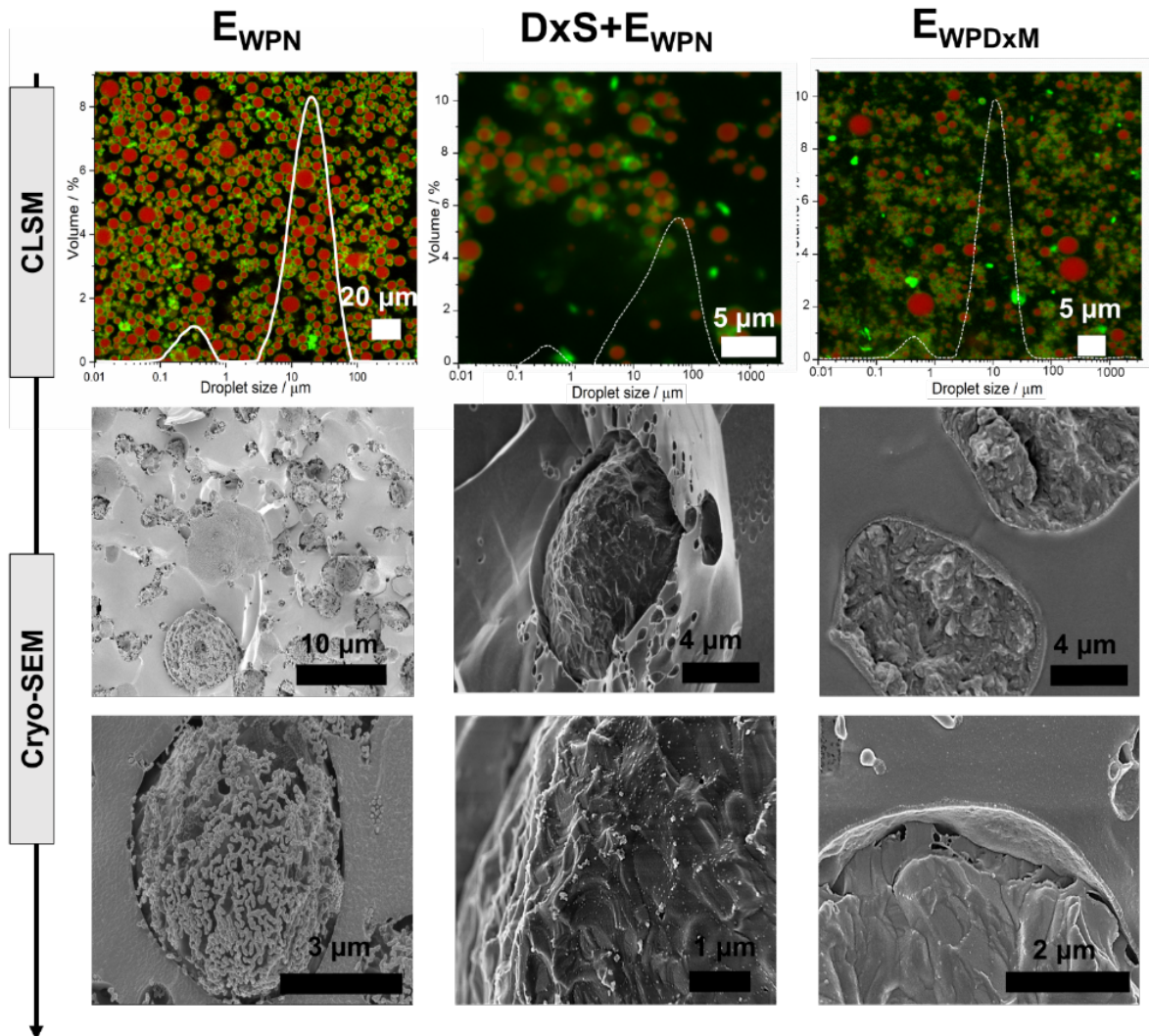


Figure 7.4. CLSM with superimposed particle size distribution and cryo-SEM images of E_{WPN} , $DxS+E_{WPN}$ and E_{WPDxM} emulsion.

~10 μm (**Chapters 2** and **5**). An interesting observation can be made in the size difference obtained for the emulsion when dextran sulphate was electrostatically attached to the surface of E_{WPN} (Table 7.3). In **Chapter 4**, the dextran sulphate-coated emulsion droplet size was around ~35 μm when using 0.2 wt% dextran sulphate (Figure 7.4). This increase might be due to the formation of polymeric bridges between anionic DxS adsorbed to WPN-laden interface and some cationic patches in the

surface of the neighbouring uncoated E_{WPN} droplets which caused droplet flocculation (Tokle et al., 2010).

Therefore, both WPN and WPD_{x10M} with similar size particle can be successfully produced using a top-down technique. In addition, complex particulate interfaces using electrostatic and covalent interactions can be effectively used to create stable Pickering emulsion systems, although the morphological and physicochemical properties of the emulsions differed only slightly.

7.2.5 Properties of emulsions during *in vitro* gastrointestinal processing using static model

The fate of E_{WPN} , $DxS+E_{WPN}$ and E_{WPDxM} Pickering emulsions (**Chapter 4 and 5**), and corresponding curcumin emulsions (**Chapter 6**), was evaluated after an *in vitro* gastric and gastrointestinal digestion, respectively. In addition to designing emulsions loaded with curcumin, bioaccessibility of the micellar phase and delivery of curcumin to the cells were assessed in **Chapter 6**. Destabilization of the emulsions was initially assessed during gastric processing, since the delivery systems should be resistant to gastric conditions (*i.e.*, enzymes, pH and ionic strength) but sensitive to intestinal conditions to enable curcumin release within the mixed micelles.

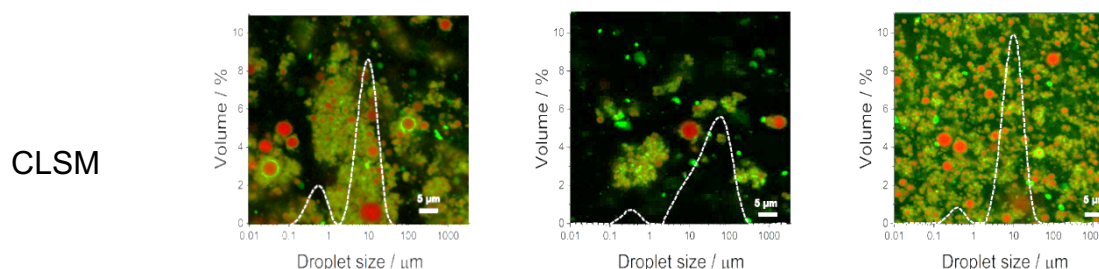
7.2.5.1 Curcumin-loaded Pickering emulsions

Curcumin-loaded Pickering emulsions showed mean droplet sizes (d_{43}) of ~ 14.93 , ~ 55 and $\sim 8 \mu m$ for $CUR-E_{WPN}$, $CUR-DxS-E_{WPN}$ and $CUR-E_{WPDxM}$, respectively (Table 7.4). Moreover, the droplet size distribution of the curcumin-loaded emulsions remained unchanged as compared to the unload (or naked) Pickering emulsions showing a bimodal size distribution with the peak in the area of $0.1 - 1 \mu m$ corresponding to unabsorbed particles and the peak in the area of $1 - 100 \mu m$ corresponding to the emulsion droplets (Table 7.4). This suggests that loading of curcumin had limited effects on the d_{43} of the droplets and droplet size distribution. In addition, viscosity measurements of the curcumin-loaded systems containing dextran (*i.e.* $CUR-DxS-E_{WPN}$ and $CUR-E_{WPDxM}$) were not significantly different ($p < 0.05$) between them but were orders of magnitude higher as compared to $CUR-E_{WPN}$. The increased viscosity of samples containing dextran might be attributed to remaining unbound DxS in the continuous phase or inter-droplet flocculation driven by negatively-charged DxS

bridging the positively-charged WPN-stabilized droplets at pH 3.0 as observed in confocal micrograph of CUR-DxS+E_{WPN} and CUR-E_{WPDxM} (Table 7.4).

Table 7.4. Comparison of the characteristics of curcumin-loaded Pickering emulsions based on their size (d_{43} , d_{32}) and ζ -potential at pH 7.0.

Characteristics	CUR-E _{WPN}	CUR-DxS+E _{WPN} *	CUR-E _{WPDxM}
d_{43} / μm	14.93 ± 3.31	54.56 ± 6.15	7.98 ± 0.20
d_{32} / μm	4.18 ± 0.15	4.49 ± 0.12	1.72 ± 0.01
ζ – potential / mV	-26.9 ± 0.52	-32.33 ± 4.85	-15.36 ± 1.11



*CUR-DxS+E_{WPN} was at pH 3.0 to allow electrostatic attractions between WPN and DxS.

7.2.5.2 Stability after *in vitro* gastric digestion

From **Chapters 4** and **6**, it was observed that after *in vitro* simulated gastric digestion, pepsin hydrolysed the protein at the surface of the emulsion droplets, or the particles bridging different droplets in both E_{WPN} and CUR-E_{WPN} with evidence of some coalescence phenomena (**Chapter 6**). However, a thin particle-laden interface was still observed in the micrographs stabilizing the majority of the droplets after the gastric digestion, which might be the peptide remnants of nanogel particles or peptides.

In comparison, the WPN-stabilized interface of DxS+E_{WPN} and CUR-DxS+E_{WPN} emulsion (DxS 500 kDa) droplets exhibited resistance to any pepsin-induced microstructural changes at gastric conditions (**Chapter 4** and **6**). In this case, the mechanical barrier properties of the polysaccharide coating might have protected the WPN from pepsinolysis by limiting the pepsin diffusion to the underlying proteinaceous particle-

stabilized interface. The CUR- E_{WPDxM} emulsion exhibited a decrease in the magnitude of surface charge and the d_{43} values increased to a certain extent but remained bimodal with no noticeable coalescence, with the intensity of the radial distribution of the protein surrounding the oil droplet presenting subtle changes after addition of pepsin (**Chapter 4**). For CUR- E_{WPDxM} , d_{43} and droplet size distribution remained unchanged (**Chapter 6**). Restricted access of digestive enzyme to the hydrophobic cleavage sites of the protein was possibly due to the complexity of the network structure formed by conjugation of WPI with dextran during the Maillard reaction. In addition, the high bulk viscosity of both, CUR-DxS+ E_{WPN} and CUR- E_{WPDxM} may have also hindered the diffusion of pepsin to the proteinaceous sides of the particle (see Figure 6.3, **Chapter 6**).

Thus, during gastric digestion, emulsions stabilized using WPDxM exhibited reduced pepsin digestibility kinetics, whereas reduced pepsin hydrolysis when using WPN was achieved when the surface of the WPN-stabilized droplets was coated with a polysaccharide (DxS). Therefore, both electrostatic and covalent interactions with polysaccharides allowed enhanced stability of Pickering emulsion droplets against gastric destabilisation and coalescence.

7.2.5.3 Behaviour during *in vitro* intestinal digestion, curcumin bioaccessibility and cellular uptake

The effect of *in vitro* intestinal digestion, bioaccessibility and cellular uptake was evaluated for CUR- E_{WPN} , CUR-DxS+ E_{WPN} and CUR- E_{WPDxM} in **Chapter 6**. During intestinal phase, destabilization is commonly expected to happen due to the action of intestinal enzymes (trypsin because of proteolytic action and lipase because of lipolytic action). Interestingly, all samples studied exhibited a significant increase in the d_{43} ranging between 60.25 and 69.25 μm corresponding to droplet coalescence, when the emulsions were mixed with simulated intestinal fluid containing pancreatin, irrespective of the initial interfacial material. These results illustrated that even if bile salts were not effective in displacing particles from the interface, lipase-co-lipase adsorption at the oil droplet surfaces occurred, enabling lipid digestion (Sarkar et al., 2019). In addition, the trypsin might have been capable of breaking down the proteinaceous particles which were somehow protected in the gastric phase particularly in case of complex particles-laden interfaces.

The rate and extent of lipolysis of curcumin-loaded Pickering emulsions was compared using the pH-stat method. The rate and the extent of the lipolysis from the amount of free fatty acids released (FFA%) was evaluated during 3 h (Figure 6.7a). The results showed that there was no significant difference between emulsion samples in terms of the rate (k) and extent (Φ_{max}) of FFAs release ($p > 0.05$). This similar FFA release behaviour during the simulated lipolysis supports the droplet size results, where no significant differences on the d_{43} between samples was observed in the intestinal stage. Similar observations about the effect of the size on FFAs release have been made in other works (Armand et al., 1992; Borel et al., 1994; McClements and Li 2010).

With respect to the bioaccessibility of curcumin between curcumin-loaded Pickering samples after the 180 min of lipolysis, there was no significant difference between emulsions ($p > 0.05$), which correlates positively with the FFA release results (Pearson correlation coefficient 0.981, p -value 0.0182). The lack of differences in the bioaccessibility can be due to the similar droplet characteristics and consequently similar FFA release after the small intestinal digestion phase. However, comparing with CUR in bulk MCT oil (*i.e.* non-emulsified sample) where bioaccessibility was significantly lower ($p < 0.05$) suggest more efficient transfer of CUR into the mixed micelles when incorporated into a Pickering emulsion system due to increased surface area in the latter systems (Salvia-Trujillo et al., 2013). Moreover, cellular uptake analysis revealed that the use of a dextran sulphate layer significantly increased ($p < 0.05$) the cellular uptake ratio from 6.3% for CUR- E_{WPN} to 7.6% and 7.36% CUR- $DxS+E_{WPN}$ and CUR- E_{WPDxM} , respectively. Therefore, Pickering emulsions designed with complex interfaces allows more efficient delivery of curcumin during the intestinal phase. The result of this thesis revealed the possibility of using structural design principles to fabricate Pickering emulsions with novel functional properties with the application of such as delivery systems for lipophilic compounds with controlled release properties.

7.3 Future directions

The work presented in this thesis has demonstrated that interfacial properties of Pickering particles can be controlled by manipulating interactions between a protein and a polysaccharide, which has implications not only on stability of the emulsion droplets but also on delivery of the encapsulated bioactive species. The main recommendations on further research that could be undertaken are summarized as follows:

Physicochemical characterization.

- It is important to understand whether the released curcumin from the three emulsions still possessed the functional properties. Therefore, antioxidant capacity of curcumin in these emulsions could be determined.
- Although large deformation rheology was used to determine the modulus of the microgel particles with an assumption that the particles had the same rheological behaviour as the heat-set gels from which they are created, atomic force microscopy (AFM) could be considered to measure the rheology of individual gel particles (Aufderhorst-Roberts et al., 2018; Bahri et al., 2019; Andablo-Reyes et al., 2019) and correlate such information with interfacial shear rheology. This would advance the field in terms of understanding the behaviour of soft particle-laden interface which has achieved limited attention until recently.
- Although, *in vitro* static model was used for understanding gastrointestinal fate of these emulsions in this thesis, new *in vitro* semi-dynamic protocol (Mulet-Cabero et al., 2020) seems to be an obvious next step to determine the kinetics of pepsinolysis of these emulsions in the gastric regime, where pH is changed as a function of time taking into account the buffering capacity of these emulsions. In addition, gastric lipase was not used in this PhD. Therefore, it is important to explore in future whether the gastric stability of the Pickering emulsions designed with complex particulate-laden interfaces such as conjugate microgel particles or polymer-coated nanogel particles are still retained once gastric lipases are introduced in the *in vitro* gastric model.

Food processing.

- It would be interesting to focus on the understanding the factors that affect the properties of the designed emulsions when incorporated into real food systems such as processing conditions (e.g. freezing, oven treatment, microwave treatments, drying etc. (Li et al., 2020)) and interactions with other components in food matrix.
- Feasibility studies of drying techniques such as spray drying and freeze-drying of these Pickering emulsions can be a subject to a future study to increase the long-term stability and improve the ease of utilization.
- The effect of using different types of biopolymers for covalent interactions such as bovine serum albumin, egg whites, pectins, maltodextrins, galactomannan etc. for creating different gastric-stable Pickering microgel stabilizers could be also interesting topic for future work.

In vivo studies and bioavailability.

- *In vivo* should be employed to validate the presented results in this PhD work which employed *in vitro* techniques and therefore can be an interesting topic for the future. From pharmacokinetics and pharmodynamic viewpoints, it is important to understand the presence of the bioactive in systemic circulation to check bioavailability to ensure its uptake by relevant tissues and organs. Hence bioavailability studies using *in vivo* animal studies are crucial with these designed Pickering emulsions to generate sufficient pre-clinical data before a clinical trial can be designed.
- It is also crucial to understand whether the knowledge on curcumin generated in this study can be translated to other bioactive compounds such as vitamin D, flavonoids (e.g. polyphenols), carotenoids (lycopene, β -carotene) etc. Hence, future studies should be performed using a different bioactive compound to check binding (if any) with the particle-laden interface that might interfere with the delivery kinetics.

7.4 References

- Ahmed, K., Li, Y., McClements, D. J. & Xiao, H. (2012). Nanoemulsion- and emulsion-based delivery systems for curcumin: Encapsulation and release properties. *Food Chemistry*, 132, 799-807.
- Andablo-Reyes, E., Yerani, D., Fu, M., Lamas, E., Connell, S., Torres, O. & Sarkar, A. (2019). Microgels as viscosity modifiers influence lubrication performance of continuum. *Soft Matter*, 15, 9614-9624.
- Armand, M., Borel, P., Ythier, P., Dutot, G., Melin, C., Senft, M., Lafont, H. & Lairon, D. (1992). Effects of droplet size, triacylglycerol composition, and calcium on the hydrolysis of complex emulsions by pancreatic lipase: an in vitro study. *The Journal of Nutritional Biochemistry*, 3, 333-341.
- Asabuwa Ngwabebhoh, F., Ilkar Erdagi, S. & Yildiz, U. (2018). Pickering emulsions stabilized nanocellulosic-based nanoparticles for coumarin and curcumin nanoencapsulations: In vitro release, anticancer and antimicrobial activities. *Carbohydrate Polymers*, 201, 317-328.
- Aufderhorst-Roberts, A., Baker, D., Foster, R. J., Cayre, O., Mattsson, J. & Connell, S. D. (2018). Nanoscale mechanics of microgel particles. *Nanoscale*, 10, 16050-16061.
- Bahri, A., Chevalier-Lucia, D., Marchesseau, S., Schmitt, C., Gergely, C. & Martin, M. (2019). Effect of pH change on size and nanomechanical behaviour of whey protein microgels. *Journal of Colloid and Interface Science*, 555, 558-568.
- Borel, P., Armand, M., Ythier, P., Dutot, G., Melin, C., Senft, M., Lafont, H. & Lairon, D. (1994). Hydrolysis of emulsions with different triglycerides and droplet sizes by gastric lipase in vitro. Effect on pancreatic lipase activity. *The Journal of Nutritional Biochemistry*, 5, 124-133.
- Li, X., Yang, Y., Murray, B. S. & Sarkar, A. (2020). Combination of egg white protein and microgels to stabilize foams: Impact of processing treatments. *Journal of Food Engineering*, 275, 109860.
- Lu, X., Li, C. & Huang, Q. (2019). Combining in vitro digestion model with cell culture model: Assessment of encapsulation and delivery of curcumin in milled starch particle stabilized Pickering emulsions. *International Journal of Biological Macromolecules*, 139, 917-924.
- Marefati, A., Bertrand, M., Sjöo, M., Dejmek, P. & Rayner, M. (2017). Storage and digestion stability of encapsulated curcumin in emulsions based on starch granule Pickering stabilization. *Food Hydrocolloids*, 63, 309-320.
- McClements, D. J. (2004). *Food Emulsions: Principles, Practices, and Techniques*. CRC Press, Taylor & Francis Group

McClements, D. J. & Li, Y. (2010). Structured emulsion-based delivery systems: Controlling the digestion and release of lipophilic food components. *Advances in Colloid and Interface Science*, 159, 213-228.

Mulet-Cabero, A.-I., Egger, L., Portmann, R., Ménard, O., Marze, S., Minekus, M., Le Feunteun, S., Sarkar, A., Grundy, M. M. L., Carrière, F., Golding, M., Dupont, D., Recio, I., Brodkorb, A. & Mackie, A. (2020). A standardised semi-dynamic in vitro digestion method suitable for food – an international consensus. *Food & Function*, 11, 1702-1720.

Salvia-Trujillo, L., Qian, C., Martín-Belloso, O. & McClements, D. J. (2013). Influence of particle size on lipid digestion and β -carotene bioaccessibility in emulsions and nanoemulsions. *Food Chemistry*, 141, 1472-1480.

Sarkar, A., Zhang, S., Holmes, M. & Ettelaie, R. (2019). Colloidal aspects of digestion of Pickering emulsions: Experiments and theoretical models of lipid digestion kinetics. *Advances in Colloid and Interface Science*, 263, 195-211.

Shah, B. R., Li, Y., Jin, W., An, Y., He, L., Li, Z., Xu, W. & Li, B. (2016a). Preparation and optimization of Pickering emulsion stabilized by chitosan-tripolyphosphate nanoparticles for curcumin encapsulation. *Food Hydrocolloids*, 52, 369-377.

Shah, B. R., Zhang, C., Li, Y. & Li, B. (2016b). Bioaccessibility and antioxidant activity of curcumin after encapsulated by nano and Pickering emulsion based on chitosan-tripolyphosphate nanoparticles. *Food Research International*, 89, 399-407.

Tang, Q., Xie, X., Li, C., Zhen, B., Cai, X., Zhang, G., Zhou, C. & Wang, L. (2019). Medium-chain triglyceride/water Pickering emulsion stabilized by phosphatidylcholine-kaolinite for encapsulation and controlled release of curcumin. *Colloids and Surfaces B: Biointerfaces*, 183, 110414.

Tikekar, R. V., Pan, Y. & Nitin, N. (2013). Fate of curcumin encapsulated in silica nanoparticle stabilized Pickering emulsion during storage and simulated digestion. *Food Research International*, 51, 370-377.

Tokle, T., Lesmes, U. & McClements, D. J. (2010). Impact of Electrostatic Deposition of Anionic Polysaccharides on the Stability of Oil Droplets Coated by Lactoferrin. *Journal of Agricultural and Food Chemistry*, 58, 9825-9832.

Wei, Z., Zhu, J., Cheng, Y. & Huang, Q. (2019). Ovotransferrin fibril-stabilized Pickering emulsions improve protection and bioaccessibility of curcumin. *Food Research International*, 125, 108602.

Appendix A

Supporting information of Chapter 3

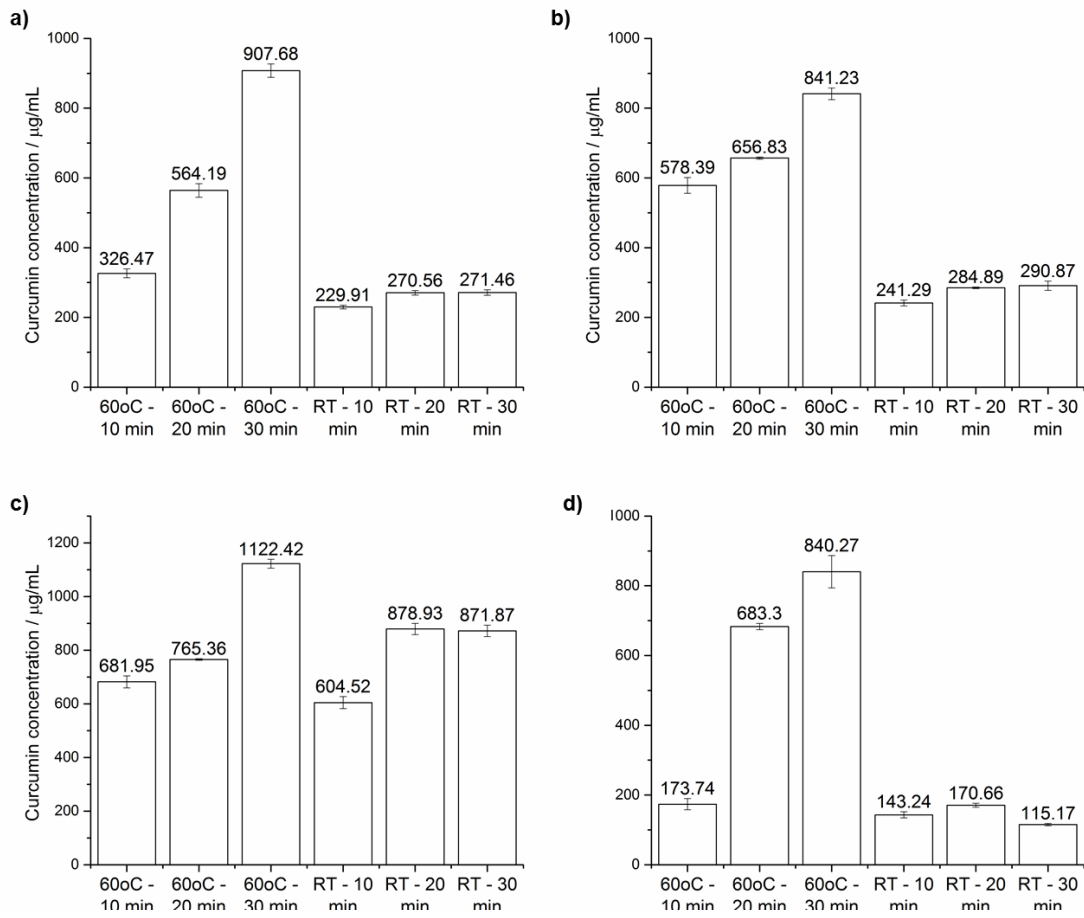


Figure A1. Solubility ($\mu\text{g}/\text{mL}$) of CUR in sunflower oil, a), soybean oil, b), medium chain triacylglycerol, c) and oleic acid, d), respectively. Error bars represent standard deviations.

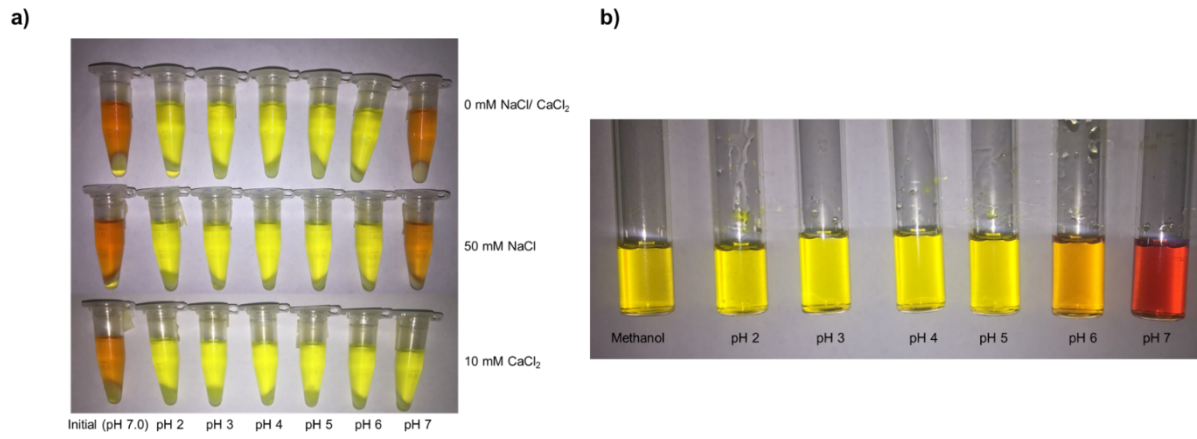


Figure A2. Visual appearance of CUR-EWPN sample extracts (methanol) a) and CUR after dilution with 1:1 (v/v) methanol/ buffer (25 oC), b) as a function of different pH.

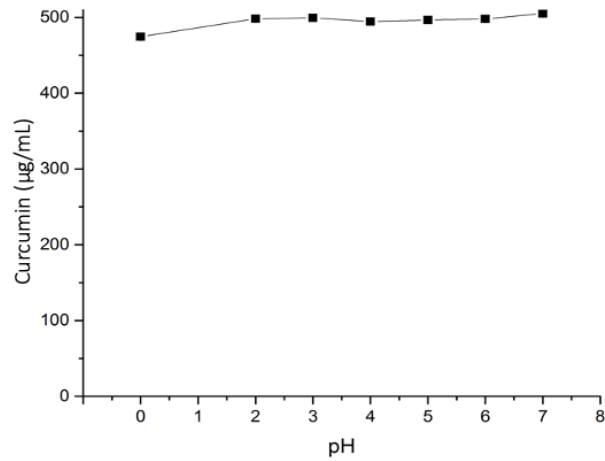


Figure A3. Mean concentration of CUR ($\mu\text{g}/\text{mL}$) estimated based on absorbance measurements (425 nm) of stock CUR-methanol solutions ($500 \mu\text{g}/\text{mL}$) in acidic state (pH 2.0) with 1:1 (v/v) methanol/ buffer (25°C), at different pH values (2.0 – 7.0) (low-to-high). Cero represent the control solution (stock CUR solution diluted in pure methanol).

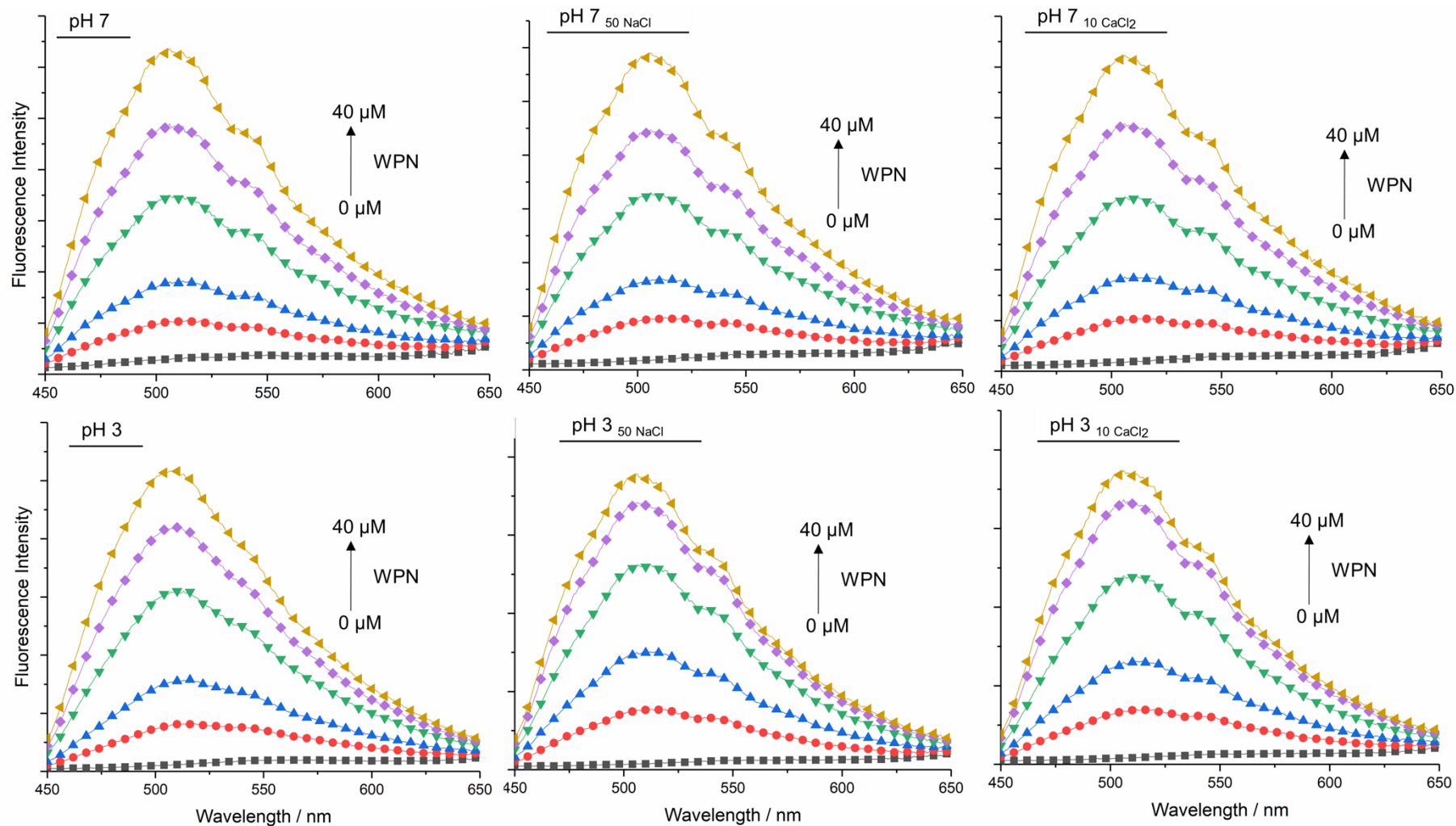


Figure A4. Emission spectra of curcumin showing the variations of curcumin fluorescence intensity and blue-shift on binding to WPN. A 10 μM concentration of curcumin was titrated against an increasing concentration of WPN (0 - 40 μM).

Appendix B

Supporting information of Chapter 4

Table B1. Mean hydrodynamic diameter (d_H), polydispersity index (Pdl) and ζ -potential values for WPN, WPN + DxS-40 and WPN+DxS-500 after formation at pH 3.0.

	WPN	WPN + DxS-40	WPN + DxS-500
d_H / nm	91.51 \pm 0.55	-	-
Pdl	0.236 \pm 0.0	-	-
ζ – potential / mV	+30.2 \pm 1.45	-21.6 \pm 2.67	-37.4 \pm 3.30

Table B2. Mean hydrodynamic diameter (d_H), polydispersity index (Pdl) and ζ -potential values of control samples for WPN, WPN + DxS-40 and WPN + DxS-500 in an *in vitro* gastric model at pH 3.0 in presence of SGF without pepsin, respectively.

Gastric digestion time / min	WPN			WPN + DxS-40	WPN + DxS-500
	d_H / nm	Pdl	ζ – potential / mV	ζ – potential / mV	ζ – potential / mV
0	93.58 ± 1.84	0.215 ± 0.03	19.13 ± 2.66	-11.51 ± 1.58	-19.26 ± 5.9
5	92.13 ± 3.35	0.333 ± 0.01	17.46 ± 2.20	-5.41 ± 2.67	-4.34 ± 0.52
30	110.16 ± 4.12	0.350 ± 0.11	17.73 ± 3.25	-1.71 ± 4.26	-9.38 ± 0.94
60	88.35 ± 2.66	0.271 ± 0.02	19.43 ± 1.43	-5.29 ± 1.48	-16.96 ± 1.05
90	89.88 ± 2.90	0.291 ± 0.00	18.2 ± 2.05	1.42 ± 0.56	-11.58 ± 1.24
120	90.22 ± 2.12	0.308 ± 0.01	17.03 ± 2.31	-4.20 ± 1.77	-14.33 ± 1.19
150	102.61 ± 7.09	0.334 ± 0.05	18.86 ± 0.70	0.67 ± 1.2	-8.89 ± 0.9

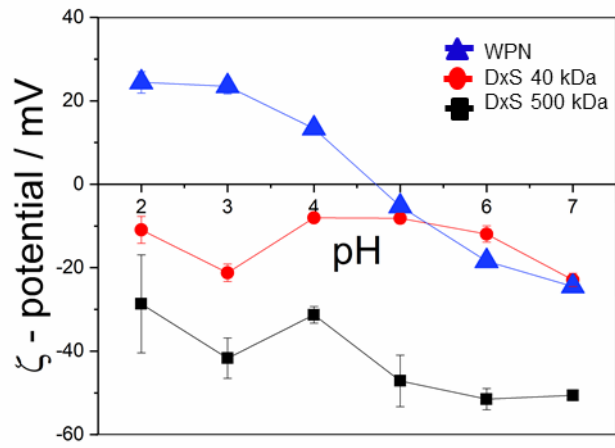


Figure B1. Mean ζ -potential values of aqueous dispersions of WPN, DxS-40 kDa and DxS-500 kDa as a function of pH, respectively.

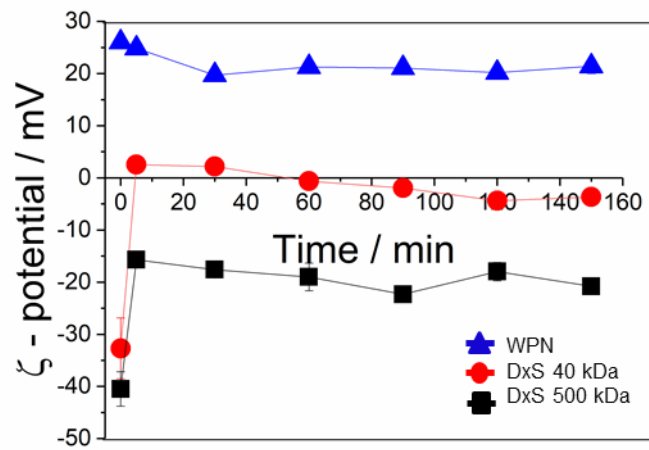


Figure B2. Change in mean ζ -potential values of 1 wt% WPN without or with the addition of 0.2 wt% DxS-40 kDa or 0.2 wt% DxS-500 kDa in an *in vitro* gastric model at pH 3.0 in presence of SGF containing pepsin, respectively.

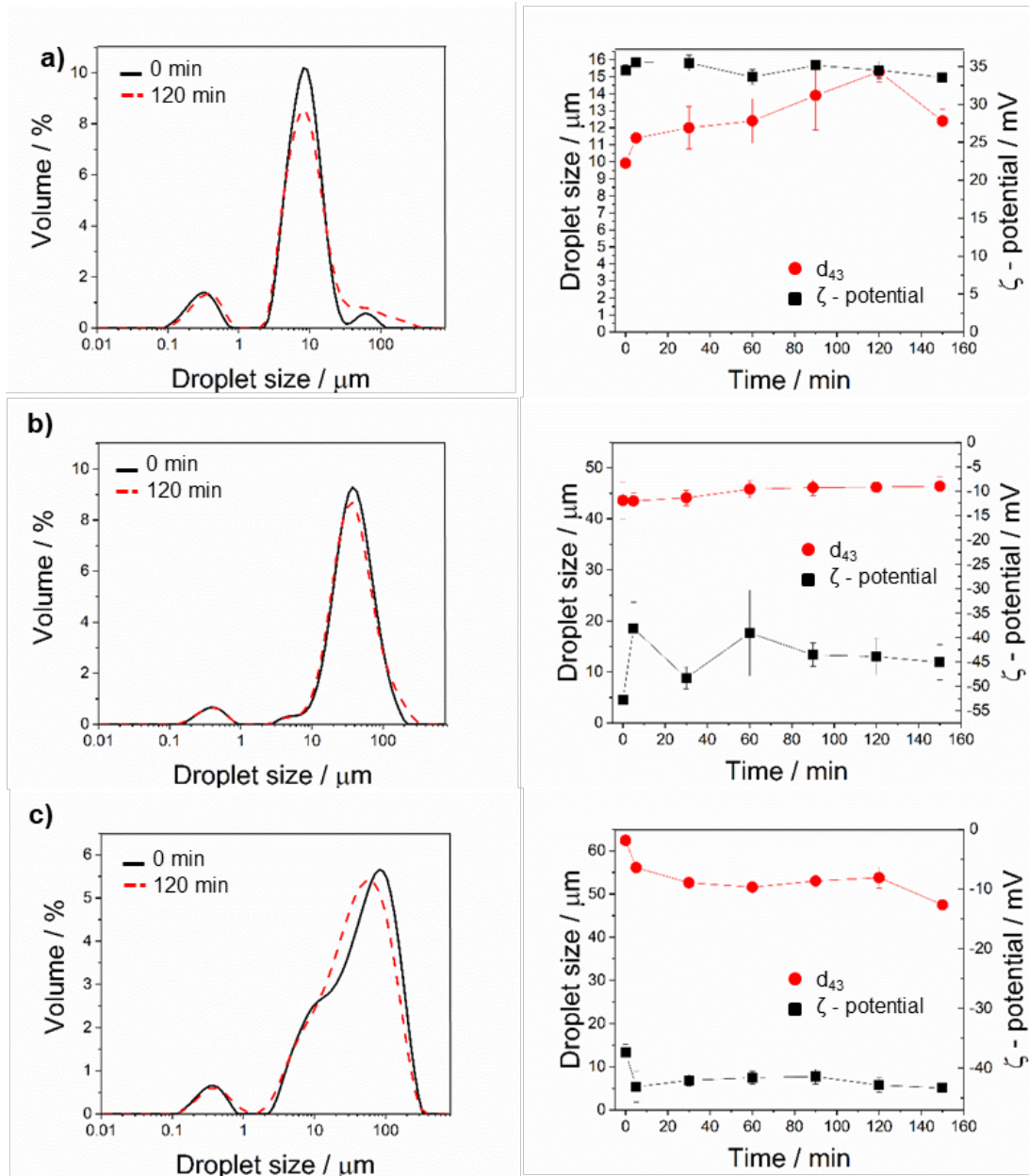


Figure B3. Droplet size distribution, mean d_{43} values and ζ -potential values of control samples for a) E_{WPN} b) DxS-E_{WPN}-40 and c) DxS-E_{WPN}-500 after *in vitro* gastric digestion in presence of SGF buffer without pepsin, respectively.

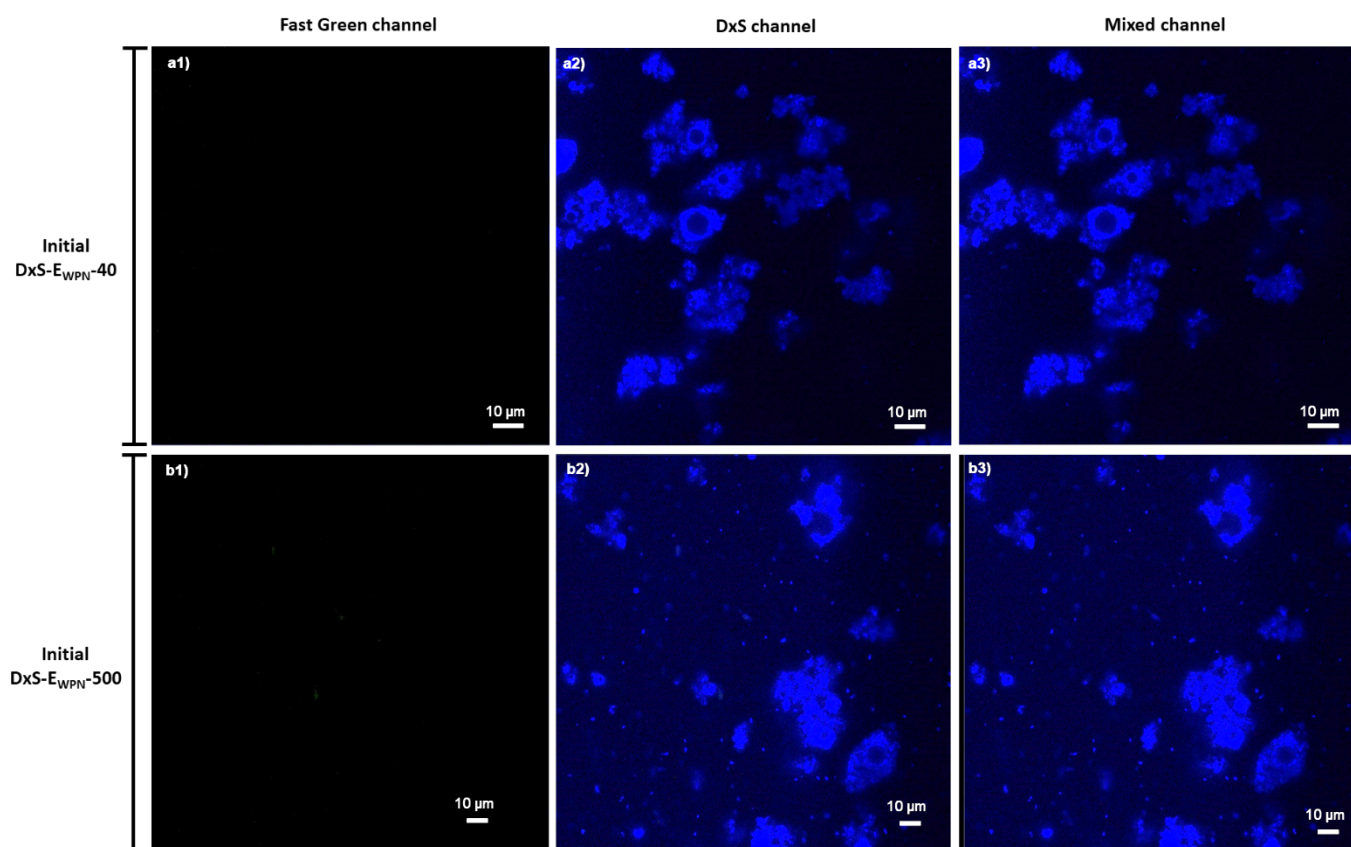


Figure B4. Confocal micrographs of initial FITC-DxS-E_{WPN}-40 and FITC-DxS-E_{WPN}-500 samples. Simultaneous recording of the emission of Fast Green and FITC-DxS dyes without the addition of Fast Green in the samples. Blue colour represents the FITC-labelled DxS.

Appendix C
Supporting information of Chapter 5

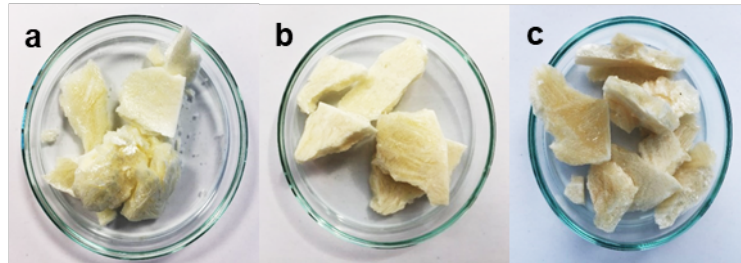


Figure C1. Images of conjugate powder of a) WPI-Dx₁₀, b) WPI-Dx₂₀, c) WPI-Dx₃₀.

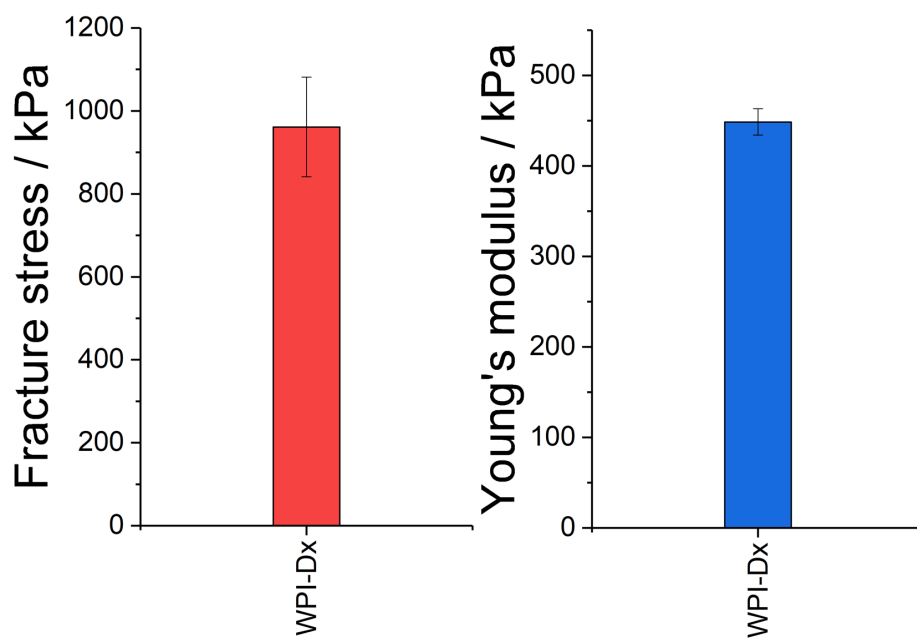


Figure C2. Fracture stress and Young's modulus of non-conjugated WPI-Dx gels.

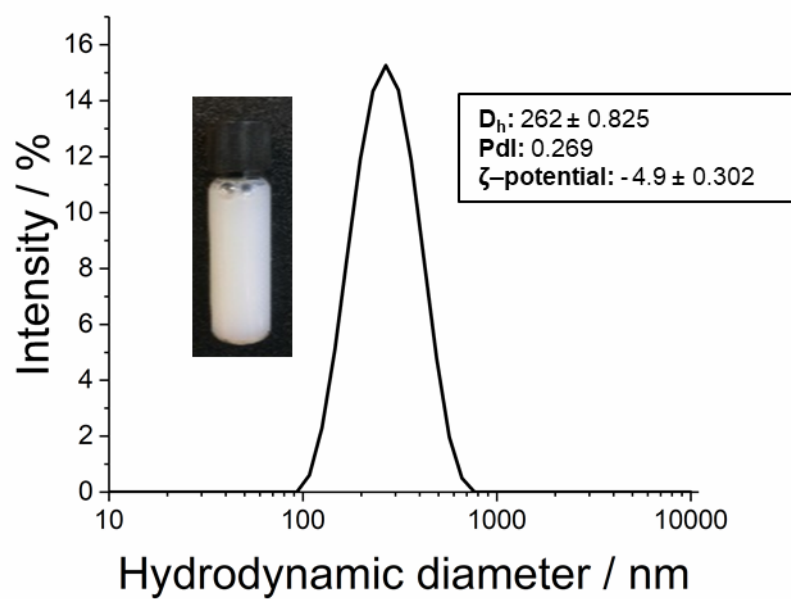


Figure C3. Intensity distribution of non-conjugated microgel particles (N-WPDxM) with inset representing the visual image and physicochemical characteristics.

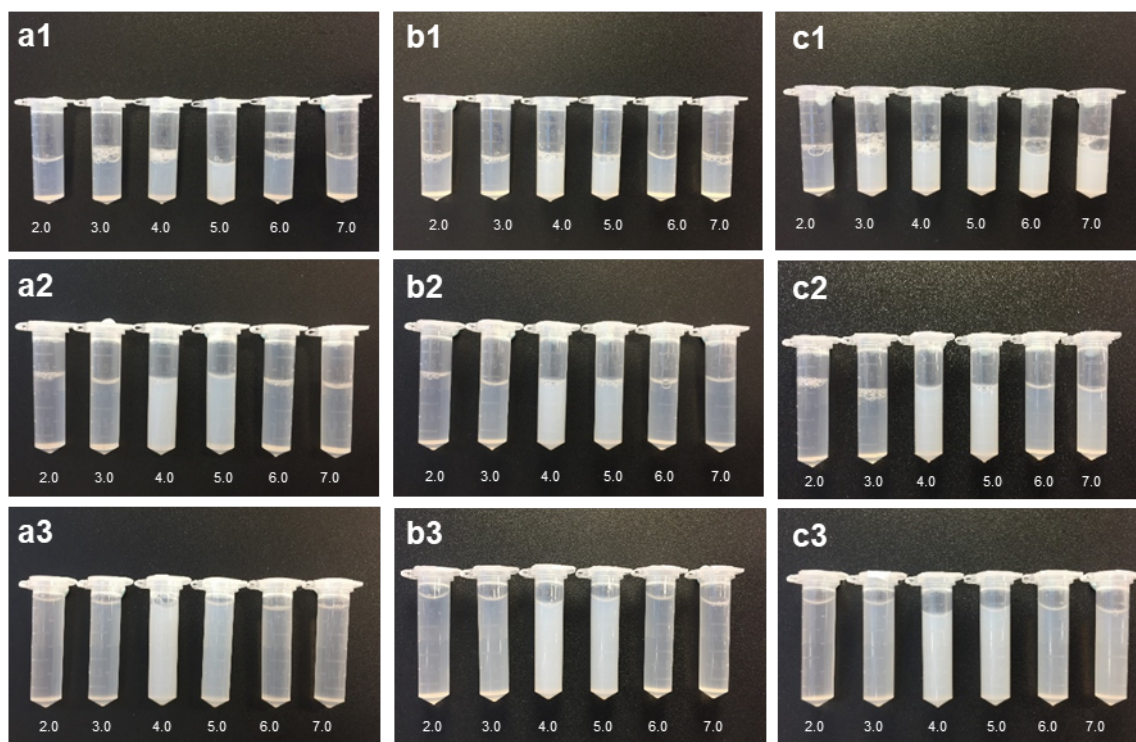


Figure C4. Photographs of vials containing 1 wt% aqueous solutions of conjugated microgel particles *i.e.* 1) WPD_{x10M}, 2) WPD_{x20M}, and 3) WPD_{x30M}, as a function of pH and ionic strength; a) 0 M NaCl/ CaCl₂, b) 50 mM NaCl and c) 10 mM CaCl₂.

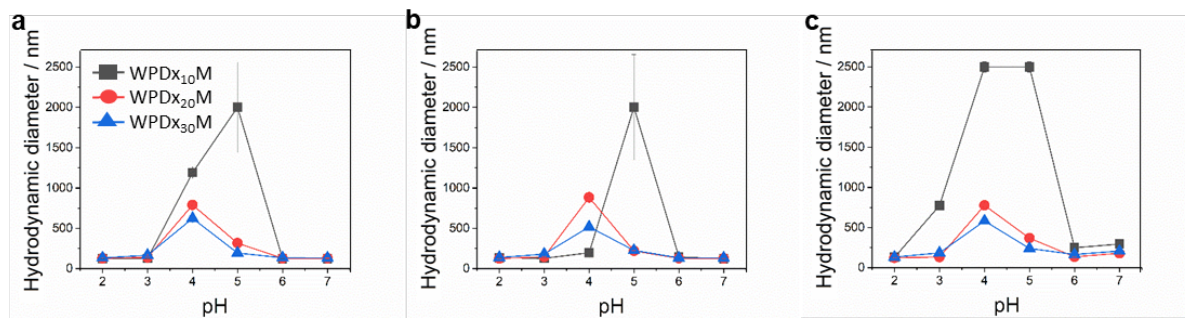


Figure C5. Hydrodynamic diameter of WPD_{x10}M, WPD_{x20}M, and WPD_{x30}M as a function of pH and ionic strength; a) 0 M NaCl/ CaCl₂, b) 50 mM NaCl and c) 10 mM CaCl₂.

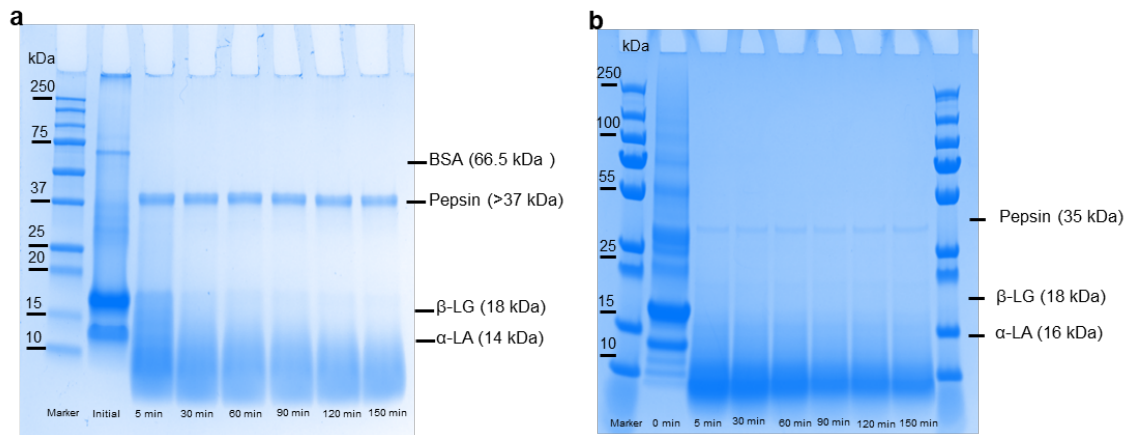


Figure C6. SDS-PAGE patterns of a) whey protein nanogel particles (WPN) (Araiza-Calahorra and Sarkar, 2019) and b) non-conjugated microgel particles as a function of in vitro gastric digestion time.

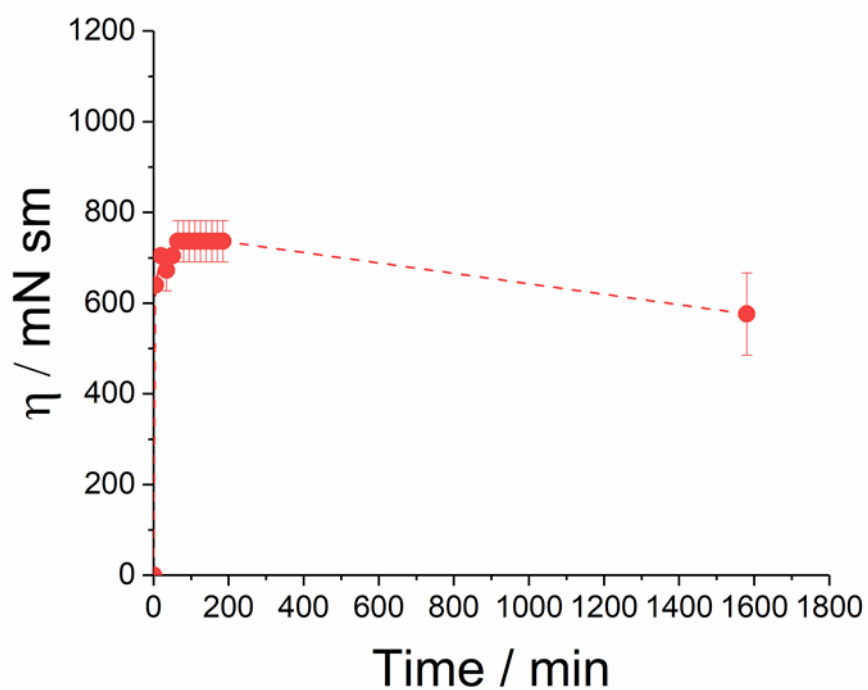


Figure C7. Interfacial shear viscosity at *n*-tetradecane-water interface against time of 0.5 wt% non-conjugated (N-WPDxM) after 24 h of adsorption. Error bars represent standard deviation.

Appendix D

Supporting information of Chapter 6

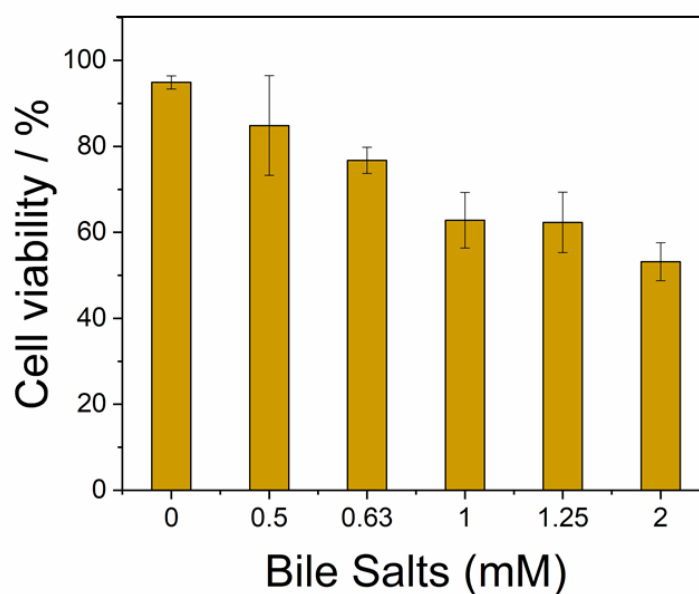


Figure D1. Cytotoxicity of bile salts towards Caco-2 cells following a 2 h incubation in the simulated digestion medium (*i.e.* simulated gastric and intestinal fluids without emulsion or CUR). Data are mean with SD from three independent experiments performed in duplicate.

